Fault Detection on an Experimental Aircraft Fuel Rig Using a Kalman Filter based FDI Scheme

by

Paul John Bennett

A DOCTORAL THESIS SUBMITTED IN PARTIAL FULFILMENT

OF THE REQUIREMENTS FOR THE AWARD OF

DOCTOR OF PHILOSOPHY

OF LOUGHBOROUGH UNIVERSITY

11 November 2010

Abstract

Reliability is an important issue across industry. This is due to a number of drivers such as the requirement of high safety levels within industries such as aviation, the need for mission success with military equipment, or to avoid monetary losses (due to unplanned outage) within the process and many other industries. The application of fault detection and identification helps to identify the presence of faults to improve mission success or increase up-time of plant equipment. Implementation of such systems can take the form of pattern recognition, statistical and geometric classifiers, soft computing methods or complex model based methods. This study deals with the latter, and focuses on a specific type of model, the Kalman filter.

The Kalman filter is an observer which estimates the states of a system, i.e. the physical variables, based upon its current state and knowledge of its inputs. This relies upon the creation of a mathematical model of the system in order to predict the outputs of the system at any given time. Feedback from the plant corrects minor deviation between the system and the Kalman filter model. Comparison between this prediction of outputs and the real output provides the indication of the presence of a fault. On systems with several inputs and outputs banks of these filters can used in order to detect and isolate the various faults that occur in the process and its sensors and actuators.

The thesis examines the application of the diagnostic techniques to a laboratory scale aircraft fuel system test-rig. The first stage of the research project required the development of a mathematical model of the fuel rig. Test data acquired by experiment is used to validate the system model against the fuel rig. This nonlinear model is then simplified to create several linear state space models of the fuel rig. These linear models are then used to develop the Kalman filter Fault Detection and Identification (FDI) system by application of appropriate tuning of the Kalman filter gains and careful choice of residual thresholds to determine fault condition boundaries and logic to identify the location of the fault. Additional performance enhancements

are also achieved by implementation of statistical evaluation of the residual signal produced and by automatic threshold calculation.

The results demonstrate the positive capture of a fault condition and identification of its location in an aircraft fuel system test-rig. The types of fault captured are hard faults such sensor malfunction and actuator failure which provide great deviation of the residual signals and softer faults such as performance degradation and fluid leaks in the tanks and pipes. Faults of a smaller magnitude are captured very well albeit within a larger time range. The performance of the Fault Diagnosis and Identification was further improved by the implementation of statistically evaluating the residual signal and by the development of automatic threshold determination. Identification of the location of the fault is managed by the use of mapping the possible fault permutations and the Kalman filter behaviour, this providing full discrimination between any faults present. Overall the Kalman filter based FDI developed provided positive results in capturing and identifying a system fault on the test-rig.

Table of Contents

Acknowledgments

This thesis is the culmination of steep learning curves, dead-ends, ups, downs and some difficult times. However, I will always be grateful to Dr. Roger Dixon for persisting till the completion of this work. Thank you for all you have done and for not giving up and for all the help and time you have given. I owe you one.

I am also very much grateful for the assistance and friendship of Dr John Pearson, industrial collaborator to the project, an integral part of making this work possible and invaluable resource.

My gratitude extends to Professor Roger Goodall, director of research, whose assistance in this project extends beyond the visible and for this, I thank you dearly.

To all my colleagues that have assisted me with technical issues, with special mention for Dr. Guy Charles and Dr. Scott Halsey for your assistance.

I will miss many colleagues, and have had good times within the group and my best wishes to you all. Hopefully I may work with some of you again some day.

Thank you to a lifelong friend, Ray Kelly, who has always supported me with his friendship.

I am grateful to my family for their time, patience, trust, support, Sunday roasts, bad jokes, but most of all for their love.

Last, but certainly not least, thank you to my wife, Karen, who has stood beside me for the ups and the downs come rain or shine and supported me whatever the situation and to my beautiful daughters Amy and Poppy – my motivation for everything.

List of Tables

List of Figures

Glossary and Acronyms

AC	Alternating Current
ANN	Artificial Neural Networks
AT	Auxiliary Tank
A_x	Area
CBM	Condition Based Maintenance
CPNN	Confidence Prediction Neural Network
c_v	Valve Conductance
DC	Direct Current
DWNN	Dynamic Wavelet Neural Network
ECU	Electronic Control Unit
EKF	Extended Kalman Filter
ENN	Ellipsoidal Neural Networks
Ev	Bulk Modulus
FADEC	Full Authority Digital Engine Controller
FDI	Fault Detection and Identification
FDIA	Fault Detection, Identification and Accommodation
FT	Flow Transducer
g	Acceleration due to Gravity
h_x	Fluidic height
KF	Kalman Filter
kg	Kilogram
L	Kalman Filter Gain
l	litres
LFR	Leak Flow Rate
LH	Left Hand
LSF	Linearization via State Feedback
m	Metres
MAD	Mean Absolute Deviation
MD	Mean Deviation
MLP	Multi-Layer Preceptron
mm	Millimetres
MSE	Mean-Square Error
N	Number of Samples
NF	Neuro-Fuzzy
NI	National Instruments
NN	Neural Networks
NSS	Nonlinear System Stabilization
Pa	Pascal
PC	Personal Computer
PCA	Principle Component Analysis

PHM	Prognostic Health Management
Psi	Pounds per Square Inch
PT	Pressure Transducer
PVC	Polyvinyl Chloride
q_x	Fluidic flow
Qn	Process Noise Covariance
ρ	Density
RH	Right Hand
RMSE	Root-Mean-Square Error
R^2	R-Square
Rn	Measurement Noise Covariance
RNN	Recurrent Neural Network
σ	Standard Deviation
S	Second
SEIC	Systems Engineering Innovation Centre
SHM	System Health Management
SSE	Sum-Square Error
SST	Total Sum of Squares
τ	Time Constant
TCP/IP	Transmission Control Protocol/ Internet Protocol
UAV	Unmanned Air Vehicle
UDP	User Datagram Protocol
V	Volts
v	Specific Volume
V_x	Volume
WNN	Wavelet Neural Network
WSSE	Weighted Sum-Square Error
WT	Wing Tank
WTI	Wing Tank Inner chamber
WTM	Wing Tank Middle chamber
WTO	Wing Tank Outer chamber
χ2-mean	Chi-Square Mean
y_v	Valve Position

Chapter 1

Introduction

The subject of this thesis is the development, application and test of a Fault Detection and Identification (FDI) tool for an aircraft fuel system simulation test rig. The FDI tool should reliably detect faults when they occur.

This chapter sets the context for the research work by discussing the project setting.

1.1 Overview

Aerospace and Defence Systems are becoming increasingly complex with higher component counts and ever more complicated components and sub-assemblies. Faults and failures are becoming harder to detect and isolate. The time that operators and maintenance technicians need to spend on faults is rising in direct relation to the complexity of the systems. With these increasing demands on reliability, maintainability and safety of systems, a wide range of fault detection and diagnostic methodologies have been proposed, and there has been considerable interest in the practical application of these fault diagnostic techniques (Leonhardt and Ayoubi, 1997; Rengaswamy *et al*, 2001; Frank *et al*, 2000; Venkatsubramanium *et al*, 2003). Reliable diagnostic techniques can contribute to reduced maintenance costs and, perhaps more importantly, to increased system availability. The selection and integration of an appropriate diagnostic tool has the potential to produce a reduction in life cycle costs for both the customer and the manufacturer. For autonomous systems on board fault diagnosis is vital as the human interface is no longer available to perform the function that needs to be performed in order to ensure the safe operation of the system.

Systems diagnostics has been around for many years and in many forms. It varies in complexity and viability from statistical and geometric algorithms and pattern recognition techniques to complex model based and soft computing methods, forms of analytical redundancy. However, it is growing in importance as advanced automated system diagnosis with little or no human interaction is becoming a requirement of our manmade systems. This is due to the ever increasing demand on reliability and the drive toward reduction of end user costs, coupled with the fact that the degree of automation within a system is constantly increasing. Systems today employ a variety of diagnosis methods from expensive simplicity to the more mathematically complex (cost reducing) solutions that are the aim of this continuing development in this area.

The approach commonly referred to as Fault Detection and Isolation (FDI), or in a broader sense System Health Management (SHM) has the potential to play major roles in human safety, reduction of monetary losses, and improving the rate of overall mission success capability.

As an example of the monetary losses incurred, the petrochemical industry alone incur an estimated $20 billion in losses every year due to process failure according to Venkatsubramian *et al.* (2003), and the cost is much more when other industries such as pharmaceutical, speciality chemicals, power, etc., also suffer significant losses. Similar process failures cost the British economy up to $27 billion every year. Therefore the need for diagnosis does not just include the high reliability required in air vehicles, but can be used in other areas as those mentioned and many more.

The project aims to demonstrate the development of such diagnostic methodology and to examine its performance in the detection of a real world test bed. The test bed consists of an aircraft fuel system simulation rig which simulates by hardware similarity the components of aircraft fuel system.

1.2 Industrial Context

The project was sponsored under the funding granted by EPSRC in collaboration with Loughborough University, UK and BAE Systems, System Engineering Innovation Centre (SEIC), Holywell Park, Loughborough.

The project supervisor is Dr. Roger Dixon and industrial collaboration via Dr. John Pearson with Prof. Roger Goodall as director of research.

The project was conceived to meet a real industrial need. To demonstrate that it is possible to design an FDI system for an aircraft fuel system.

1.3 Project Scope and Aims

The project aims to create a Fault Detection and Identification (FDI) tool for the detection and identification of faults on the avionic fuel system simulator rig. The fuel rig is a piece of hardware based at the BAE Systems (BAES), Systems Engineering Innovation Centre (SEIC), Holywell Park, Loughborough. The fuel rig represents the fuel system of a modern aircraft and consists of a number of pumps, pipes, valves and tanks representing those on the aircraft. The early stages of the project shall be concerned with the development and commissioning of the fuel rig. Following this it is necessary to develop various stages of model in order to eventually achieve the goal of creating the FDI tool. The sequence of development leading to this goal is detailed in the numbered list below.

1) Create nonlinear simulink system model representing the fuel rig and validate against the fuel rig.

2) Develop a linear state space models representing the main dynamics of key components of the simulink system model.

3) Use the linear state space model to create a Kalman filter based FDI to apply to the simulink system model.

4) Apply the Kalman filter based FDI to the fuel rig to correctly detect and identify fault conditions.

5) Develop improvements to the FDI scheme by using statistical residual evaluation and automatic threshold determination.

1.4 The Thesis

1.4.1 General

The work addressed in this thesis incorporates the development of the fuel rig and the path to achieving a fault detection system capable of reliably detecting faults as they occur and to classify the location of the fault so as to aid in the maintenance of said systems.

1.4.2 Thesis organization

The thesis chapters are organized as set out in the list below.

i) Chapter 2 provides a literature review identifying other important or relevant publications in a similar field.
ii) Chapter 3 describes the fuel rig and its functionality and interface.
iii) Chapter 4 covers the nonlinear simulink system model development and the validation of this model.
iv) Chapter 5 investigates the implementation of a simple Kalman filter based FDI scheme on a single tank and the effect of statistical residual evaluation upon injected leak faults.
v) Chapter 6 introduces development of the bank of Kalman filters. The Kalman filters are applied to the simulink system model in order to detect faults and correctly identify the location of the fault.
vi) Chapter 7 contains the process of applying the Kalman filter based fault detection to the fuel rig and presents and discusses the results from various faults injected into the fuel rig.
vii) Chapter 8 provides a conclusion on the overall thesis results.

Appendices

i) Appendix A contains the fuel rig electric power system cabinet schematic drawings.

1.5 List of Publications

i) Bennett P., Dixon R., Pearson J.; "*Comparing residual evaluation methods for leak detection on an aircraft fuel system test-rig*"; Systems Science Journal, Vol. 34, 2008; ISSN: 0137-1223; pp 63-74.

ii) Bennett P., Dixon R., Pearson J.; "*Comparing residual evaluation methods for leak detection on an aircraft fuel system test-rig*"; Proceedings of the 16th International Conference on Systems Science, Wroclaw, Poland, 4-6 September 2007.

iii) Bennett, P.J., Pearson, J.T., Martin, A., Dixon, R.; "*Application of diagnostic techniques to an experimental aircraft fuel rig*"; Proc. Of 6th IFAC Symposium on Fault Detection, Supervision and Safety of Technical Processes 2006. Beijing, China, Sept. 2006.

iv) Bennett P., Dixon R., Pearson J.; "*Dynamic model development and validation for an aircraft fuel test-rig"*; Proc of 6th UKACC International Control Conference, Glasgow, UK, Aug 2006.

v) Future submission - Bennett P., Dixon R., Pearson J.; "*Application of a bank of Kalman filters to an aircraft fuel system test-rig*"; UKACC Internation Conference on Control 2010, Coventry, UK, 7-10 September 2010.

1.6 Thesis Contributions

The thesis contributions cover a number of areas are as listed in the list below.

i) The contribution of Chapter 2, *literature survey*, is the identification of publications presenting current methodology concerned with the development of diagnostic systems or similar related material to aid the development of the fault detection and identification scheme.

ii) The contribution claimed in Chapter 3, *Fuel Rig Plant Description*, is to provide a full functioning fuel rig that can be used for the validation and evaluation of methods and algorithms for fault detection and health monitoring.

iii) The contribution of Chapter 4, *Fuel Rig Modelling and Validation*, is to create and document the development and validation of a simulink model based upon the fuel rig to be used in the production of a Kalman filter based Fault Diagnostic and Identification (FDI) development.

iv) The contribution claimed in Chapter 5, *Application of Fault Diagnosis to a Single Tank,* are application of fault detection to a real tank successfully detecting a leak and the evaluation of different methods utilised in detection of a fault to determine which offers greatest sensitivity whilst remaining robust to false alarms.

v) The contribution of Chapter 6, *Design and Evaluation of Fault Diagnosis and Identification for the System Simulation Model*, is the development of the fault detection and identification system and its correct operation in identifying faults correctly when applied to the simulink system model representing the fuel rig. This validates the design prior to applying it to the real system.

vi) The contribution claimed in Chapter 7, *Application of Fault Diagnosis and Identification to the UAV Fuel Rig*, is the application and successful demonstration of the Fault Detection and Identification scheme to the real life system in order to detect and identify faults reliably.

The overall contribution of the thesis is the development of a Fault Detection and Identification (FDI) tool to detect faults on a test rig emulating the operation of aircraft fuel system. It utilizes a Kalman filter to detect the faults and statistical evaluation of the resultant signal to attain increased performance. The thesis presents results applied to the physical test rig and also lays out the design approach.

Chapter 2

Literature Survey

The overall aim of the project is the development and application of fault diagnosis and identification. It is necessary in the early stage of a project to identify alternative methods similar to the intended path to justify the direction of the research in order to confirm suitability of the intended method.

This chapter aims to provide an insight into current research trends and a summary of current methodology and technology. The literature survey will be broad in the sense that it will analyse a wide range of diagnostic techniques to encompass varying methodology within the field, rather than provide an in depth review of a single specific method.

The contribution of this chapter is the identification of publications presenting current methodology concerned with the development of diagnostic systems or similar related material to aid the development of the fault detection and identification scheme.

There has been considerable interest in the practical application of these fault diagnostic techniques and some of the prominent authors include Leonhardt and Ayoubi, 1997; Rengaswamy et al, 2001; Frank et al, 2000; Venkatsubramanium et al, 2003. Review of these and other publications are included in this chapter.

2.1 Overview of Technology

The structure of health management can be subdivided into main tasks of fault detection by analytic and heuristic symptom generation, and fault diagnosis as illustrated in Figure 1, Isermann, (1997).

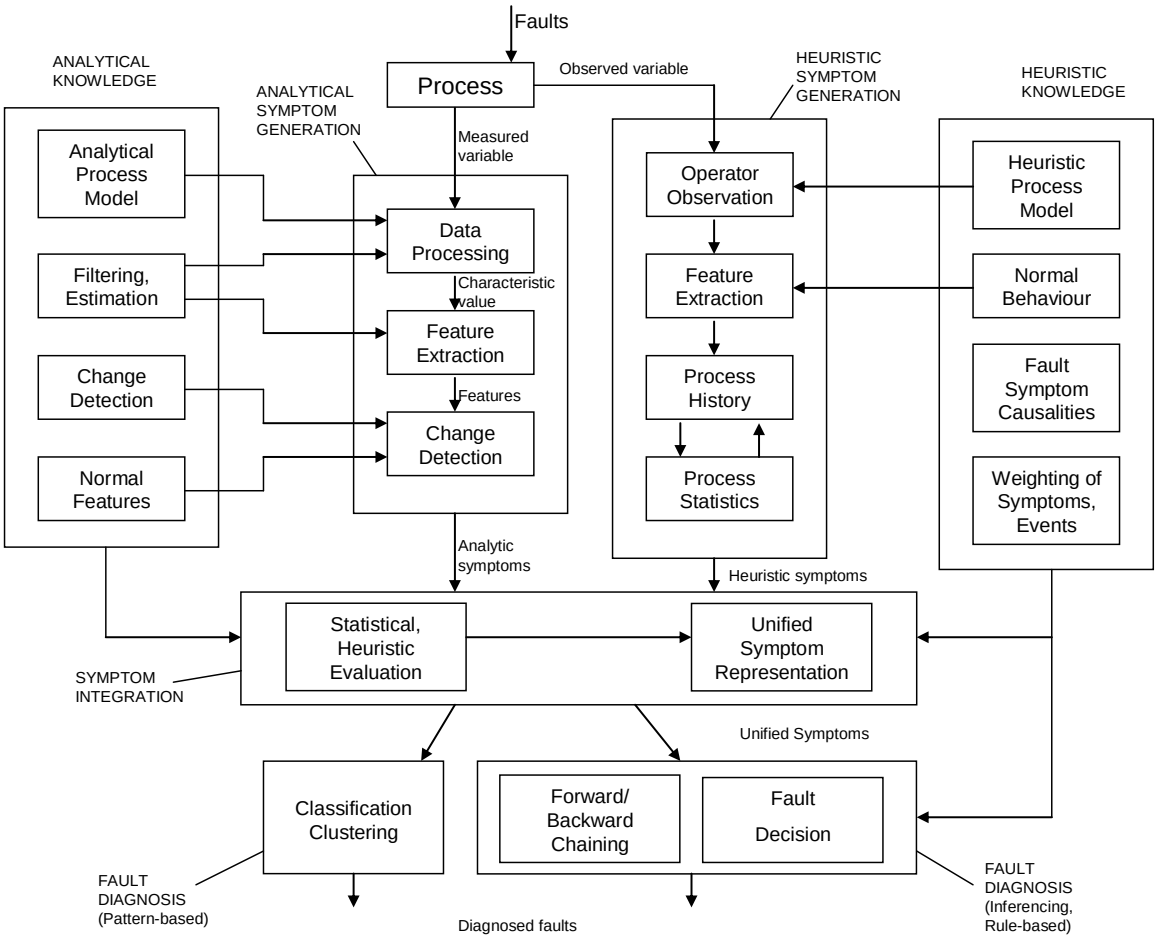

Figure 1: Health Management Methods Hierarchy

Figure 2 shows a tree structure depicting the areas that the diagnostic disciplines are generalised into. They are Quantitative, Qualitative, and process history based. This project aimed to mainly look into and develop the quantitative methods. A further breakdown of the hierarchy of the diagnostic methods shows that this subsection consists of Kalman filters, observers and parity space methodologies.

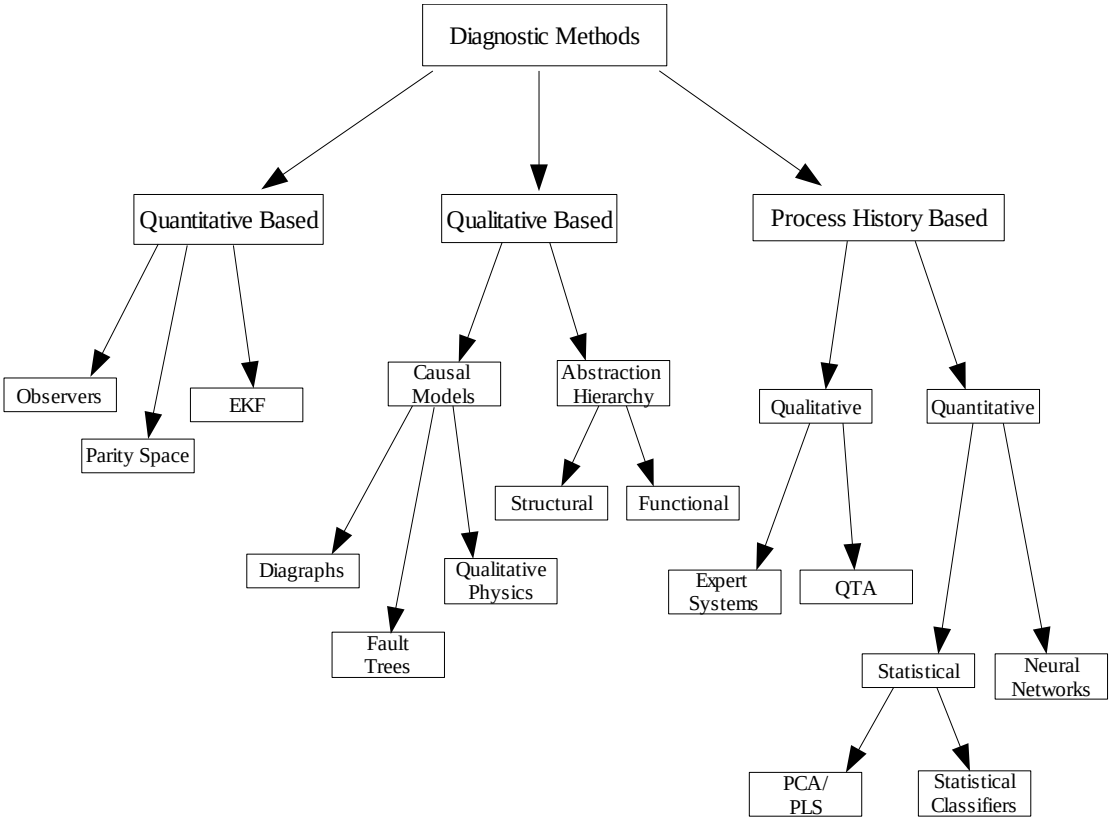

Figure 2: Diagnostic Methods Hierarchy

2.2 Existing Industrial Practice

2.2.1 Hardware Redundancy

In a hardware redundant based diagnosis system the physical hardware is duplicated and any discrepancy leading to diagnosis of a failure causes the failure free hardware to take control. Hardware redundancy can be used at system, sub-system or component level. Some Avionic Full Authority Digital Engine Control (FADEC) systems use a system level redundancy and voting based software decision as to determine the health of each system resulting in the healthier FADEC taking control of the engine. This scheme offers high reliability yet is subject to high system cost. Advances in redundancy schemes use highly redundant systems such as the highly redundant actuator developed by Du *et al.* (2007) and further work carried on by Davies *et al.* (2008) which extends the physical hardware of an actuation system to include series and parallel redundancy to provide a highly reliable system.

2.2.2 Signal Processing

Signal processing based fault diagnosis involves the identification of a fault achieved by suitable signal processing by monitoring symptoms such as time domain functions like magnitudes, arithmetic or quadratic mean values, limit values, trends, statistical moments of the amplitude distribution or envelope, or frequency domain functions like spectral power densities, frequency spectral lines, spectrum, etc. This is discussed by Frank *et al.* (2001). A method for condition based maintenance using signal processing techniques for gearbox tooth failure is discussed by Lin *et al.* (2004).

2.3 Current Diagnostic Research

This section identifies current publications for work involving diagnostics within the areas of model based diagnostics, fuzzy logic, neural networks, hybrid neuro-fuzzy and some others.

2.3.1 Model Based Diagnostics

Model based diagnostics uses a model of the system as a comparative measure of the system under diagnosis. Model-based diagnosis relies on the ability to produce an exact model of the system without influence from unknown external disturbances and because of this is not suitable in all industrial processes. Therefore it is not available to all industries as some, such as the chemical process industry, may suffer the inability of its use due to too many external disturbances and difficult to model process dynamics. Whereas, modelling of a mechanical or electrical system is in most cases possible and is especially viable when modelling is used in the design process due to the availability of the model.

The difference between the output(s) of model and the real world system (often called the residual) is used to evaluate the condition of the real world system as summarized in Figure 3. This method, known as parity equations, is subject to errors due to disturbances, noise and modelling errors; however, methods are available to reduce the effects of these on the diagnostic process and these will be discussed later. An overview of model based fault detection is provided in detail by Isserman (2004), Rengaswamy *et al*. (2001), Frank *et al*. (2000) and Venkatsubramanium *et al*. (2003). The flexibility of a model-based system is limited as it is designed for an individual system and may require more adaptability in some situations; for example, following overhaul of an aircraft if any of the modelled parameters or operating conditions change.

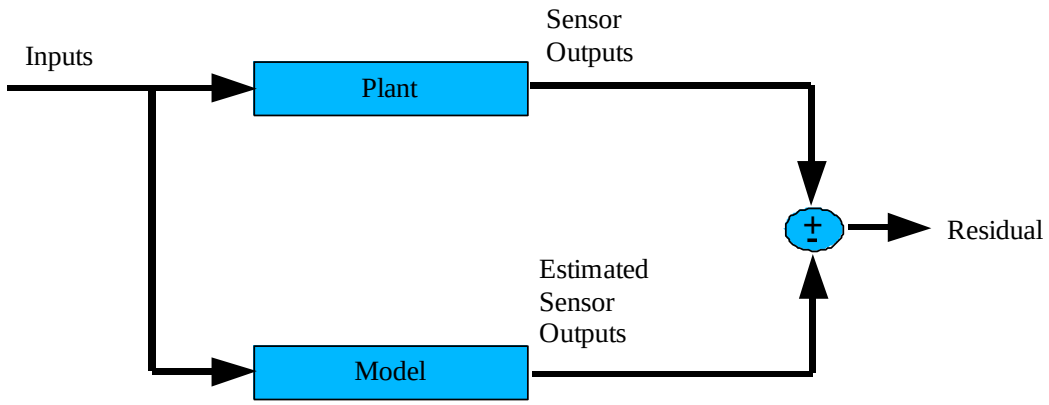

Figure 3: Summarised Diagram for a Model Based Diagnostic Scheme.

When the system is operating exactly as modelled then the residual is equal to zero and any significant deviation from this will be due to a fault in the system. However, in practice, this will not be the case due to the previously mentioned disturbances and modelling errors are cumulative over time. The cumulative effect of modelling errors can lead to a large divergence between model and plant over time.

Numerous publications on model-based diagnostics have been produced, each employing slightly different methods for a variety of end user purposes. One such method by Rengaswamy *et al.* (2001) employs the use of the diagnostic model processor (DMP) and uses a priori knowledge in terms of first principles-based model equations. The process model is represented as a set of model equations in residuals form. When a fault is present the residual will tend toward 1 or –1 due to an applied non-linear transformation, giving a magnitude and direction to the fault. To account for modelling errors and noise, each equation is given an associated pair of tolerance limits giving a range around zero for which the equation is satisfied. The tolerance limits can be symmetric or asymmetric, since the residual is not uniform in magnitude.

An interesting paper on model-based process failure identification is that of Frank *et al.* (2001). It covers the subject of model-based diagnostics thoroughly and weighs the

benefits and associated problems of modelling as a fault diagnostic tool. The paper discusses in detail the methods and issues regarding model-based diagnostics including the residual generation and several variants of failure identifier already developed. This paper covers residual generation and the mathematics involved for linear and nonlinear processes. The author describes the methods of linearisation via state feedback (LSF), theory of nonlinear system stabilization (NSS) and an FDI scheme based on the integration of LSF and NSS. One of the problems associated with model-based diagnostics is filtering of model errors, disturbances and other variants in the residuals to distinguish between faults and signals of no interest. This problem is discussed by Frank *et al.* (2001), who give a description for fault detection filter, diagnostic observer and parity space approach methods.

A paper by Wang (2003) described a successful implementation of a model-based diagnostic system using a generalized state-space model. The paper highlights the issue of the inefficiency of a purely model-based diagnostic tool. The implementation therefore included neural net classification to improve the diagnostic performance. The paper gives details of implementation of a purely neural net-based diagnostic system having the ability to diagnose 140 fault patterns correctly whereas a generalized state-space model-based system using neural net classification will diagnose 170 faults on the same test case.

2.3.1.1 Observers

FDIA, (Fault Detection, Identification and Accommodation), by Dixon (2004), uses a model based diagnostic tool to identify failure of a DC motor and gearbox driven actuator based test bed. A residual is created based on a comparison of the system and the model. Kalman filtering is then applied to reduce the effect of system disturbances. In addition to this, the developed system can accommodate a failure ensuring the system can continue to operate as efficiently as possible. Each observer in the observer bank can generate estimates of all three sensor outputs on the test bed allowing reasonable system operation to continue in the case of multi modal failure.

In the case of two out of three sensor faults the system can generate estimated readings of the faulty sensors by approximation based on the reading on the one working sensor. Failure modes of drift, noise and open circuit sensor outputs in two of three sensors are discussed.

A survey paper, by Isermann (1984), presents a study on estimation methods for fault detection. The fault detection is examined using the test case of a pump and an associated pipeline using a Kalman filter and discusses the tuning of the feedback matrix, the application of further processing of the residual signal. Also, the determination of threshold levels and estimation of the position of a leak in a pipe is presented using cross-correlation methodology. The author demonstrates the development of the process model of motor, pump and pipework and produces the linear state space model of the system and extends this to a fault detection system. Practical results are given for the application of the fault detection to an industrial pipeline spanning many kilometres with two 400kW pumps delivering a maximum of $330m^3/h$ at an initial pressure of 69 bar, the pressure at the other end of the pipe was dispensed with as it was constantly approximately atmospheric. Thus only the volume into and out of the pipe and the initial pressure were used to detect leaks in the pipe. A leak was induced at a distance of 3.8km at a leakage rate of 0.19% (0.2l/s) and the trigger level of the fault detection was exceeded at 98 seconds. The position of the leak was estimated with a precision of ±0.7% (±500m) at a time of 90 seconds after the alarm.

Luemberger observers and Kalman filters and Beard fault detection filter are a few of the many types of observer, also known as state estimators, and can be used as a residual generation function for detection and isolation of faults. They have the advantages of systematic design procedure, defined noise handling, they can be extended to non-linear systems and a very sensitive reaction to instrument faults can be achieved as discussed by Betta and Pietrosano (2000).

The Beard Fault detection filter, a special class of full order observer, has a specially designed feedback matrix which can make the output estimation of error have

unidirectional characteristics associated with some fault directions and offer further robustness over some other types of observer as shown in Chen and Patton (1999).

Further papers of interest covering model-based diagnosis include one by Ding *et al*. (2004), which investigates model based vehicle braking systems sensor faults.

2.3.1.2 Artificial Neural Networks

Artificial Neural Networks are networks of simple processing nodes loosely based on the structures of the human biological nervous system. The processing nodes are usually based on the Mc-Culloch-Pitts Neuron, as shown in Figure 4.

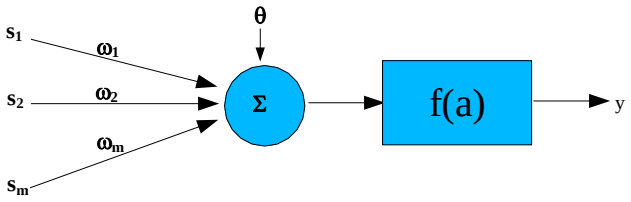

Figure 4: Mc-Culloch-Pitts Neuron

The process consists of calculation of the scalar product of an input vector, "s", and a synaptic weight vector, "ω", plus an offset, "θ", as shown in Equation 1.

$$a = \sum_{j=1}^{m} w_j . s_j + \theta \qquad \textbf{(1)}$$

Therefore, the activation status, "a", is mapped to the output via a non-linear activation function, "f_{akt}". The case of a sigmoidal function is shown in Equation 2.

$$f_{sig}.(a) = \frac{1}{1+e^{-a}} \qquad \textbf{(2)}$$

Within network architectures the best known is the multi-layer preceptron (MLP). An MLP consists of several layers, each of which has a certain number of processing nodes. The case of a three layer MLP is shown in Figure 5.

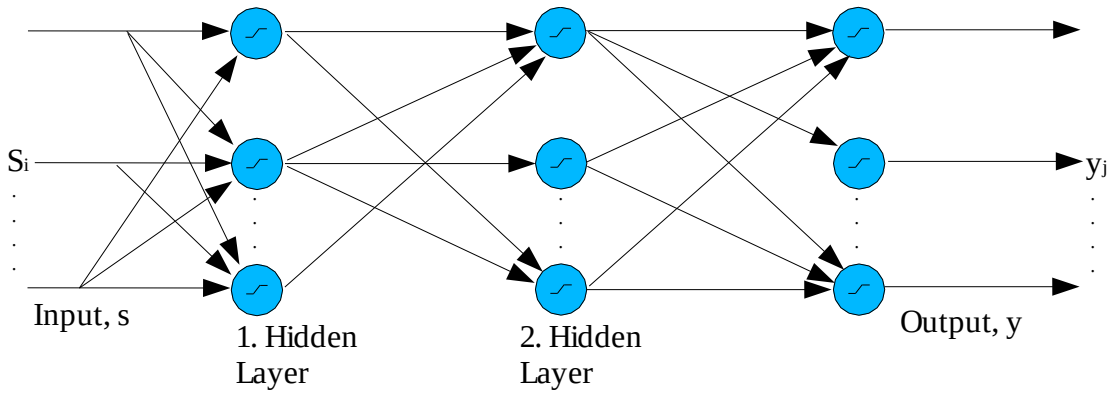

Figure 5: Three Layer MLP

All neural networks need to be trained and the most common method for this being back-propagation, although this method is sensitive and slow as described by Leonhardt and Ayoubi (1997). There has been much research into reducing the

training time of neural networks, however, this still remains a disadvantage of this method as large amounts of fault free operating data is required.

Figure 6 illustrates the training process of neural networks.

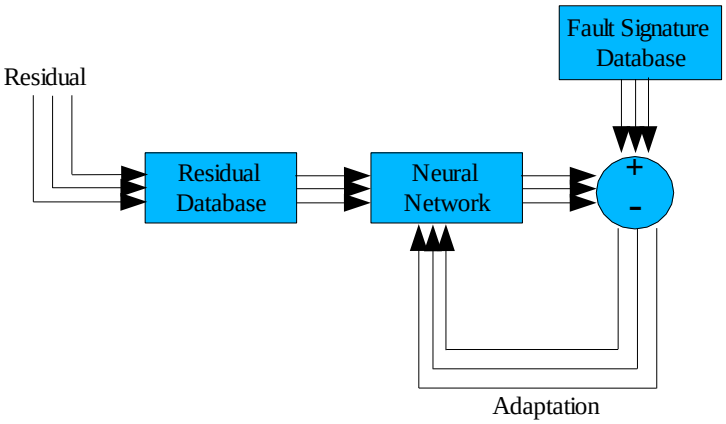

Figure 6: Neural Network Training.

Figure 7 illustrates the use of a purely neural network based diagnostic scheme used for the purpose of residual generation and offers the same function as seen in model based diagnostics. It is worth noting that neural networks can be used for both residual generation and for classification of a model based residual.

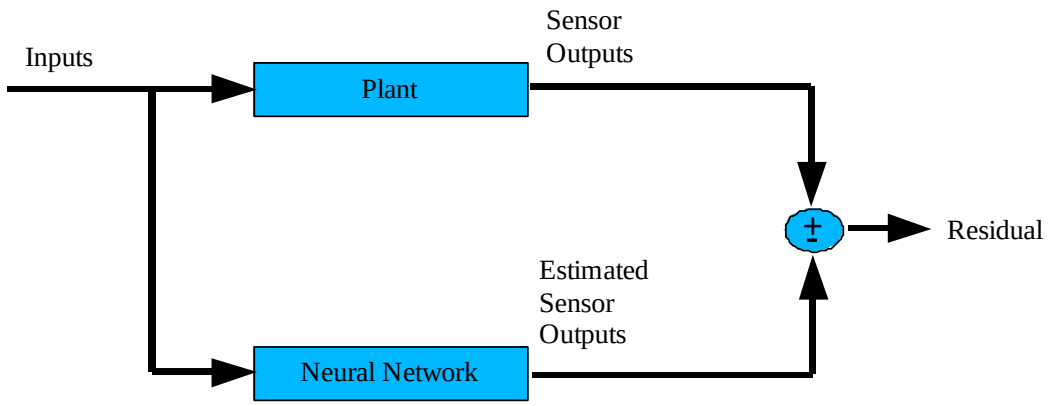

Figure 7: Neural Network Residual Generation.

Fault detection and diagnosis using neural networks is achieved by exploiting their non-linear pattern classification properties. There are certain requirements a neural networks classifier has to meet for successful fault diagnosis. When measurements patterns are presented, the classifier should be able to distinguish and classify the result into one of the following three categories.

Normal behaviour: From a definition of normal system behaviour, through the training patterns observed, the neural network should be able to determine no fault is present and should not be affected by noise.

Abnormal and known fault: If the observation pattern falls into the region of a recognised training pattern for a known fault should be announced while simultaneously announcing that other faults have not occurred.

Abnormal and unknown fault: When the observation pattern falls far from the training patterns the classifier should announce that abnormal behaviour has occurred and that the fault is of unknown class.

Thus based on sensor measurements the neural network should be able to determine fault condition and corresponding failure mode or determine fault condition with unknown failure mode.

The diagnostic ability of a neural network depends on the arbitration of the network to classify a fault condition to the corresponding training region. However, since in the real world systems are subject to natural differences from the ideal, there has to be identification of a boundary that reflects the correct region in which the network identifies a fault. Ellipsoidal Neural Networks (ENN) claims to overcome these classification boundary problems and is discussed by Rengaswamy *et al.* (2001).

The successful implementation of a model-based diagnostic system coupled with a neural net-based classifier as discussed by Wang and Lui (2003) resulted in good

evidence of the improvement in performance a neural net-based classifier can have over a qualitative model based diagnostic tool.

Further papers covering artificial neural networks include Kong *et al.*, (2004) and Joly *et al.*, (2003) who both demonstrate the application of a neural network based fault detection scheme applied to a gas turbine engine.

Further detailed explanation of artificial neural networks can be found in survey papers by Frank *et al.* (2001) and by Leonhardt and Ayoubi (1997).

2.3.2 Fuzzy Logic

Fuzzy logic is an extension of a classical expert system approach which follows rule based reasoning such as IF – THEN – ELSE. For the case of classical expert system and its binary logical systems, they do not offer the required gradual nature of a real world diagnostic problem. The problem of diagnostic reasoning using value information was solved by Zadah (1973), who introduced the concept of fuzzy logic. With classical expert systems the concept of fault identification followed rules such as:

IF s1 AND s2 OR s3 NOT s4 THEN F1 = TRUE

Whereas fuzzy logic follows rules such as:

IF s1=LARGE AND s2=LARGE OR s3=LARGE AND s4=SMALL THEN F1=LARGE=TRUE

A fuzzy logic system consists of three parts, namely, fuzzification, inference and de-fuzzification.

Fuzzification of a crisp value/ signal involves the evaluation according to its degree of membership to a certain membership function. This gives the signal a “weight” and is usually expressed within the limits 0…1 and is based on heuristic knowledge,

statistical distribution functions, subjective knowledge or by learning with the aid of ANN's. Inference is the application of the rule based decision making process, and is applied to the symptom membership function and not the symptom itself. De-fuzzification is the process of obtaining a crisp output from the resultant, making a decision based on the "weight" of the defuzzified result as to whether it constitutes a fault as discussed by Leonhardt and Ayoubi (1997).

A method for diagnosing wear and fatigue is presented in a two-part publication by Du and Yeung (2004), which describes a novel method of diagnosis. Fuzzy transition probability combines transition probability (markov process) with fuzzy logic. This method uses available information from the training samples to the maximum extent, finding both the transition probability and the fuzzy membership, and is claimed by the author to outperform artificial neural networks based on the test results.

Further papers on fuzzy logic include Frank *et al*., (2000) which provides a review of fuzzy logic in fault diagnosis employing a fuzzy qualitative observer and a fuzzy relational observer.

2.3.3 Hybrid Neuro-Fuzzy

Neuro-fuzzy fault diagnosis is a hybrid method employing the gradual nature of fuzzy logic for dealing with inaccuracy and approximate reasoning while artificial neural networks provide tools for approximate reasoning and adaptation. Another step further to this could make use of systematic stochastic search and optimisation properties of genetic algorithms.

A neuro-fuzzy based hybrid system comes in a variety of forms each biased in a slightly different direction. A publication by Leonhardt and Ayoubi (1997) gives a brief overview of varying neuro-fuzzy systems. The different forms discussed include neural networks influenced by fuzzy logic, fuzzy models within neural networks, fuzzy based adaptation of neural networks, fuzzy systems influenced by neural networks, neural network based adaptation of fuzzy systems and hybrid fuzzy-neuro

systems. The author concludes that none of the presented methods offer "completeness", and in practical applications unexpected symptom combinations may still cause problems if they are not covered by a rule or data set.

Further papers on neuro-fuzzy hybrid architecture include Garcia *et al.* (1997) who uses neuro-fuzzy classification to identify faults following fault detection from an observer based FDI scheme and Kuo (1995) who looks at the use of neural networks and fuzzy logic in the identification of faults on turbine blades.

2.3.4 Pattern Recognition Using Geometric and Statistical Classification

A method using pattern recognition techniques by Aretakis (2003), claims possible 100% success in the identification of examined sensor faults. It is based on the principle that, if a measurement set is fed to an adaptive performance algorithm, a set of component performance modification factors (fault parameters) is produced. Faults, which may be present in the measurement set, may be recognised by the patterns they produce on the modification parameters. In this study, three kinds of pattern recognition techniques with increasing complexity are used in order to correctly identify the examined sensor faults on the test case of a gas turbine engine model. The three types of pattern recognition used are geometric, statistical, and statistical using optimal directions.

2.3.5 Current Signature Analysis & Wavelet Packet Transform

An alternative method, current signature analysis using wavelet packet decomposition, as discussed by Eren and Devaney (2004) monitors the stator current of a motor. When bearings in a motor deteriorate, a most common fault, this then causes vibration in the motor and resulting in a modulation of the stator current. The stator current is then notch filtered to eliminate power harmonics and observed using a wavelet transform, an alternative to short time Fourier transform in nonstationary signal processing, achieving a finer resolution.

2.3.6 Vibration Analysis

The analysis of vibration at strategic points in the monitoring of a mechanical component can identify faults or even incipient faults. Its usage is associated with gear and bearing surface defects causing an increase or inconsistency in the analysed vibration signature. Gearbox defects are presented via vibration analysis in a paper by Lin *et al.* (2004), and the diagnosis of vacuum cleaner motors by Tinta *et al.* (2005).

2.3.7 Sensor Validation

A note must be made on the importance of robust sensor readings, as a diagnostic system with uncertain sensor readings does not offer consistency. This is not to say that all indifferences can be eradicated but the diagnostic system must be able to discriminate a faulty sensor with a system fault. Papers discussing sensor validation include Wang and Wang (2002) and Alag *et al.* (2001).

2.3.8 Data/ Information Fusion

With methods such as neural network architectures relying heavily on historical data in their training, there becomes a requirement to analyse all available data/ information to aid increased knowledge within the diagnostic system by means of fusing the data to form a "best informed" result. If a diagnostic system, whether neural network or other, can make use of historical data, heuristic information, sensor readings, etc., then the diagnostic system can make a better informed decision than if the data/ information was not available. Three types of fusion architecture are currently used, centralised, autonomous, and hybrid fusion. Descriptions of each of the architectures and their usage is discussed by Schroer (2002), Alag *et al.* (2001) and Goebel (2000).

2.4 Prognostics

With diagnostics an error is either present or not, binary in format, but with prognostics the ability must be present to determine a trend toward an incipient failure. If this is taken further to recognise a trend toward a fault condition and the rate of change toward the fault condition and the limit at which a fault is diagnosed is known then the Prognostic Health Management (PHM) System is capable of estimating the remaining useful life of the component and its impact on the system, therefore offering failure precursor detection or reconfiguration options.

Prognostic Enhancements to Diagnostic Systems for Improved Condition-Based Maintenance by Byington *et al.* (2002) discusses the different methods used in prognosis at component/ sub system level and also the incorporation of the prognostic techniques into an overall prognostic system. It provides examples of some prognostic modules including gas turbine fuel nozzle, gas turbine compressor wash and gearbox prognostics.

2.4.1 Model Based

Model based prognostics, as with model based diagnostics, offers a method for comparative analysis between a mathematical model of the system and the system itself. The difference between the model and real world system being the residual and defines the behaviour of the real world system.

There has been little research into the development of model based prognostics, however one publication by Luo *et al.* (2003) gives an overview of the design process for an automotive ECU (Electronic Control Unit) and provides a full mathematical example of the process used for implementation of model based prognostics for a half car suspension system.

Predictive maintenance of pumps discussed by Higham and Perovic (2001) is a model based prognostic development using the signal analysis of pressure and differential pressure (flow) measurements. It develops and discusses techniques in signal analysis using practical experiment subjected upon a centrifugal pump, and is carried out on pumps with blockages and with damaged impellors

Watchdog Agent – An infotronics based prognostics approach for product performance degradation assessment and prediction by Djurdjanovic *et al.* (2003) discusses a tool, the watchdog agent, for multi-sensor assessment and prediction of machine/ process performance. This is a tool that can be utilised to predict Condition Based Maintenance (CBM) as well as identification of components with significant remaining useful life.

2.4.2 Artificial Neural Netorks

Wavelet based methods for the prognosis of mechanical and electrical failures in electric motors is discussed by Zanardelli *et al.* (2005) and looks at three wavelet based methods for prognosis of incipient faults with dc motors. Wavelet and filter bank theory, nearest neighbour rule and linear discriminant functions are reviewed. An experimental set-up for a wiper blade and a fuel pump is used and results from testing presented in this paper.

The use of neuro-fuzzy (NF) systems for the prognosis of machine health condition is discussed by Wang *et al.* (2004) and compares neuro–fuzzy prognostics against recurrent neural networks (RNNs) for the application of machine health condition. Through this comparison, the paper highlights that, if properly trained, an NF system performs better than an RNN system. The investigation within this paper evaluates the comparison using three test cases, namely, a worn gear, a cracked gear and a chipped gear as well as using data sets from previous studies corresponding to gear pitting damage and shaft misalignment.

A paper by Zhang *et al.* (2002) introduces an integrated diagnostic/ prognostic architecture that builds upon means to identify the systems operating mode and usage pattern using concepts from hybrid system theory and petri networks as decision support tools. These are mechanisms to extract an optimum feature vector based on data mining and diagnostic/ prognostic algorithms that are designed to employ fuzzy logic expert system estimation of the remaining useful lifetime of a failing component.

Long term prediction of remaining life entails a large uncertainty therefore a prognosis system must incorporate the measurement and management of uncertainty. Confidence metrics and uncertainty management within prognostics are discussed by Barlas *et al.* (2002) and provide a method for the calculation of confidence given for a prediction such as the amount of useful life remaining in a component. The paper discusses a data driven Confidence Prediction Neural Network (CPNN) that estimates the uncertainty bounds by predicting the possible future values as more information becomes available. Also, a variation of the CPNN architecture is introduced in the paper that accommodates a learning scheme intended to reduce the uncertainty bounds as more information becomes available.

An excellent overview of the use of dynamic wavelet neural networks (DWNNs) for single component prognostics is provided in a paper by Wang and Vachtsevanos (2001). The paper describes the use of a Wavelet Neural network (WNNs) in the use as a virtual sensor where real data is not available and the use of a DWNN as a predictor for use in determining the remaining life of the system. The paper also covers uncertainty management and performance assessment. The paper also provides an illustrative example using a test case of vibration measurement of a bearing.

2.5 Conclusion

This chapter has given a brief overview of literature identified which encompasses the field of diagnostics and prognostics. The amount of material published in the field of diagnostics is vast and all of it could not be included, however, the more relevant publications were included within this review.

The chapter has introduced model based diagnostics and identified its limitations in its simplest form, i.e. parity equations. However with feedback applied in the form of model based observers further performance is achieved. Many papers discuss the use of and associated problems of discriminating fault and non-fault condition behaviour. Fault accommodation is also achieved by some authors.

Neural networks, fuzzy logic and various incarnations of the two are included to give a view of possible other diagnostic methodology and attempt to compare performance claims between the methods. Authors of one publication mentioned in this section claim 100% successful detection of sensor faults utilising pattern recognition techniques, however, does not examine the detection of actuator or plant faults. Application of neural networks and fuzzy logic to the formulation of FDI schemes is common and presented with great success as are observer based fault detection schemes.

An overview of literature for prognostic systems is also included as this is a closely related field and is a possible path for further extension of the project.

The approach to be used is that of a Kalman filter based FDI methodology to detect any system, actuator or sensor fault on an aircraft fuel system test rig. This method leads itself to a structured approach, is comparatively simple therefore easily understood by engineers at large.

Chapter 3

Fuel Rig Plant Description

The rig on which this research project has focused is an aircraft fuel simulation rig which, during the initial stage of the project, was required to be installed, refurbished and commissioned at the BAE site at which it is based. The rig was installed at BAE Systems SEIC (Systems Engineering Innovation Centre) at Loughborough.

The author's contribution in the early part of the project was to aid in the refurbishing and commissioning of the fuel rig. Refurbishment was to include expansion to the sensing ability of the rig and redevelop hardware and to implement a fully functioning control software interface to control the interoperability and measurement capabilities. The direct involvement of the author was to redesign and commission a new power supply cabinet with the added function of fault injection in the separate phases of the supply and to individual motors and the measurement instrumentation. This has now placed the rig in a state where it can used for the authors own research (described in the following chapters) and for other research at the SEIC. Examples of other research carried out on the rig include the use of digraphs by Kelly and Bartlett (2007) and digraphs and fault tree analysis by Bartlett et al. (2008).

Hence the contribution claimed in this chapter is to provide a full functioning fuel rig that can be used for the validation and evaluation of methods and algorithms for fault detection and health monitoring.

3.1 Plant Description

The target system for the research described in this thesis is an aircraft fuel system simulator rig. This section provides the background to the fuel rig including its functional capability, the control and monitoring interface and associated electrical systems. The fuel rig is located at the Systems Engineering Innovation Centre (BAE Systems) Prognostic Health Management (PHM) laboratory. The rig can be physically reconfigured to represent fuel systems from a number of different aircraft. The configurations considered in this study are representative of a fuel system on a an unmanned air vehicle (UAV). A photograph of the fuel rig can be seen in Figure 8 below, the electrical cabinet in Figure 9 and the control and monitoring computers in Figure 10.

Figure 8: Photograph of fuel rig at SEIC.

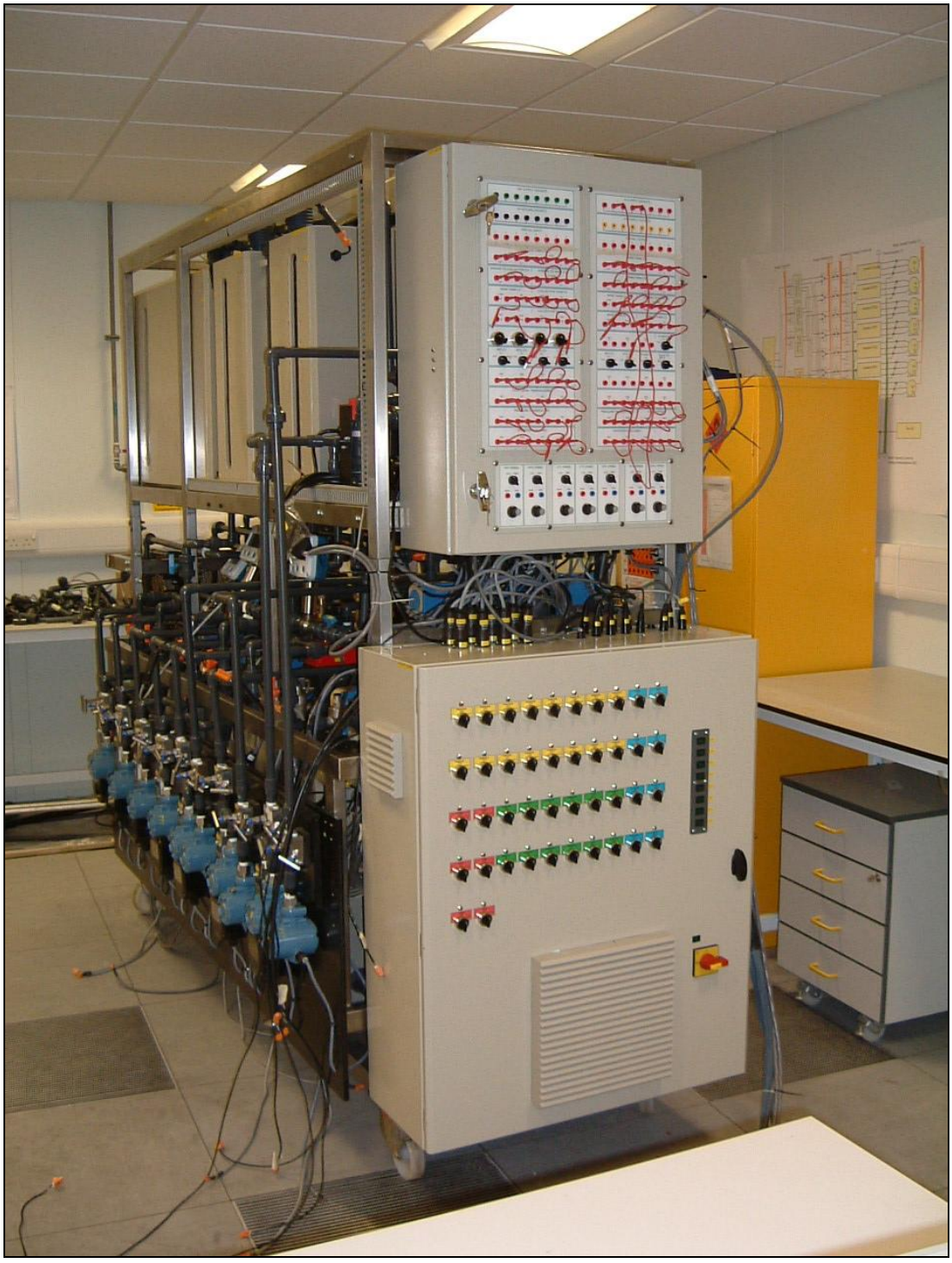

Figure 9: Photograph of fuel rig showing electrical interface.

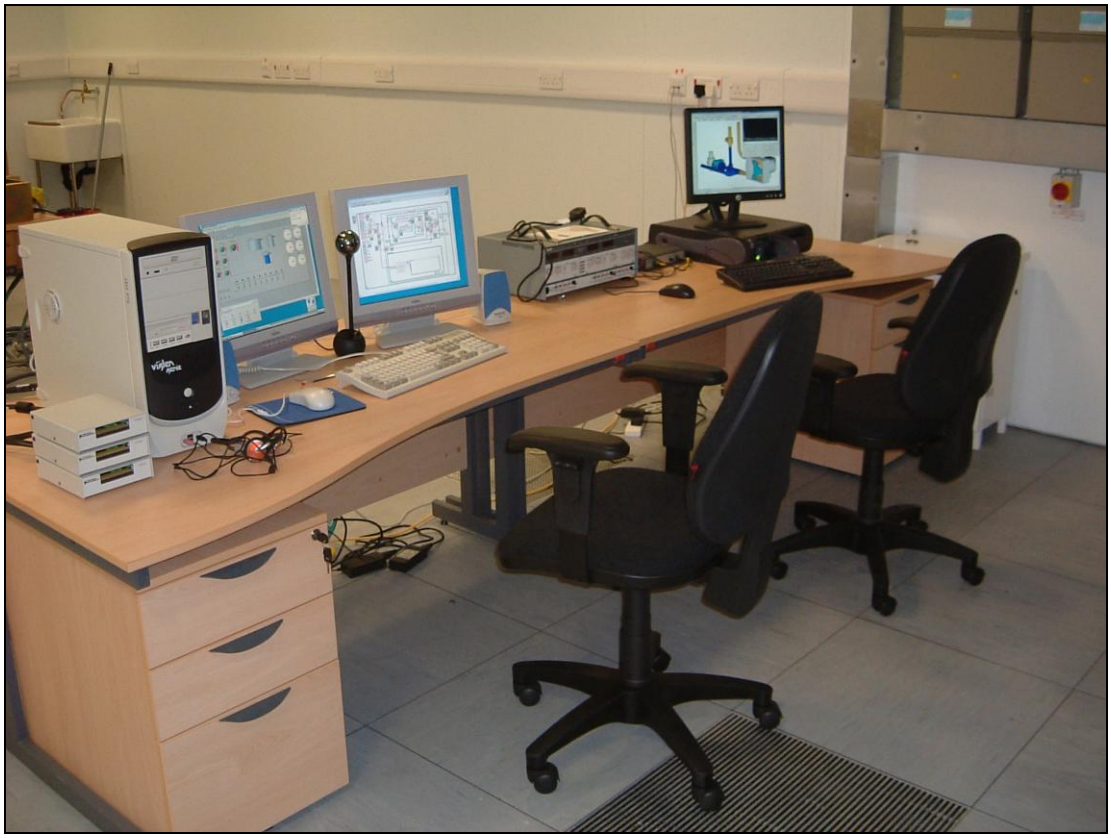

Figure 10: Photograph of fuel rig control and monitoring system.

3.2 Fuel Rig Functional Description

The fuel rig simulates, by hardware similarity, the fuel supply of an aircraft. The rig has a number of tanks representing the storage of fuel, a series of pumps representing the supply of fuel to the engine and interconnecting tanks – the process flow being dependant upon the position of various valves within the system. One of the tanks has a dividing wall in the centre which can be effectively removed by opening an interconnecting valve allowing the option to run the rig with either three or four physical tanks. This allows simulation of fuel systems representative of different aircraft. A further tank is situated at the bottom of the rig and simulates the engines (i.e. receiving spent fuel). The rig also includes various process equipment, i.e. actuators and sensors, involved in control and monitoring the flow of fluid throughout the system which is described in more detail in later sections.

This study is based upon the structure of an unmanned air vehicle (UAV). In UAV configuration one pump normally supplies one engine, i.e. the left pump supplies the left engine and the right pump supplies the right engine, however it has the ability to cross feed tanks by means of switching a 3-way valve so that for instance, a left tank can supply a right engine. In addition to this the UAV fuel simulation configuration can transfer fuel between left wing and right wing tanks. It also has a left and right auxiliary tank to act as further redundancy in the case of failure. The top level UAV configuration is depicted in Figure 11.

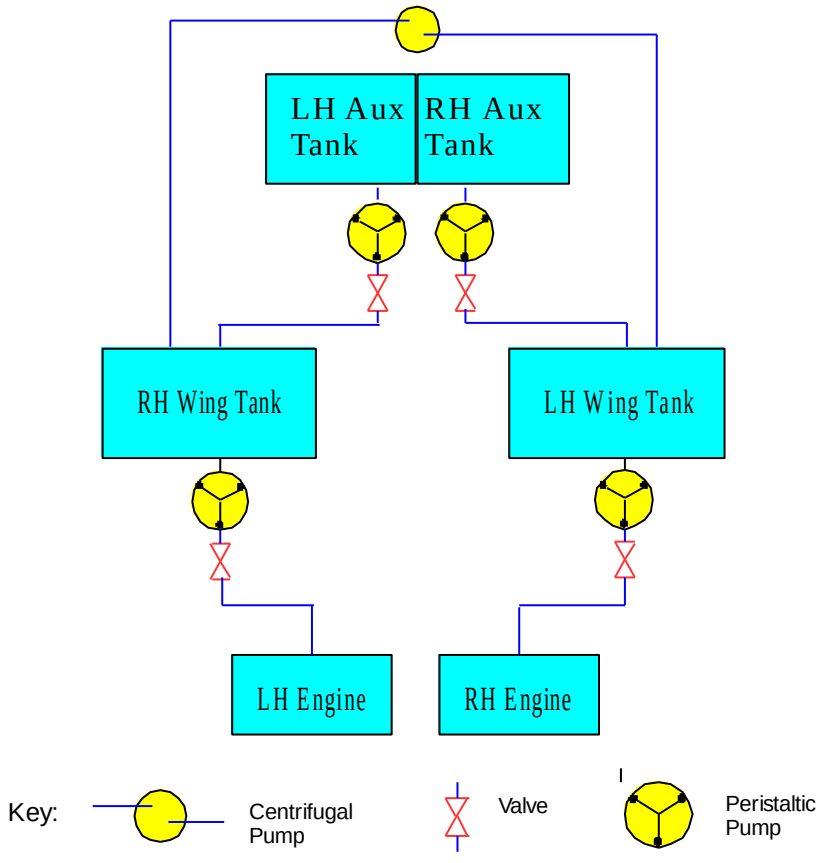

Figure 11: Top Level Diagram of Overall UAV Fuel Rig Functionality

A more complex diagram of the fuel rig in UAV configuration is shown in Figure 12 below. In this diagram the three level sensors of the baffled right and left wing tanks

can be seen. The three way valves can also be seen whereby changing the position of the valve will reconfigure the flow path of the system. The rig is also fitted with an array of valves offering pressure relief, unidirectional flow, isolation, control and reconfiguration. The main pumps are peristaltic pumps driven by a reduction gearbox and all motors controlled by 0-5V DC signal to a corresponding inverter. The transfer pump is centrifugal. All pipe work is 15NB (15mm) PVC rated at 15 bar. Pressure relief valves are set at 7 psi (0.48 bar/ 48263 Pa). Fault injection is achieved by manipulation of control and sensor variables to physically inject a fault condition whether it is a process, actuator or sensor fault.

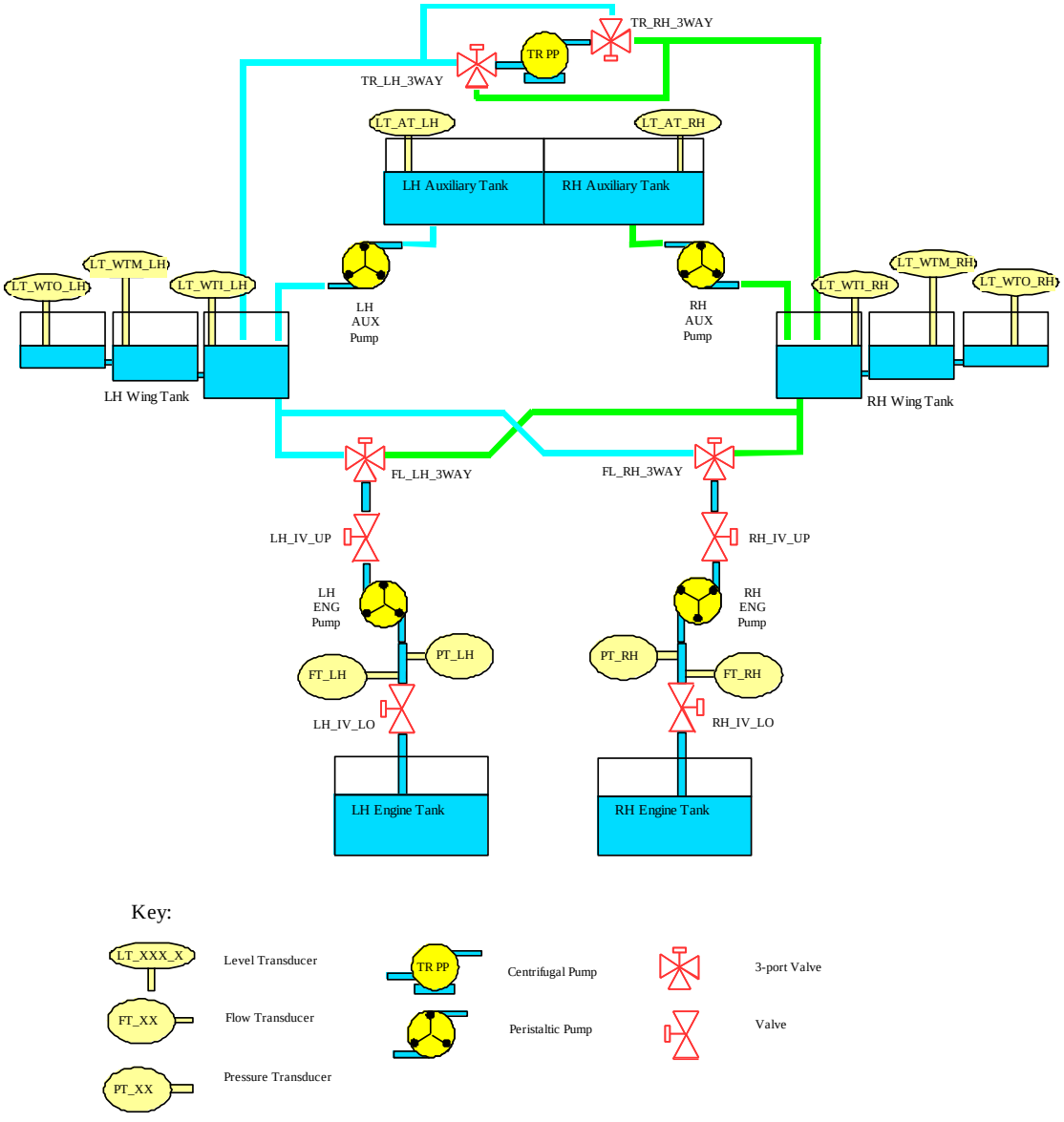

Figure 12: Diagram of UAV Fuel Rig Configuration

As previously stated, there are four 3-way valves on the fuel rig. One for each of the supply paths for each engine which directs fluid to an engine from either of the wing tanks, and another two which work non-independently to switch the fluid flow path when directing fluid between each of the wing tanks. This ability of transferring fluid between tanks is implemented on the aircraft to help maintain a central centre of gravity when in flight, or to move fuel in the presence of a fault.

3.3 Control and Monitoring Interface

The control and monitoring interface provides input signals to drive the pumps and valves on the fuel rig and monitors the sensor output signals and displays them in a computer graphical interface. It also has the ability to provide automatic control of various aspects of the fuel rig function.

The fuel rig is controlled by National Instruments (NI) Labview designed interface on a computer via NI interface cards. The rig has measurements of tank height, pressure, pump speed, fluid flow and other discrete controls such as valve position and tank level limit switches as summarised in Figure 13.

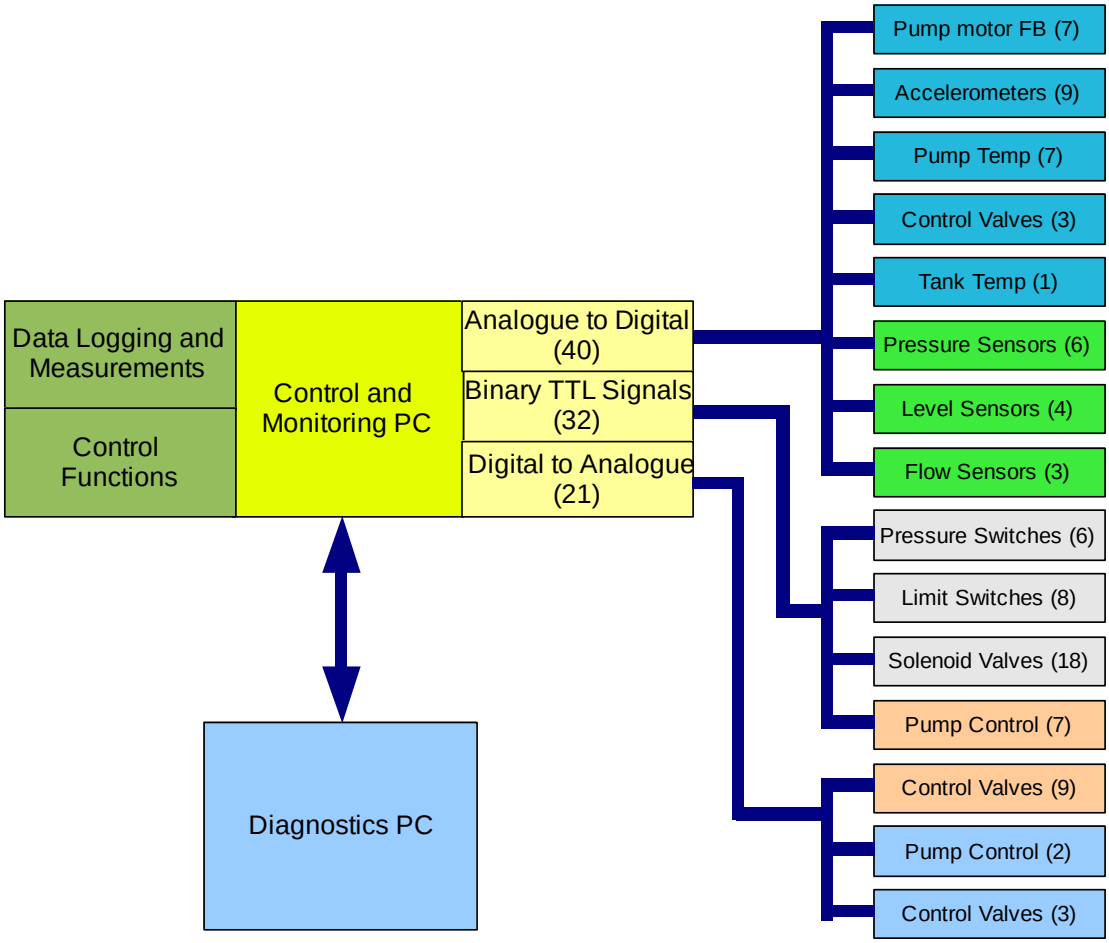

Figure 13: Fuel Rig control variables and measurements.

A screenshot of the NI labview interface is shown below in Figure 14.

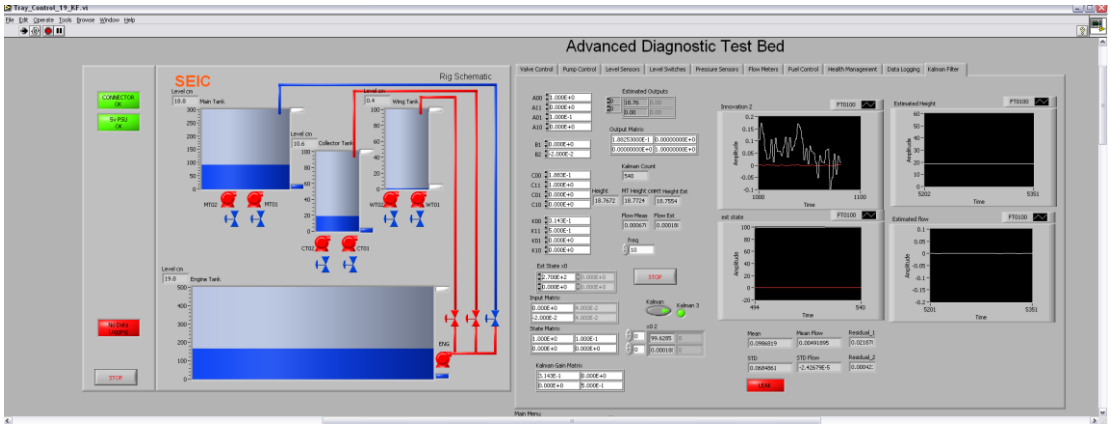

Figure 14: Fuel Rig control and monitoring interface.

The pump speed input from the control and monitoring interface is 0-5V to the inverter, whereby the inverter determines the three phase motor control. The valve position control is open loop and discrete in its demand position, i.e. open or closed.
The fuel rig has the ability to enable automatic control which maintains an equal amount of fuel in each wing tank, therefore maintaining a central gravity point and is programmed into the Labview interface. It does this by switching the source of fuel between tanks in the case of imbalance.

Faults and part faults can be injected using the interface such as pump failure/ degradation, valve failure/ incorrect operation, leaks, blockages and part blockages and all manner of sensor malfunction.

This interface is then logged via UDP communication channel to another computer on which a model based diagnostic system runs in real time in Matlab/ simulink. This then detects the presence of any faults within the system and identifies the location of the faults which can be seen in later sections.

3.4 Electrical Interface

Work was carried out into the redesign of the fuel rig power supply cabinet during the initial commissioning work, which involved a complete redesign. The redesign included an integrated fault injection system and reconfiguration control.

A simplified schematic of the design is shown in Figure 15. This shows a single motor and its corresponding inverter and its associated power supply. The power can be drawn from one of two places dependant upon the position of the double throw relay. The other relays in the schematic are to induce open circuit fault conditions.

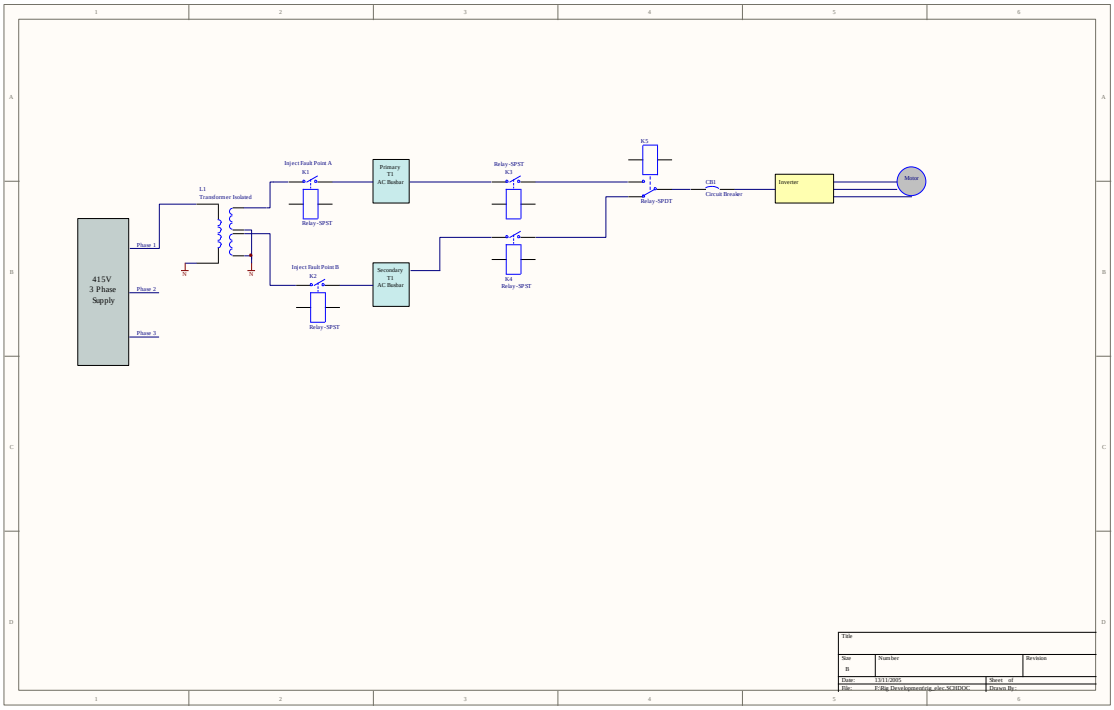

Figure 15: Simplified Electrical Schematic showing Fault Injection and Reconfiguration.

The complete reconfiguration and fault injection system for all inverters and supplies is shown in Figure 16. Each main fuel supply motor and its corresponding inverter draws its operating power from an single busbar, i.e. an individual coil on a series of three transformers. The three transformers each draw power from a single phase of a three phase electrical supply. Any open circuit fault can be injected into the power

supplies by the Labview control system. In the case of loss of a single busbar the electrical system can be reconfigured using the double throw relay to supply power from a different busbar.

The redesigned power supply cabinet provides all power to the fuel rig, contains the pump motor control inverters, and provides feedback measurements of pump motor voltage and current. It also has manual and automatic user settings for switching between Labview control and manual control via switches and includes an external display of reconfiguration and fault injection relay position.

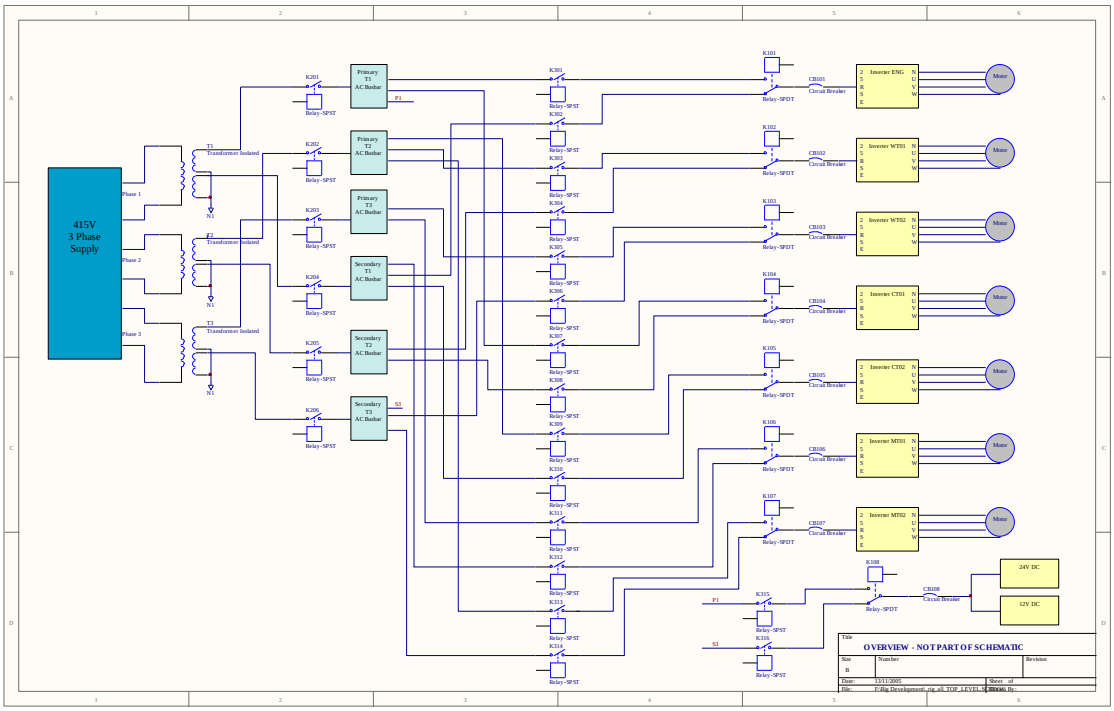

Figure 16: Electrical Schematic showing Fault Injection and Reconfiguration.

The full schematics for the fuel rig power cabinet redesign are included in Appendix A.

3.5 Conclusion

This section has introduced the fuel rig and its operational capabilities. The early stages of the project included the re-commissioning the fuel rig to get it into a functioning state as it was delivered as a non functioning rig. This included a complete overhaul of the pumps, pipe work, valves, all sensor interfaces, a complete interface control system developed using Labview and PC interfacing cards and power supply redesign. The author's contribution to this was the redesign of the power supply and control cabinet. This then provided the basis for development of the diagnostic functions and also provided a rig on which other people could develop other projects as mentioned earlier in this chapter. Hence the contribution claimed in this chapter is to provide a fully functioning fuel rig that can be used for the validation and evaluation of methods and algorithms for fault detection and health monitoring.

Chapter 4

Fuel Rig Modelling and Validation

This chapter describes the development of the nonlinear simulink model representing the fuel rig and the validation of this against its real life counterpart. The nonlinear simulink model development is for the purpose of developing the diagnostic methodology upon. The models performance in comparison to the fuel rig is required to be as similar in function as possible to enable the simulink based diagnostic algorithm development to be transferred to use on the fuel rig as seamlessly as possible. The validation of the model determines its performance against the fuel rig hardware.

The contribution of this chapter is to create and document the development and validation of a simulink model based upon the fuel rig to be used in the production of a Kalman filter based Fault Diagnostic and Identification (FDI) development.

4.1 Introduction

The modelling approach used is mechanistic/physical modelling based upon the hardware of the fuel rig and the fluid properties. A library of component models are created which when interconnected shall create overall fuel rig system models. The sub-systems created include models of tanks, pumps, pipes, valves and 3-way valves. These are developed in a modular fashion to allow interconnections between resistive elements such as pumps and valves to capacitative devices such as tanks and pipes to create an overall system model representing the fuel rig. This chapter will also provide the validation of the developed subsystem models and furthermore the validation of the overall fuel rig system model.

4.2 Tank Model

4.2.1 Description and Model Derivation

The three physical tanks in the fuel rig system are cubic in shape and as stated previously the working fluid is water. The outlet from the tank is situated at the bottom of each tank as shown in Figure 17.

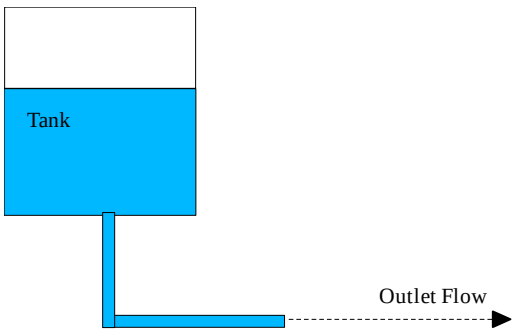

Figure 17: Diagram of a Tank.

Equation 3 is the defining dynamic equation that provides solution to the model for height, h, given flow in, q_{in}, and flow out, q_{out}.

$$h = \frac{\int (q_{in} - q_{out})dt}{a} \quad \textbf{(3)}$$

Where: h = height (m)

a = area (m^2)

q = volumetric flow rate (l/s)

Figure 18 below shows the simulink model for the tank. The inputs to this sub-model are flows, either in or out, and the output is the height. The initial condition of the integrator is the start height of fluid in the tank. During operation this can initially be set to the same as seen on the rig in order to give the same fluid level initial conditions. The boxes placed in the path of the model are in order to add noise to the signal, the one on the left adds noise to the process and the one on the right adds sensor noise. The box on the input is the injection of a fault condition, in this case of a leak fault, which is set by substituting a positive flow magnitude in l/s in the relevant simulation workspace variable.

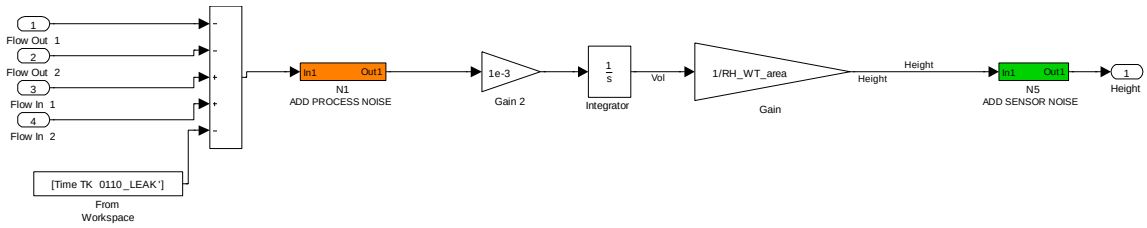

Figure 18: Simulink model for tank.

With the fuel rig in the configuration of UAV the labview interface applies software scaling which makes the tanks look like they have the inner, middle and outer chamber as depicted in Figure 19 and make them look like the real aircraft tank size of 990 litres. Therefore it is required to also within the model apply software scaling to the tank model which simulates this effect which is achieved by a scaling factor of 0.1 on the flow input and a difference of heights of 0.081m and 0.053m as illustrated in Figure 19 below.

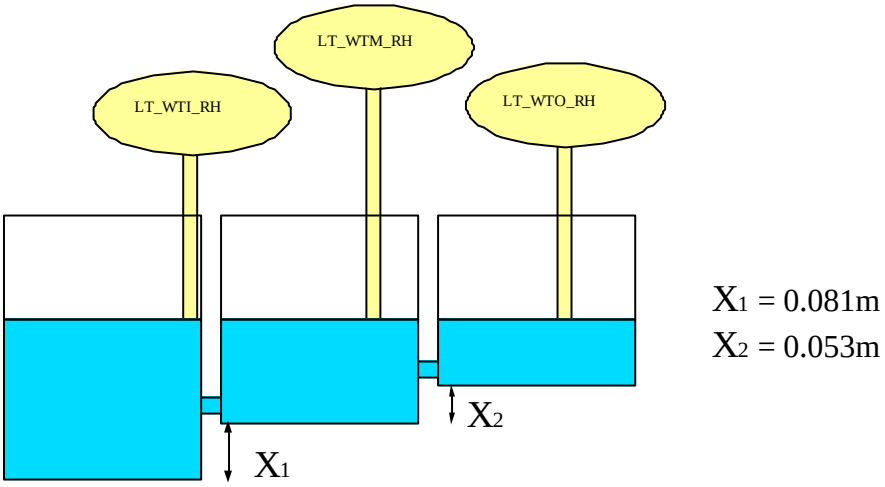

Figure 19: Simulink model for UAV tank.

4.2.2 Model Mathematical Verification

The tank model is verified by providing an input to the model in terms of a flow, in this test case 0.361 l/s. The corresponding tank level is then analysed to confirm correct drop in level for the given flow. Note, this will validate both input and output flow since both work the same way albeit in positive and negative directions. The rate of change of height, can then be calculated as in Equation 4 and with a given area of $0.5312m^2$ for this tank and given that $1m^3$ = 1000 litres then the flow required for a drop in level of this rate calculated as per Equation 5 which show a rate of change of volume, i.e. flow. The calculated flow, based upon the drop in tank level seen, is 0.361 l/s, as shown in Figure 20, which verifies this model.

$$m = \frac{\Delta h}{\Delta t} = \frac{0.068m}{100s} = 0.00068\,m/s \quad \textbf{(4)}$$

$$6.8\times10^{-4}\times0.5312 = 3.61\times10^{-4}\,m^3/s = 0.361l/s \quad \textbf{(5)}$$

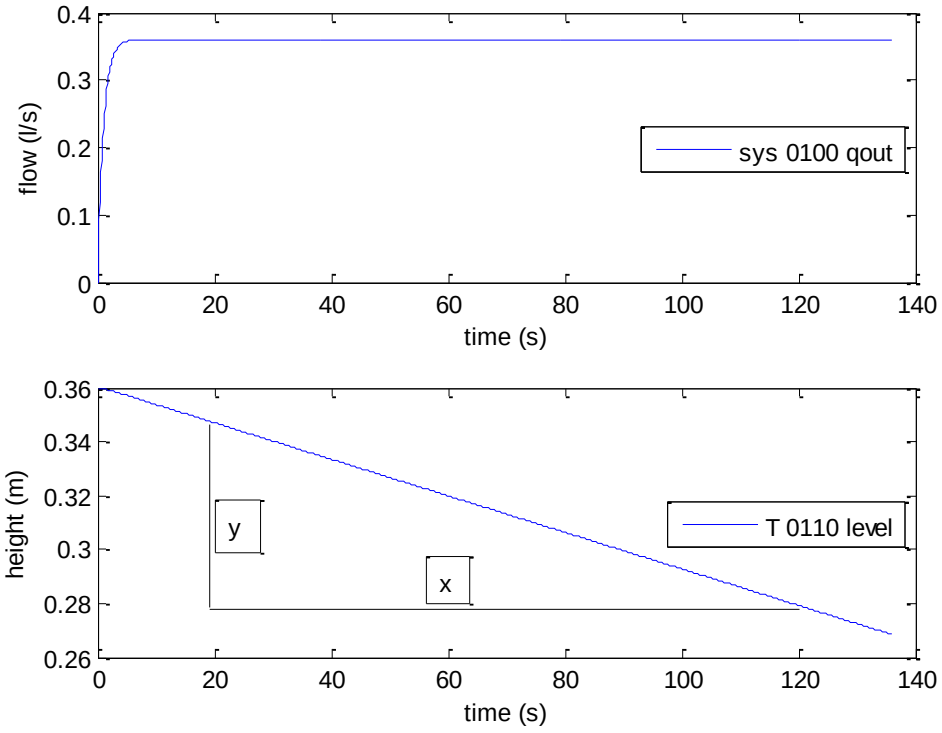

Figure 20: Simulink tank model verification results.

4.2.3 Model Validation Simulation Results

The model is now validated against the real fuel rig to confirm its correct operation. A plot of the fuel rig results for right hand wing tank flow (Rig RH WT Flow) and right hand wing tank level (Rig RH WTI Lev) alongside the simulink model right hand wing tank flow (Sim RH WT Flow) and right hand wing tank level (Sim RH WTI Lev) are shown below in Figure 21. The pump control signal (RH WT Dem) is also shown to show clearly the transients of the pump. Of course it is possible to have the measured flow (rather than simulated, as shown in the figure) as an input to the tank model. This produces almost identical results from the validation as the flow prediction can be seen to be very close to the actual. These results illustrate the tank models ability to represent the real tanks level for given flow inputs and therefore validates the subsystem model.

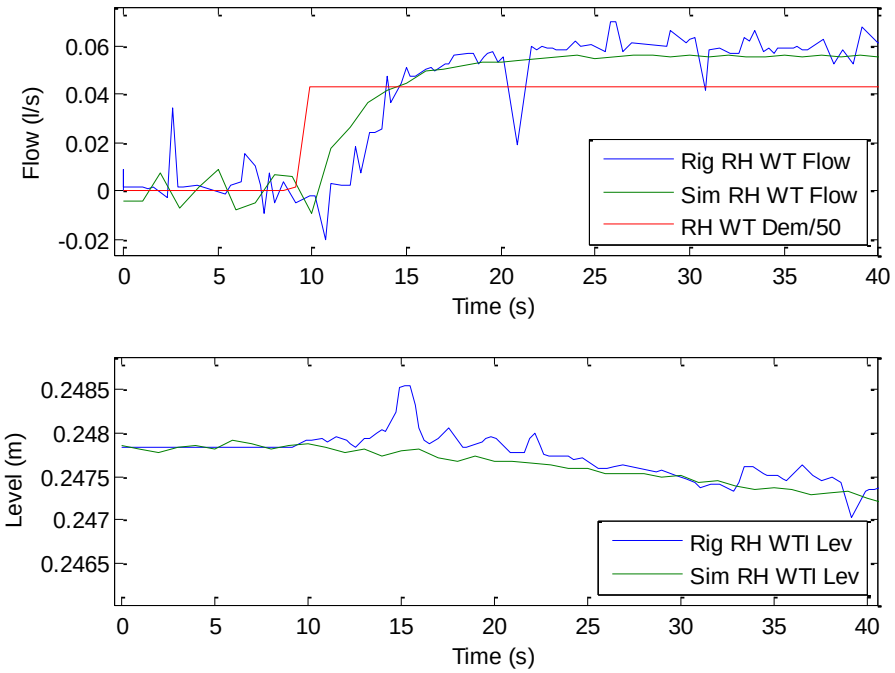

Figure 21: Simulink tank model validation results.

4.3 Pump Model

4.3.1 Description and Model Derivation

The six main pumps used on the fuel rig are peristaltic pumps, and these provide a flow that is directly proportional to the 3 phase motor speed. The pump motor is in turn is driven by an inverter which applies a controlled signals to each phase of the motor to control the motor commutation and limit its rate of change of motor velocity, which is the acceleration. The inverter is driven by a demand signal from the control and data logging system. The control signal as per the inverter data sheet follows a straight line taking 5 seconds for the ramp between full scale change control signal, i.e. from stationary to maximum motor speed, and is implemented in the simulink model as a rate limiter set to govern maximum input at this rate. The pump, motor and gearbox are represented in the model as a first order transfer function, where the time constant and gain were found to be 3 seconds and 0.026 l/s/V respectively and were

found empirically. The transfer function to represent the peristaltic pump operation is shown in Equation 6.

$$q = \frac{K_{mp}}{T_{mp}.s + 1} \times V_{in} \quad \textbf{(6)}$$

Where: q = flow (l/s)

K_{mp} = Pump motor gain = 0.026l/s/V

T_{mp} = Time constant for motor response = 3s

V_{in} = Voltage demand input (V)

Figure 22 shows the simulink model for the pump motor. The model also includes the addition of a bias to the input voltage to allow the injection of a fault on the input of the motor in order to simulate mechanical or electrical breakdown in the motor. The saturation block in the figure limits the input to the motor to values in the range as produced by the rig.

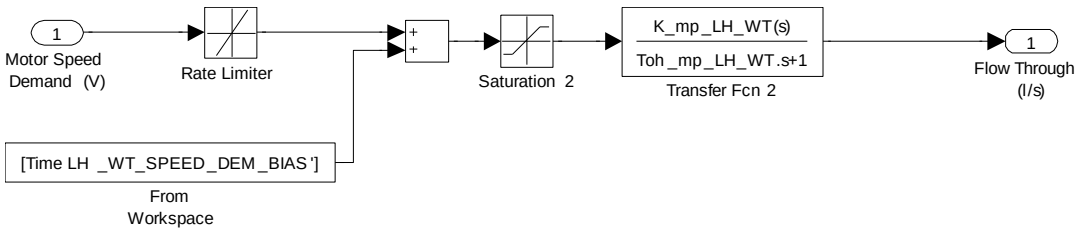

Figure 22: Simulink model for pumps with fault injection.

4.3.2 Model Mathematical Verification

In order to verify the mathematical model by calculation, the input to the pump is stepped from 0V to full scale input of 2.5V. The results from the model show expected output of 0.065 l/s at 2.5V as shown in Equation 7.

$$q_p = 0.026 \times Vin = 0.026 \times 2.5 = 0.065 l/s \quad \textbf{(7)}$$

The response of the simulink model of the pump and its associated tank are shown in Figure 23. The response is subject to input step to full scale input.

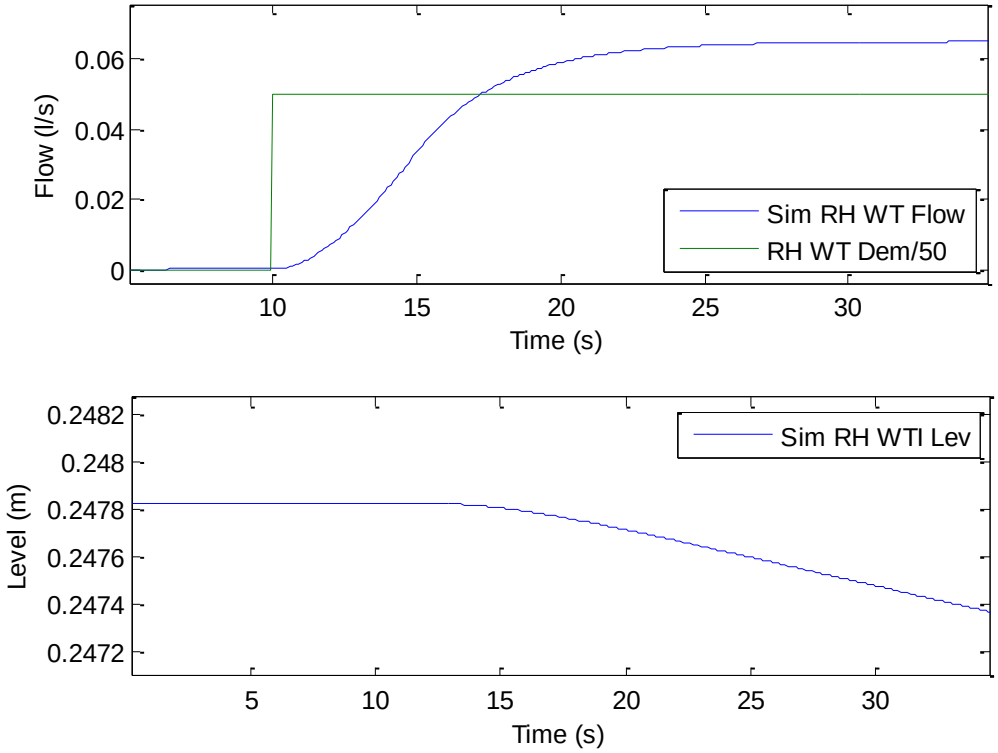

Figure 23: Simulink model pump motor and associated tank level simulation results.

4.3.3 Model Validation Simulation Results

Running the fuel rig and the simulink model alongside each other produces the plot as can be seen in Figure 24 below. This shows the flow as measured by the flow sensor on the fuel (Rig RH WT Flow) and the simulink model flow (Sim RH WT Flow) when driven by the same input signal (RH WT Dem/50).

The addition of noise to the tank level, as shown in Figure 25, the model produces a reasonable representation of the rig sensor result.

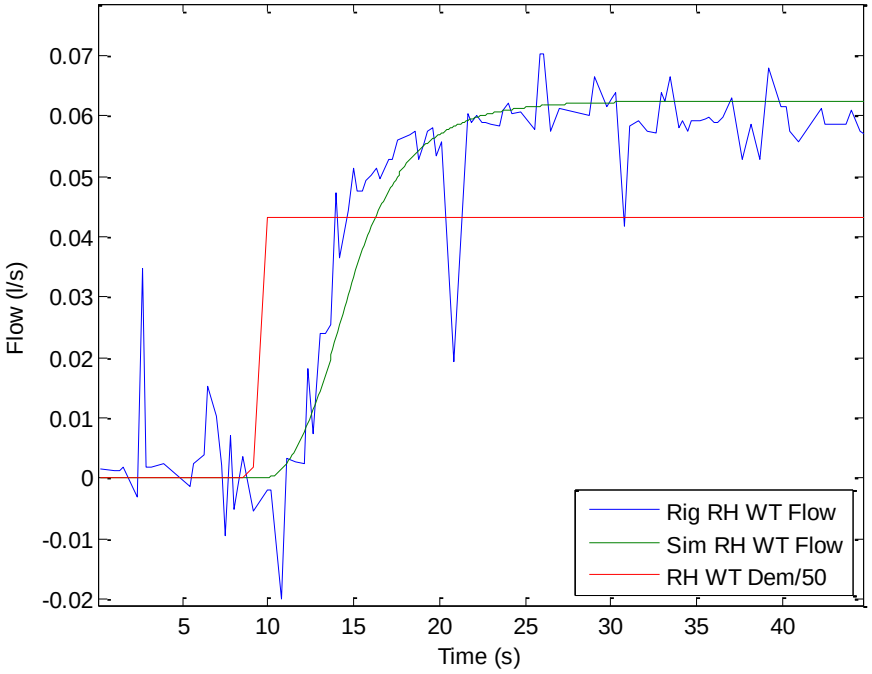

Figure 24: Fuel rig and simulink peristaltic pump response.

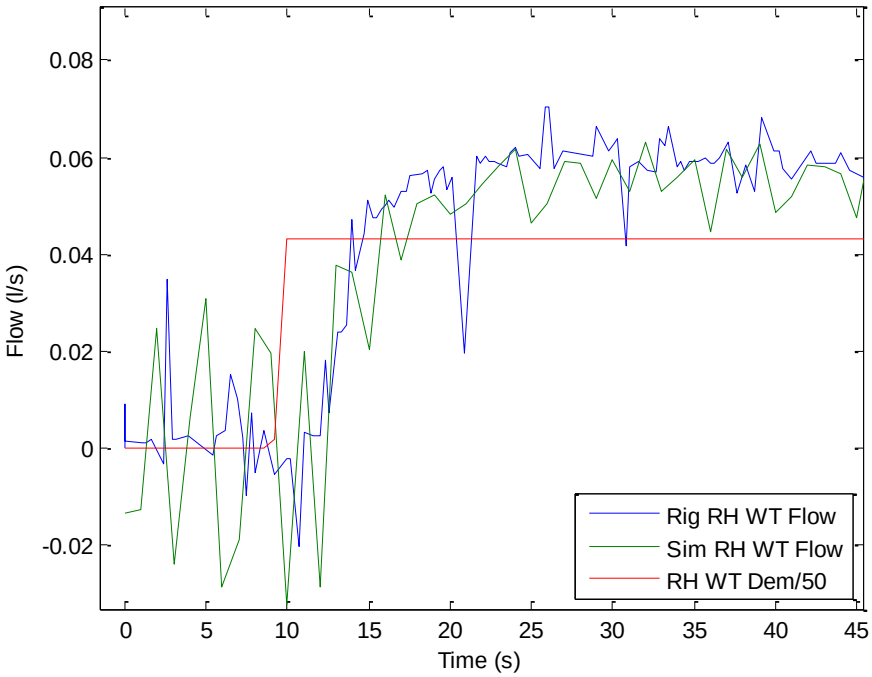

Figure 25: Fuel rig and simulink peristaltic pump response with noise addition.

4.4 Valve Model

4.4.1 Description and Model Derivation

The valve model gives the volumetric flow rate from the valve with a given valve position and a given pressure differential across the valve. The defining equation for flow through the valve is shown in Equation 8, and is referenced in Thomas, (1999). The rig valves are controlled via motors, which are switchable between open and closed only and have a transition rate of 6 seconds between each state. The valve conductance is representative of the pressure requirement to overcome valve orifices, pipe surfaces, and changes of fluid direction in a laminar fluid system. The model assumes only laminar flow and the fluid is compressible. The simulink model for a valve is shown in Figure 26.

$$q = \frac{c_v . y_v \sqrt{\frac{\Delta P}{v}}}{\rho} \qquad \textbf{(8)}$$

Where: v = specific volume = 1.0022×10^{-3} m^3/kg

ρ = density = $997.78 kg/m^3$

c_v = valve conductance = 1.52×10^{-4} m^2

ΔP = pressure difference (Pa)

q = flow (m^3/s)

y_v = proportional valve opening (range 0 to 1)

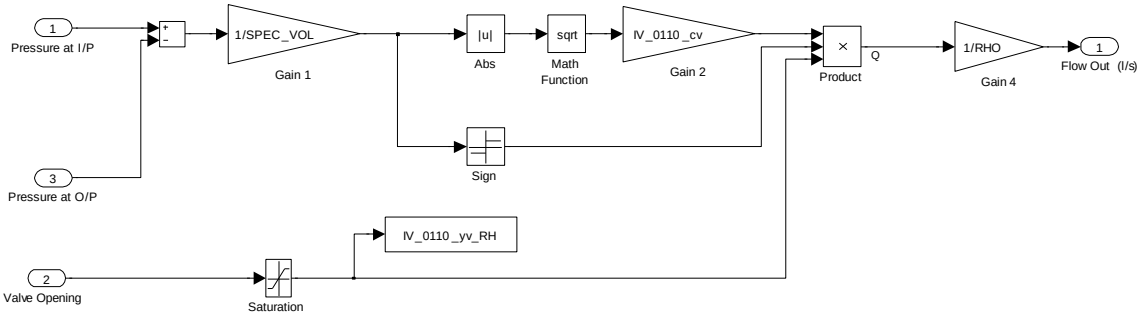

Figure 26: Valve Model.

4.4.2 Model Verification

The valve model is verified by using a constant pressure drop of 10,000 Pa and comparing the calculated pressure drop with the simulink based test results of the pressure model to validate the numerical function of the valve model. Theoretically the flow for the given pressure drop of 10,000 Pa, with a valve conductance of 1.52×10^{-4} m^2 and a proportional opening of 0.85 should be as in Equation 9. As shown in this equation the output flow for this given pressure differential should produce a flow through the valve of 4.1 l/s which, as shown in Figure 27, it complies with. Figure 27 also highlights the nonlinear relationship between pressure and flow.

$$q = \frac{c_v . y_v \sqrt{\frac{\Delta P}{v}}}{\rho} = \frac{1 \times 10^3 \times 15.2 \times 10^{-5} \times 0.85 \sqrt{\frac{1 \times 10^4}{1.0022 \times 10^{-5}}}}{997.78} = 4.1 l / s \qquad \textbf{(9)}$$

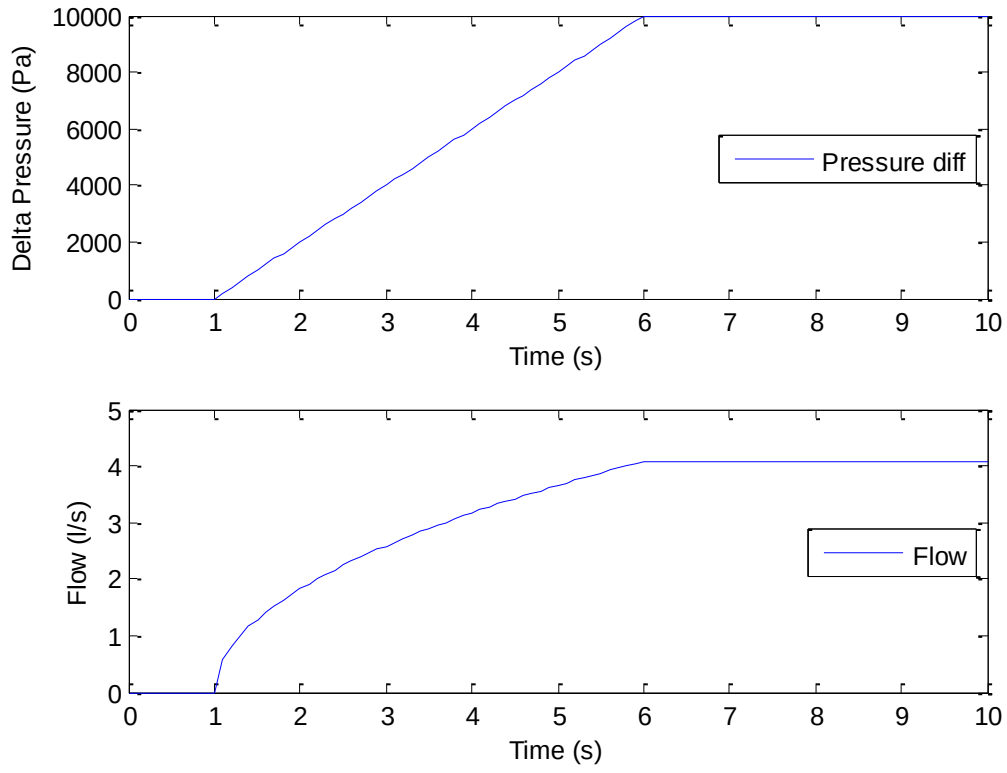

Figure 27: Verification of simulink valve model.

4.4.3 Model Validation Simulation Results

The validation of the valve model can only be done together with the pipe model and will be carried out in later sections. In practice, the valve relies on the presence of a pipe in order to function correctly. This is because the valve itself is a static model and relies on the pipe model to introduce dynamic behaviour.

4.5 Pipe Model

4.5.1 Description and Model Derivation

The pipe is modelled as a pressure device. The pipe model equation which gives pressure as a function of flow is shown below in Equation 10. It is based on Pressure being a ratio of change in volume multiplied by the bulk modulus of the working liquid, in this case water. This assumes compressibility of the fluid, and although the pipe elasticity is present it is assumed negligible since working pressures are low.

$$P = \frac{E_v}{V_o}(\int q_{in} - q_{out})dt \qquad \textbf{(10)}$$

Where: E_v = Bulk Modulus = $2.15*10^9$Pa P = Pressure (Pa)

V_o = Original Volume (pipe) = $1.0261*10^{-4}$ m^3 q = Flow (l/s)

The pipe model is shown in Figure 28. It includes both the pipe and a function to simulate the release of fluid in the instance of an over-pressure situation, thus simulating the pressure release valves which are present on the fuel rig to perform a function of safety. This is implemented by switching the flow to be directed back to the tank when the overpressure condition is reached. However, where a pressure release valve is not present the release valve function is inhibited by setting the pressure threshold to infinity.

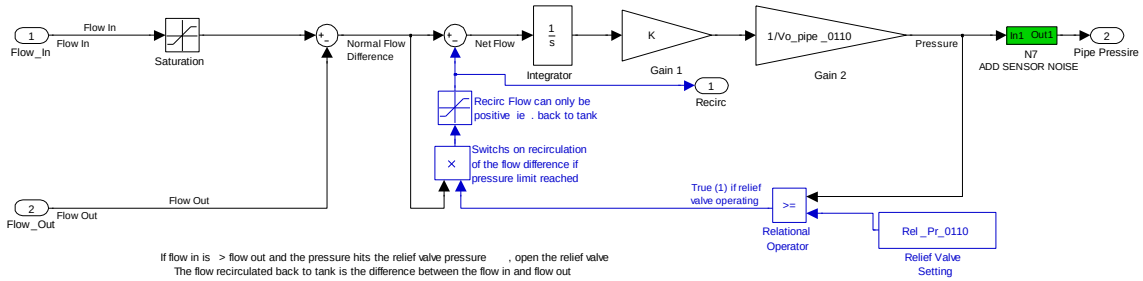

Figure 28: Simulink model for pipe.

The calculation for the original volume in the pipe is based on the cross sectional area multiplied by the sum of length for all the sections for all pipes. The pipe volumes are model dependant and can be seen in the relevant system model sections. Note that in a section of pipe where a pressure relief valve is not fitted this function can be disabled by setting the relief threshold to infinity.

4.5.2 Model Verification

The simulation is based on ramping the pump up from zero to full power whilst having a constant proportional valve opening of 0.3 causing a build up of pressure within the pipe. The pipe characteristics used in the simulation are of 0.81m length with a cross sectional diameter of 12.7mm. An estimated valve conductance of 15.2×10^{-5} is used at this stage and the correct value will be found in the section containing the validation for the two pump trays. As can be seen in the results, in Figure 29 and Figure 30, flow and pressure increase at the expected rate with the increase of pump speed. Proving the simulation results by calculation to ensure that the valve is operating correctly. The pressure seen at the output of the pipe is assumed to be zero, therefore $P = \Delta P$. Rearranging Equation 9 for pressure, P, gives Equation 11 and shows the solution for the pressure seen in the pipe using the flow and is proven to correlate with the simulation results seen in Figure 29 and Figure 30.

$$P = v.\left(\frac{q\rho}{c_v.y_v}\right)^2 = 1.0022*10^{-3}\left(\frac{0.18*10^{-3}*997.78}{15.2*10^{-5}*0.3}\right)^2 = 1.555*10^4\,Pa \qquad \textbf{(11)}$$

Where: v = specific volume = $1.0022*10^{-3}$ m^3/kg

ρ = density = $997.78kg/m^3$

c_v = valve conductance = $15.2*10^{-5}m^2$

ΔP = pressure difference (Pa)

q = flow (m^3/s)

y_v = proportional valve opening = 0.3

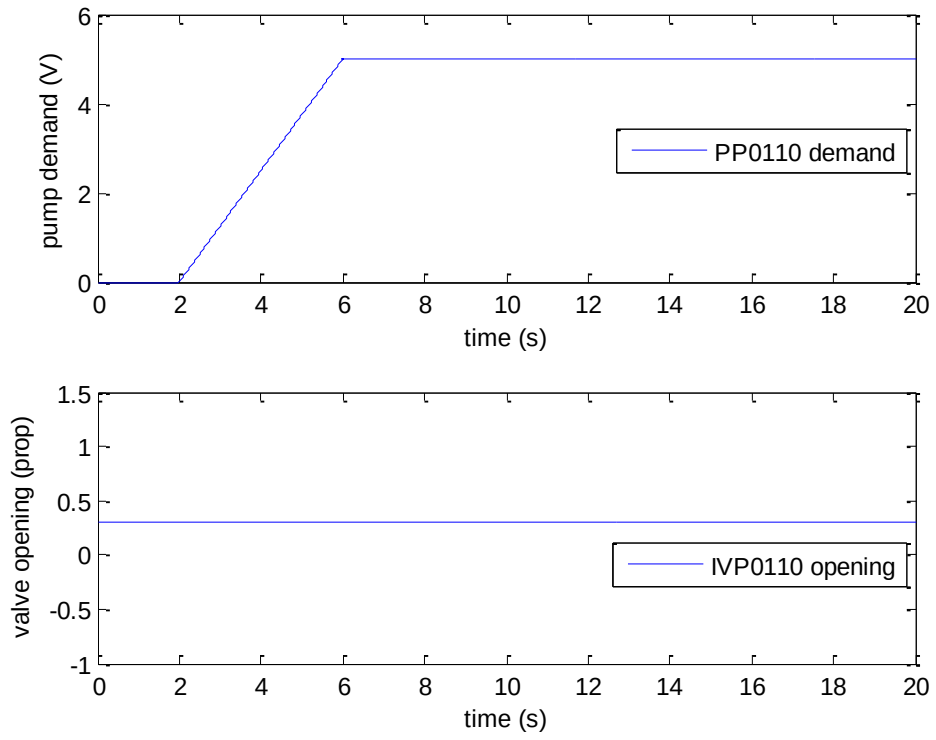

Figure 29: Simulation Results for Pipe Model.

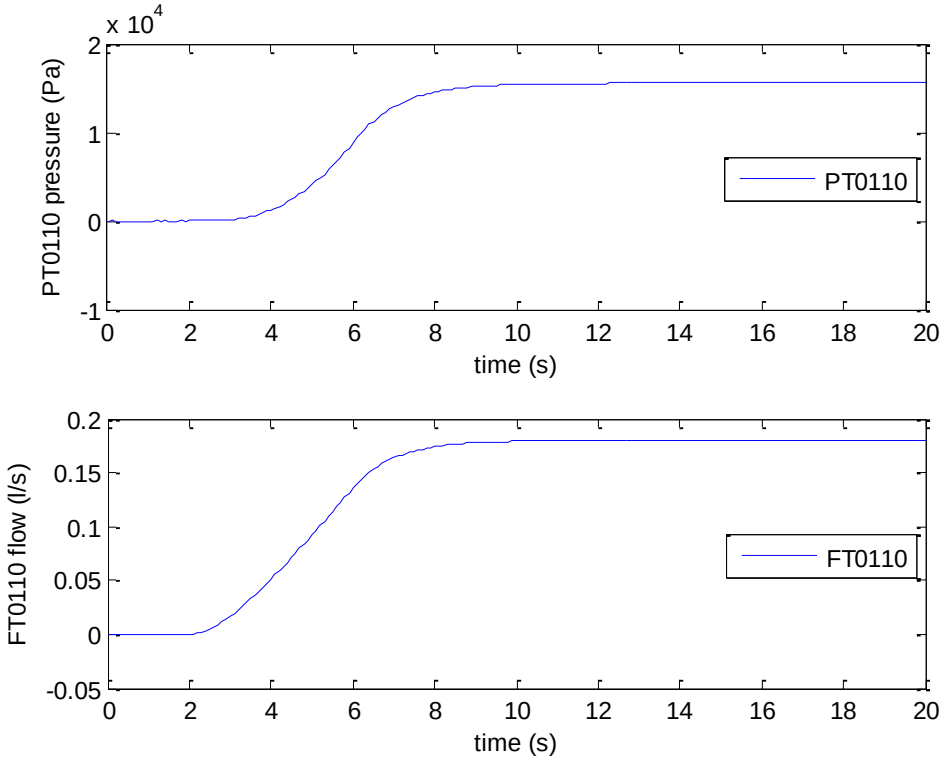

Figure 30: Simulation Results for Pipe Model.

The next set of verification results test the valve opening over all possible positions by using a ramp function to close it. The valves initial condition will be open and will be ramped closed at 2 seconds taking 6 seconds for the transition. Figure 31. Figure 32 and Figure 33 show motor demand (PP0110 demand), valve position (IVP0110 opening), the pressure (PT0110), flow (FT0110), flow through the pressure relief return path (PSV0110) and tank level (LT0110). The flow through the return path is not affected until 7 seconds at which point the valve has reached a proportional opening of 0.165. When the valve is fully closed the flow through the return path is equal to that through the pump and therefore the level in the tank at this point remains unchanged.

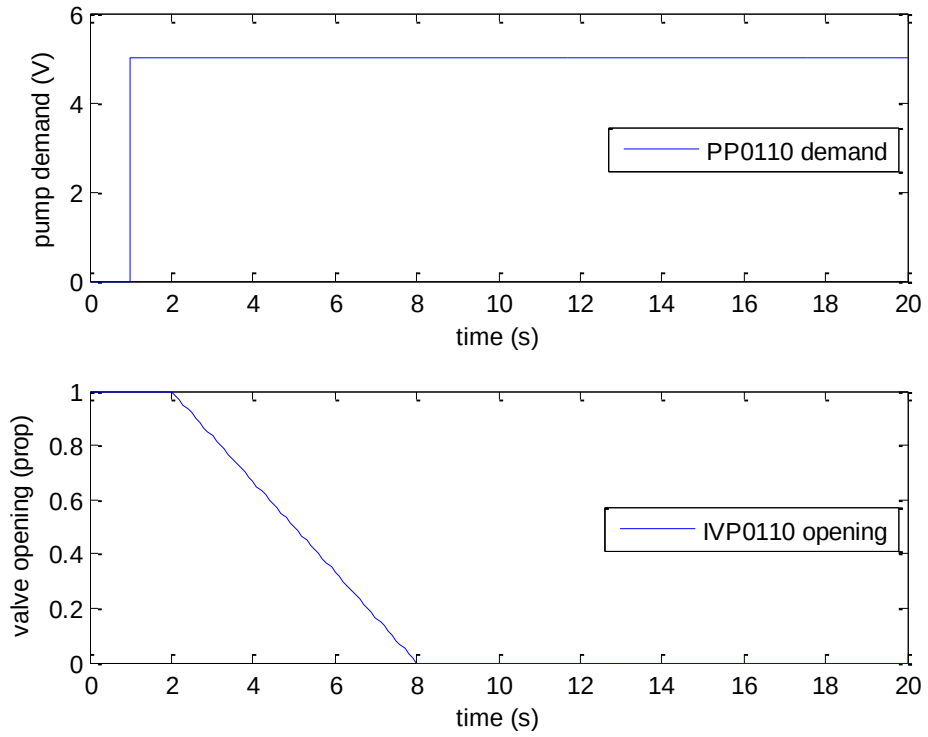

Figure 31: Simulation Results for verification of Pipe Model.

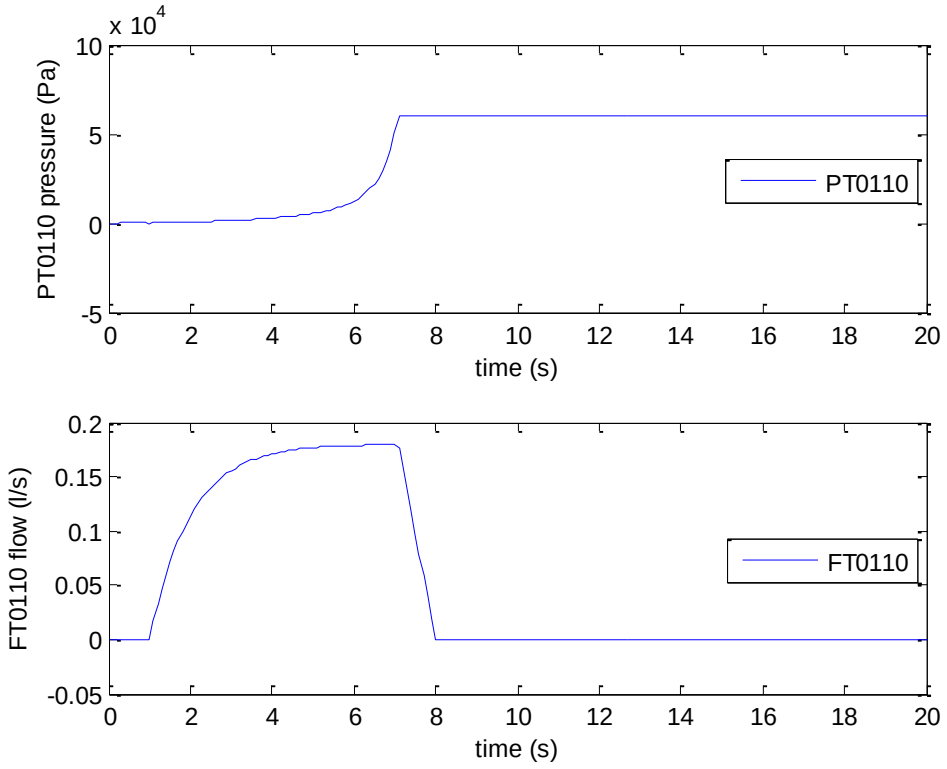

Figure 32: Simulation Results for verification of Pipe Model.

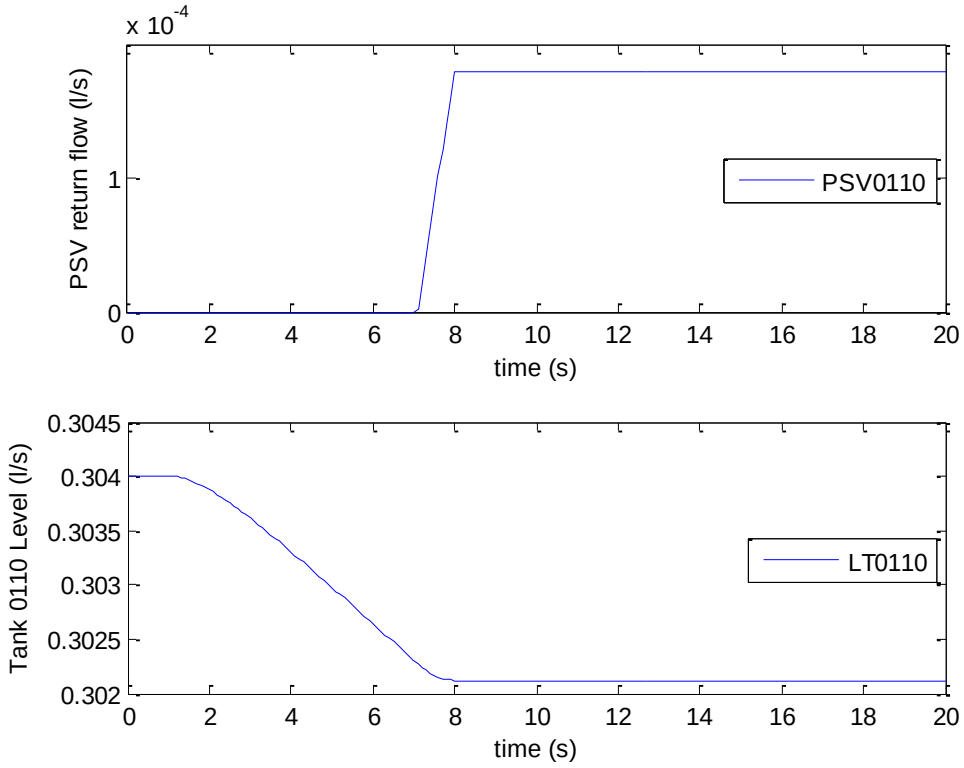

Figure 33: Simulation Results for verification of Pipe Model.

4.5.3 Model Validation Simulation Results

The validation of the pipe model can only be done together with the valve model as with the valve alone and will be validated in the following sections.

4.6 Pipe and Valve Model

4.6.1 Description and Model Derivation

The pipe and valve model is based on the valve model and pipe model described in previous sections. The modelling interconnections between valve and pipe are as shown in the block diagram seen in Figure 34. The input of atmospheric pressure will be suited to a pipe at the end of a run and therefore assumed zero, as all pressure measurements are relative, however this input can be replaced by the pressure output

from a pipe if situated in the middle of a run therefore enabling multiple interconnecting subsystems of modular design. If a series section of pipes are interconnected in the real system, these would normally be modelled as a single pipe. If for some reason it was necessary to model them as separate sections, then a valve model representing the resistance of the pipes is required between the two pipe interconnections.

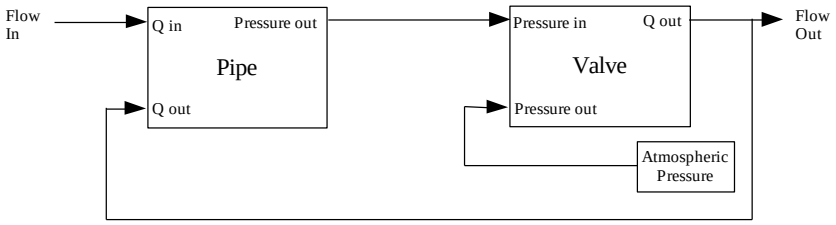

Figure 34: Diagram of Pipe and Valve Model Component Interconnections.

4.6.2 Model Verification

No further model verification is required for the pipe or valve model sections as this has been covered fully in previous sections.

4.6.3 Model Validation Simulation Results

The test system used for validation of the simulink model against the fuel rig will be the flow through a valve and pressure within the pipe work driven by a single pump as shown in Figure 35 below. The pump is required to validate the pipe and valve model as it is the only physically measurable input signal available to the drive the pipe and valve subsystem model.

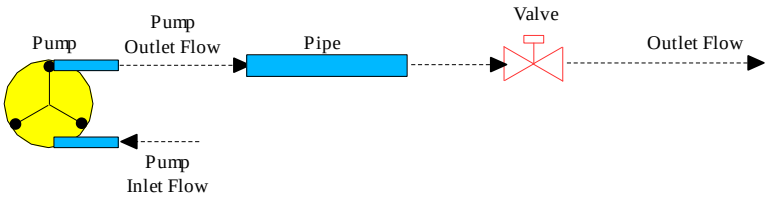

Figure 35: Diagram of Pipe and Valve Model Validation Components.

The model validation has been carried out using pump model parameters of transfer function gain of 0.026 and time constant of 3 second for pump response, a valve conductance of 2.05e-2 and an overall pipe length of 2.79 metres. As can be seen in Figure 36 and Figure 37 below the model reproduces the dominant (first order) dynamics of the fuel rig results for flow for rig (Rig LH WT Flow) and model (Sim LH WT Flow) and pressure for rig (Rig LH WT Press) an model (Sim LH WT Press) respectively. Some offset error is noted in the wing-tank steady state pressure. This is thought to due to poor repeatability of the pressure sensors at low pressures and, most importantly, it does not have a deleterious effect on the models ability to predict the flow.

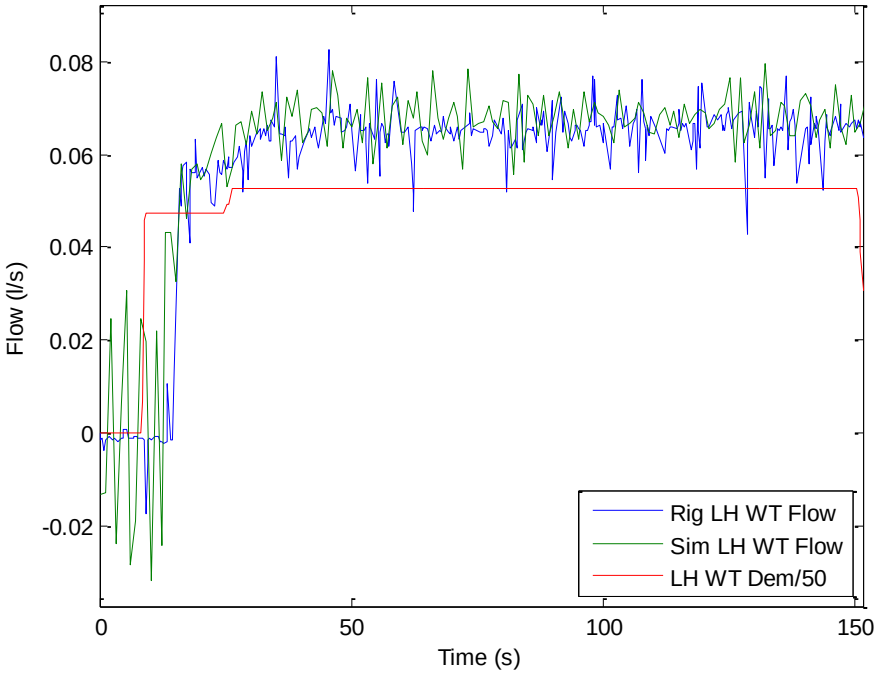

Figure 36: Pipe/ Valve Model – Left Hand Wing Tank Flow.

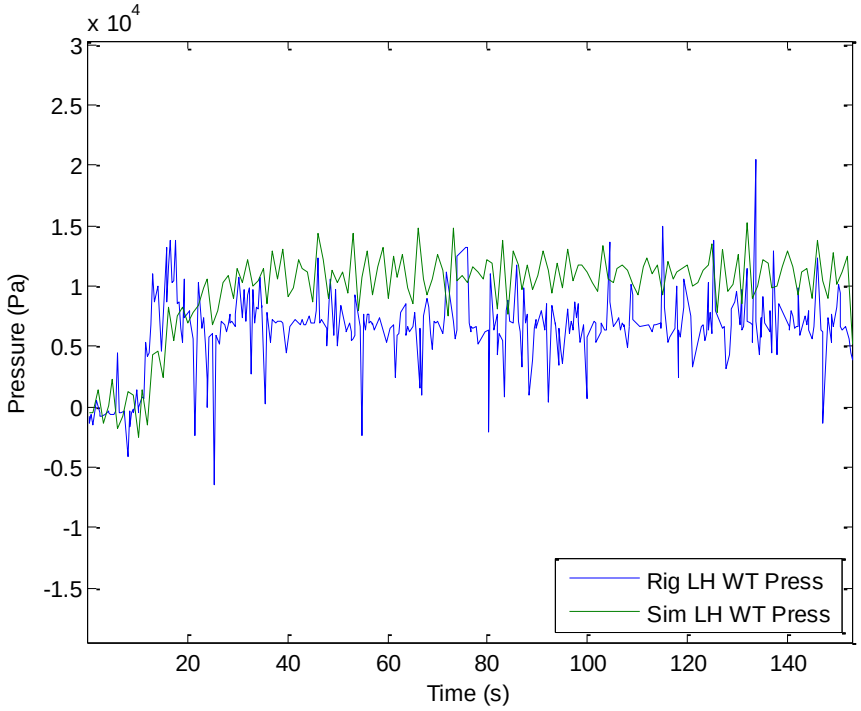

Figure 37: Pipe/ Valve Model - Left Hand Wing Tank Pressure.

4.7 Three-way Valve Model

4.7.1 Description and Model Derivation

As previously stated, there are four 3-way valves on the fuel rig. One for each of the supply paths for each engine which directs fluid to an engine from either of the wing tanks, and another two which work non-independently to switch the fluid flow path when directing fluid between each of the wing tanks. This ability of transferring fluid between tanks is implemented on the aircraft to help maintain a central centre of gravity when in flight, or to move fuel in the presence of a fault. The input to the three way valves is of discrete form and can be 0, 1, 2 or 3. Table 1 below shows the action for each of these inputs. Figure 38 demonstrates the flow paths for normal and cross-feed engine fuel supply.

	Output from 3-way			
	0	1	2	3
Xfeed Valve Response (UAV)	Initial response (position not yet known)	Normal flow	Cross-feed flow	State Transition
Transfer Pump Valve Response (UAV)	Right Hand Wing Tank to Right Hand Auxiliary Tank	Left Hand Wing Tank to Right Hand Wing Tank	Position not known	State Transition

Table 1: Three way valve response.

When the rig is first started up as the valve does not yet know the position it is in the output corresponds to this. When the left engine directs fluid from the left tank to the left engine, for example, then this is normal flow position, i.e. position 1. The valve has the ability to switch this to supply the left engine from the right tank and this is position 2. As the valve is in a transitional state between 1 and 2 the valve position sensor outputs a 3. The simulink model, as shown in Figure 39, will use the last known state of either state 1 or 2 until it has fully switched. This will give the equivalent flow between tanks over time.

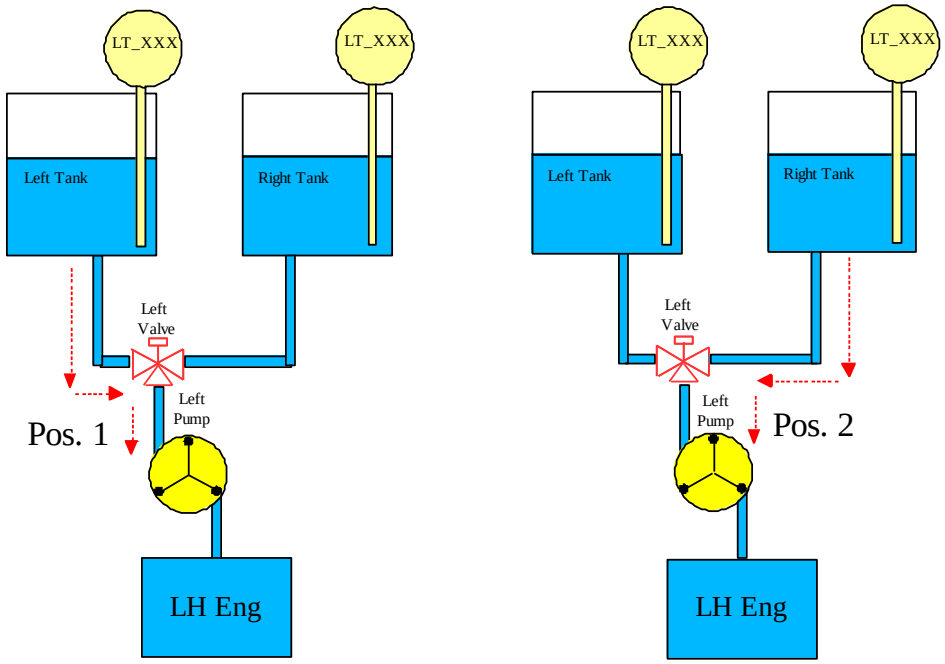

Figure 38: UAV Cross Feed Valve Positions

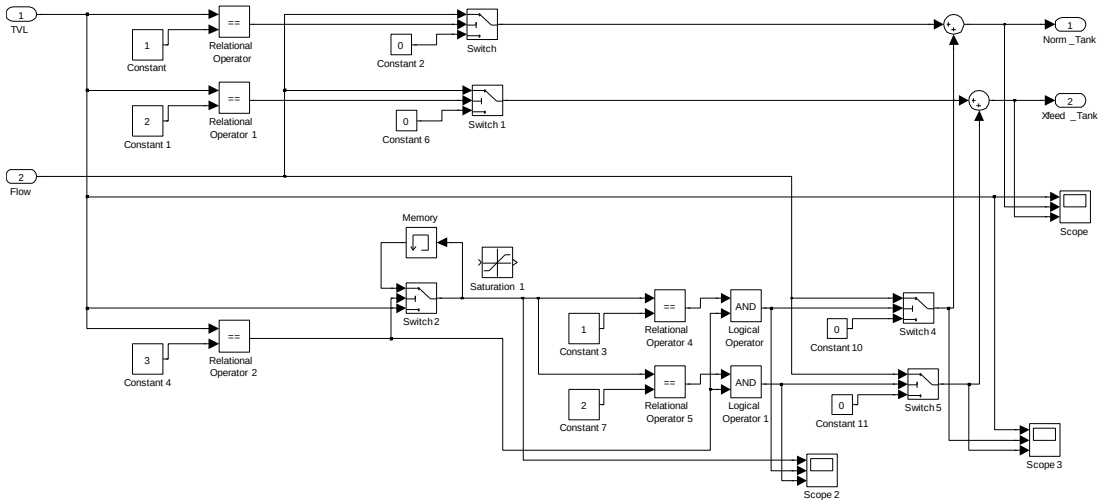

Figure 39: UAV 3 Way Valve simulink logic model.

4.7.2 Model Validation Simulation Results

It is not necessary to mathematically verify the operation of the three way valve since its operation is one of discrete switching of the direction of fuel supply; however this section contains the validation results for the operation of the simulink model against

the fuel rig. The test consists of switching between normal and cross-feed, as demonstrated in Figure 38, flow paths to validate correct 3-way valve operation. The positions that the discrete valve position represents is shown in Table 1. As can be seen in Figure 40 below, the three way valve is switched from normal to cross feed at 60 seconds and back to normal at 120 seconds. In the plots following, Figure 42 shows the tank level for left hand inner, middle and outer tanks from which the pump is supplied from 0 to 60 seconds and highlights the tank levels acting accordingly. Figure 41 shows the right hand inner, middle and outer tank level and although not as clear, since fuel is being pumped from the tank throughout the time span of the plots, an increase in the rate of fuel pumped from this increases at 60 seconds thus justifying correct operation of the 3-way valve model.

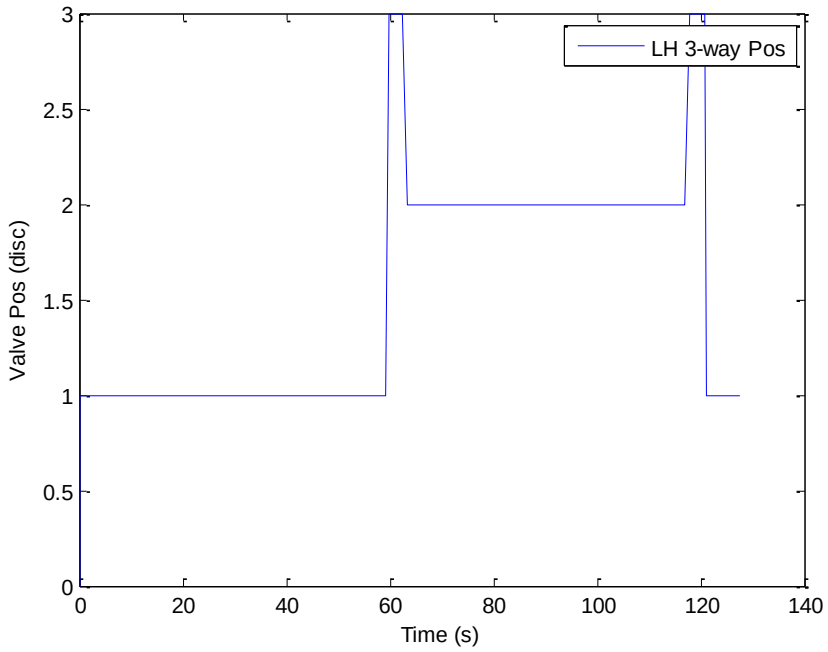

Figure 40: Left Hand 3-way valve position.

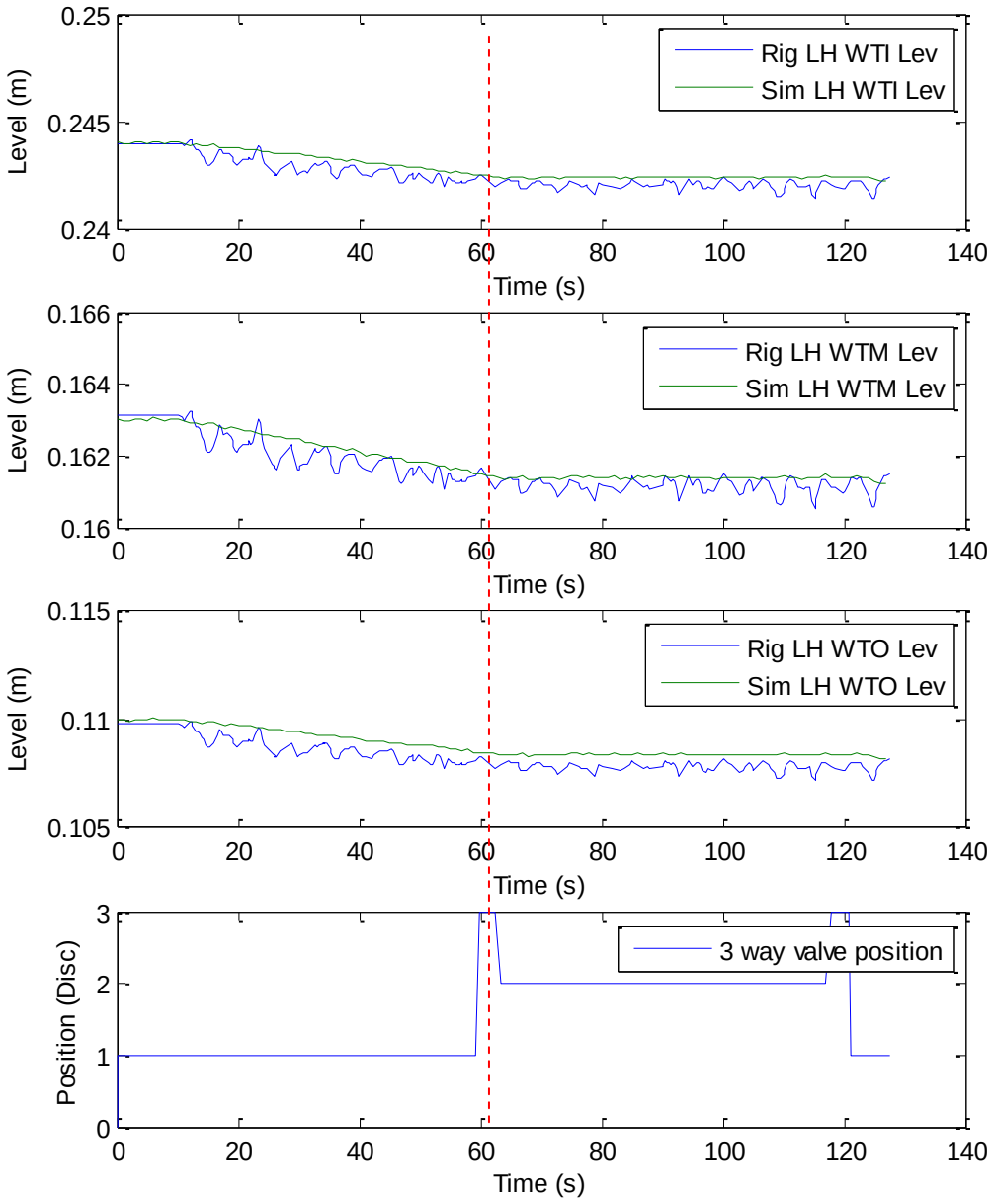

Figure 41: Left Hand Wing Tank levels for Inner, Middle and Outer tanks (top to bottom).

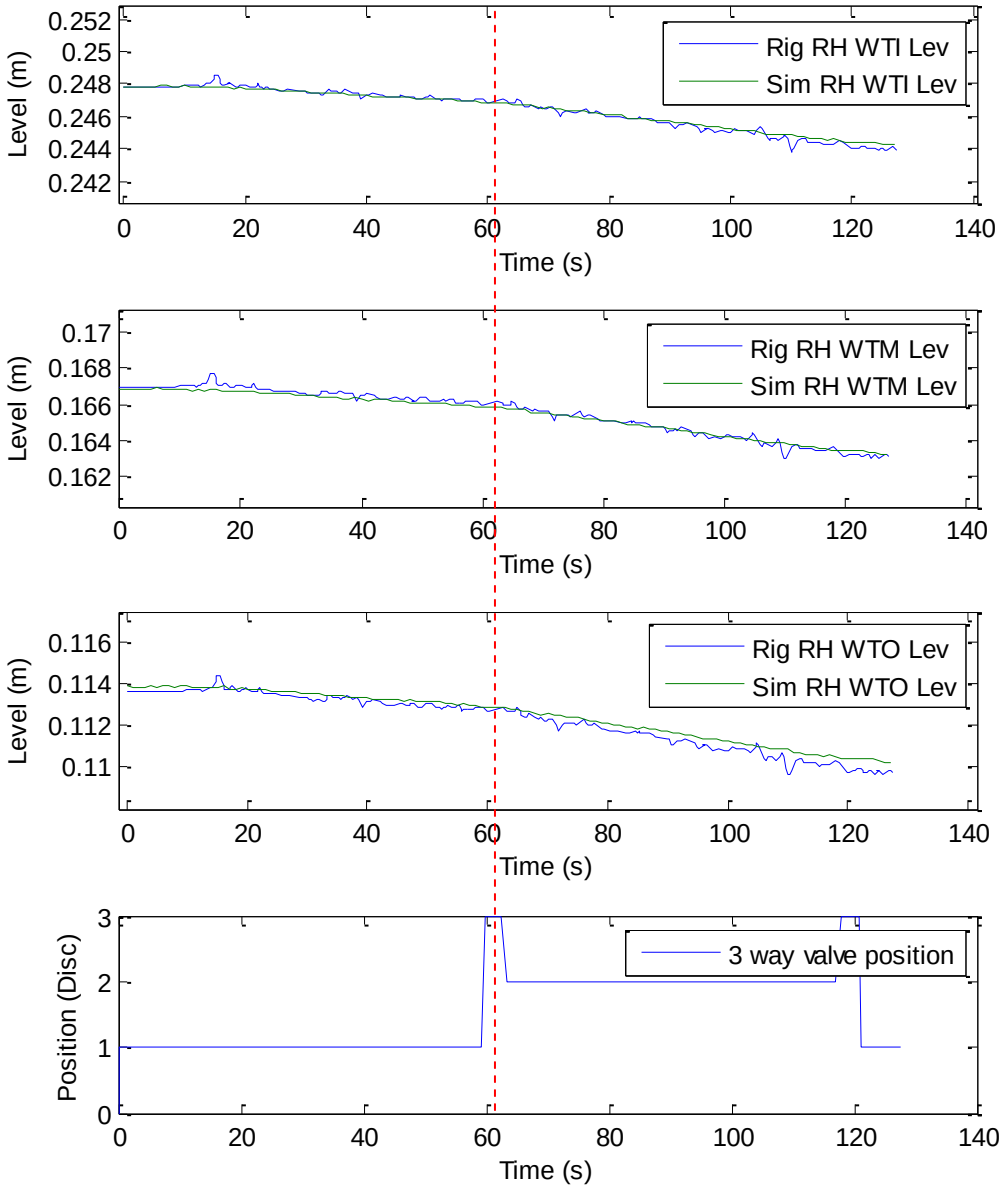

Figure 42: Right Hand Wing Tank levels for Inner, Middle and Outer tanks (top to bottom).

4.8 UAV Pump Tray Model

4.8.1 Description and Model Derivation

Having previously validated the components individually, this section looks at validation of the components within a subsystem. A pump tray in the fuel rig is shown below in Figure 43. Using the modular approach capacitive model elements, for example tanks and pipes, are connected to resistive model elements such as pumps and valves. The pump, a resistive element, provides the flow within the subsystem and is connected to the capacitive element of the pipe. The pipe is, in turn, connected to a valve and this provides the resistive element within the pump tray. The tanks are shown at either end provide the capacitive storage element which represent the store of fluid in the systems. The simulnk model of the pump tray is shown in Figure 44. The red blocks in the model are for the purpose of fault injection which is covered later and the green block is for the purpose of noise addition.

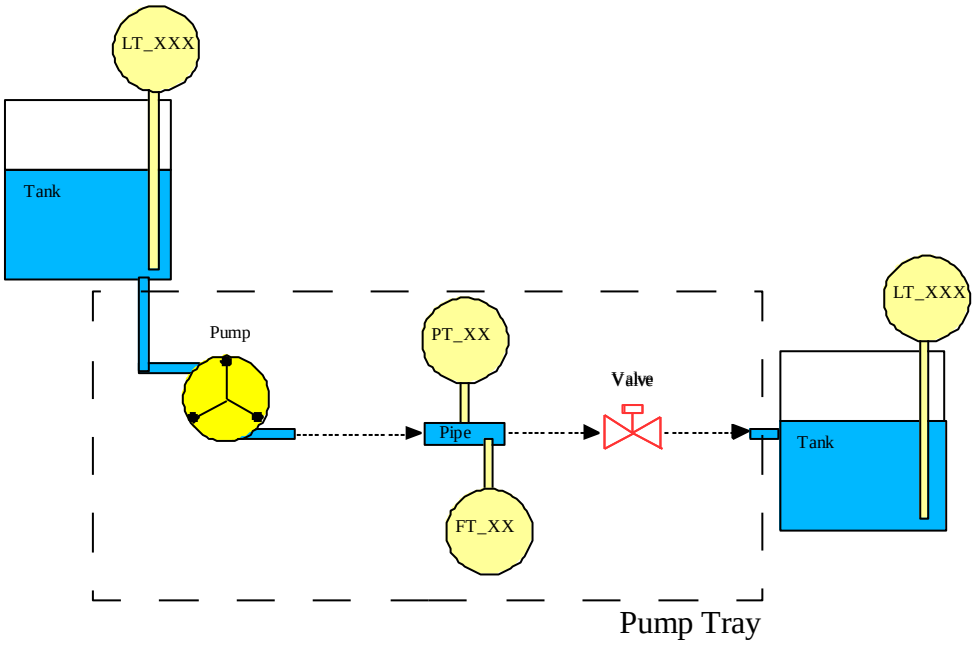

Figure 43: UAV Pump tray diagram.

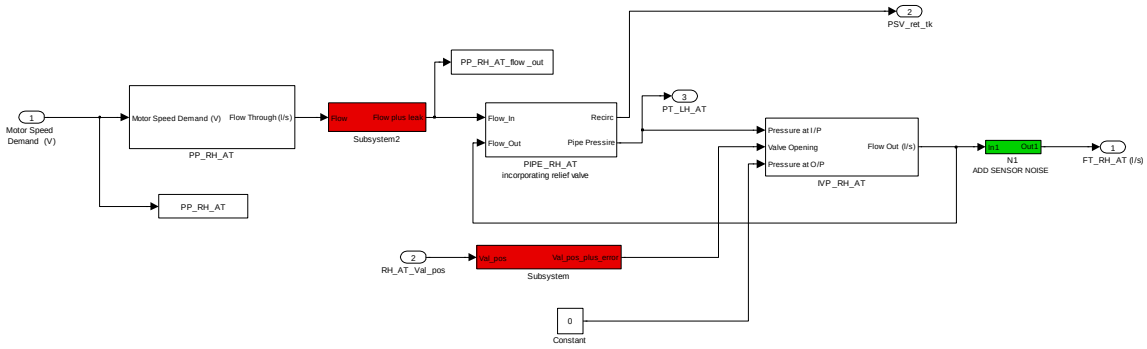

Figure 44: UAV Pump tray simulink model.

Testing of a single pump tray on its own will validate the correct operation of the pump, pipe and valve models in its complete configuration to be further used as a subsystem block in its own right for the development of the simulink model. The various physical parameters of the UAV pump tray model are given in Table 2.

Name	Description	Value (units)
E_v	Bulk modulus	2.15×10^{9} Pa
v	Specific volume (water)	1.0022×10^{-3} m^3/kg
ρ	Density (water)	997.78×10^{-4} kg/m^3
g	Acceleration due to Gravity	9.81 m/s^2
V_o	Original Volume of pipe	3.5343×10^{-4} m^3
y_v	Valve opening	1 (no units – proportional 0=>1)
c_v	Valve conductance	2.05×10^{-2} m^2

Table 2: UAV pump tray model parameters

4.8.2 Model Validation Simulation Results

The following results demonstrate the validity of the simulink model for a single pump tray as illustrated in Figure 44.

This test includes a step input to the main pump from zero to full scale output, i.e. 2.5V. The result can be seen by the rig flow sensor (Rig LH WT Flow) and the model output (Sim LH WT Flow) can be seen in Figure 45. Figure 46 shows the response of the fuel rig pressure sensor (Rig LH WT Press) and the response of the model (Sim LH WT Press). The pressure sensors are the least accurate as this is a difficult variable to measure due to the relatively low pressure levels seen on the fuel rig. (Note: This can be accommodated later, in the FDI design, by using greater Kalman feedback gains; however it also means larger thresholds need to be adopted). The last plot, Figure 47, shows the fall in left hand inner, middle and outer tanks level due to the liquid being pumped from it for the period of 0 to 60 seconds. The flow from this tank is stemmed at 60 seconds due to the 3 way valve being changed over in order to supply fuel to the other engine. Therefore the level in the tanks, between rig and model, correspond accordingly thus proving validity of the model within this functional domain.

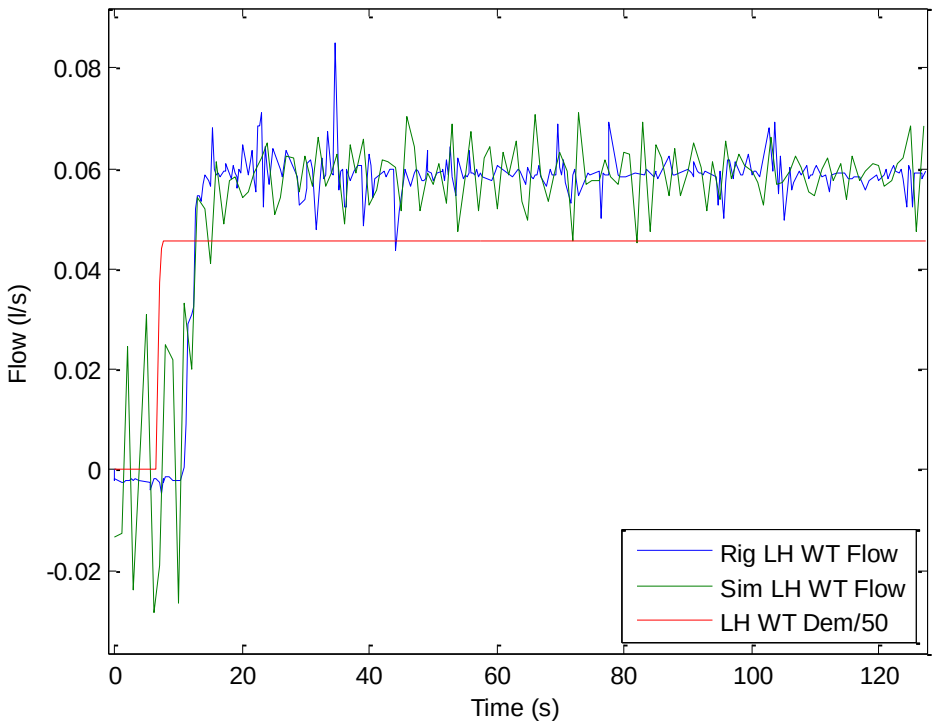

Figure 45: UAV pump tray model validation fuel flow

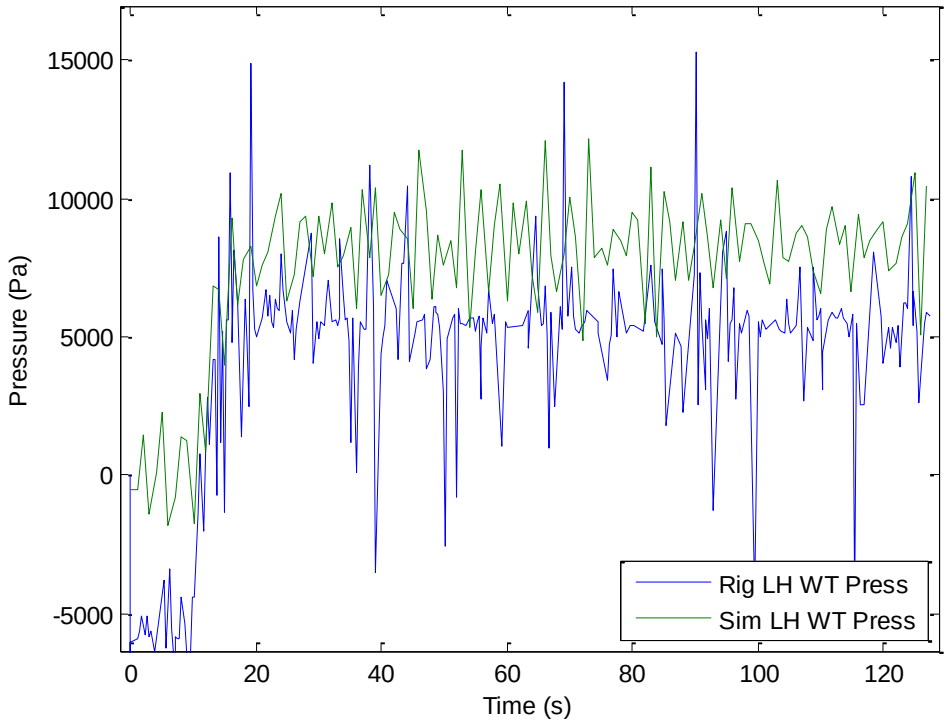

Figure 46: UAV pump tray model validation fuel pressure

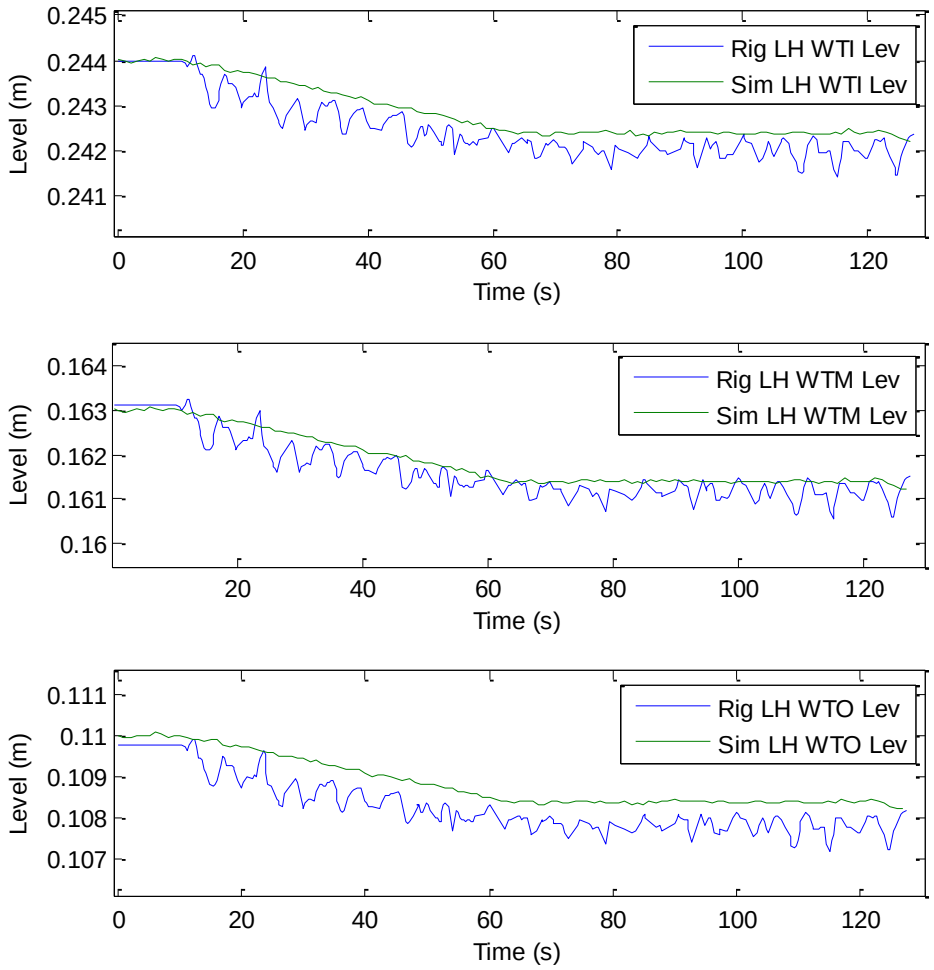

Figure 47: Left Hand Wing Tank inner (WTI), middle (WTM) and outer (WTO) levels.

4.9 UAV Fuel Rig System Model

4.9.1 Description and Model Derivation

In UAV configuration the fuel rig takes on the form as shown in Figure 48, whereby one pump supplies the right hand engine and another pump supplies the left hand engine. The right hand engine is usually fed by the right hand tank and the left hand engine by the left tank, however this is reconfigurable so that any tank can supply any pump. Further to the main left and right tanks is an auxiliary tank for each side, with a pump feed and the ability to transfer fluid from one to the other for such in flight functionality as adjusting the centre of gravity. Level, flow and pressure sensors are located as shown in Figure 48.

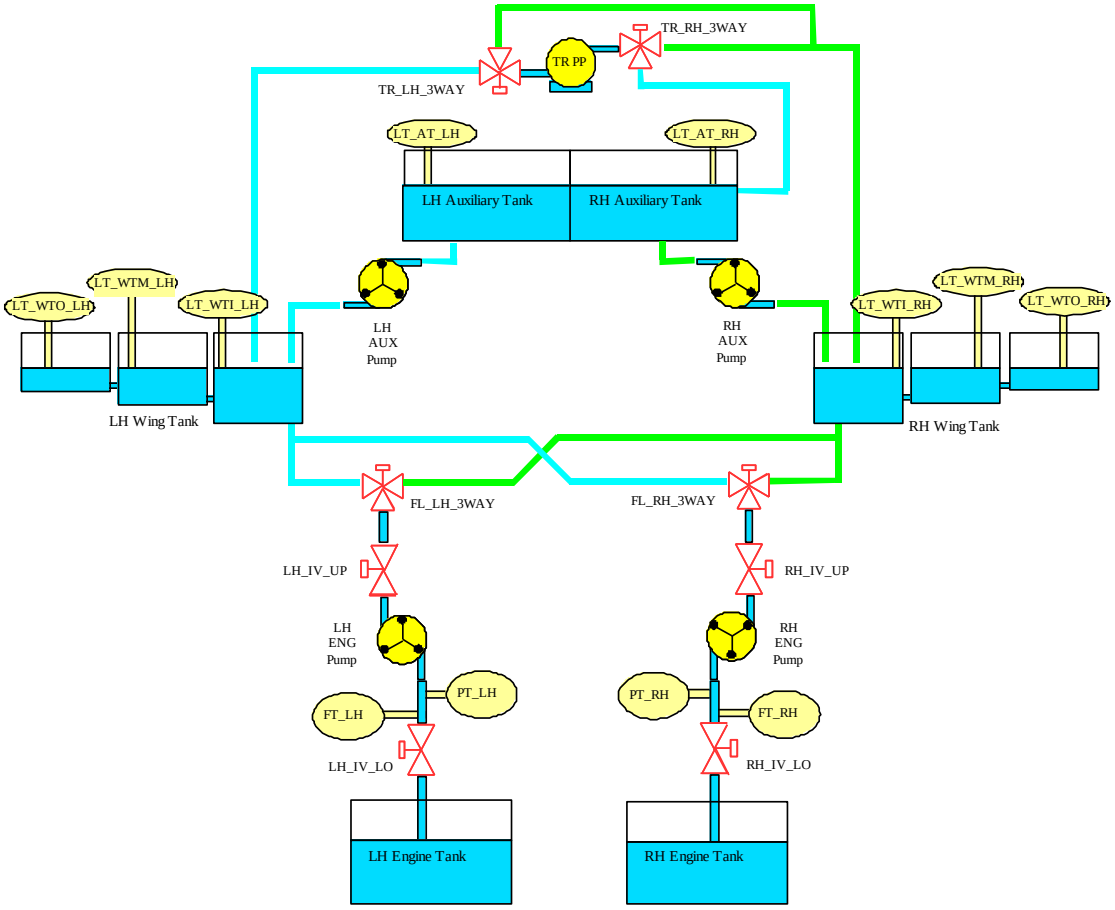

Figure 48: UAV fuel system functional diagram

This has been developed in simulink using the previously developed subsystems. Four UAV pump tray block subsystems which contain pump, pipe and valve models are connected as shown in Figure 49 below. The tanks and 3 way valve logic is also incorporated into the model. The blue blocks represent tanks, the yellows blocks represent pump trays, the grey blocks represent three way valve associated with the main fluid path and the orange block represents the transfer pump and its associated valves.

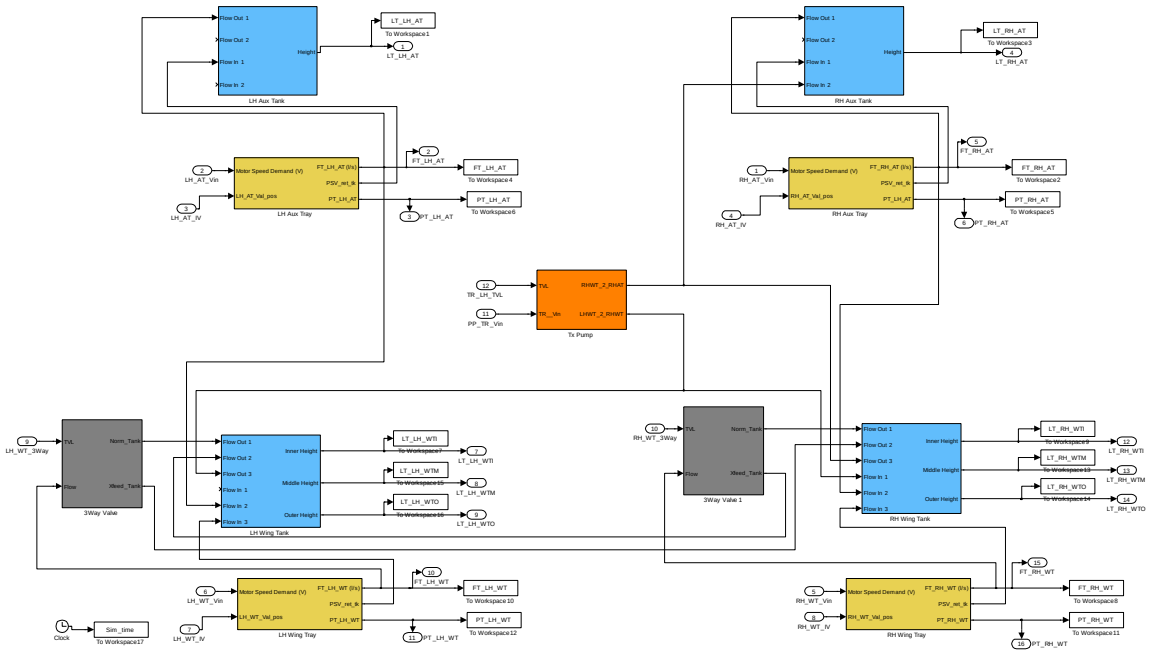

Figure 49: UAV fuel rig simulink model.

All of the variables, parameter and constants for the UAV simulink non-linear model are shown below the following tables. Table 3 shows the model inputs. Table 4 shows the model outputs. Table 5 shows the model constants. Table 6 shows the model parameters and Table 7 shows the noise input magnitudes. The noise additions are Gaussian deviation and were found empirically and proved to provide results similar to the noise seen on the fuel rig sensor outputs. The process noise is on the input of the sub-model so simulate the splashing about of fluid entering the tank, therefore is measured in l/s and is very small as it is propagated through the model to affect the output in the manner seen in the sensor.

Inputs			
Name	Description	Range	Units
CP_FL_RH	Right Hand Engine Pump Demand Voltage	0 – 2.5	V
CP_FL_LH	Left Hand Engine Pump Demand Voltage	0 – 2.5	V
CP_AT_RH	Right Hand Aux. Pump Demand Voltage	0 – 2.5	V
CP_AT_LH	Left Hand Aux. Pump Demand Voltage	0 – 2.5	V
CP_TR	Transfer Pump Demand Voltage	0 – 5	V
YV_RH_IV_UP	Valve Opening Upper RH Isolation Valve	0 – 1	-
YV_LH_IV_UP	Valve Opening Upper LH Isolation Valve	0 – 1	-
YV_RH_IV_LO	Valve Opening Lower RH Isolation Valve	0 – 1	-
YV_LH_IV_LO	Valve Opening Lower LH Isolation Valve	0 – 1	-
FL_LH_TVL	Left Hand Fuel Supply 3-way Valve	0 – 3 (Disc.)	-
FL_RH_TVL	Right Hand Fuel Supply 3-way Valve	0 – 3 (Disc.)	-
TR_LH_TVL	Left Hand Transfer Pump 3-way Valve	0 – 3 (Disc.)	-

Table 3: UAV simulink model input variables.

Outputs		
Name	Description	Units
LT_WTI_RH	Right Hand Wing Inner Tank Height	m
LT_WTM_RH	Right Hand Wing Middle Tank Height	m
LT_WTO_RH	Right Hand Wing Outer Tank Height	m
LT_WTI_LH	Left Hand Wing Inner Tank Height	m
LT_WTM_LH	Left Hand Wing Middle Tank Height	m
LT_WTO_LH	Left Hand Wing Outer Tank Height	m
LT_AT_RH	Right Hand Auxiliary Tank Height	m
LT_AT_LH	Left Hand Auxiliary Tank Height	m
PT_RH	Right Hand Pressure Transducer	Pa
PT_LH	Left Hand Pressure Transducer	Pa
FT_RH	Right Hand Flow Transducer	l/s
FT_LH	Left Hand Flow Transducer	l/s

Table 4: UAV simulink model output variables.

Model Constants (Standard Engineering Units)			
Name	Description	Value	Units
g	Acceleration due to Gravity	9.81	m/s^2
v	Specific Volume	$1.0022*10^{-3}$	m^3/kg
ρ	Density	997.78	kg/m^3
g	Acceleration due to Gravity	9.81	m/s^2
Ev	Bulk Modulus	$2.15*10^9$	Pa

Table 5: UAV simulink model constants.

Model Parameters			
Name	Description	Value	Units
K_mp_LH_WT	Gain for LH WT peristaltic pump T.F.	0.026	l/s/V
Toh_mp_LH_WT	Time constant for LH WT peristaltic pump T.F.	1	Sec
K_mp_RH_WT	Gain for RH WT peristaltic pump T.F.	0.026	l/s/V
Toh_mp_RH_WT	Time constant for RH WT peristaltic pump T.F.	1	Sec
K_mp_LH_AT	Gain for LH AT peristaltic pump T.F.	0.026	l/s/V
Toh_mp_LH_AT	Time constant for LH AT peristaltic pump T.F.	1	Sec
K_mp_RH_AT	Gain for RH AT peristaltic pump T.F.	0.026	l/s/V
Toh_mp_RH_AT	Time constant for RH AT peristaltic pump T.F.	1	Sec
K_mp_TR	Gain for transfer centrifugal pump T.F.	0.026	l/s/V
Toh_mp_TR	Time constant for transfer centrifugal pump T.F.	1	Sec
Vo_LH_WT_pipe	Starting Volume of LH WT Pipe	$3.5343*10^{-4}$ *	m^3
Vo_RH_WT_pipe	Starting Volume of RH WT Pipe	$3.5343*10^{-4}$ *	m^3
Vo_LH_AT_pipe	Starting Volume of LH AT Pipe	$3.5343*10^{-4}$ *	m^3
Vo_RH_AT_pipe	Starting Volume of RH AT Pipe	$3.5343*10^{-4}$ *	m^3
Rel_Pr_LH_WT	LH WT pressure relief valve operational limit	6e6	Pa
Rel_Pr_RH_WT	RH WT pressure relief valve operational limit	6e6	Pa
Rel_Pr_LH_AT	LH AT pressure relief valve operational limit	6e6	Pa
Rel_Pr_RH_AT	RH AT pressure relief valve operational limit	6e6	Pa
LH_WT_IV_cv	Valve Conductance of LH WT valve	$2.05*10^{-2}$	m^2
RH_WT_IV_cv	Valve Conductance of RH WT valve	$2.05*10^{-2}$	m^2
LH_AT_IV_cv	Valve Conductance of LH AT valve	$2.05*10^{-2}$	m^2
RH_AT_IV_cv	Valve Conductance of RH AT valve	$2.05*10^{-2}$	m^2
RH_WTI_area	Right Hand Inner Wing Tank Area	0.1278	m^2
RH_WTM_area	Right Hand Middle Wing Tank Area	0.1278	m^2
RH_WTO_area	Right Hand Outer Wing Tank Area	0.1278	m^2
LH_WTI_area	Left Hand Inner Wing Tank Area	0.1278	m^2
LH_WTM_area	Left Hand Middle Wing Tank Area	0.1278	m^2
LH_WTO_area	Left Hand Outer Wing Tank Area	0.1278	m^2

Table 6: UAV simulink model parameters.

Noise addition			
Name	Description	Value	Units
Tank_process_noise	Noise seen in input to tank due to ,e.g., splashing etc	1e-10	l/s
Tank_sensor_noise	Electrical noise seen on the tank level sensor	1e-9	m
Flow_sensor_noise	Electrical noise seen in the flow sensor	1e-5	l/s
Pipe_sensor_noise	Electrical noise seen in the Pressure sensor	1e5	Pa

Table 7: UAV simulink model noise parameters.

4.10 Validation of Simulink Model

In order to validate the full simulink model, as shown in Figure 49 (whole rig), the model was run alongside offline data in Matlab/ simulink environment. The tests should exercise all of the functions and prove that the simulink model corresponds to the dynamics of the fuel rig.

Testing full system functionality on top of what has already been tested is simply case of exercising all fluid flow paths by operating all motors and fluid directional control, and observing the correct corresponding action in the tank fluid level, fluid flows and pressures. This will cover the fuel rig normal operating conditions. Further control inputs are available to the fuel rig model by means of isolation valves, however, their intended use is not of normal operation but of simulation of fault injection and will be covered later.

4.10.1 Test 1

The first functional test involves exercising the main function of the fuel system, i.e. pumping fuel from the main wing tanks to the engines. At around 60 seconds the fluid path is changed by operation of the three way valve thus providing fluid supply from

the right hand wing tank only. Figure 50 shows the demand to the right hand wing tank pumps (RH WT Dem), the flow produced by this demand for both the rig and the simulink model (Rig RH WT Flow and Sim RH WT Flow) and the pressure produced by the rig and simulink model in the bottom half of these plots also (Rig RH WT Press and Sim RH WT Press). Figure 51 is similar being the result for the left hand wing tank on the fuel rig. In both left hand and right hand flow sensing the results seem good, however, some difficulty in accuracy for the pressure sensing is noticed on both sides as pressure is notably sensitive in its measurement. In theory these results should be of the same value, however one pressure sensor reads higher than expected pressure and the other slightly lower pressure therefore a best estimate is resulted in an approximation in between these two.

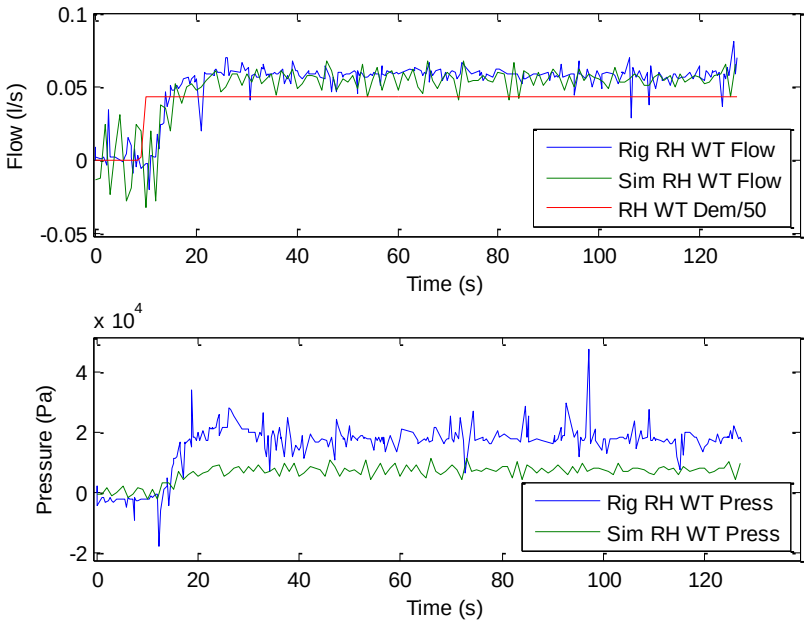

Figure 50: UAV Validation – Test 1 – RH WT Flow & Press.

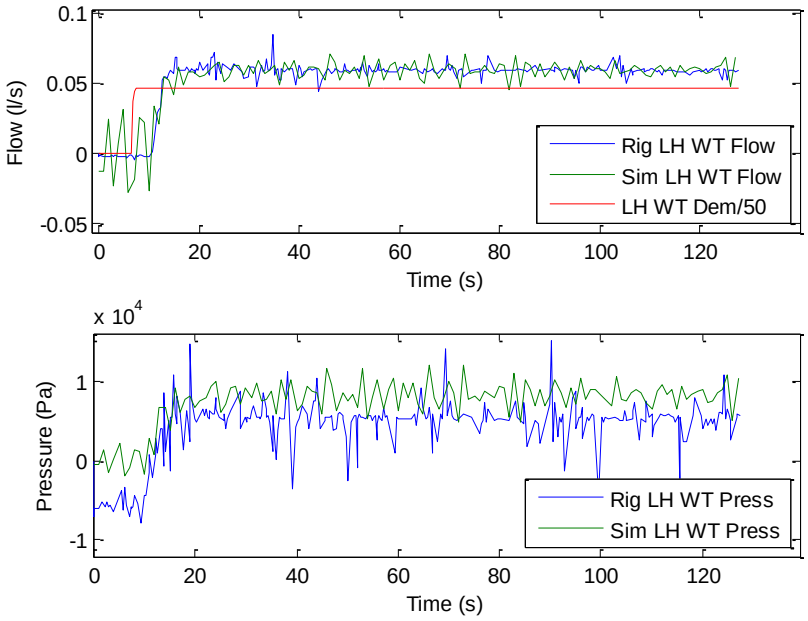

Figure 51: UAV Validation– Test 1 – LH WT Flow & Press.

Figure 52 and Figure 53 show the levels for right hand tanks and left hand tanks respectively. Each of these plots is split into three subplots representing the inner, middle and outer sub-tanks simulating the position of the tanks on the UAV. For example, the right hand wing inner tank for the fuel rig is 'Rig RH WTI Lev' and for the simulink model is 'Sim RH WTI Lev'. This is repeated throughout the plots, LH denoting left hand, WTM denoting Wing tank Middle, WTO denoting Wing tank Outer. The plots show reasonable predictions of model in comparison to the real fuel rig system.

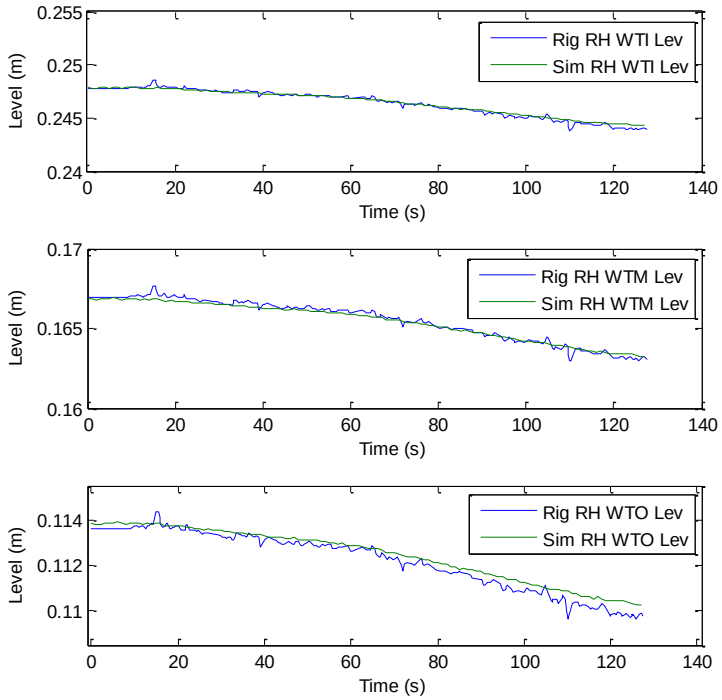

Figure 52: UAV Validation – Test 1 – Right Hand Wing Tank Levels.

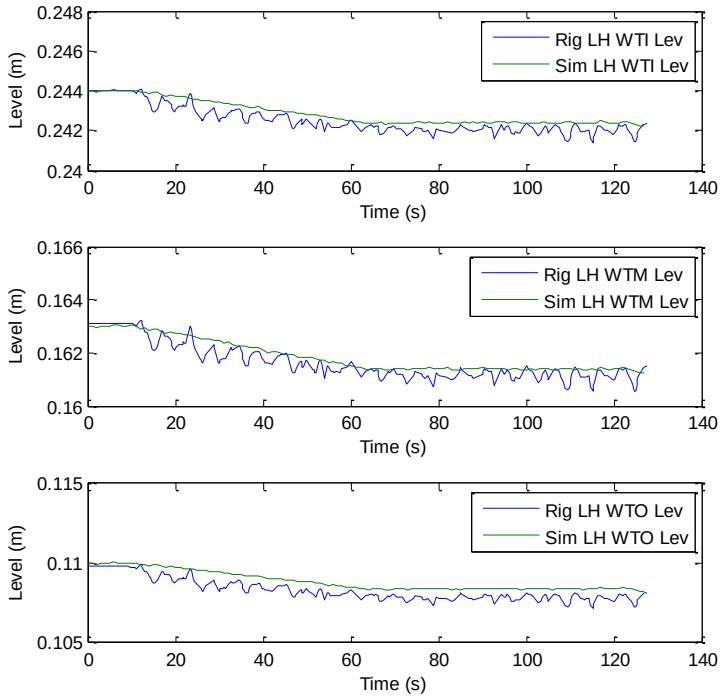

Figure 53: UAV Validation – Test 1 – Left Hand Wing Tank Levels.

4.10.2 Test 2

The second validation test for the UAV fuel rig configuration exercises the auxiliary tank paths supplying fuel to the wing tanks. Figure 54 shows the input demand (LH AT Dem) to the Left hand Auxiliary tank pumps and auxiliary tank level fuel rig (Rig LH AT Lev.) and Simulink model (Sim LH AT Lev). There are no flow or pressure sensors within this flow path, therefore correct flow has to be determined via the change in levels between tanks when this flow path is active. Figure 55 shows the corresponding left hand wing tank levels for inner (LH WTI Lev), middle (LH WTM Lev) and outer tanks (LH WTO Lev) which follow the corresponding auxiliary pump demand level reasonably well.

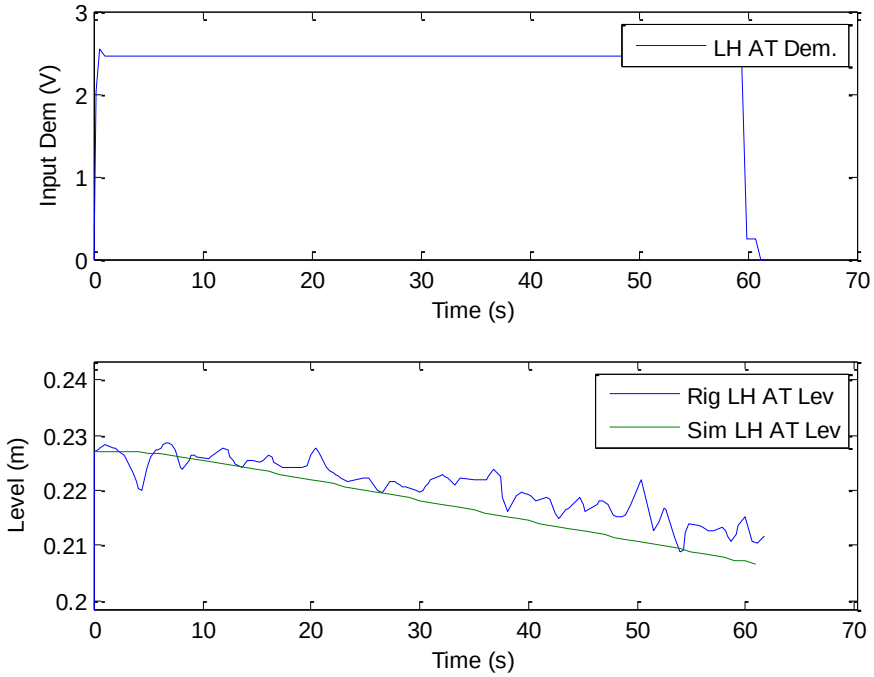

Figure 54: UAV Validation – Test 2 – Left Hand Auxiliary Pump Demand and Tank Level.

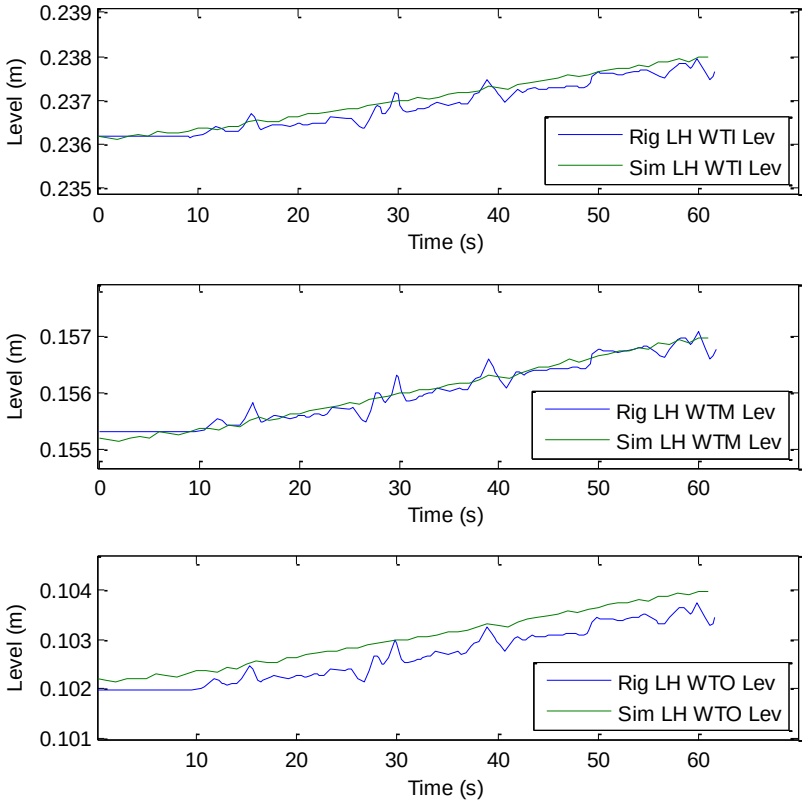

Figure 55: UAV Validation – Test 2 – Left Hand Wing Tank Level.

This validates the correct operation of the simulink model and sufficient accuracy compared to the real fuel rig.

4.11 Noise Addition

Sensor noise is added to the model signals to simulate noise physically seen on the fuel rig sensors for the purpose of developing the Kalman filter using the Simulink model as the design model application. The amplitude of the noise is estimated based on real rig results. The amplitudes of all noise in the model are shown in Table 8. Input noise signals are based on white noise signals and separate noise injection points are subject to different seed values in the simulation to avoid correlation.

Sensor type	Noise amplitude
Tank level sensor	1e-9 m
Pressure sensor	1e5 Pa
Flow sensor	1e-5 l/s

Table 8: Sensor noise addition inputs values.

4.12 Fault Injection

Simulated faults are injected into the model to simulate fault conditions for all possible rig faults. Faults that can be injected into the model include tank leak, pipe leak, pipe blockage, valve position bias and valve position stuck, pump drive voltage error, pump performance degradation, pump abrupt failure, 3-way valve position error and any sensor fault. However, this will be described in more detail in following sections.

4.13 Conclusion

This chapter has presented the model development of the subsystem level models which are used in the production of the fuel rig system level model. The subsystem models have been structured in order to allow modular implementation of system level models by interconnecting capacitative, i.e. storage devices such as pipes and tanks, to resistive model elements, such as pumps and valves. This modular design also allows quick development of further system configurations by using a series of interconnected subsystems to create an overall system model. Validation of the subsystem level models has demonstrated that they are fit for the intended purpose of creating the overall system model of the fuel rig. Finally, the model has been validated against the fuel sensor data sets during various experiments and the results indicate that the overall model fidelity is sufficient for its use as a simulation model for testing the fault detection system prior to implementation on the rig. Nonlinearities in the model are only seen in the valve flow therefore the model could be considered approximately linear and consequently the use of linear observers, Kalman filters, for fault detection is justified.

Chapter 5

Application of Fault Diagnosis to a Single Tank

As a preliminary investigation into the performance of the diagnostic algorithms a simple diagnostic method is implemented for a single fuel rig tank. The purpose of the implementation of the diagnostics is to determine the presence of a fault. In the case of a single tank the only fault to be diagnosed is a fuel leak in the tank. It is necessary to make this detection as robust as possible to eliminate the possibility of false alarms whilst being sensitive enough to detect faults. A simple steady state Kalman Filter is used to detect the faults by means of the production of a residual signal. The residual identifies the presence of a fault with its divergence from zero. Improvement in the sensitivity to faults is then applied to the residual by use of various statistical methods which are compared and evaluated.

The contributions of this chapter are application of fault detection to a real tank successfully detecting a leak and the evaluation of different methods utilised in detection of a fault to determine which offers greatest sensitivity whilst remaining robust to false alarms.

5.1 Introduction

This section will deal with a single tank to demonstrate that it is possible to diagnose leak faults and evaluate the performance of several alternative methods of residual evaluation. The model used in this evaluation is that of a simple tank. Model dynamics use a physical/ mechanistic approach. A discrete time state space model is designed and validated against the fuel rig tank. This is then used to develop the steady state Kalman Filter which produces a normally zero residual, significant divergence of which identifies the presence of a fault. The application of a range of statistical methods the Kalman Filter residual is evaluated to identify the methods offering best performance.

5.2 Description and Model Derivation

The physical dynamic model is developed using the assumptions of water being the working fluid at room temperature under atmospheric pressure.

The three tanks in the system are cubic in shape and as stated previously the working fluid is water The outlet feed to the other parts of the system is situated at the bottom of the tank as shown in Figure 56.

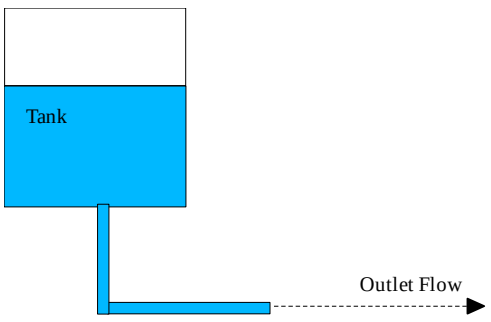

Figure 56: Diagram of a Tank.

The system subject to this investigation is a single tank of the fuel-rig with sampled dynamic inputs of volumetric flow in, $Q_{in}(k)$, and flow out, $Q_{out}(k)$, (in l/s) and the sampled output of tank level or height, *h(k)* (in m). For modelling, the main dynamics of interest are those of the fluid system, and can be represented by the linear equations for fluid height and flow rate. A simple discrete model of the tank can be defined as per Equation 12, where: cross-sectional Area = 0.1728m^2 and the flow, Q_x, in m^3/s.

$$h(k+1) - h(k) = \frac{Q_{in}(k)\Delta T}{Area} - \frac{Q_{out}(k)\Delta T}{Area} \qquad \textbf{(12)}$$

5.3 State Space Model

One of the most common modern control systems design methodologies is design in a state space form. The state space design method is inherited from the state variable method of describing differential equations. In this method the differential equations describing a dynamic system are organized as a set of first order differential equations. If a dynamic system can be described by the set of first order differential equations as seen in Equation 13.

$$\begin{aligned}
\dot{x}_1 &= a_{11}x_1 + a_{12}x_2 + \ldots + a_{1n}x_n + b_{11}u_1 + \ldots + b_{1m}u_m \\
\dot{x}_2 &= a_{21}x_1 + a_{22}x_2 + \ldots + a_{2n}x_n + b_{21}u_1 + \ldots + b_{2m}u_m \\
&\vdots \\
\dot{x}_n &= a_{n1}x_1 + a_{n2}x_2 + \ldots + a_{mn}x_n + b_{n1}u_1 + \ldots + b_{nm}u_m
\end{aligned} \qquad \textbf{(13)}$$

Then, the system can be modelled in state space form by writing this set of simultaneous differential equations in matrix form as shown in Equation 14.

$$\begin{bmatrix} \dot{x}_1 \\ \dot{x}_2 \\ \vdots \\ \dot{x}_n \end{bmatrix} = \begin{bmatrix} a_{11} & a_{12} & \dots & a_{1n} \\ a_{21} & a_{22} & \dots & a_{2n} \\ \vdots & \vdots & \vdots & \vdots \\ a_{n1} & a_{n2} & \dots & a_{nn} \end{bmatrix} \begin{bmatrix} x_1 \\ x_2 \\ \vdots \\ x_n \end{bmatrix} + \begin{bmatrix} b_{11} & \dots & b_{1m} \\ \vdots & & \vdots \\ b_{n1} & \dots & b_{nm} \end{bmatrix} \begin{bmatrix} u_1 \\ \vdots \\ u_m \end{bmatrix} \quad \textbf{(14)}$$

Which in standard compact notation of the state differential equation is as shown in Equation 15.

$$\dot{x} = Ax + Bu \quad \textbf{(15)}$$

The matrix A is an n x n square matrix and B is an n x m matrix. The state differential equation relates the rate of change of the state of the system to the state of the system and the input signals. In general the outputs of a linear system can be related to the state variables and the input signals by the output equation which is shown in Equation 16.

$$y = Cx + Du \quad \textbf{(16)}$$

Where y is the set of output signals expressed in column vector form.

Notation for a discrete time state space system is shown below in Equation 17 and Equation 18 whereby ‘k’ denotes the sample time.

$$\mathbf{x}_{k+1} = \mathbf{A}\mathbf{x}_k + \mathbf{B}\mathbf{u}_k \quad \textbf{(17)}$$

$$y_{k+1} = \mathbf{C}\mathbf{x}_{k+1} + \mathbf{D}\mathbf{u}_{k+1} \quad \textbf{(18)}$$

As previously mentioned the system subject to this investigation is a single tank of the fuel-rig with sampled dynamic inputs of volumetric flow in, $Q_{\text{in}}(k)$, and flow out, $Q_{\text{out}}(k)$, (in l/s) and the sampled output of tank level or height, $h(k)$ (in m). For

modelling, the main dynamics of interest are those of the fluid system, and can be represented by the linear equations for fluid height and flow rate. A simple discrete model of the tank can be defined as per Equation 19, where: cross-sectional Area = $0.1728m^2$, the flow, Q_x, in m^3/s and $\Delta T = 0.1$ seconds. This is re-written in state-space form as described previously and shown in Equation 20, with the measurement equation as shown in Equation 21.

Also, Γ, the process noise, which is the effect of all system disturbances, modelling errors and so on is shown in Equation 20 and υ, the measurement noise representing the sensor noise and discretisation errors are shown in Equation 21 and these represent the total noise seen in the system.

$$h(k+1) - h(k) = \frac{Q_{in}(k)\Delta T}{Area} - \frac{Q_{out}(k)\Delta T}{Area} \quad \textbf{(19)}$$

$$\mathbf{x}_{k+1} = \mathbf{A}\mathbf{x}_k + \mathbf{B}\mathbf{u}_k + \Gamma_k \quad \textbf{(20)}$$

$$y_{k+1} = \mathbf{C}\mathbf{x}_{k+1} + \mathbf{D}\mathbf{u}_{k+1} + v_{k+1} \quad \textbf{(21)}$$

The state vector $\boldsymbol{x}_k$, the input vector, u_k, and the state, input, observation, and feed-forward matrices, A, B, C and D respectively are shown below in Equation 22 to Equation 27.

$$x_k = \begin{bmatrix} h_k \end{bmatrix} \quad \textbf{(22)}$$

$$u_k = \begin{bmatrix} Q_{in}(k) & Q_{out}(k) \end{bmatrix}^T \quad \textbf{(23)}$$

$$A = \begin{bmatrix} 1 \end{bmatrix} \quad \textbf{(24)}$$

$$B = \begin{bmatrix} \Delta T / A & -\Delta T / A \end{bmatrix} \quad \textbf{(25)}$$

$$C = \begin{bmatrix} 1 \end{bmatrix} \quad \textbf{(26)}$$

$$D = \begin{bmatrix} 0 & 0 \end{bmatrix} \quad \textbf{(27)}$$

The state space system can be modelled in simulink using the block layout shown in Figure 57.

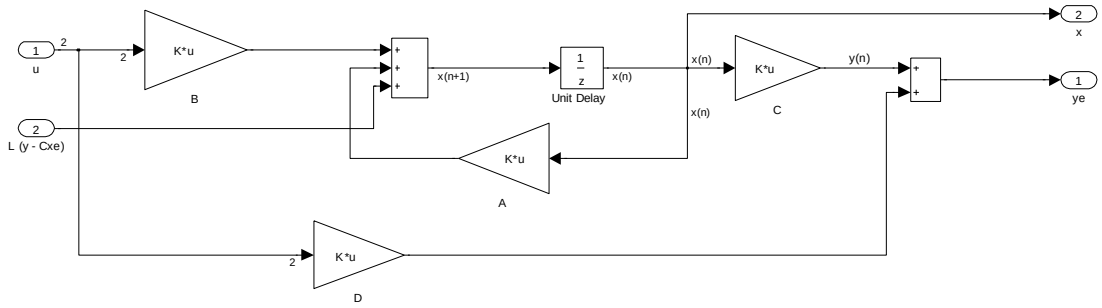

Figure 57: Discrete time state space model implementation in simulink.

5.4 Model validation

The model has been validated against real rig data by means of a direct comparison of the model and real rig data imported into the Matlab workspace. The results shown below in Figure 58 shows the flow from tank and Figure 59 shows the tank level on the fuel rig and the simulation tank level. As can be seen on the plots the function of the model is ascertained by this test. The noise seen in Figure 59 is that of quantisation error seen on the fuel rig height sensor. A number of different inputs were tested for validity and successful results achieved however addition results have been omitted for brevity.

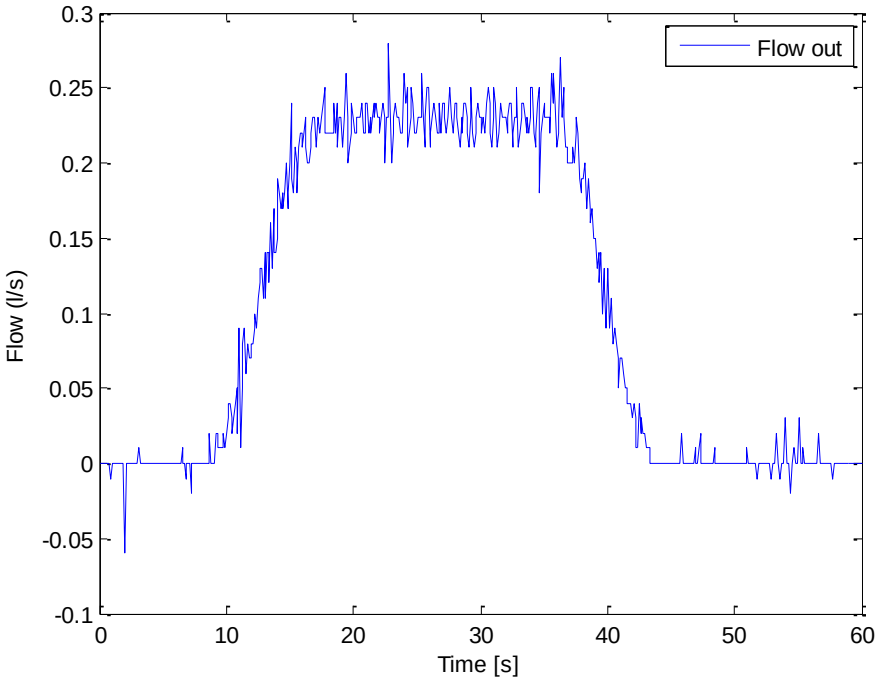

Figure 58: Fuel rig flow out of tank for validation of tank model.

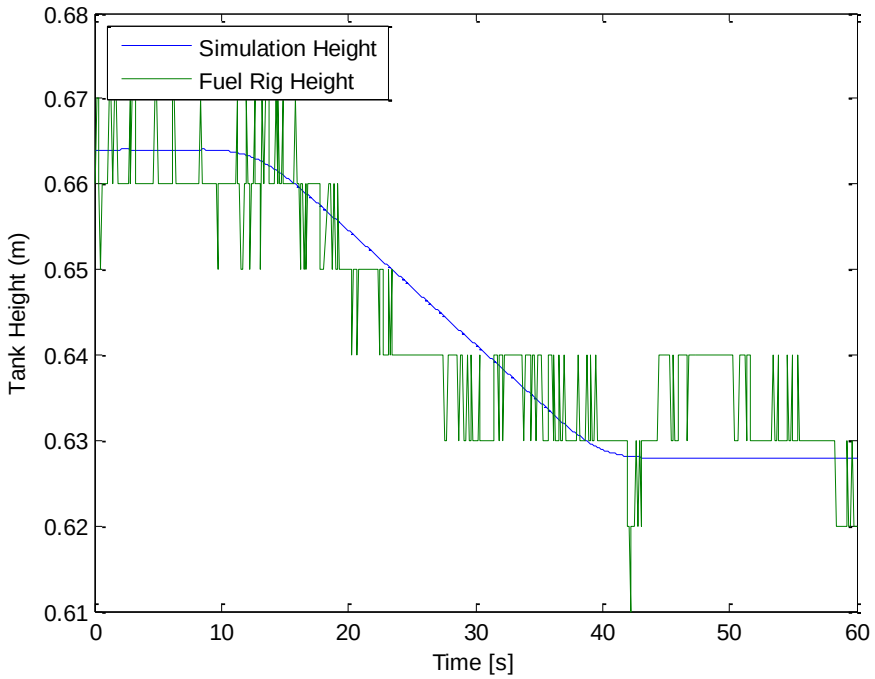

Figure 59: Fuel rig and simulated tank height for validation of tank model.

5.5 Kalman Filter Development

A steady state Kalman filter can be developed based on the state space model shown in Equation 28 below. From Equation 28, 'L' is the Kalman gain which in the part of the development is calculated based on known or estimated process and measurement noise. This is calculated by use of the riccati equation for steady state computation of the Kalman filter gain matrix within the Matlab mathematical modelling environment.

For the case of the single tank the kalman filter parameters on which Matlab uses to calculate the kalman filter gain are a process noise covariance, Q_n = 1e-8, and a measurement noise covariance, R_n = 1e-1, giving, L = 1.83e-1. This produced excellent practical results on the rig. With higher Kalman filter gain the faulty signals are tracked which would be incorrect as the faults will be masked. In the instance of a fault condition divergence of sensor data and Kalman estimation should occur. With too little Kalman filter gain the system becomes only representative of the open loop model therefore in the instance of small process drift or model errors, for example, divergence would occur incorrectly indicating the presence of a fault. The output equation shown in Equation 29 produces the prediction of the output of the system.

$$\hat{\mathbf{x}}_{k+1/k+1} = \mathbf{A}\hat{\mathbf{x}}_{k/k} + \mathbf{B}\mathbf{u}_k + \mathbf{L}(\hat{y}_{k+1} - Cx_{k+1/k}) \quad \textbf{(28)}$$

$$\hat{y}_{k+1/k+1} = \mathbf{C}\mathbf{x}_{k+1/k+1} \quad \textbf{(29)}$$

A block diagram of this arrangement is shown below in Figure 60.

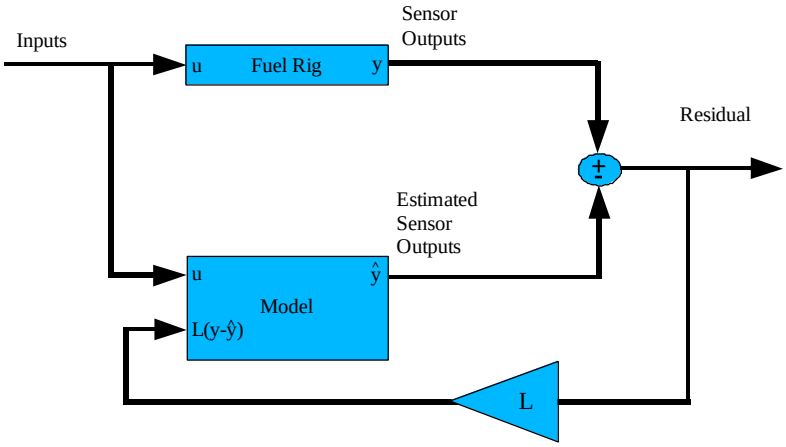

Figure 60: Diagram of Steady State Kalman filter.

The Kalman filter implemented in Simulink is shown below in Figure 61.

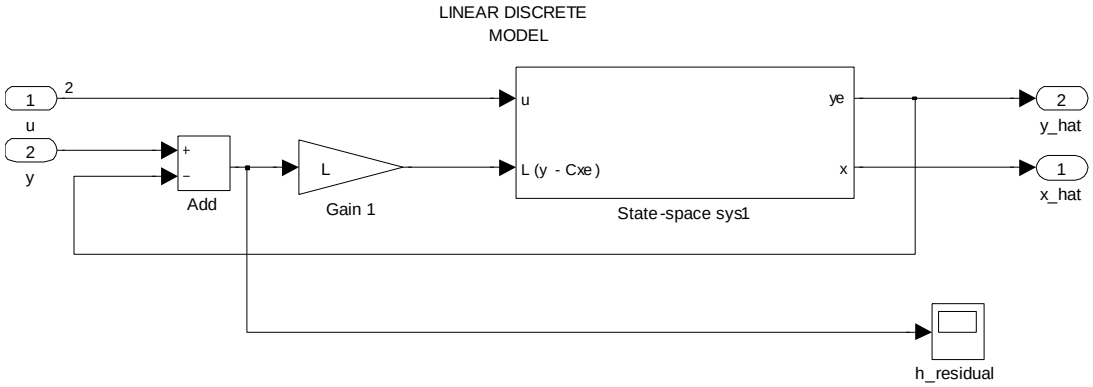

Figure 61: Diagram of Kalman filter in Simulink.

The difference between the observed output, $\hat{y}$, and the system output, y , is known as the residual, see Equation 30 and Figure 60. Ideally this is a zero mean white noise signal when the system is in a "healthy" state. Hence significant deviations in the signal properties can be used to indicate a fault.

$$R = y - \hat{y} \qquad \textbf{(30)}$$

For abnormal conditions to be identified the residual value has to exceed a predetermined value, i.e. a threshold. The threshold value can be determined in a number of ways. Heuristically determined thresholds are common and rely on human judgement via examination of the system. Statistical calculation of fixed thresholds based on a statistical function of known good data is also possible, as are adaptive thresholds which can change to accommodate changes in the system. In the following example a fixed statistically calculated threshold has been calculated.

5.6 Kalman Filter Results

Four separate tests were carried out on the fuel rig in order to collect data for the analysis. First, in the fault free case; secondly a leak flow of 1.03 l/s injected at 35.5 seconds, thirdly a smaller leak of 0.42 l/s at 44.1 seconds and, finally, 0.22 l/s at 50.1 seconds. The aim of the latter three tests is to see if the performance is similar across a range of fault magnitudes.

The Kalman filter described previously is applied to the system in order to examine the performance of the Kalman filter with respect to identifying the faults. All tests are carry out using a volume of fluid in the tank equal to around 200-300 litres. Therefore the tank would empty in 200-300 seconds at the highest flow leak rate and around 1000 seconds at the slowest flow leak rate.

Below in Table 9 are the results for the three varying leak flow rates under test. The time to detect the fault is shown and also the fluid lost in the system before the fault is detected. The fluid lost is also included in the table as it gives a realistic and meaningful comparison between different fault magnitudes. A graph of the Kalman filter residual results for a leak flow rate of 0.42 l/s is shown in Figure 62. The results in Table 9 show good detection of the faults. For low magnitude faults the total fluid lost is similar to that of high magnitude faults, whereas there seems to be peak fluid loss at around fluid loss rates of 0.42 l/s.

Leak Flow Rate (l/s)	Time To Fault Detection (s)	Total Fluid Lost (l)
1.04	8.0	8.29
0.42	25.3	10.71
0.22	26.8	5.95

Table 9: Fault detection results for KF.

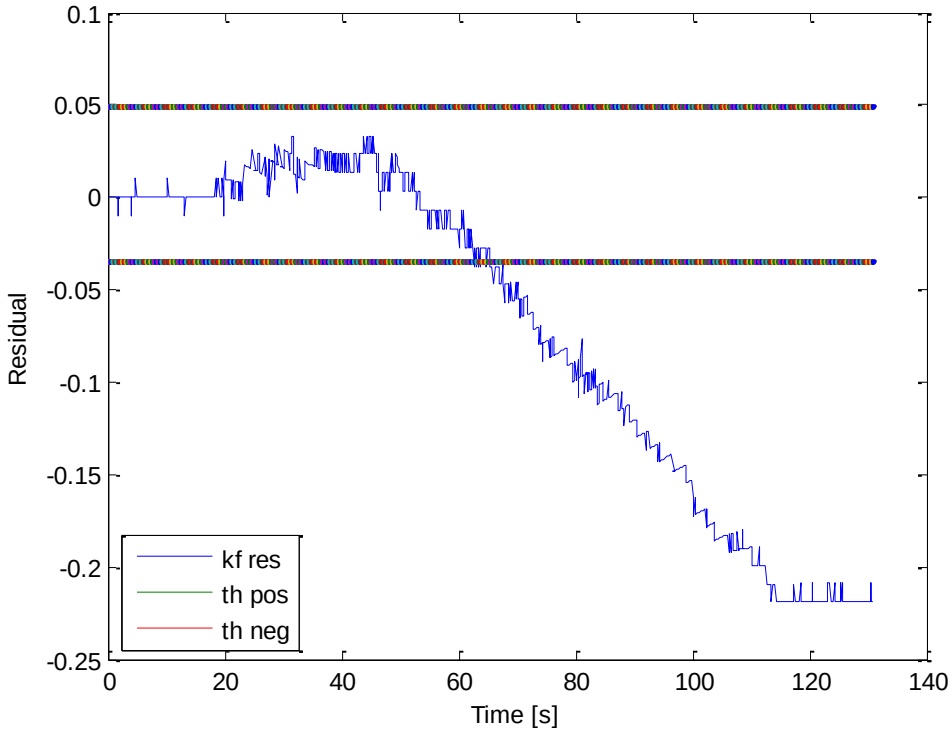

Figure 62: KF residual showing fault at t=44.1 s.

5.7 Statistical Residual Evaluation

Coupled with the ability to create a residual is the requirement of additional filtering to increase the ability to detect a fault and to eliminate the sensitivity to erroneous

false fault conditions. This has been achieved by the inclusion of a statistical based residual evaluation. This means that the residual is subjected to further processing albeit not very much. In this section the rig is used to test detection of a leak from a single tank, using a Kalman Filter and several different residual evaluation methods. The aim is to make a recommendation as to which residual evaluation approach offers the greatest performance. The methods considered are: mean deviation (MD), mean absolute deviation (MAD), sum of square error (SSE), weighted sum of square error (WSSE), root mean square error (RMSE), paired-t test, chi-square mean (χ^2-mean) and R-square (R^2). These different methods are described in sections 5.7.1 to 5.7.9. The overall results are summarised in section 5.8.

Each of the different evaluation methods is applied with sample windows of N=5, N=10, N=20, N=40, N=80, N=160 in order to get an impression of the most appropriate window size for the different methods.

Although other methods exist such as adaptive threshold theory (Chen and Patton, 1999), (Frank and Ding, 1997) and Sequential Probability Ratio testing (Granger et al., 1995), (Piatyszek et al., 2000). These methods are not demonstrated here as they were judged to be beyond the scope of this study.

In order to evaluate the different methods on a fair basis it was necessary to remove the vagaries and potential bias generated by the manual tuning of threshold levels. This was achieved by calculating the threshold levels based on the standard deviation of the residual (or evaluated residual). For example, the threshold for the Kalman filter was calculated on the basis of ±5 standard deviations from the mean over a known good data set (i.e., with no faults present). A representation of a typical set of residual data is shown in Figure 63, where the mean, $\mu=0$ and standard deviation, σ = 0.00734. The unit of standard deviation covers 68.2% of the distribution, i.e. ±34.1%. This leads to 5 x σ thresholds positioned at ±0.0367. This method provides automatic threshold calculation based on a known good data set and allows good fault detection even at low fault injection magnitudes producing minimal erroneous faults during testing. As an example of calculating the threshold for SSE, the threshold for SSE at a

sample window size of N = 80 is calculated by taking the sum square over 80 samples of the Kalman filter threshold.

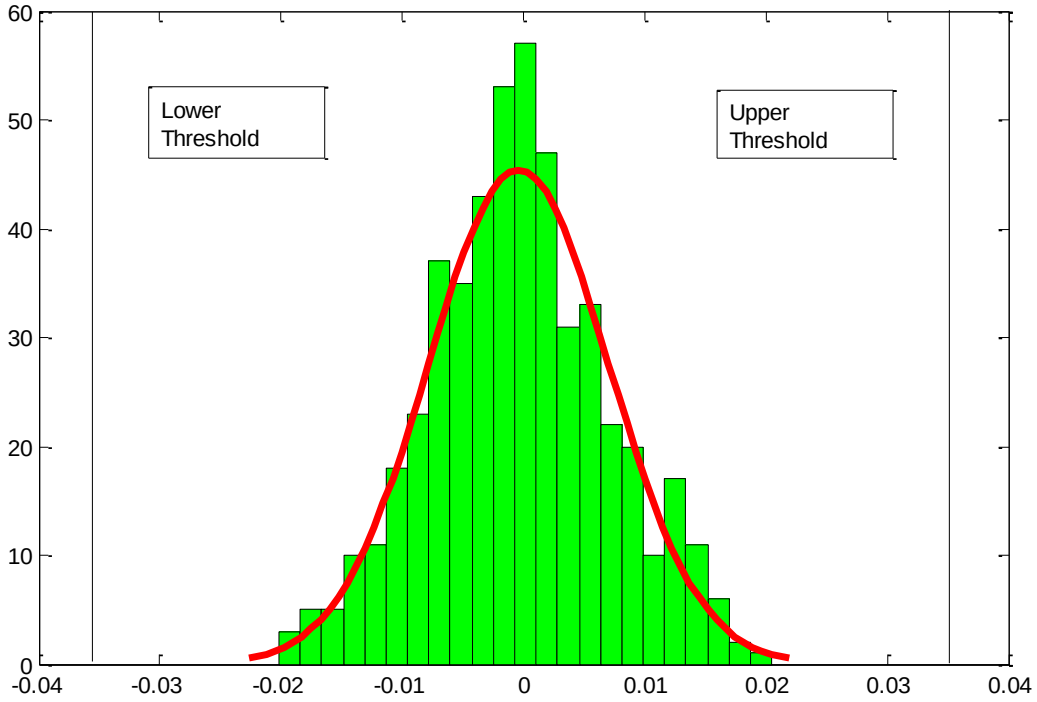

Figure 63: Histogram showing threshold calculation

5.7.1 Summed Square of Errors

The sum square of errors (SSE) is the sum of the square of the residual over a moving sample window, as shown in Equation 31.

$$SSE = \sum_{i=k-N+1}^{k} (y_i - \hat{y}_i)^2 \qquad \textbf{(31)}$$

Figure 64 shows the plot of the SSE of the residual over a moving window of N = 40 samples for a leak flow rate of 1.03l/s. The addition of SSE statistic to the Kalman filter residual offers marginally faster fault detection over use of the Kalman filter

alone at small sample window size and high fault magnitude. However, the method offers some delay, in terms of detection time, in all other cases. The time to detect the fault increases with greater moving window sample size, N, as a moving average provides low pass filtering, the larger the sample size, the lower the pass band. This will be used as the benchmark test for comparison to the other statistical methods in order to determine which offers the best performance. The full results from the addition of the SSE statistic are shown below in Table 10 below.

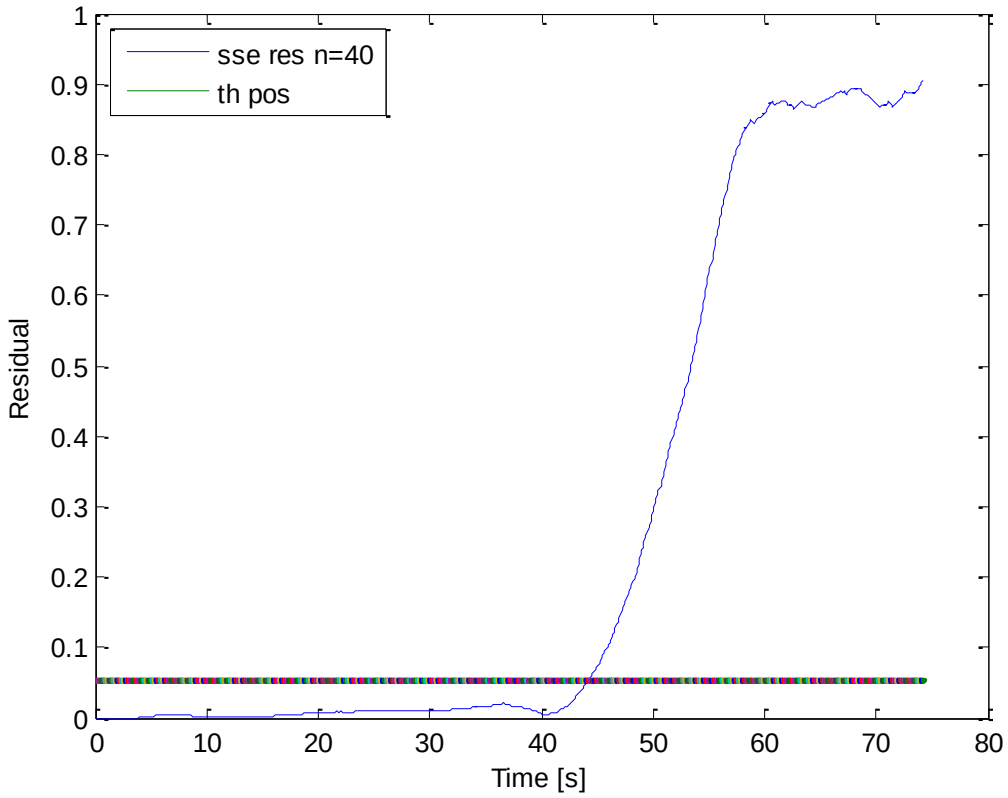

Figure 64: SSE evaluation for Leak Flow Rate = 1.03 l/s (N=40).

	SSE					
	LFR = 1.0366 l/s		LFR = 0.4231 l/s		LFR = 0.2219 l/s	
N	Time to Fault Detection (s)	Total Fluid Loss Before Detection (l)	Time to Fault Detection (s)	Total Fluid Loss Before Detection (l)	Time to Fault Detection (s)	Total Fluid Loss Before Detection (l)
5	7.8	8.09	25.2	10.66	27.3	6.06
10	8.1	8.40	25.2	10.66	27.5	6.10
20	8.7	9.02	25.9	10.96	27.7	6.15
40	9.4	9.74	27.1	11.47	28.3	6.28
80	11.0	11.40	29.1	12.31	30.8	6.83
160	12.5	12.96	32.1	13.58	34.6	7.68

Table 10: Fault detection results for SSE.

5.7.2 Mean Deviation

The mean deviation is one of the most common measures of systematic deviation and is simply the mean of the residual over a moving window. It is calculated as shown in Equation 32.

$$MD = \frac{\sum_{i=k-N+1}^{k} (y_i - \hat{y}_i)}{N} \quad \textbf{(32)}$$

Below, in Figure 65, the plot of mean deviation of the residual is shown for 0.22 l/s leak flow rate for sample window of N=5. It is worth noting the greater noise seen with a small sample window size as is illustrated in this plot.

Like the Kalman filter residual this retains the direction of fault which in the realm of diagnostics may aid the identification of the cause of fault although this will not be examined here. The mean deviation results, shown in Table 11 below, show that, as with SSE, there is marginally faster fault detection over use of the Kalman filter alone at small sample window size and high fault magnitude. However, there is some delay,

in terms of detection time, in all other cases and greater delay generally when compared to SSE.

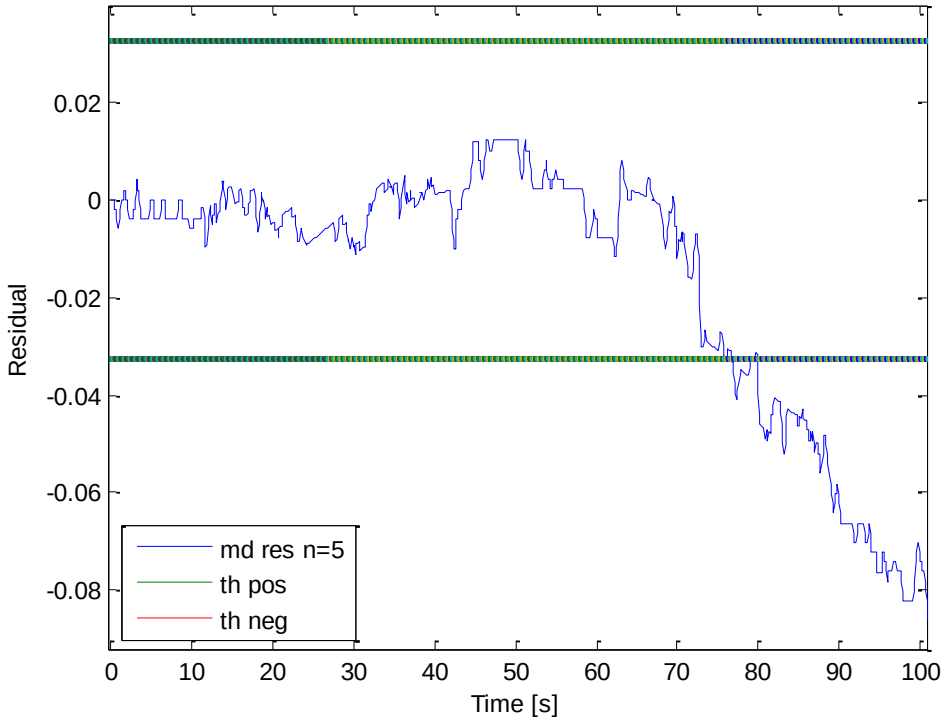

Figure 65: MD evaluation for Leak Flow Rate = 0.22 l/s (N=5).

	MD					
	LFR = 1.0366 l/s		LFR = 0.4231 l/s		LFR = 0.2219 l/s	
N	Time to Fault Detection (s)	Total Fluid Loss Before Detection (l)	Time to Fault Detection (s)	Total Fluid Loss Before Detection (l)	Time to Fault Detection (s)	Total Fluid Loss Before Detection (l)
5	7.8	8.09	25.2	10.66	27.3	6.06
10	8.2	8.50	25.3	10.71	27.5	6.10
20	8.7	9.02	26.0	11.00	27.8	6.17
40	9.7	10.06	27.2	11.51	28.6	6.35
80	11.8	12.23	29.4	12.44	31.0	6.88
160	15.8	16.38	33.1	14.01	36.1	8.01

Table 11: Fault detection results for MD.

5.7.3 Mean Absolute Deviation

The mean absolute deviation is the modulus of the MD and is calculated as in Equation 33.

$$MAD = \frac{\sum_{i=k-N+1}^{k} |y_i - \hat{y}_i|}{N} \quad \textbf{(33)}$$

The results for MAD, are quite similar to that of MD, albeit unidirectional. Figure 66 shows the MAD of the residual for a leak flow rate of 1.03 l/s for N=160 samples. Additional smoothing of the waveform can be seen over this longer sample window over that seen in previous plots for lesser number of samples. This additional smoothing, with thresholds set based on the standard deviation, causes a "tighter" set of threshold bounds, although the large sample window also causes a lag in the resultant waveform adding time to the fault detection. The results for MAD are shown below in Table 12 producing almost identical results to MD.

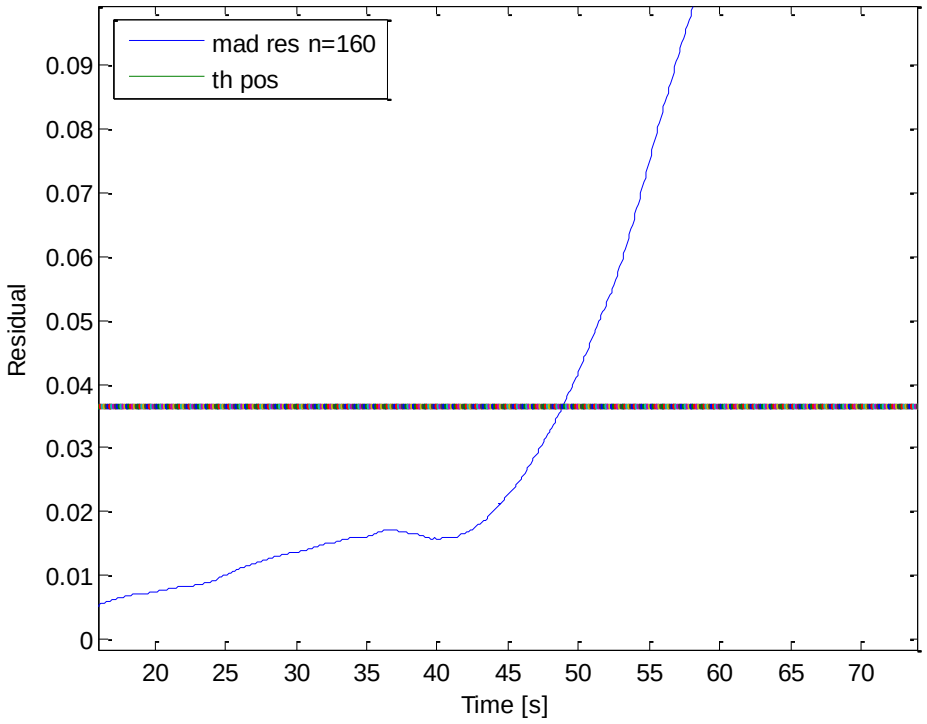

Figure 66: MAD evaluation for Leak Flow Rate = 1.03 l/s (N=160).

	MAD					
	LFR = 1.0366 l/s		LFR = 0.4231 l/s		LFR = 0.2219 l/s	
N	Time to Fault Detection (s)	Total Fluid Loss Before Detection (l)	Time to Fault Detection (s)	Total Fluid Loss Before Detection (l)	Time to Fault Detection (s)	Total Fluid Loss Before Detection (l)
5	7.8	8.09	25.2	10.66	27.3	6.06
10	8.2	8.50	25.3	10.71	27.5	6.10
20	8.7	9.02	26.0	11.00	27.8	6.17
40	9.7	10.06	27.2	11.51	28.6	6.35
80	11.8	12.23	29.4	12.44	31.0	6.88
160	14.2	14.72	33.1	14.01	36.1	8.01

Table 12: Fault detection results for MAD.

5.7.4 Mean Square of Errors

The mean square error (MSE) is a statistic based on the mean of the squared error and is calculated as shown in Equation 34.

$$MSE = \frac{\sum_{i=k-N+1}^{k} (y_i - \hat{y}_i)^2}{N} \quad \textbf{(34)}$$

Comparison of Equation 23 and Equation 20 reveals that the MSE is simply the SSE divided by the window size, N. Not surprisingly, the results (in terms of detection times) are identical to those of SSE in Table 10. For this reason the results are not repeated here.

5.7.5 Root Mean Square of Errors

The root mean square error (RMSE) is calculated as shown in Equation 35.

$$RMSE = \sqrt{\frac{\sum_{i=k-N+1}^{k} (y_i - \hat{y}_i)^2}{N}} \quad \textbf{(35)}$$

Essentially the RMSE is the square root of MSE. In Figure 67 the plot of the RMSE of the residual is shown over a moving window of N = 20 samples for a leak flow rate of 0.42 l/s. The addition of the RMSE statistic to the Kalman filter residual provides an improvement over the SSE statistic all round in terms of fault detection time as shown in Table 13.

It offers improvement over the use of Kalman filter alone up to N = 20 for LFR = 1.03 l/s and 0.42 l/s and for all sample window sizes at a LFR = 0.22 l/s under test.

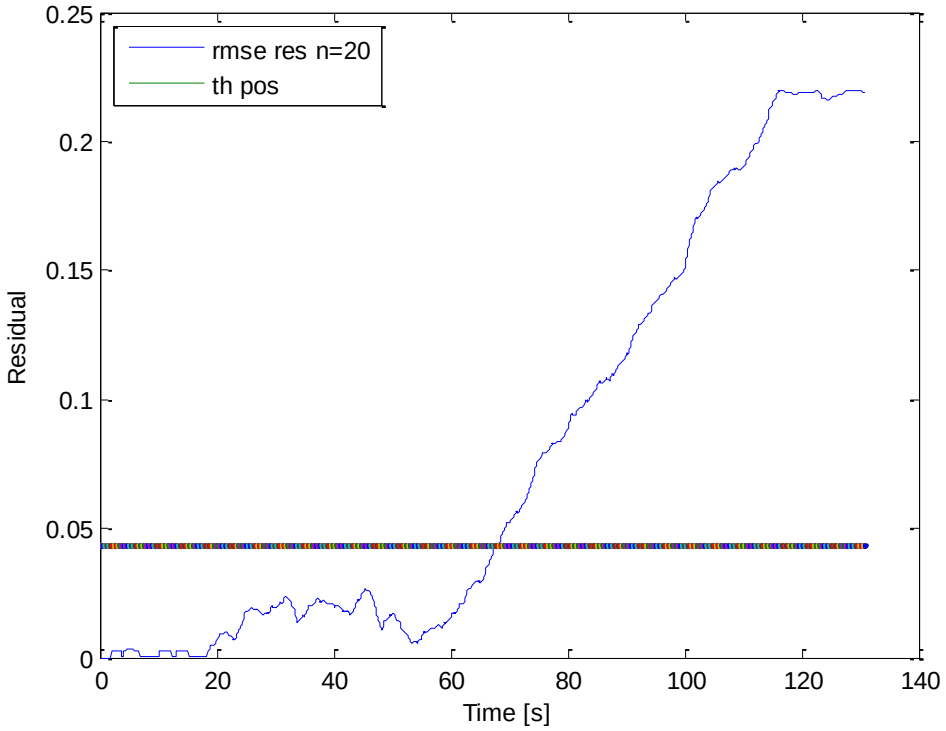

Figure 67: RMSE evaluation for Leak Flow Rate = 0.42 l/s (N=20).

	RMSE					
	LFR = 1.0366 l/s		LFR = 0.4231 l/s		LFR = 0.2219 l/s	
N	Time to Fault Detection (s)	Total Fluid Loss Before Detection (l)	Time to Fault Detection (s)	Total Fluid Loss Before Detection (l)	Time to Fault Detection (s)	Total Fluid Loss Before Detection (l)
5	7.4	7.67	24.4	10.33	23.3	5.17
10	7.4	7.67	24.3	10.28	22.6	5.01
20	7.8	8.09	24.4	10.33	22.5	4.99
40	8.6	8.92	25.3	10.71	23.4	5.19
80	10.0	10.37	26.9	11.38	24.0	5.33
160	11.6	12.03	29.1	12.31	26.0	5.77

Table 13: Fault detection results for RMSE.

5.7.6 Paired T-Test

The paired t-test is shown below in Equation 36 and Equation 37. The paired-t test follows a t-distribution and the resultant is usually compared to critical values from a table. However, for the purpose of maintaining fairness it is based on the calculation previously outlined.

$$s_d^{\,2} = \frac{\sum_{i=k-N+1}^{k} ((y_i - \hat{y}_i) - (\overline{y_i - \hat{y}_i}))^2}{N-1} \quad \textbf{(36)}$$

$$|t| = \frac{|y_i - \hat{y}_i|}{s_d^{\,2}/N} \quad \textbf{(37)}$$

Below, in Figure 68, the plot of the paired-t test of the residual is shown over a moving window of N = 40 samples for a leak flow rate of 1.03 l/s. The addition of the paired-t test statistic to the Kalman filter residual results in delayed detection time at smaller leak flow rates However, it offers a slightly faster detection time at high leak flow rates. The results for paired-t test are shown in Table 14.

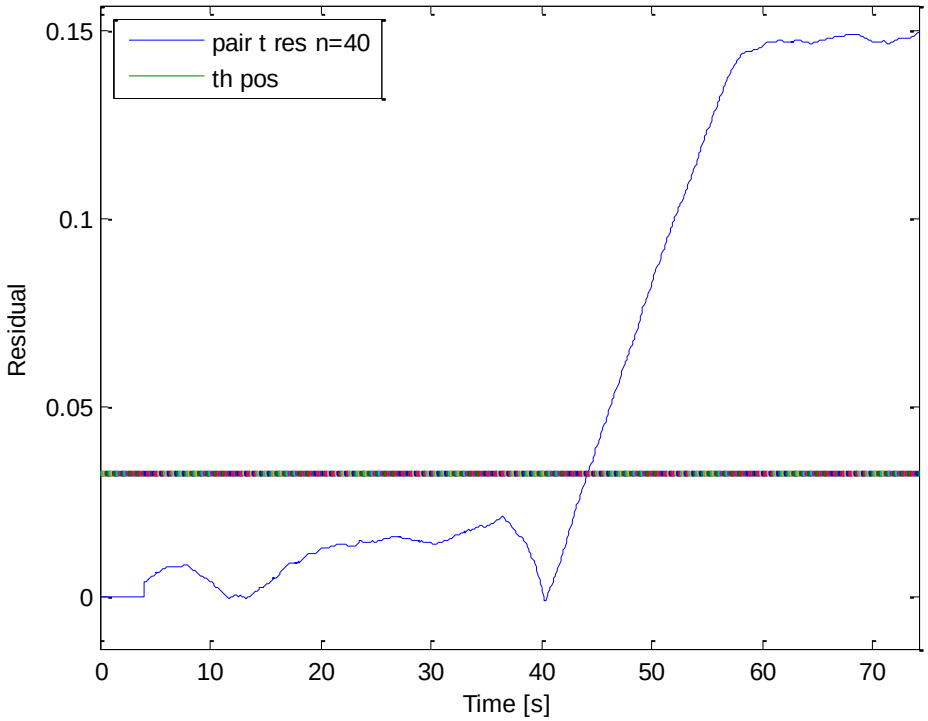

Figure 68: Paired t-test for Leak Flow Rate = 1.03 l/s (N=40).

	PAIRED T-TEST					
	LFR = 1.0366 l/s		LFR = 0.4231 l/s		LFR = 0.2219 l/s	
N	Time to Fault Detection (s)	Total Fluid Loss Before Detection (l)	Time to Fault Detection (s)	Total Fluid Loss Before Detection (l)	Time to Fault Detection (s)	Total Fluid Loss Before Detection (l)
5	7.7	7.98	22.2	9.39	27.3	6.06
10	8.0	8.29	22.5	9.52	27.8	6.17
20	8.3	8.60	22.8	9.65	27.9	6.19
40	9.4	9.74	23.6	9.99	29.1	6.46
80	11.6	12.03	25.3	10.71	31.1	6.90
160	15.6	16.17	29.0	12.27	36.5	8.10

Table 14: Fault detection results for Paired t-test.

5.7.7 Chi-Square Mean

The chi-square mean is calculated by the observed signal minus the expected value squared and summed over a moving window and divided by the expected value as shown in Equation 38.

$$\chi^2 = \frac{\sum_{i=k-N+1}^{k} (y_i - \hat{y}_i)^2}{\hat{y}_i} \quad \textbf{(38)}$$

Figure 69 shows the plot of the chi-square mean of the residual for a sample window size of N=40 for a leak flow rate of 0.42 l/s. Compared to SSE, chi-square mean offers similar fault detection speeds at smaller sample window sizes but faster fault detection at large sample window sizes as shown in Table 15.

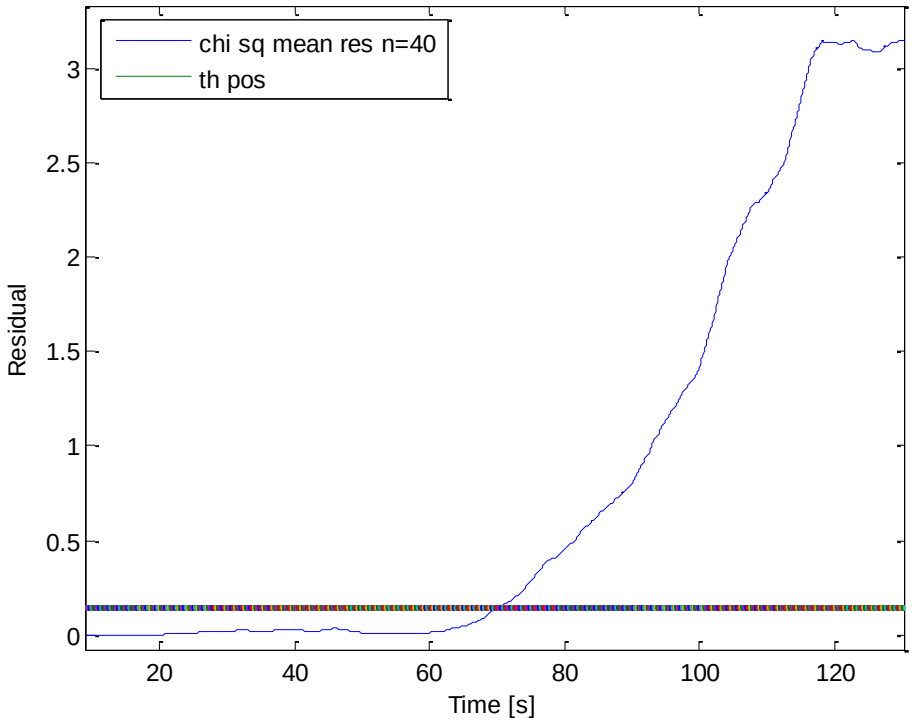

Figure 69: Chi-square for Leak Flow Rate = 0.42 l/s (N=40).

	SSE					
	LFR = 1.0366 l/s		LFR = 0.4231 l/s		LFR = 0.2219 l/s	
N	Time to Fault Detection (s)	Total Fluid Loss Before Detection (l)	Time to Fault Detection (s)	Total Fluid Loss Before Detection (l)	Time to Fault Detection (s)	Total Fluid Loss Before Detection (l)
5	8.0	8.29	25.2	10.66	27.3	6.06
10	8.2	8.50	25.5	10.79	27.5	6.10
20	8.8	9.12	26.0	11.00	27.6	6.12
40	9.6	9.95	27.2	11.51	28.3	6.28
80	11.3	11.71	29.3	12.40	30.8	6.83
160	12.8	13.27	32.2	13.63	34.7	7.70

Table 15: Fault detection results for Chi-square mean.

5.7.8 R-Square

The R-square (R^2) statistic is commonly used for in system identification for goodness of fit evaluation. Hence, it was anticipated that it might be useful in residual evaluation for fault detection. R^2 normally takes a value between 0 and 1 and, in model fitting, an R^2 value close to 1 indicates a good fit. The R^2 statistic is the difference between 1 and the ratio of SSE to SST as shown in Equation 39, where SST is the total sum of squares and is as shown in Equation 40. SSE is shown previously in Equation 31.

$$R^2 = 1 - \frac{SSE}{SST} \quad \textbf{(39)}$$

$$SST = \sum_{i=k-N+1}^{k} \left(y_i - \bar{y}_i\right)^2 \quad \textbf{(40)}$$

When tested, the R^2 statistic gave a very prominent spike shortly after the fault was injected, as can be seen in Figure 70. However, it returned to its normal operational area shortly afterward thereby incorrectly indicating no fault present. Further investigation revealed that during non-fault operation both SSE and SST are small. When a fault is injected SSE becomes large and SST small therefore producing a spike like signal. As the fault remains SSE continues to get larger but SST, although lagging SSE, increases at a much faster rate and quite quickly attenuates the R^2 signal. It was thought that the response may be fast enough to give early fault detection but it does not, being slower than all other methods under test. This result would indicate that the R^2 is not useful for fault detection. Hence the full set of results have been omitted from section 4.8 for brevity.

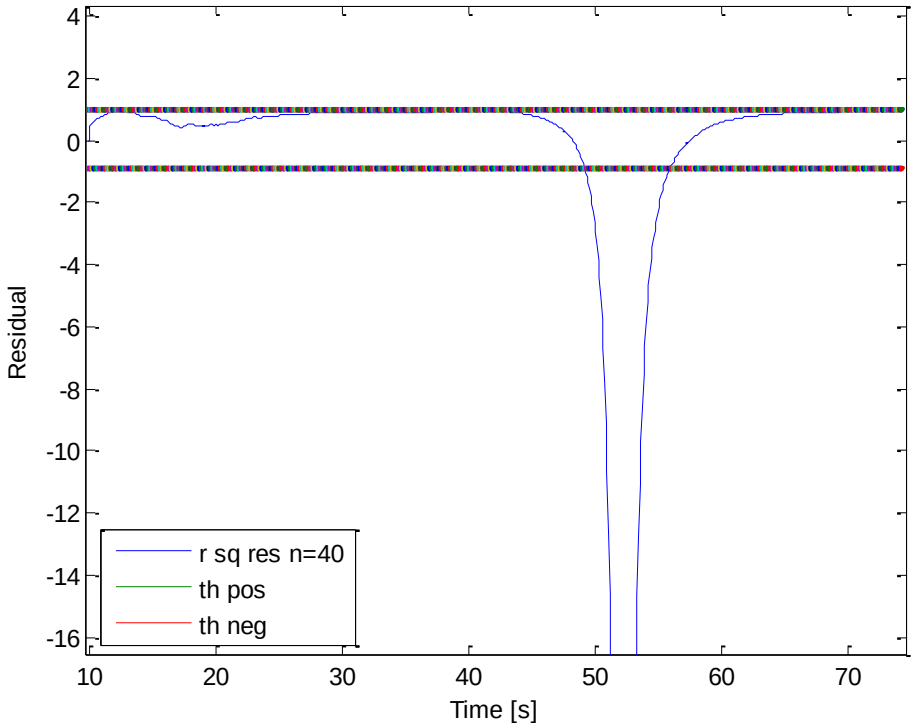

Figure 70: R^2 for Leak Flow Rate = 1.03 l/s (N=40).

5.7.9 Weighted Summed Square of Errors

A number of authors (see e.g., (Candy et al., 2004), (Chen and Patton, 1999), (Kobayashi and Donald, 2003), (Sohlberg, 1998).) have discussed the use of the weighted sum square of error (WSSE) which is the same as the SSE statistic but with the addition of a weighting based on the reciprocal of the variance. It is calculated as shown in Equation 41 and Equation 42.

$$WSSE = \sum_{i=k-N+1}^{k} \omega_i \left(y_i - \hat{y}_i\right)^2 \quad \textbf{(41)}$$

$$\omega_i = 1/\sigma^2 \quad \textbf{(42)}$$

There are two ways of interpreting σ (and hence ω_i) in Equation 42. First, σ could be calculated for the N samples of the moving window. Alternatively it could be calculated from "good" or no fault data (similar to the thresholds) and adopt a fixed value thereafter. The latter would appear to be the most appropriate interpretation, but the results obtained using this are (not surprisingly) the same as for the SSE (Table 10). The problem with continuously recalculating (as per the first approach) is as follows: If the residual remains close to zero, i.e. little variance, by cause of a non-fault state, then the reciprocal of the variance, i.e. the weighting, will be large. However when a fault occurs the residual will detract from its close to zero normal state and approach a value much higher than its normal operating area causing the variance to increase. This in turn will cause the weighting to decrease and attenuate the SSE when a fault condition occurs. For this reason this interpretation was not considered a suitable test, and a constant weighting is assumed.

5.8 Summary of Results

A summary of the tabulated results for the time taken for the Kalman filter residual to exceed the thresholds for each of the methods is shown below in Table 16. This is represented graphically for each of the leak flow rates in order to have a comparison of the methods and their time to fault detection. The comparison of the methods for the leak flow of 1,04 l/s is shown in FIG, for 0.42 l/s in FIG and 0.22 l/s in FIG.

		SSE	MD	MAD	MSE	RMSE	CHI SQ MEAN	WSSE	PAIR-T	KF Res.
LFR (l/s)	N	Time To Detect (s)	Time To Detect (s)	Time To Detect (s)	Time To Detect (s)	Time To Detect (s)	Time To Detect (s)	Time To Detect (s)	Time To Detect (s)	Time To Detect (s)
1.0366	5	6.8	5.9	8	6.8	8	6.8	0	8.4	8
1.0366	10	1.1	5.8	8.2	1.1	8.1	7	0	8.3	8
1.0366	20	7.5	6.4	8.7	7.5	8.3	7.6	16.2	8.9	8
1.0366	40	8.1	7.3	9.4	8.1	9	8.1	15.3	9.8	8
1.0366	80	8.7	9.1	11.1	8.7	10	8.7	22.2	11.6	8
1.0366	160	8.8	11.1	11.5	8.8	9.9	8.8	28.5	14.9	8
0.4231	5	22.1	22.1	25.2	22.1	25.4	22.1	0	24.9	25.3
0.4231	10	22.2	22.1	25.2	22.2	25.5	22.2	78.9	25.1	25.3
0.4231	20	22.5	22.3	25.7	22.5	25.7	22.5	0	25.4	25.3
0.4231	40	22.7	22.5	26.7	22.7	26.6	22.7	54.3	26.3	25.3
0.4231	80	24.1	23.7	28.6	24.1	28.3	24.2	29.8	28.6	25.3
0.4231	160	26	25.3	30.8	26	29.9	26	40.1	31	25.3
0.2219	5	23.3	23.5	23.4	23.3	23.4	23.3	0	23.5	26.8
0.2219	10	23	23.9	23.5	23	23.5	23	0	23.8	26.8
0.2219	20	23.3	24.6	23.5	23.3	23.4	23.3	0	24.2	26.8
0.2219	40	23.4	25.2	23.9	23.4	23.5	23.4	26.9	24.6	26.8
0.2219	80	23.5	26.3	24.6	23.5	23.9	23.5	29	25.3	26.8
0.2219	160	23.5	28.4	24.5	23.5	23.7	23.5	32.6	26.4	26.8

Table 16: Summary of results for fault detection times for residual evaluation.

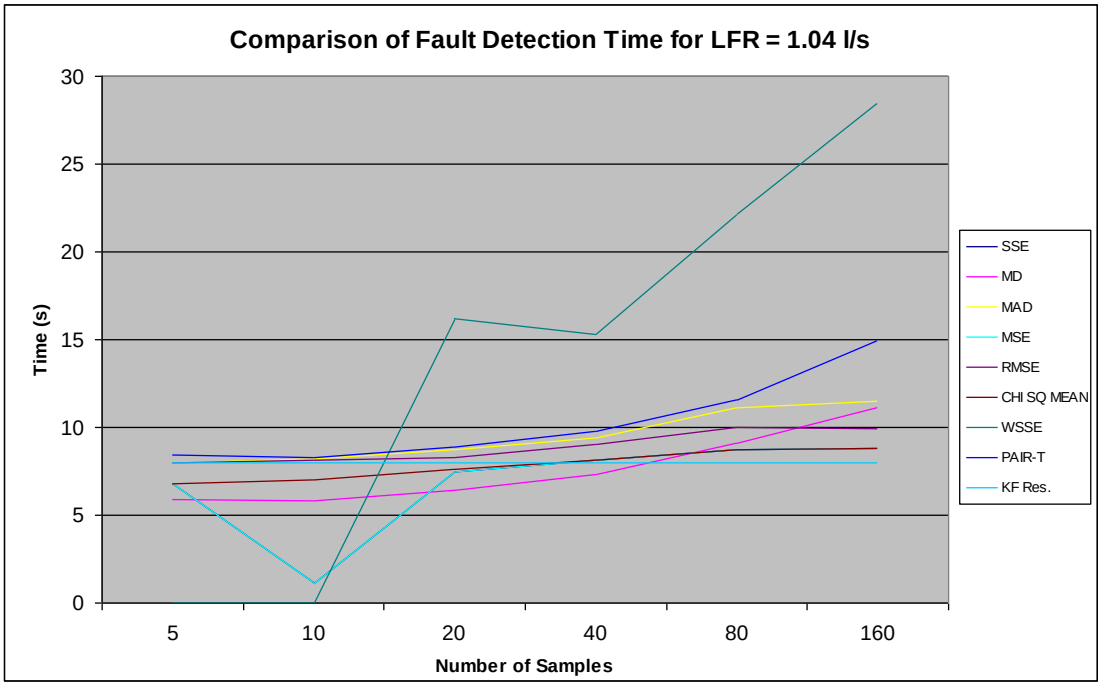

Figure 71: Comparison of Fault Detection for LFR = 1.04 l/s

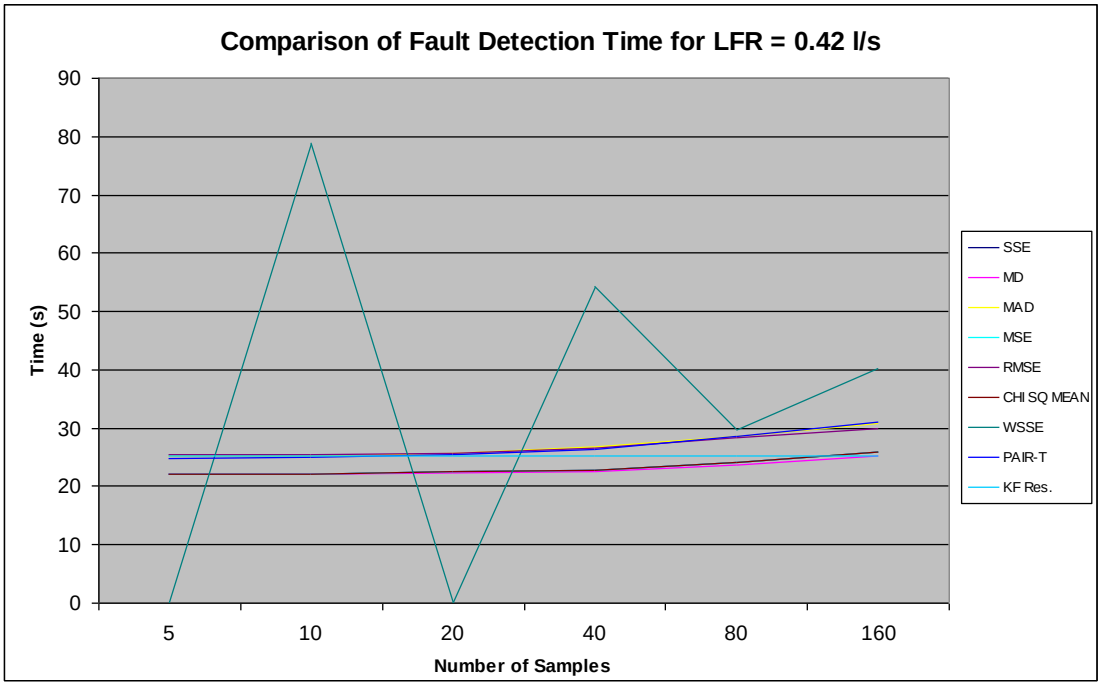

Figure 72: Comparison of Fault Detection for LFR = 0.42 l/s

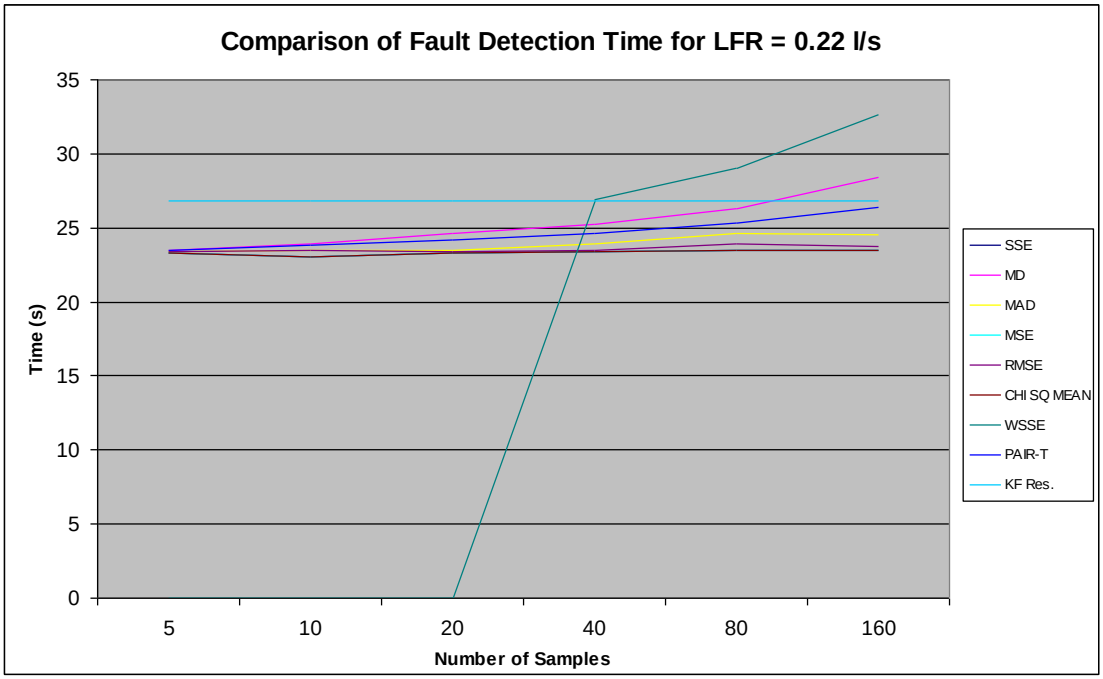

Figure 73: Comparison of Fault Detection for LFR = 0.22 l/s

Table 17 shows the fluid lost from the tank caused by the leak before the fault is detected and is considered of practical interest. These results allow cross comparison of all methods for all sample sizes, N, for each of the leak flow rates tested. Results equal to zero are where faults were not correctly detected.

This is represented graphically for each of the leak flow rates in order to have a comparison of the methods and the fluid lost before fault detection. The comparison of the methods for the leak flow of 1,04 l/s is shown in FIG, for 0.42 l/s in FIG and 0.22 l/s in FIG.

		SSE	MD	MAD	MSE	RMSE	CHI SQ MEAN	WSSE	PAIR-T	KF Res.
LFR (l/s)	N	Total Fluid Lost (l)	Total Fluid Lost (l)	Total Fluid Lost (l)	Total Fluid Lost (l)	Total Fluid Lost (l)	Total Fluid Lost (l)	Total Fluid Lost (l)	Total Fluid Lost (l)	Total Fluid Lost (l)
1.0366	5	7.04	6.11	8.29	7.05	8.3	7.05	0	8.71	8.29
1.0366	10	1.14	6.01	8.5	1.14	8.4	7.26	0	8.6	8.29
1.0366	20	7.77	6.63	9.01	7.77	8.6	7.88	16.79	9.23	8.29
1.0366	40	8.39	7.56	9.74	8.4	9.33	8.4	15.86	10.16	8.29
1.0366	80	9.01	9.43	11.5	9.02	10.37	9.02	23.01	12.02	8.29
1.0366	160	9.12	11.5	11.92	9.12	10.26	9.12	29.54	15.45	8.29
0.4231	5	9.35	9.35	10.66	9.35	10.75	9.35	0	10.54	10.71
0.4231	10	9.39	9.53	10.66	9.4	10.8	9.39	33.39	10.62	10.71
0.4231	20	9.52	9.43	10.87	9.52	10.88	9.52	0	10.75	10.71
0.4231	40	9.6	9.52	11.29	9.61	11.26	9.6	22.96	11.13	10.71
0.4231	80	10.19	9.65	12.1	10.2	12	10.24	12.61	12.1	10.71
0.4231	160	11	10.02	13.03	11	12.65	11	16.97	13.12	10.71
0.2219	5	5.17	10.7	5.19	5.17	5.2	5.17	0	5.21	5.95
0.2219	10	5.1	5.21	5.21	5.1	5.21	5.1	0	5.28	5.95
0.2219	20	5.17	5.21	5.21	7.05	8.29	7.05	0	5.37	5.95
0.2219	40	5.19	5.3	5.3	1.14	8.4	7.26	5.97	5.46	5.95
0.2219	80	5.21	5.45	5.46	7.77	8.6	7.9	6.44	5.61	5.95
0.2219	160	5.21	5.43	5.44	8.4	9.33	8.4	7.23	5.86	5.95

Table 17: Summary of results for fluid lost before fault detection for residual evaluation.

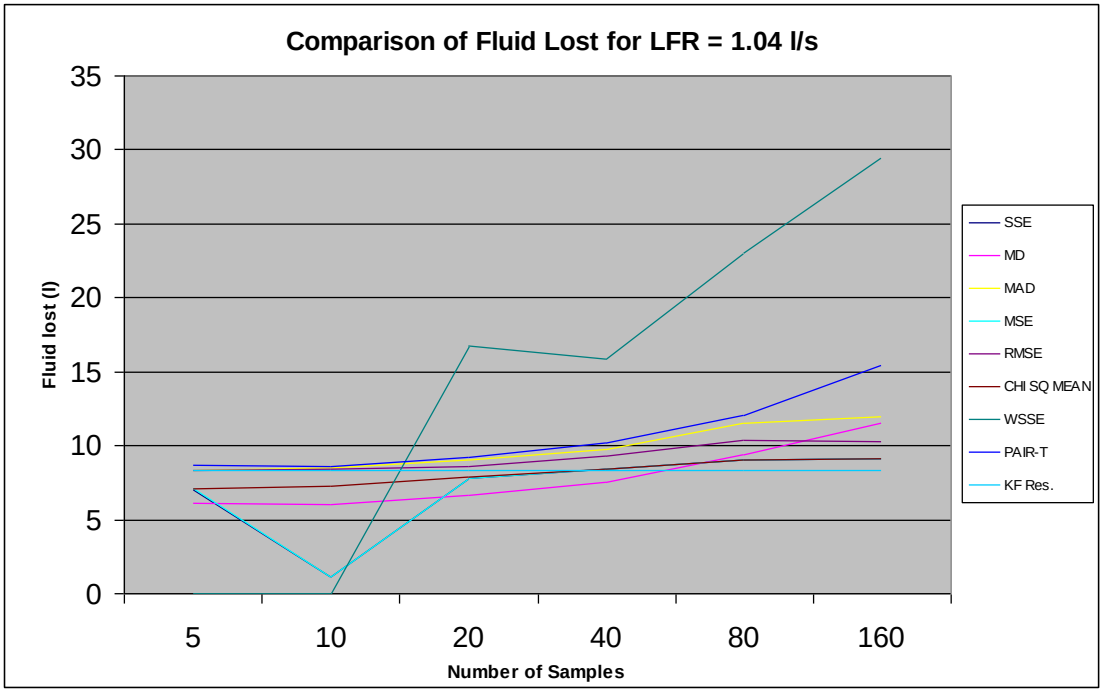

Figure 74: Comparison of Fluid Lost for LFR = 1.04 l/s

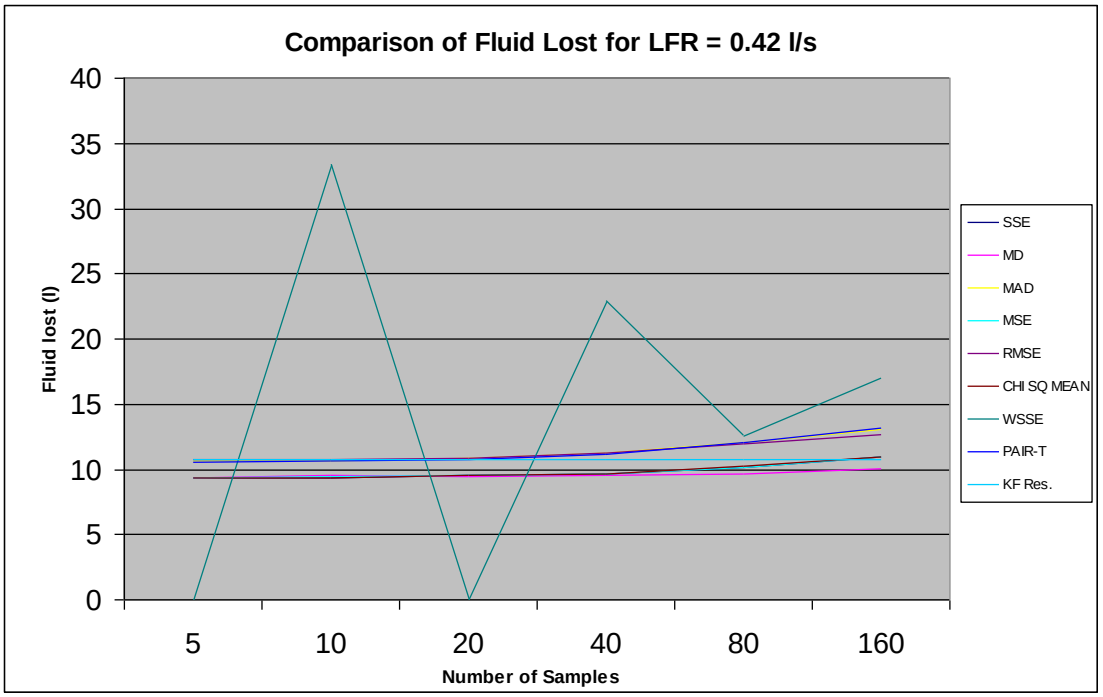

Figure 75: Comparison of Fluid Lost for LFR = 0.42 l/s

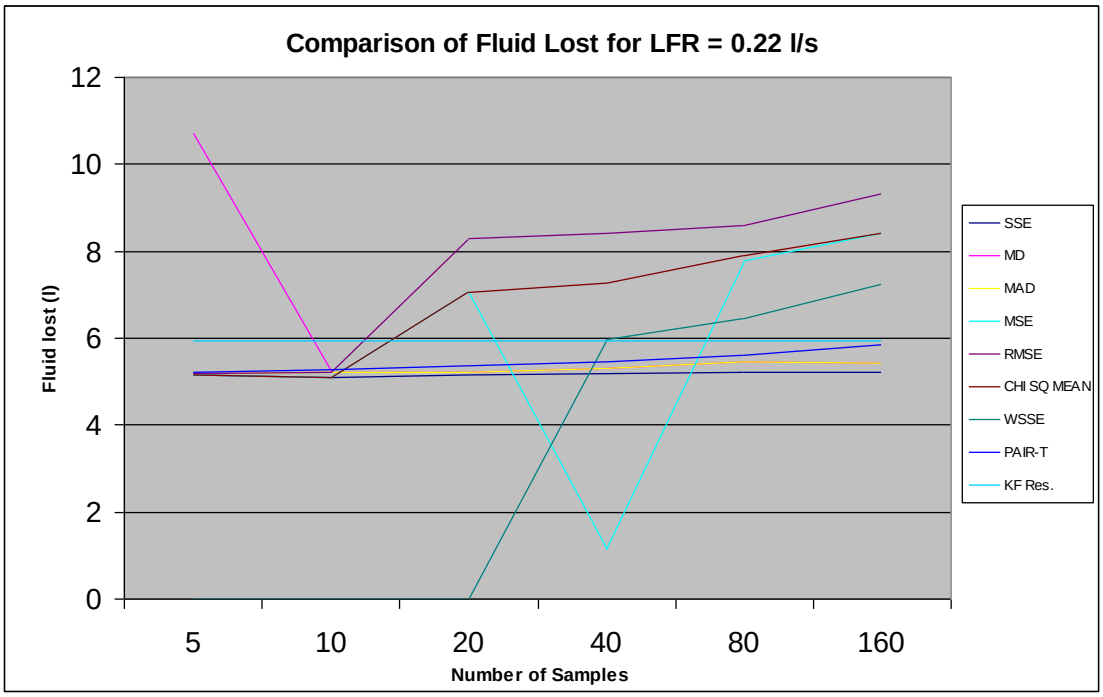

Figure 76: Comparison of Fluid Lost for LFR = 0.22 l/s

5.9 Conclusion

The use of the statistical evaluation of the residual, significantly improves the capability to detect faults at much lower fault magnitudes, resulting in significantly reduced detection times when compared to thresholding of the raw residual signal.

The previous sections have demonstrated a method for automatic determination of threshold bounds based on the standard deviation of a known good sample and applied this to the statistical methods evaluated. The methodologies discussed were mean deviation, mean absolute deviation, mean square error, root mean square error, sum of square error, weighted sum of square error, paired-t test and chi-square mean and R-square.

Based on the overall results, RMSE produces the fastest fault detection time in this test case. SSE is slightly slower, as is MSE which gives identical detection time results. The advantage of MSE over SSE being that the MSE residual threshold will be the same value for all sample window sizes and can be calculated by taking a constant multiplying factor of the standard deviation of the Kalman residual (e.g. as 5 was used in the tests).

With the greater number of samples, N, an attenuation of noise can be achieved thus causing a "tighter set of bounds to be achieved. This, however, comes with the cost of a greater delay in time to detect the presence of a fault. Therefore, it is recommended that a sample window of between 5 and 20 samples is used, since this causes least delay and even improvement of fault detection time in some instances. For example, if a large sample window is a requirement, (say to further reduce the chance of erroneous fault detections) then chi-square mean produced better results compared to SSE, however this method is still not matching the performance of RMSE. WSSE seemed to have little to offer beyond that already given by SSE for this application and fault type. It may be that it is application dependant as several other authors appear to use it with some success. Similarly, R^2 seemed to have little to offer and failed to maintain the identification of the presence of a fault even though the fault

was persisting. The use of Paired-t test gave comparable results to SSE at high fault magnitudes, however, did not perform comparably at low fault magnitudes. MD and MAD gave similar results, neither of which were as good as SSE.

To conclude, RMSE outperforms all the other statistical methods evaluated in this test case. In particular, at small fault magnitudes it performs extremely well. If used with a sample window of N=20, this statistical method improves the detection time compared to the Kalman filter residual alone and improves the robustness of the fault detection scheme.

The contribution of this chapter has been to demonstrate leak detection of a tank and to highlight the advantage of using statistical evaluation of the Kalman filter residual and recommend which one offers the best performance in the test case given.

Chapter 6

Design and Evaluation of Fault Diagnosis and Identification on the System Simulation Model

The application of the Fault Diagnosis and Identification is based upon a model based approach, namely a steady state Kalman Filter. The Kalman filter is an observer with optimal gain. Its implementation offers an observed signal to be compared to the real fuel rig signals – the difference of which is the residual. It allows faults to be detected by the monitoring of the Kalman filter residuals divergence from zero, a large divergence of which indicates the presence of a fault condition. This requires suitable tuning of the Kalman filter parameters in order to prevent false detection of faults and the masking of faults, i.e. the condition whereby no fault flag is raised when a fault is present. A suitable threshold also needs to be determined for the same reasons. The identification of the location of the faults is then required to indicate to the operator which part of the system is at fault and the type of fault.

The contribution of this chapter is the development of the fault detection and identification system and verification its correct operation in identifying faults correctly when applied to the simulink system model representing the fuel rig. Thereby validating the design.

6.1 Introduction

This section includes the development of the Kalman filter based Fault Detection and Identification (FDI) scheme which is then validated by checking that it correctly detects and identifies the location of faults introduced into the fuel rig simulink system model. The development of the Kalman filter is achieved by using state space models of key elements of the fuel rig to produce a bank of filters. Tuning of the filters is performed and threshold levels applied to determine the level at which a fault condition is triggered. Fault identification using logic tables of symptoms and the corresponding fault condition is achieved. The resulting Kalman filter bank scheme is applied to the simulink model created in the previous sections to perform the process of Fault Diagnosis and Identification.

6.2 Development of the Kalman Filter for the Fuel Rig

The first stage of the development of a Kalman filter model is to develop the state-space model and to validate this against the already developed non-linear simulink system model. Note that the simulink model has already been developed and validated against the real fuel rig.

First, the Kalman filter elements shall be designed for the elements in a single pump tray, as shown in Figure 77, as the elements contained within this are repeated throughout the whole system. The only difference being the fuel supply interconnections. All Kalman filters utilise a sample frequency of 1 Hz as this the sampling rate at which data is captured from the fuel rig and captures enough data to reconstruct the highest frequency component of the signals as per Nyquist theory of the sampling frequency being at least twice the frequency of the highest frequency component, as stated in Diniz et al..

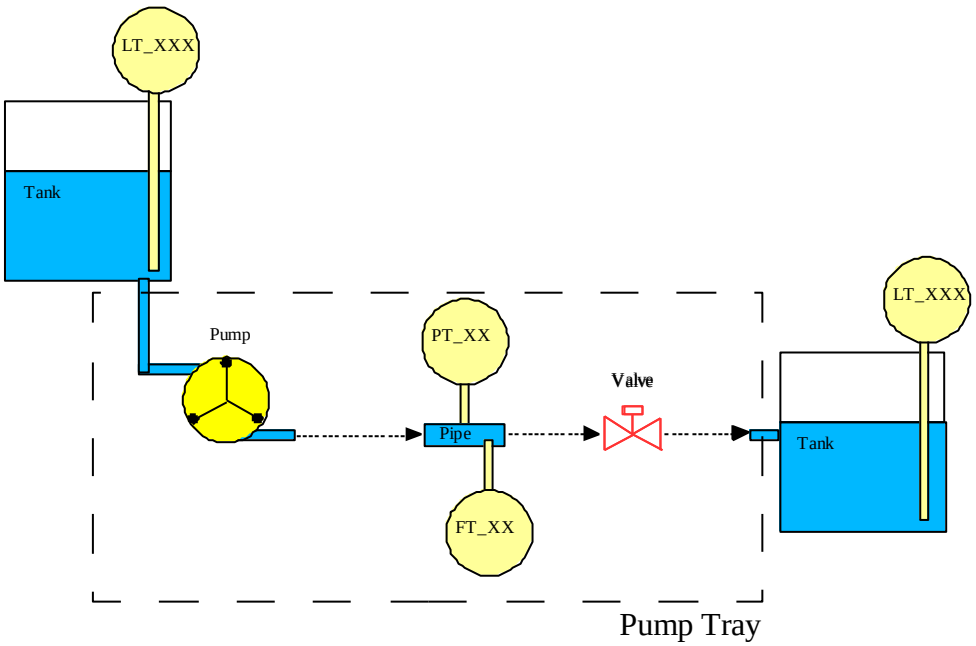

Figure 77: UAV pump tray.

A number of problems were encountered when developing the Kalman filters intended for use as the fault diagnosis tool. The greatest of which was the stiffness seen in the model restricting its ability to be discretised. Stiffness is where the discrete model dynamics are too large for the integration solver algorithm to provide a sensible numerical solution to the model data, thus the solution becomes unstable as huge order numbers are produced. Therefore the same Kalman filter implementation was used whereby a bank of Kalman filters are used for level and flow measurements and a steady state solution is obtained for achieving pressure measurement estimation based upon the estimation of flow. Note: this Kalman filter design could be implemented in one large MIMO system design; however it aids transparency and engineering understanding if modelled individually as a bank of filters.

6.2.1 Flow system state space model derivation

The dynamic response for flow through the valve is the same as the flow through the pump when the system is in a steady state, i.e., no change in rate of flow. Therefore, for use with the Kalman filter, the flow through the pump model shall be compared with the measured flow through the pipe/valve.

The flow out of the pump, Q_{pp1}, for given voltage input, $V_{pp1,}$ is shown in the transfer function shown in Equation 43 and the dynamic system equation derived from this shown in Equation 44.

$$Q_{pp1} = \frac{K_{vpp1}}{\tau s + 1}.V_{pp1} \qquad \textbf{(43)}$$

$$\vdots$$

$$Q_{pp1}.(\tau s + 1) = K_{vpp1}.V_{pp1}$$

$$Q_{pp1}.\tau s + Q_{pp1} = K_{vpp1}.V_{pp1}$$

$$Q_{pp1}.\tau s = K_{vpp1}.V_{pp1} - Q_{pp1}$$

$$\vdots$$

$$\dot{Q}_{pp1} = \frac{K_{vpp1}.V_{pp1}}{\tau} - \frac{Q_{pp1}}{\tau} \qquad \textbf{(44)}$$

Where: Q_{pp1} = volumetric flow rate through pump (l/s)

τ = Motor response time constant = 3 s

K_{vpp1} = Motor response gain constant = 0.026

V_{pp1} = Motor input voltage

Representation of this in continuous time state-space form is shown in Equation 45. Continuous time state space form, $\dot{x} = Ax + Bu$, for pump model with state vector, $x = \lfloor Q_{pp1} \rfloor$, and input vector, $u = \lfloor V_{pp1} \rfloor$, and output equation of $y = Cx + Du$.

$$A = \lfloor -1/\tau \rfloor \qquad B = \lfloor K_{vpp1}/\tau \rfloor \qquad \textbf{(45)}$$

$$C = \lfloor 1 \rfloor \qquad D = \lfloor 0 \rfloor$$

This is however subject to a nonlinear function applied to the input which represents the independent control of the motors by the inverters. This is modelled in the simulink model as a rate limiter to the motor input providing a maximum of full scale change, from 0 V to 2.5 V, of 5 seconds in both positive and negative directions. The rate of change of the input voltage is calculated as shown in equation 46, where $u_{(i)}$ is the current input voltage, $t_{(i)}$ is the current time, $y_{(i-1)}$ is the previous output voltage and $t_{(i-1)}$ is the previous time.

$$V_{input\_rate} = \frac{u_{(i)} - y_{(i-1)}}{t_{(i)} - t_{(i-1)}} \qquad \textbf{(46)}$$

Therefore, if the input, V_{input_rate}, is greater than or less than the maximum slew rate of +/- 0.5 Volts/ second (denoted as R_{max}) then the output is calculated as per equation 47.

$$y_{(i)} = \Delta t.R_{\max} + y_{(i-1)} \quad \textbf{(47)}$$

Else no rate limiting is applied and thus equation 48 applies.

$$y_{(i)} = u_{(i)} \quad \textbf{(48)}$$

There is one final pump to be modelled which is the transfer pump which has the same characteristics as the previously modelled pumps and therefore be developed using identical system parameters.

6.2.2 Tank system state space model derivation

The dynamic response for height, h, for given inputs of Q_{in} and Q_{out} is shown in Equation 49.

$$\dot{h}_x = \frac{1\times10^3 \times Q_{in}}{A_x} - \frac{1\times10^3 \times Q_{out}}{A_x} \quad \textbf{(49)}$$

Where: h = height (m)

A_x= Tank cross sectional area (m^2)

Q_{in} = volumetric flow rate in (l/s)

Q_{out} = volumetric flow rate out (l/s)

6.2.2.1 Auxiliary Tanks

The auxiliary tank height measurement uses the voltage input to the relative pump to estimate the flow through from that tank and then from this estimates the fluid height.

6.2.2.1.1 Left Hand Auxiliary Tank

The left hand auxiliary tank supplies fluid to the left hand wing tank only. Continuous time state space form, $\dot{x} = Ax + Bu$, for left hand auxiliary tank model with state vector, $x = [h \quad Q_{aux}]^T$, and input vector, $u = [V_{aux}]$, and output equation of $y = Cx + Du$ is shown in Equation 50.

$$A = \begin{bmatrix} 0 & -1/A_x \\ 0 & -1/\tau \end{bmatrix} \qquad B = \begin{bmatrix} 0 \\ K_{vpp1}/\tau \end{bmatrix} \qquad \textbf{(50)}$$

$$C = [1 \quad 0] \qquad D = [0]$$

Where: τ = Motor response time constant = 3 s

K_{vpp1} = Motor response gain constant = 0.026

A_x= 0.1728m^2

6.2.2.1.2 Right Hand Auxiliary Tank

The right hand auxiliary tank supplies fluid to the right hand wing tank and can also receive fluid from the right hand wing tank if the transfer pump is activated and the transfer pump 3 way valve is in the appropriate position. Continuous time state space form, $\dot{x} = Ax + Bu$, for left hand auxiliary tank model with state vector, $x = [h \quad Q_{aux} \quad Q_{tx1}]^T$, and input vector, $u = [V_{aux} \quad V_{tx1}]^T$, and output equation of $y = Cx + Du$ is shown in Equation 51.

$$A = \begin{bmatrix} 0 & -1/A_x & 1/A_x \\ 0 & -1/\tau & 0 \\ 0 & 0 & -1/\tau \end{bmatrix} \qquad B = \begin{bmatrix} 0 & 0 \\ K_{vpp1}/\tau & 0 \\ 0 & K_{vpp1}/\tau \end{bmatrix} \qquad \textbf{(51)}$$

$$C = \begin{bmatrix} 1 & 0 & 0 \end{bmatrix} \qquad D = \begin{bmatrix} 0 & 0 \end{bmatrix}$$

Where: τ = Motor response time constant = 3 s

K_{vpp1} = Motor response gain constant = 0.026

A_x= 0.1728m^2

However since the flow from the transfer pump is determined by valve position (TVL) then some additional logic is required in order to provide this functionality. If the transfer pump associated three way valve is in position '0' then the active path of fluid flow is from the right hand wing tank to the right hand auxiliary tank. A logic function is implemented in the model to switch the input on or off to this part of the state space model. If the valve position is in any other position than '0' or '1' then it remains in its last state. The logic, as shown in Equation 52, is implemented in Simulink.

$$\begin{aligned} &\text{If TVL} = 0: && V_{aux(i)} = V_{demand(i)}, V_{tx1(i)} = 0 \\ &\text{If TVL} = 1: && V_{tx1(i)} = V_{demand(i)}, V_{aux(i)} = 0 \\ &\text{Else:} && V_{aux(i)} = V_{aux(i-1)}, V_{tx1(i)} = V_{tx1(i-1)} \end{aligned} \qquad \textbf{(52)}$$

6.2.2.2 Wing Tanks

There are two sets of wing tanks on the fuel rig, namely the left hand wing tank and right hand wing tank. These two sets of tanks are each made up of three baffled tanks which have different heights to simulate the position of the section of tank in the wing section of the aircraft. As the wing tanks have separate baffled sections they will remain at the same level for each section, therefore the Kalmn filter for the left hand

tank is the same for inner, middle and outer tanks and is described in this section as a single entity. However, it is distinguished in the model by using different constants.

6.2.2.2.1 Left Hand Wing Tank

The left hand wing tank receives fluid from the left hand auxiliary tank. It supplies fluid to the left hand engine, the right hand engine and the right hand wing tank dependant upon the associated three way valve positions. The wing tank models are developed by utilising the estimates of flow calculated using the voltage demand on he pump. It is also possible to utilise the flow sensor reading as a model input, however upon testing was found to be too noisy to use.

Modelling the left hand wing tank in a continuous time state space form, $\dot{x} = Ax + Bu$, with state vector, $x = \begin{bmatrix} h & Q_{aux\_L} & Q_L & Q_R & Q_{TX} \end{bmatrix}^T$, and input vector, $u = \begin{bmatrix} V_{aux\_L} & V_{eng\_L} & V_{eng\_R} & V_{TX} \end{bmatrix}^T$, and output equation of $y = Cx + Du$ is shown in Equation 53.

$$A = \begin{bmatrix} 0 & K_{LWT}/A_X & -K_{LWT}/A_X & -K_{LWT}/A_X & -K_{LWT}/A_X \\ 0 & -1/\tau & 0 & 0 & 0 \\ 0 & 0 & -1/\tau & 0 & 0 \\ 0 & 0 & 0 & -1/\tau & 0 \\ 0 & 0 & 0 & 0 & -1/\tau \end{bmatrix}$$

$$B = \begin{bmatrix} 0 & 0 & 0 & 0 \\ K_{vpp1}/\tau & 0 & 0 & 0 \\ 0 & K_{vpp1}/\tau & 0 & 0 \\ 0 & 0 & K_{vpp1}/\tau & 0 \\ 0 & 0 & 0 & K_{vpp1}/\tau \end{bmatrix} \quad \textbf{(53)}$$

$$C = \begin{bmatrix} 1 & 0 & 0 & 0 & 0 \end{bmatrix} \qquad D = \begin{bmatrix} 0 & 0 & 0 & 0 \end{bmatrix}$$

Where: τ = Motor response time constant = 3 s

K_{vpp1} = Motor response gain constant = 0.026

K_{LWT} = Wing tank constant = 9 x 10^{-5}

A_x= 0.1728m^2

The position of the transfer pump 3 way valve affects the input of this model and the input associated to the transfer pump flow is switched on or off by some logic.

In addition to this some logic is required to simulate the behaviour of the 3 way valve changing the fluid flow paths within the fuel rig, i.e. right pump receiving fluid from left hand wing tank. The logic therefore determines which one of the tanks the fluid is drawn from when a pump is active. There are two of these, one for each of the main fluid path 3 way valves on the rig. Again if the valve is in an unknown state, as in when it is in a transition stage, then it remains in its last known position until a determined position is reported. This logic is shown in equation 54.

$$\begin{aligned} &\text{If TVL} = 1: && V_{eng\_L(i)} = V_{demand(i)}, V_{eng\_R(i)} = 0 \\ &\text{If TVL} = 2: && V_{eng\_R(i)} = V_{demand(i)}, V_{eng\_L(i)} = 0 \\ &\text{Else:} && V_{eng\_L(i)} = V_{eng\_L(i-1)}, V_{eng\_R(i)} = V_{eng\_R(i-1)} \end{aligned} \quad \textbf{(54)}$$

6.2.2.2.2 Right Hand Wing Tank

The right hand wing tank receives fluid from the right hand auxiliary tank and from the left hand wing tank. It supplies fluid to the right hand engine, the left hand engine and the right hand auxiliary tank dependant upon the associated three way valve positions. The wing tank models are developed by utilising the estimates of flow calculated using the voltage demand on the pump.

Modelling the left hand wing tank in a continuous time state space form, $\dot{x} = Ax + Bu$, with state vector, $x = \begin{bmatrix} h & Q_{aux\_L} & Q_L & Q_R & Q_{TX} \end{bmatrix}^T$, and input vector,

$u = \begin{bmatrix} V_{aux\_L} & V_{eng\_L} & V_{eng\_R} & V_{TX} \end{bmatrix}^T$, and output equation of $y = Cx + Du$ is shown in Equation 55. This is almost identical to the left hand wing tank developed previously, however the input of the transfer pump is now positive. Logic shall be applied on this input dependant upon the position of the three way valve as to whether fluid is pumped to or drawn from this tank.

$$A = \begin{bmatrix} 0 & K_{RWT}/A_X & K_{RWT}/A_X & K_{RWT}/A_X & K_{RWT}/A_X \\ 0 & -1/\tau & 0 & 0 & 0 \\ 0 & 0 & -1/\tau & 0 & 0 \\ 0 & 0 & 0 & -1/\tau & 0 \\ 0 & 0 & 0 & 0 & -1/\tau \end{bmatrix}$$

$$B = \begin{bmatrix} 0 & 0 & 0 & 0 \\ K_{vpp1}/\tau & 0 & 0 & 0 \\ 0 & K_{vpp1}/\tau & 0 & 0 \\ 0 & 0 & K_{vpp1}/\tau & 0 \\ 0 & 0 & 0 & K_{vpp1}/\tau \end{bmatrix} \quad \textbf{(55)}$$

$$C = \begin{bmatrix} 1 & 0 & 0 & 0 & 0 \end{bmatrix} \qquad D = \begin{bmatrix} 0 & 0 & 0 & 0 \end{bmatrix}$$

Where: τ = Motor response time constant = 3 s

K_{vpp1} = Motor response gain constant = 0.026

K_{RWT} = Wing tank constant = 2 x 10^{-4}

A_x= 0.5312m^2

The right hand wing tank inputs are subject to the action of the transfer pump and this is defined by the logic seen in equation 56.

$$\begin{aligned} &\text{If TVL} = 1: && V_{eng\_R(i)} = V_{demand(i)},\ V_{eng\_L(i)} = 0 \\ &\text{If TVL} = 2: && V_{eng\_L(i)} = V_{demand(i)},\ V_{eng\_R(i)} = 0 \\ &\text{Else:} && V_{eng\_L(i)} = V_{eng\_L(i-1)},\ V_{eng\_R(i)} = V_{eng\_R(i-1)} \end{aligned} \quad \textbf{(56)}$$

6.2.3 Pressure system state space model derivation

The stiffness seen in the pressure model did not allow development of the Kalman filter using the method as per the previous models for fluid flow and tank height. Therefore a steady state solution based upon measured flow, model calculated flow or Kalman filter based estimation of flow is used. This can be used based upon Equation 58, which is derived from Equation 57, (Thomas, 1999). Substituting values into this gives Equation 59 where Q = flow and y_v = valve position. Testing of this method gave good results.

$$Q = \frac{c_v . y_v}{\rho} . \sqrt{\frac{1}{v}} . \sqrt{P} \qquad \textbf{(57)}$$

$$P = \frac{Q^2}{y_v^2} . \frac{1}{1\times10^{-3} . \left(c_v . \sqrt{\frac{1}{v}}\right)^2} = \frac{Q^2}{y_v^2} . \frac{1}{1\times10^{-3} . \left(2.05\times10^{-2} . \sqrt{\frac{1}{1.0022\times10^{-3}}}\right)^2} \qquad \textbf{(58)}$$

$$P = \frac{Q^2}{y_v^2} . \frac{1}{4.212\times10^{-7}} \qquad \textbf{(59)}$$

Where: $c_v = 2.05 \times 10^{-2}$ m^2 $v = 1.0022 \times 10^{-3}$ m^3/kg

6.2.4 Application of Kalman Filters on Simulation Model

The bank of Kalman filters are applied to the positions illustrated in Figure 78. Note this is a simplified diagram to aid clarity. These provide estimates, and therefore residual error, for the levels, flows and pressures. This diagram illustrates the right hand half of the fuel rig and is extended to the left hand side although not illustrated in this diagram.

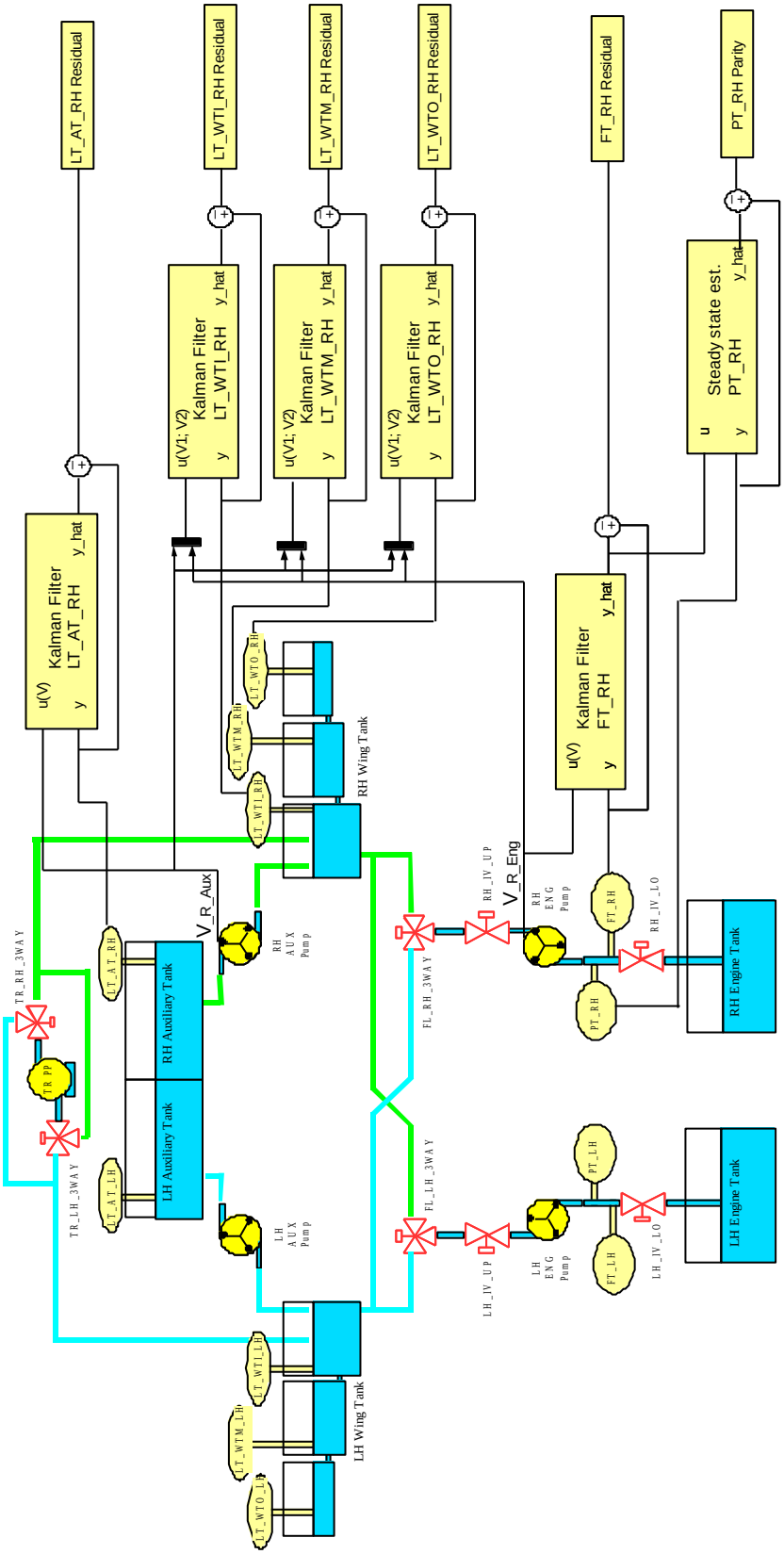

Figure 78: Application of the bank of Kalman Filters to the fuel rig.

6.2.5 Kalman filter tuning

The method adopted here uses a calculated sensor covariance based upon real data. The covariance attained for the UAV rig sensor set of interest is shown below in Table 18.

Sensor Name	Description	Sensor Noise Covariance
LT_WTI_RH	Right Hand Wing Inner Tank Level Transducer	1.5×10^{-4}
LT_WTM_RH	Right Hand Wing Middle Tank Level Transducer	1.5×10^{-4}
LT_WTO_RH	Right Hand Wing Tank Outer Level Transducer	1.5×10^{-4}
LT_WTI_LH	Left Hand Wing Inner Tank Level Transducer	1.5×10^{-4}
LT_WTM_LH	Left Hand Wing Middle Tank Level Transducer	1.5×10^{-4}
LT_WTO_LH	Left Hand Wing Outer Tank Level Transducer	1.5×10^{-4}
LT_AT_RH	Right Hand Auxiliary Tank Level Transducer	3.9×10^{-4}
LT_AT_LH	Left Hand Auxiliary Tank Level Transducer	3.9×10^{-4}
FT_RH	Right Hand Flow Transducer	6.7×10^{-4}
FT_LH	Left Hand Flow Transducer	4.9×10^{-4}

Table 18: Sensor noise covariance

With noise covariance set to as shown in the table the process covariance can then be successively estimated to produce a reasonable estimation of the fuel rig sensor signal whilst not being too high a gain as to mask faults when they occur. The tuning in this case is achieved by setting the noise covariance to a values attained by sampling of the sensor data. Then heuristically tuning the process covariance to provide a result that provides a reasonable estimation of the required sensor signals allowing for correction in the estimation for model error but allowing fault to be captured, i.e. ensuring they are not masked by the Kalman filter. It may be possible to provide an algorithmic solution for this process using sets of rig sample data to achieve the same result. Tuning produced the process noise covariance in Table 19 below. Note that the

left hand and right hand auxiliary tank level transducer are significantly different due to their physical size.

Sensor Name	Description	Process Noise Covariance
LT_WTI_RH	Right Hand Wing Inner Tank Level Transducer	30
LT_WTM_RH	Right Hand Wing Middle Tank Level Transducer	30
LT_WTO_RH	Right Hand Wing Tank Outer Level Transducer	30
LT_WTI_LH	Left Hand Wing Inner Tank Level Transducer	3
LT_WTM_LH	Left Hand Wing Middle Tank Level Transducer	3
LT_WTO_LH	Left Hand Wing Outer Tank Level Transducer	3
LT_AT_RH	Right Hand Auxiliary Tank Level Transducer	1.1
LT_AT_LH	Left Hand Auxiliary Tank Level Transducer	1.05×10^{-6}
FT_RH	Right Hand Flow Transducer	1
FT_LH	Left Hand Flow Transducer	0.7

Table 19: Process noise covariance

6.2.6 Fault condition determination

It is necessary to set a level at which, when the Kalman filter residual has exceeded, a fault condition is determined to have occurred. This can be set by identifying normal behaviour and producing the threshold heuristically at a level at which false fault conditions will not occur, however a fault condition will be captured. Each Kalman filter requires its own heuristically set threshold.

An arbitrary fault of a leak from the left hand wing tank is simulated in the simulink model to demonstrate the application of the thresholds. The leak is set to leak fluid at a rate of 0.05l/s at 30 seconds. The tank levels for inner, middle and outer tanks for both simulink simulation and the Kalman filter are shown in Figure 79. The residuals for these measurements and their associated thresholds for the left hand wing tank are shown in Figure 80. As can be seen the Kalman filter estimation and the simulink

model output diverge causing the residual to exceed the preset thresholds. Hence, the fault is detected at 42 seconds, taking 12 seconds for the residual to exceed the threshold.

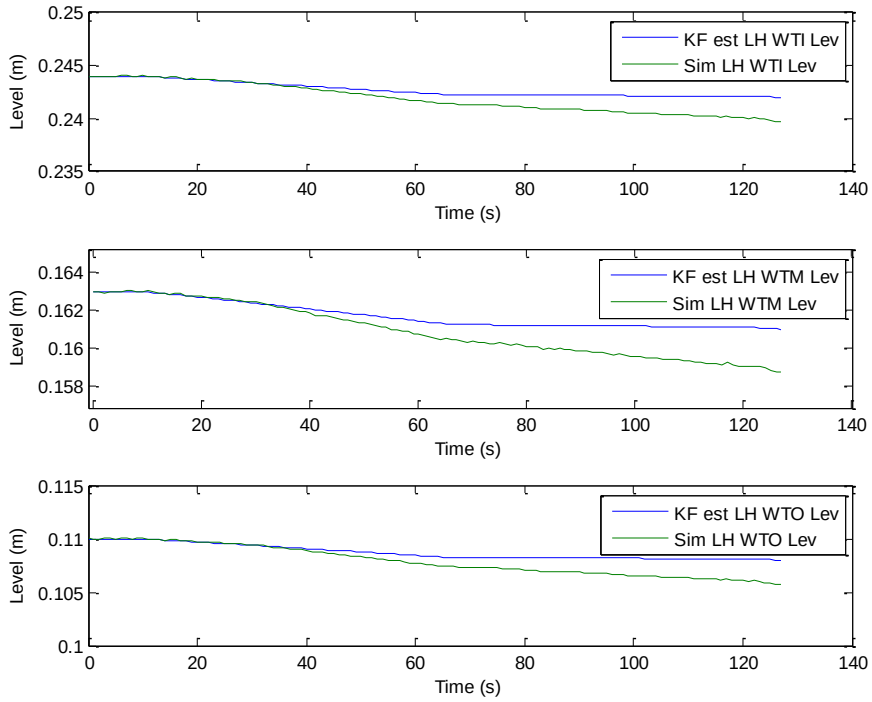

Figure 79: Left hand inner, middle and outer wing tank levels.

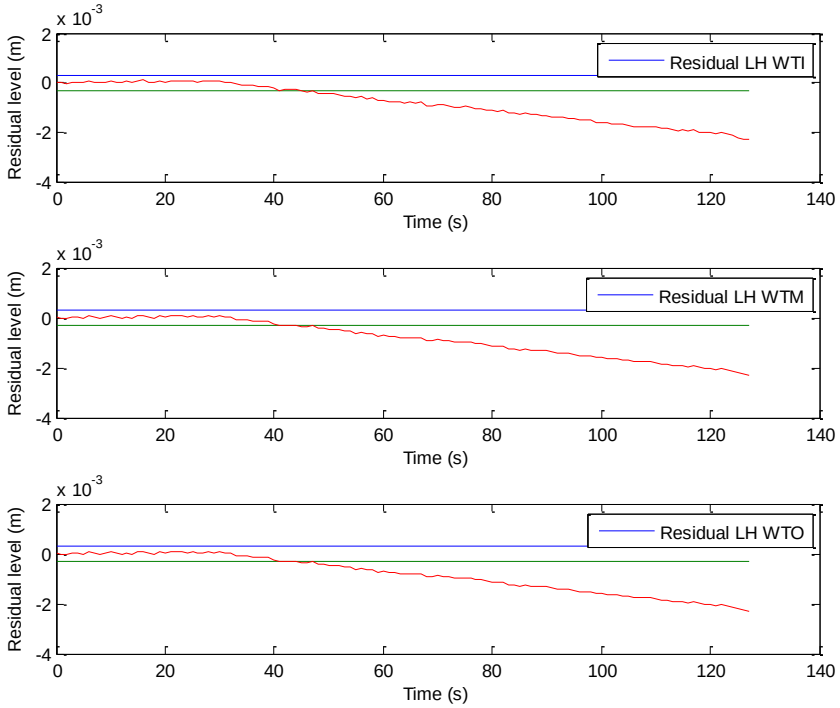

Figure 80: Left hand inner, middle and outer wing tank residuals.

6.2.7 Fault Identification

It is necessary to identify the location of the fault. Therefore using analysis of the combination of Kalman filters which are in a fault state, the behaviour of the Kalman filter and the behaviour of the sensor it is possible to discriminate between possible faults and identify the location.

Faults have been separated into different types, namely process faults, actuation faults and sensor faults. Process faults include physical plant based faults which affect the operational ability of the plant itself such as a pipe or joint cracking. Actuation faults occur within the actuated parts of the plant such as pump or valve failure and sensor faults occur wholly with regard to the sensor operation.

The tabulation of possible actuator faults within the system is shown below in Table 20. The possible process faults in Table 21 and sensor faults in Table 22. For each fault both the sensor behaviour and the Kalman filter residual behaviour is mapped to determine, if possible, total discrimination of all permutations of faults. As an example of discrimination of faults using multiple Kalman filter residuals, for example, if a flow sensor fails completely on the right hand engine flow path then FT_RH residual is negative, whereas if a leak occurs located within the pipe this also causes FT_RH residual to go negative. However, discrimination can be achieved by the fact that that the residuals for the right hand pressure sensor and wing tank also are affected with regard to the pipe leak and do not when sensor failure occurs. Further to this if a level sensor in the right hand wing tank, for example, fails abruptly this cause the LT_RH_WT residual to be negative, whereas a leak in the right hand wing tank will also cause the LT_RH_WT residual to be negative. These can however be discriminated by the action of the sensor signal, i.e. if LT_RH_WT is negative and LT_RH_WT sensor signal is 0 or constant, k, then the probable cause is sensor failure. However, if LT_RH_WT residual is negative and dropping at a constant rate (or just not equal to 0 or k) then it is probable that a leak in the tank has occurred.

Although the list provides almost complete discrimination between each fault by use of the Kalman residual behaviour and sensor behaviour there is one set of faults which do provide the same resultant characteristic. This is faults F27 and F52 which both result in a positive error of the left hand pressure transducer Kalman residual and a constant error in the sensor reading.

Fault F27 is a blockage in the range of 0% to 85% and thus will cause an increase in pressure read from the sensor, whereas the Kalman estimate pressure sensor value will read what the pressure should be if a fault was not present, therefore producing a positive residual and the variance between real sensor and Kalman estimated pressures will be constant relative to the increase in pressure caused by the blockage.

Fault F52 is a sensor fault caused by an offset or bias in the sensor signal causing a positive or negative residual and sensor behaviour of a constant offset, in the case of bias, which is what will be examined here as this result is the same as the previously mentioned F27. This causes a problem as the resultant characteristics of the Kalman filter and sensor behaviour are the same for both faults. One solution in this special case the operator must be made aware that the action that caused the fault could be possibly from two faults and further human intervention is required to locate the source of the fault. The second possible solution is to reduce flow to zero and therefore pressure also to zero. If the source of the fault is a biased sensor then a bias will still show, however if it is the fault of a blockage then the pressure will read zero.

As an example of determining the location of a fault, if a fault was determined by the Kalman filters that LT_RH_WT (level transducer right hand wing tank) was in error, whereby the residual exceeded the negative threshold, then it could be determined by the tables below that this could correspond to a fault signature of faults F7, F17, F21, F31, F32, F33 or F34. However, since no other Kalman filters are reporting faults then this is narrowed down to faults F17, F31, F32, F33 or F34. Then by looking at the behaviour of the sensor signals at this time it would be possible to discriminate further, for example if the sensor value was constant zero then it is due to an abrupt failure of the sensor.

	Fault type	Fault position	Type	Sensor Behaviour	Kalman Residual Behaviour
F1	Actuator	PP_FL_RH	Abrupt failure	FT_RH = 0	FT_RH = -ve
				PT_RH = 0	PT_RH = -ve
				LT_RH_WT = flow from AT pump only	LT_RH_WT = +ve
F2			Pump underrun bias	FT_RH = FT_RH - k OR = FT_RH * (-k)	FT_RH = -ve
				LT_RH_WT = LT_RH_WT + k	LT_RH_WT = +ve
F3			Pump overrun bias	FT_RH = FT_RH + k OR = FT_RH * (+k)	FT_RH = +ve
				LT_RH_WT = LT_RH_WT - k	LT_RH_WT = -ve
F4	Actuator	PP_FL_LH	Abrupt failure	FT_LH = 0	FT_LH = -ve
				PT_LH = 0	PT_LH = -ve
				LT_RH_WT = flow from AT pump only	LT_LH_WT = +ve
F5			Pump underrun bias	FT_LH = FT_LH - k OR = FT_LH * (-k)	FT_LH = -ve
				LT_LH_WT = LT_LH_WT + k	LT_LH_WT = +ve
F6			Pump overrun bias	FT_LH = FT_LH + k OR = FT_LH * (+k)	FT_LH = +ve
				LT_LH_WT = LT_LH_WT - k	LT_LH_WT = -ve
F7	Actuator	PP_AT_RH	Abrupt failure	LT_RH_AT = Static	LT_RH_AT = -ve
				LT_RH_WT = Static	LT_RH_WT = -ve
F8			Pump underrun bias	LT_RH_AT = LT_RH_AT + k	LT_RH_AT = -ve
				LT_RH_WT = LT_RH_WT - k	LT_RH_WT = +ve
F9			Pump overrun bias	LT_RH_AT = LT_RH_AT - k	LT_RH_AT = -ve
				LT_RH_WT = LT_RH_WT - k	LT_RH_WT = +ve
F10	Actuator	PP_AT_LH	Abrupt failure	LT_LH_AT = Static	LT_LH_AT = -ve
				LT_LH_WT = Static	LT_LH_WT = -ve
F11			Pump underrun bias	LT_LH_AT = LT_LH_AT + k	LT_LH_AT = -ve
				LT_LH_WT = LT_LH_WT - k	LT_LH_WT = +ve
F12			Pump overrun bias	LT_LH_AT = LT_LH_AT - k	LT_LH_AT = -ve
				LT_LH_WT = LT_LH_WT - k	LT_LH_WT = +ve
F13	Actuator	IV_FL_RH	Position stuck	PT_RH = constant offset dependant on Vin	PT_RH = +ve
F14			Position bias	PT_RH = PT_RH +/- k	PT_RH = +ve
F15	Actuator	IV_FL_LH	Position stuck	PT_LH = constant offset dependant on Vin	PT_LH = +ve
F16			Position bias	PT_LH = PT_LH +/- k	PT_LH = +ve

Table 20: Fault behaviour for pump and actuator fault conditions

	Fault type	Fault position	Type	Sensor Behaviour	Kalman Residual Behaviour
F17	Process	LT_RH_WT	Leak	LT_RH_WT = LT_RH_WT - k	LT_RH_WT -ve
F18	Process	LT_LH_WT	Leak	LT_LH_WT = LT_LH_WT - k	LT_LH_WT -ve
F19	Process	LT_RH_AT	Leak	LT_RH_AT = LT_RH_AT - k	LT_RH_AT -ve
F20	Process	LT_LH_AT	Leak	LT_LH_AT = LT_LH_AT - k	LT_LH_AT -ve
F21	Process	IV_FL_RH	Leak (in pipe)	LT_RH_WT = LT_RH_WT - k	FT_RH = -ve
					PT_RH = -ve
					LT_RH_WT -ve
F22	Process	IV_FL_LH	Leak (in pipe)	LT_LH_WT = LT_LH_WT - k	FT_LH = -ve
					PT_LH = -ve
					LT_LH_WT -ve
F23	Process	IV_AT_RH	Leak (in pipe)	LT_RH_AT = LT_RH_AT - k	LT_RH_AT -ve
F24	Process	IV_AT_LH	Leak (in pipe)	LT_LH_AT = LT_LH_AT - k	LT_LH_AT -ve
F25	Process	IV_FL_RH	Blockage 0 => 85% cl.	PT_RH = PT_RH + k	PT_RH = +ve
F26	Process	IV_FL_RH	Blockage 85 => 100% cl.	PT_RH = PT_RH + k	PT_RH = +ve
				FT_RH = FT_RH - k	FT_RH = +ve
F27	Process	IV_FL_LH	Blockage 0 => 85% cl.	PT_LH = PT_LH + k	PT_LH = +ve
F28	Process	IV_FL_LH	Blockage 85 => 100% cl.	PT_LH = PT_LH + k	PT_LH = +ve
				FT_LH = FT_LH - k	FT_LH = +ve

Table 21: Fault behaviour for process fault conditions

	Fault type	Fault position	Type	Sensor Behaviour	Kalman Residual Behaviour
F31	Sensor	RH_WT	Abrupt failure	RH_WT = 0 OR k	RH_WT -ve or +ve
F32			Gain/ offset bias	RH_WT = RH_WT +/- k OR * k	RH_WT -ve or +ve
F33			Hysteresis	RH_WT = RH_WT - k on POS; + k on NEG.	RH_WT -ve or +ve
F34			Excessive noise	RH_WT = RH_WT + k AND - k random	RH_WT -ve or +ve
F35	Sensor	LH_WT	Abrupt failure	LH_WT = 0 OR k	LH_WT -ve or +ve
F36			Gain/ offset bias	LH_WT = LH_WT +/- k OR * k	LH_WT -ve or +ve
F37			Hysteresis	LH_WT = LH_WT - k on POS; + k on NEG.	LH_WT -ve or +ve
F38			Excessive noise	LH_WT = LH_WT + k AND - k random	LH_WT -ve or +ve
F39	Sensor	RH_AT	Abrupt failure	RH_AT = 0 OR k	RH_AT -ve or +ve
F40			Gain/ offset bias	RH_AT = RH_AT +/- k OR * k	RH_AT -ve or +ve
F41			Hysteresis	RH_AT = RH_AT - k on POS; + k on NEG.	RH_AT -ve or +ve
F42			Excessive noise	RH_AT = RH_AT + k AND - k random	RH_AT -ve or +ve
F43	Sensor	LH_AT	Abrupt failure	LH_AT = 0 OR k	LH_AT -ve or +ve
F44			Gain/ offset bias	LH_AT = LH_AT +/- k OR * k	LH_AT -ve or +ve
F45			Hysteresis	LH_AT = LH_AT - k on POS; + k on NEG.	LH_AT -ve or +ve
F46			Excessive noise	LH_AT = LH_AT + k AND - k random	LH_AT -ve or +ve
F47	Sensor	PT_RH	Abrupt failure	PT_RH = 0 OR k	PT_RH -ve or +ve
F48			Gain/ offset bias	PT_RH = PT_RH +/- k OR * k	PT_RH -ve or +ve
F49			Hysteresis	PT_RH = PT_RH - k on POS; + k on NEG.	PT_RH -ve or +ve
F50			Excessive noise	PT_RH = PT_RH + k AND - k random	PT_RH -ve or +ve
F51	Sensor	PT_LH	Abrupt failure	PT_LH = 0 OR k	PT_LH -ve or +ve
F52			Gain/ offset bias	PT_LH = PT_LH +/- k OR * k	PT_LH -ve or +ve
F53			Hysteresis	PT_LH = PT_LH - k on POS; + k on NEG.	PT_LH -ve or +ve
F54			Excessive noise	PT_LH = PT_LH + k AND - k random	PT_LH -ve or +ve
F55	Sensor	FT_RH	Abrupt failure	FT_RH = 0 OR k	FT_RH -ve or +ve
F56			Gain/ offset bias	FT_RH = FT_RH +/- k OR * k	FT_RH -ve or +ve
F57			Hysteresis	FT_RH = FT_RH - k on POS; + k on NEG.	FT_RH -ve or +ve
F58			Excessive noise	FT_RH = FT_RH + k AND - k random	FT_RH -ve or +ve
F59	Sensor	FT_LH	Abrupt failure	FT_LH = 0 OR k	FT_LH -ve or +ve
F60			Gain/ offset bias	FT_LH = FT_LH +/- k OR * k	FT_LH -ve or +ve
F61			Hysteresis	FT_LH = FT_LH - k on POS; + k on NEG.	FT_LH -ve or +ve
F62			Excessive noise	FT_LH = FT_LH + k AND - k random	FT_LH -ve or +ve

Table 22: Fault behaviour for sensor fault conditions

6.2.8 Testing of Kalman filter FDI on Simulink Model

In order to provide verification of the action of the fault detection and the fault identification process a number of tests are run in order to exercise a number of fault conditions. The fault identification process is, at this stage, demonstrated by injecting fault into the simulink model and using the Kalman filters to diagnose the fault and discrimination logic to determine or identify the locality of the fault.

6.2.8.1 Test 1 – Left hand wing tank leak

The first fault injection test applied to the simulink model is that of a leak fault in the left hand wing tank at a rate of 0.25 l/s at 40 seconds. The graph below, in Figure 81, shows tank level for simulink model (Sim LH WTI Lev, Sim LH WTM Lev and Sim LH WTO Lev for inner, middle and outer respectively) and for Kalman filter estimation of this output (KF est LH WTI Lev, KF est LH WTM Lev and KF est LH WTO Lev for inner, middle and outer respectively). It is clear to see the divergence of the simulink model and Kalman filter levels.

Figure 82 shows the residual, i.e. the differential of, the estimation of the level sensor and the actual level sensor. It shows the residual exceeding the manually set threshold after a few seconds.

By analysis of the behaviour of the signals for the left hand wing tank, the sensor signal is greater than simulation signal and the divergence increases by an approximately constant amount. No other residuals are affected. This produces a negative direction residual and cross-referencing back to the fault behaviour tabulations in the previous section it can be determined that the fault is either that of a leak in the left hand wing tank (F18). As an example of an alternative, but similar, fault condition, if this behaviour occurred and the pressure sensor residual also exceeded its threshold also then the resultant fault condition based on the fault permutations in the table would be a leak in the left hand pipe (F22).

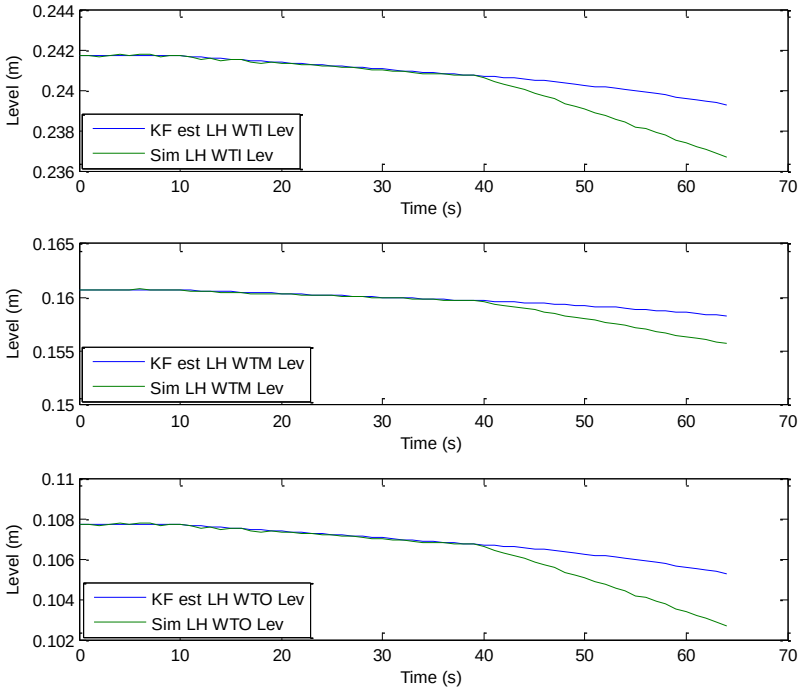

Figure 81: Left hand wing tank level and Kalman filter estimate for leak fault injection.

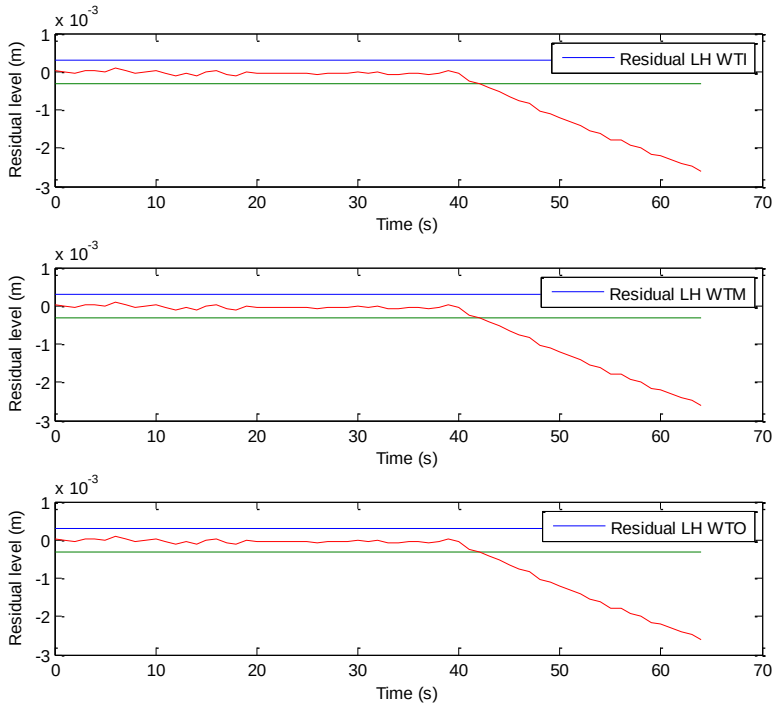

Figure 82: Left hand wing tank residuals for leak fault injection.

6.2.8.2 Test 2 – Degraded pump

The second test involves the left hand pump running under degraded performance characteristics. A failure of this pump is injected at 20 seconds whereby the pump is run at 1V whereas the Kalman filter thinks it is running at 2.5V simulating degraded performance. The results for flow pressure for the left hand wing tank pump tray are shown in Figure 83. This plot captures the divergence of both flow and pressures signals at the time the fault is injected. The fluid levels seen in the left hand wing tank for inner (LH WTI Lev), middle (LH WTM Lev) and outer (LH WTO Lev) are shown in Figure 84. The residuals are observed exceeding the threshold for flow as is shown in Figure 85. The left hand wing tank threshold is also exceeded by the residual; however, this is much less sensitive to this fault taking around 15 seconds to exceed the threshold as is shown in Figure 86.

Although it was assumed that in theory such a test of pump performance degradation would cause not only flow to exceed its residual but also for pressure to drop significantly also and to cause an error condition in the pressure residual. However, by examination of the pressure signal behaviour in Figure 83 and Figure 85 it is seen that only a complete loss of pressure signal is required to instigate a fault condition being triggered by exceeding the threshold. This is due to the inaccuracy of the pressure sensor at low pressure, which is the normal operating pressure of the fluid system. This requires thresholds at which a fault condition is triggered to be wide. It is however more accurate over a larger range and useful in the case of a system blockage as this would register as an increase greater than the required large threshold.

Referencing the faults back to the tabulations of possible faults, the negative residual for flow and positive residual for tank level produces a fault of pump failure which correctly identifies the fault.

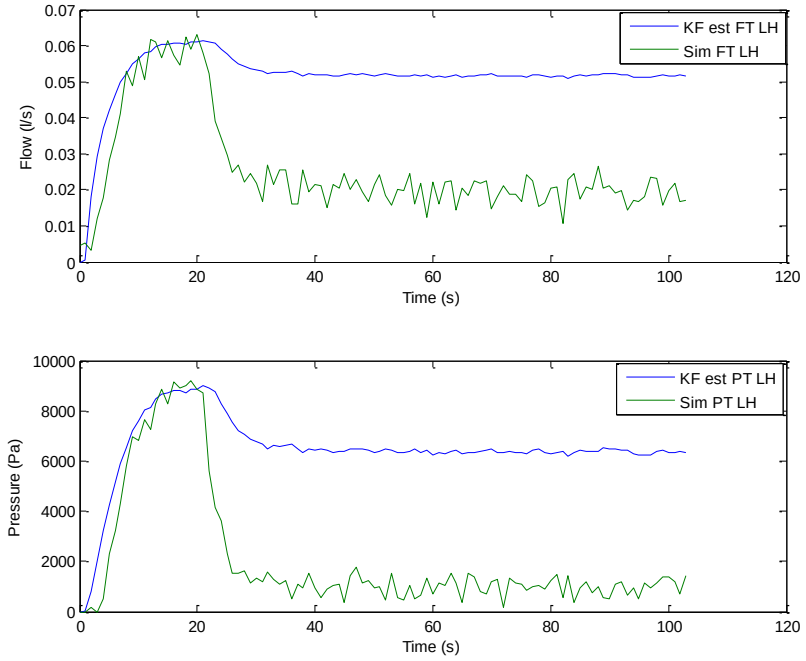

Figure 83: Flow and pressure sensor results for pump degradation fault injection.

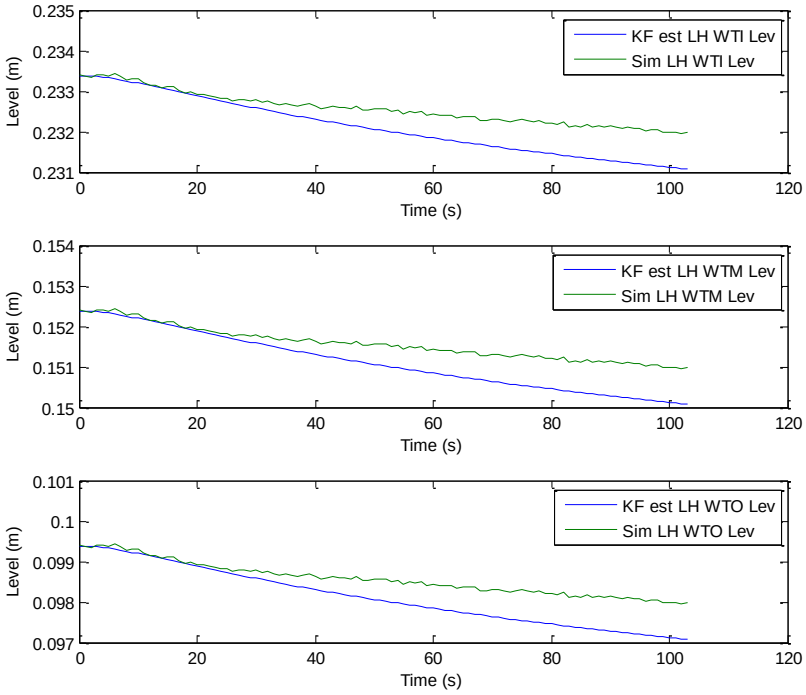

Figure 84: Left hand wing tank level sensor results for pump degradation fault injection.

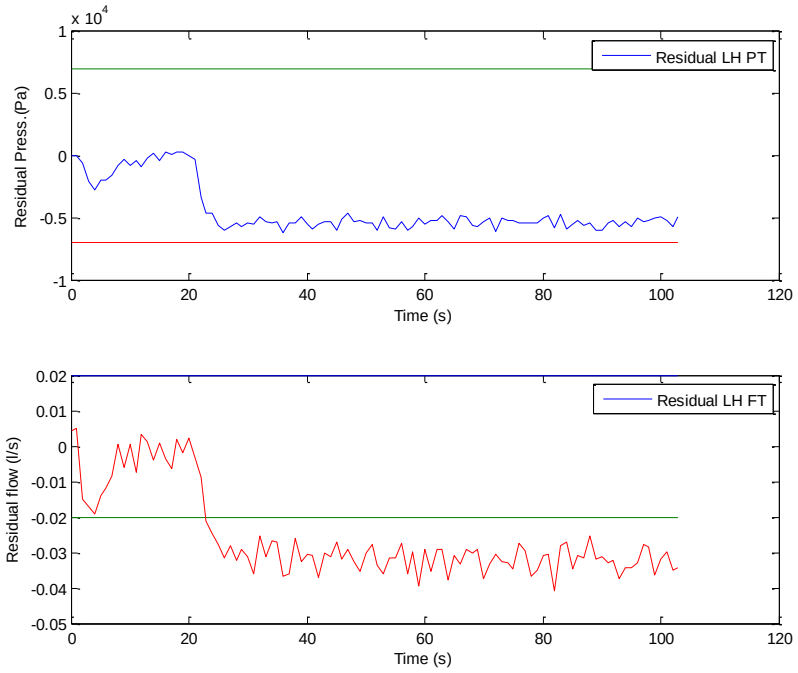

Figure 85: Pressure and flow residuals for pump degradation fault injection.

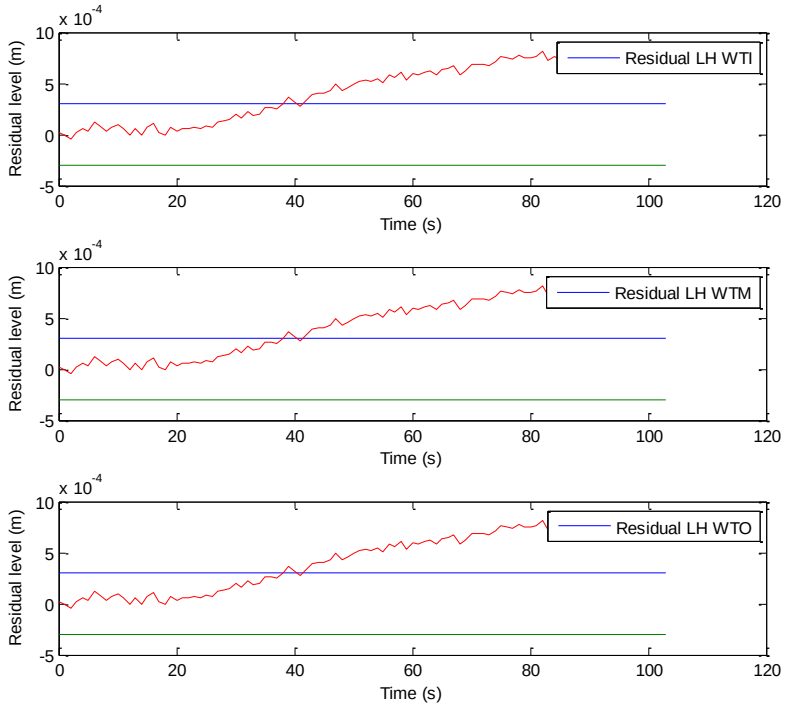

Figure 86: Left hand wing tank level sensor residuals for pump degradation fault injection.

6.2.8.3 Test 3 – Pipe blockage fault

A blockage fault was injected into the left hand pipe between the left hand wing tank and left hand engine of the simulink system model. The blockage was represented by closing of a valve in the simulink model only. Varying magnitudes of fault was injected over the test period. A blockage representing the pipe being 50% closed is injected at 30 seconds, and then a blockage of 80% closed at 70 seconds and finally fully closed at 110 seconds.

The flow transducer and pressure transducer signals with the Kalman filter estimate for each are shown in Figure 87 which shows clear divergence of pressure signals at each stage of fault injection and divergence of the flow transducer estimate for fully closed position only.

Figure 88 shows the residuals for pressure and for flow signals. The pressure signal residual clearly exceeds the threshold for all levels of blockage. At fully closed the pressure limit is reached a pressure release valve directs the fluid flow back to the tank. The flow residual only deviates and produces an error when the valve is fully closed.

Mapping these fault condition parameters back to the tabulated fault permutations identifies that at 50% and 80% blockage the fault identified is F27, which is a blockage of 0 to 85% closed in left hand main flow isolation valve. At 100% closed whereby a negative residual of flow is also produced the fault identified is F28, which is a blockage of 85 to 100% closed in left hand main flow isolation valve.

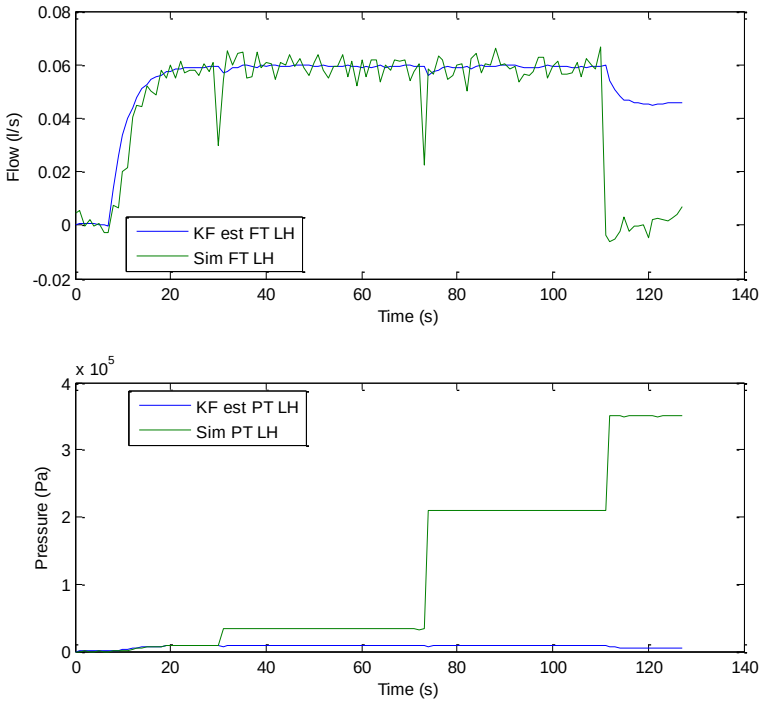

Figure 87: Left hand wing tank flow and pressure sensor results for pipe blockage fault injection.

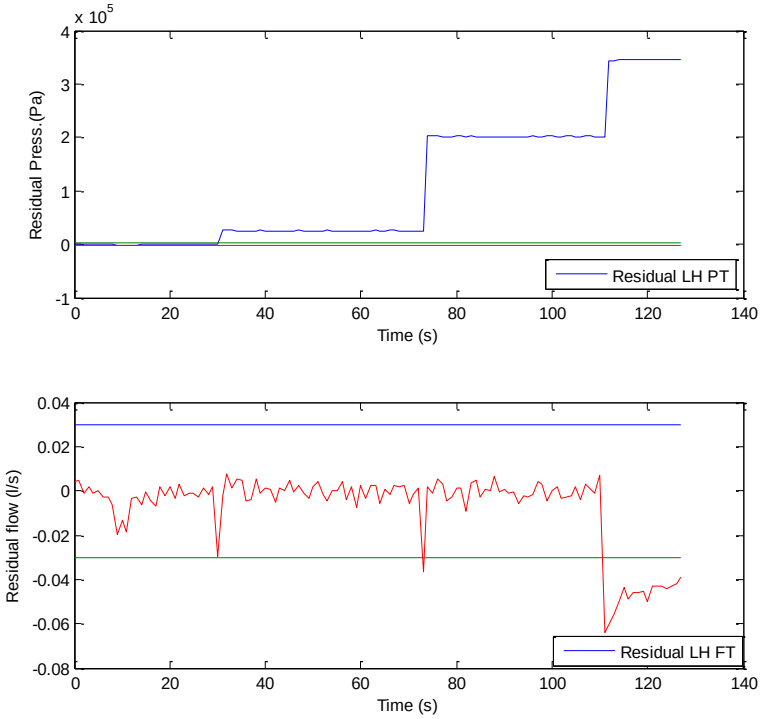

Figure 88: Left hand wing tank pressure and flow residuals for pipe blockage fault injection.

6.2.8.4 Test 4 – Pressure sensor fault

Injecting a pressure sensor abrupt failure in the left hand pressure sensor at 39 seconds causes the residual to exceed its threshold after only 0.1 seconds. No other residuals are affected. Also note that in order to differentiate between some faults sensor behaviour can help to discriminate. The sensor behaviour, i.e. the sensor signal and the estimated signal, can be seen in Figure 89. Note how when the fault is injected the sensor signal is equal to zero. The residual is shown in Figure 90.

It is worth noting that although the negative residual is exceeded for anything much less than full output of the appropriate pump then the fault condition will not be captured. This is due to the poor performance of the pressure transducers at low pressure. Referencing the nature of the fault back to the fault tables ties in with the expected behaviour for a fault of this type.

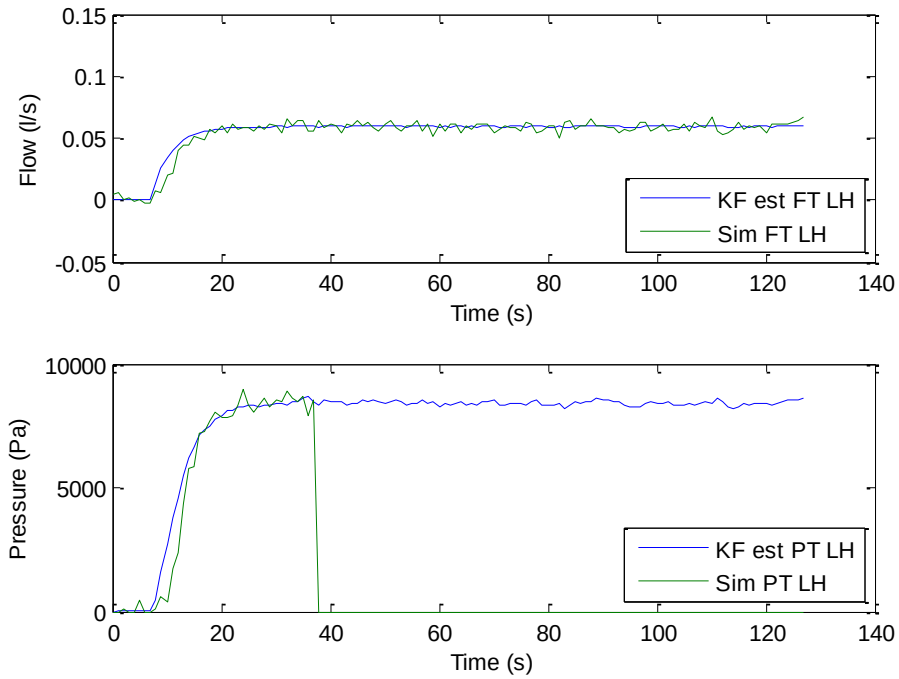

Figure 89: Flow and pressure sensor reading and Kalman estimate for pressure sensor fault.

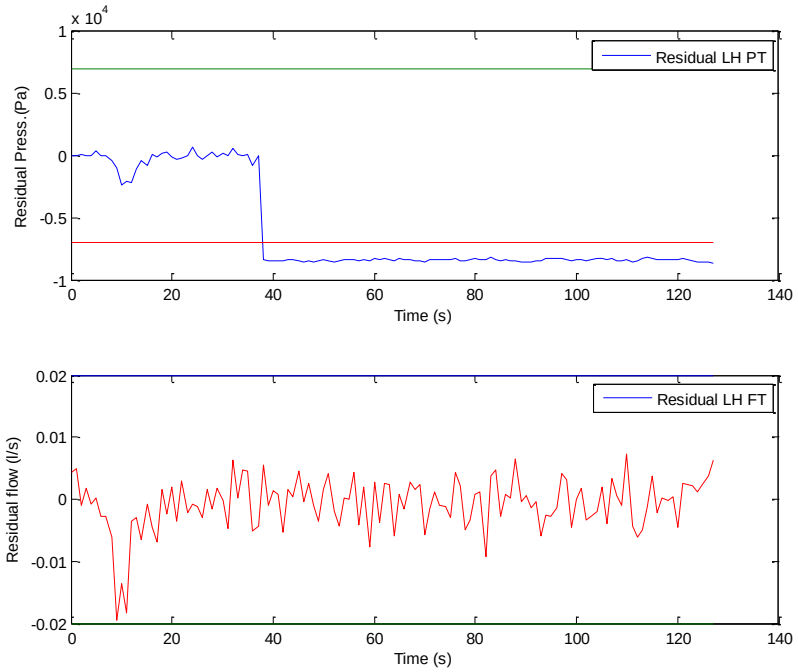

Figure 90: Left hand pressure sensor and flow sensor residuals showing pressure sensor fault.

6.3 Conclusion

This chapter has discussed the development and evaluation of the Kalman filter based Fault Diagnosis and Identification (FDI) applied to the simulink system model of the fuel rig. It has introduced the sub-system dynamics and from this produced state space models of various parts of the fuel rig in order to develop these into a bank of Kalman filters capable of identifying the presence of a fault.

The Kalman filters are then tuned in such a way as to identify the presence of a fault. This requires being sensitive enough to not mask the presence of faults but not so sensitive as to trigger false fault alarms.

Threshold determination has been briefly discussed and a simple heuristic methodology adopted for the purpose of this part of the development. The requirement to discriminate between faults has been introduced and all fault permutations tabulated. The possibility to discriminate further by not only identifying the Kalman filter behavior but also by monitoring the sensor signal behavior has been identified. For example, if two faults had the same Kalman filter residual behavior but in one case the sensor signal was static and equal to zero then the fault would most likely be a failure of the sensor.

Three test cases were evaluated and resulted in positive fault detection and identification.

Chapter 7

Application of Fault Diagnosis and Identification to the UAV Fuel Rig

This chapter describes the application of the Fault Diagnosis and Identification (FDI) to the fuel rig. The application of the FDI uses the bank of Kalman filters developed in the previous chapter, Chapter 6. The bank of Kalman filters is applied to the fuel rig in real time and faults injected into the fuel rig in order to demonstrate the FDI capability and these results presented.

In addition to the Kalman filter FDI applied to the fuel rig, additional residual evaluation using statistical methods is adopted and the use of automatic threshold determination applied to improve robustness and usability of the design process.

The contribution of this chapter is the application of the Fault Detection and Identification scheme to the real life system in order to detect and identify faults reliably. This verifies that this approach is viable for real engineering processes such as the fuel rig.

7.1 Introduction

This Chapter includes the application of the Kalman filter based Fault Detection to the fuel rig with the added benefit of statistical residual evaluation and automatic threshold determination. The residual evaluation filters the signal over a period of samples but amplifies errors as the Kalman filter residual diverges from its normally zero position when a fault is present and examples of this will be given.

The automatic threshold determination aids usability in that it does not require the user to manually determine threshold levels heuristically, which is a very time consuming task.

A series of faults are injected which include a leak fault, pump performance degradation, pipe blockages and sensor failure. This covers failure in actuation, sensors and failure with the physical process. The results are presented for all these faults and conclusions given.

7.2 Application of Kalman Filter FDI to Fuel Rig

Before the Kalman filter is applied to the fuel rig it is necessary to implement a communications interface between the command and control interface and the simulink model. It is also necessary to determine threshold levels and to implement the root mean squared error statistic which is applied to the residual.

7.2.1 Fuel Rig communication interface

The Kalman filter is run in real time against the fuel rig again within the simulink environment. This method requires a communication interface over a network for which UDP is used. UDP is a communication protocol similar to TCP/IP but does not utilise handshaking functionality. Timing is a key issue with the Kalman filter as it is time dependant and the sensor signals are required to be at exactly or as close as possible to 1 second, i.e. ΔT for the model. The timestamp within the Matlab/ simulink environment was not judged to be robust enough as processor control is decided by windows and therefore latency can be caused and not necessarily detected. The labview control and data logging environment produces a timestamp at each data sample which is taken from the system clock and does not rely on the operating system. Therefore as data is sent to simulink it captures all data but picks out the closest data to 1 second and uses this in its calculation. Where data is not available an interpolation of available data is calculated and used for the Kalman filter calculations.

7.2.2 Kalman filter tuning

Having validated the Kalman filter bank on the detailed simulink system model in Chapter 6, it is then possible to implement the same Kalman filter bank on the experimental fuel rig. The Kalman filter gains developed when using the Kalman

filter on the simulink system model are exactly the same as used for the Kalman filter on the fuel rig.

7.2.3 Statistical residual evaluation

The application of the statistical residual processing allows more sensitivity in the residual allowing fault conditions to be amplified whilst not having the same effect on near zero signals as was explained in Chapter 4. The root mean squared error (RMSE) of the residual is used with a sample size of 10 samples as this offered good overall performance. As an example in this instance a tank leak is injected at 39 seconds in the left hand wing tank. The Rig sensor data and KF estimate are shown in Figure 91 and highlights the divergence shortly after the fault is injected. The difference of these signals, the residual, is shown in Figure 92 along with positive and negative thresholds. The residual can be seen exceeding the threshold at around 42 seconds and therefore detecting the fault. The RMSE of the residual is shown in Figure 93 and shows how when the fault occurs the divergence from zero is much greater, zero being no separation between estimate and sensor signal. This figure highlights the overall filtering effect the RMSE function over 10 samples has on the residual and smoothing of the RMSE signal allows tighter thresholds to be applied.

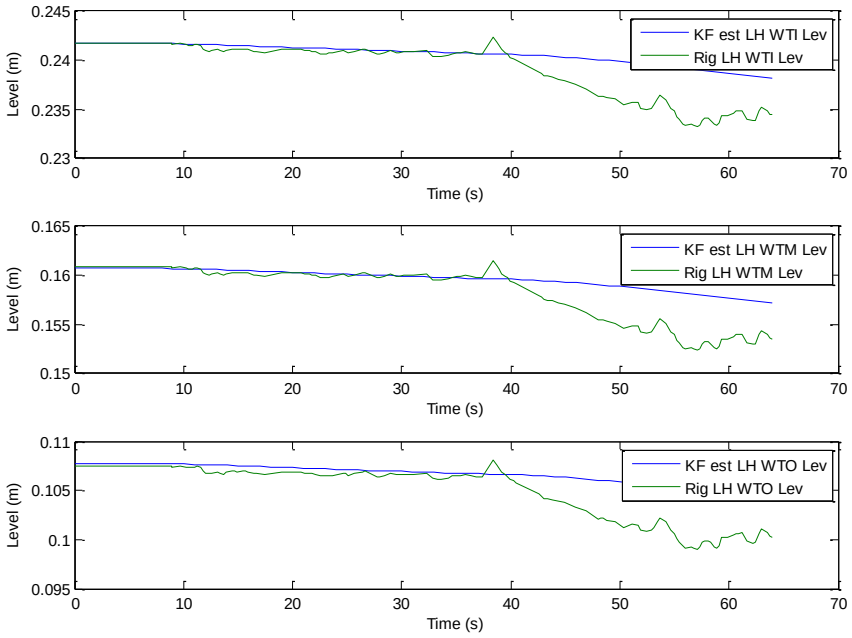

Figure 91: Left hand wing tank rig sensor and KF estimate.

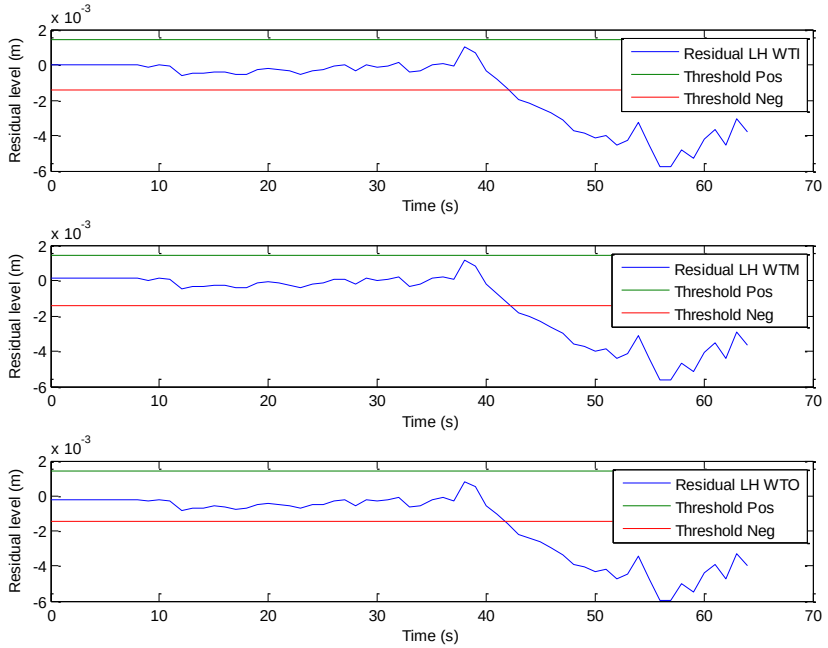

Figure 92: Left hand wing tank residual.

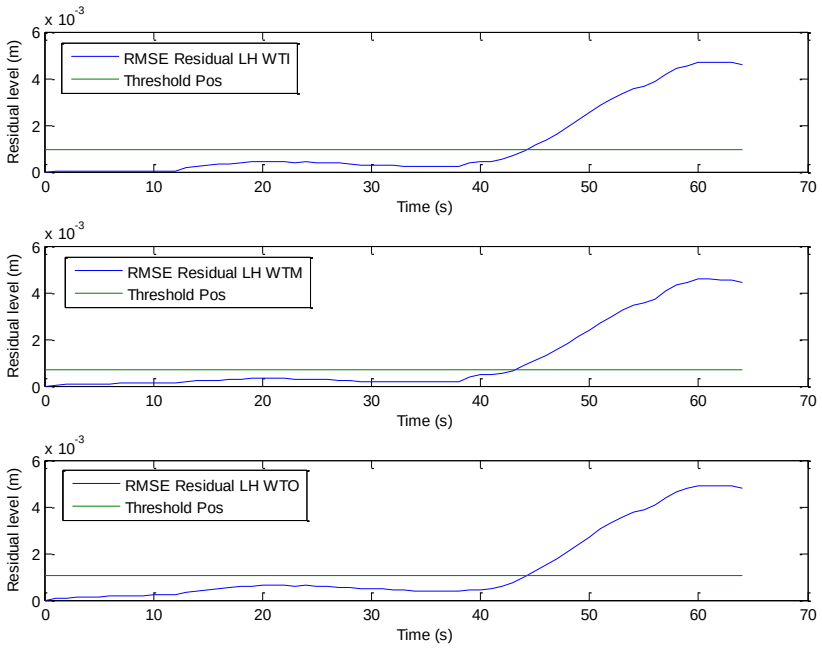

Figure 93: Left hand wing tank RMSE residual.

7.2.4 Threshold determination

Up until this stage all thresholds have been determined heuristically, by examination of data results and the user choosing a value for positive, and if necessary negative, threshold values. The threshold values need to be far enough away from the mean of the normal operation residual values as not to trigger false alarms but close enough as to capture lower magnitude fault conditions. The resultant Kalman residual is of normal distribution with a zero mean value.

For this part of the development the thresholds are determined by a statistical test of known good data. The data is collated and the standard deviation calculated and this used to determine the thresholds. The thresholds are set at a value of 6σ of the distribution and in practice this gave a good overhead as not to trigger false fault condition but also not miss relatively small magnitude faults.

An example of this type of calculation is shown below whereby a known good active sample of 127 seconds is run as shown in Figure 94 below. The 6σ deviation over the sample is also shown in this plot. The final value at the end of this test run is the point at which the thresholds are set. In this case the threshold is 1.25×10^{4} for the left hand pressure transducer (LH PT) and 2.52×10^{-2} for the left hand flow transducer (LH FT). The residual signal showing the set threshold is shown in Figure 95.

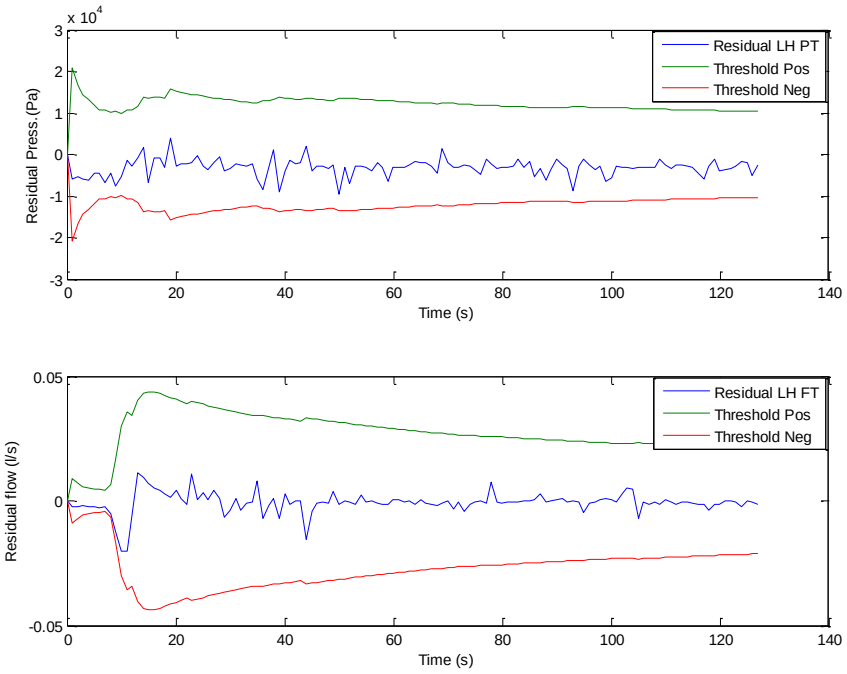

Figure 94: Residual signal for flow and pressure sensor and statistically determined threshold calculation.

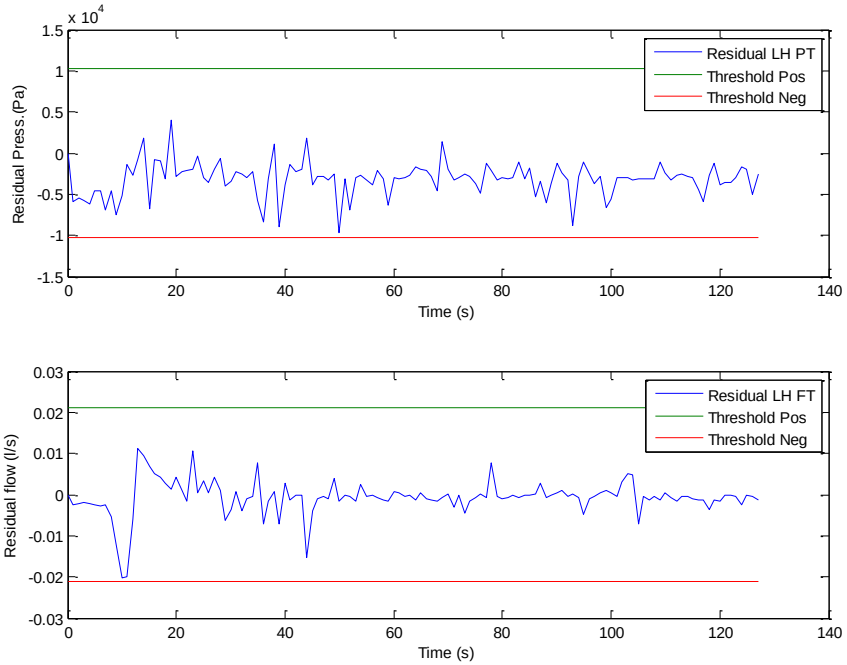

Figure 95: Residual signal and threshold for flow and pressure sensor.

The threshold levels used in the following tests are shown below in Table 23.

	Positive threshold	Negative threshold
Flow Transducer LH WT	2.52×10^{-2}	-2.52×10^{-2}
Pressure Transducer LH WT	1.25×10^{4}	-1.25×10^{4}
Level Transducer LH WT Inner	1.44×10^{-3}	-1.44×10^{-3}
Level Transducer LH WT Middle	1.44×10^{-3}	-1.44×10^{-3}
Level Transducer LH WT Outer	1.44×10^{-3}	-1.44×10^{-3}
Flow Transducer RH WT	3.0×10^{-2}	-3.0×10^{-2}
Pressure Transducer RH WT	3.24×10^{4}	-3.24×10^{4}
Level Transducer RH WT Inner	1.2×10^{-3}	-1.2×10^{-3}
Level Transducer RH WT Middle	1.2×10^{-3}	-1.2×10^{-3}
Level Transducer RH WT Outer	1.2×10^{-3}	-1.2×10^{-3}
Level Transducer LH AT	7.9×10^{-3}	-7.9×10^{-3}
Level Transducer RH AT	1.0×10^{-4}	-1.0×10^{-4}

Table 23: Diagnostic system calculated thresholds for residuals.

The threshold levels used for the RMSE of the residual are calculated in the same way and are shown below in Table 24.

	Positive threshold
Flow Transducer LH WT RMSE	1.56×10^{-2}
Pressure Transducer LH WT RMSE	1.92×10^{4}
Level Transducer LH WT Inner RMSE	9.7×10^{-4}
Level Transducer LH WT Middle RMSE	7.0×10^{-4}
Level Transducer LH WT Outer RMSE	1.0×10^{-3}
Flow Transducer RH WT RMSE	1.56×10^{-2}
Pressure Transducer RH WT RMSE	2.28×10^{4}
Level Transducer RH WT Inner RMSE	6.6×10^{-4}
Level Transducer RH WT Middle RMSE	5.4×10^{-4}
Level Transducer RH WT Outer RMSE	8.8×10^{-4}
Level Transducer LH AT RMSE	3.4×10^{-3}
Level Transducer RH AT RMSE	3.8×10^{-3}

Table 24: Diagnostic system calculated thresholds for RMSE residuals.

7.3 Testing of Kalman filter FDI implementation on fuel rig

Faults are injected on the fuel rig which includes tank leak, pump performance degradation, part and full blockage and sensor failure which are demonstrated in following subsections.

7.3.1 Test 1

This test case is an example of the fault diagnostic system running in a fault free scenario. The left hand pump is driven at full scale input of 2.5V producing a flow of 0.06 l/s to the left engine. In Figure 96, flow and pressure rig sensors and the corresponding Kalman filter estimates are shown for the left hand side main system components, i.e. flow to the engine. Figure 97 shows the left hand wing tank levels for rig and the Kalman filter estimates for inner, middle and outer tanks. Figure 98 shows the residual for flow and pressure and highlights that the residual remains within the threshold bounds in this non-malfunctioning scenario. Figure 99 shows the residual and Kalman filter estimate for the left hand wing tank levels which also remain within the bounds of the predetermined thresholds. Figure 100 shows the root mean squared error (RMSE) of the pressure and flow residuals. These RMSE signals for pressure and flow also remain within the thresholds. Figure 101 shows the RMSE of the residual for the inner, middle and outer left hand wing tank levels. Again these remain within the thresholds.

All of the residuals and RMSE of the residuals have remained within the bounds of the thresholds as intended for this fault free scenario and therefore agrees with the non-fault condition of the fuel rig.

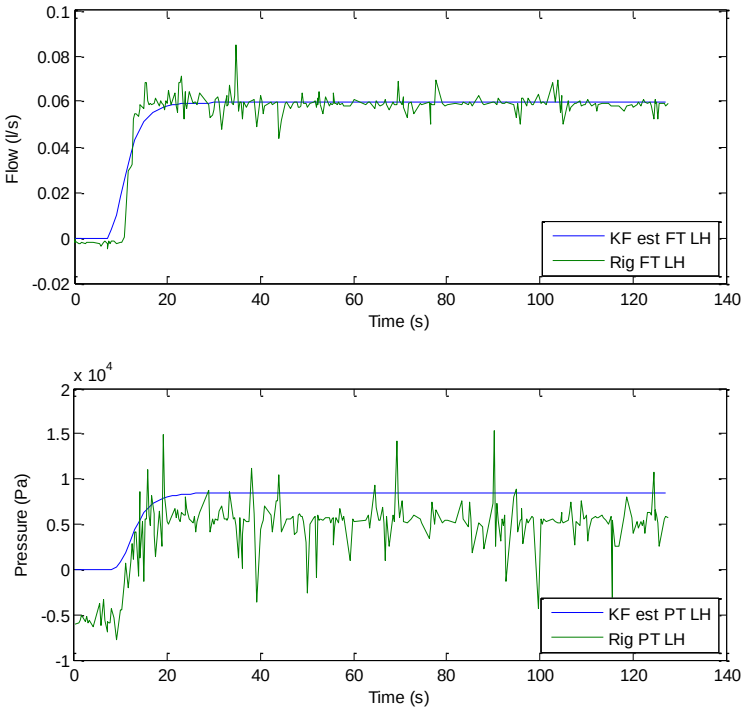

Figure 96: Fuel rig and KF estimate for flow and pressure sensor.

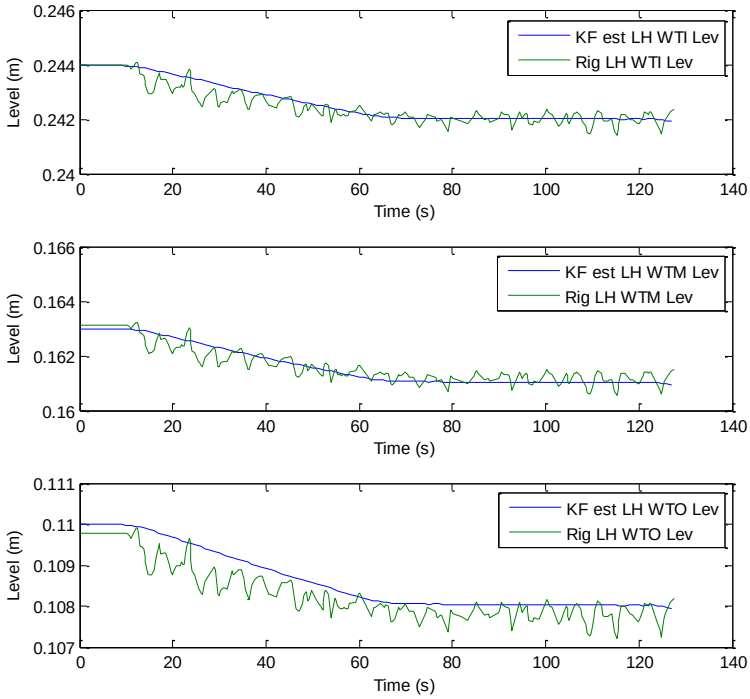

Figure 97: Fuel rig and KF estimate for tank level sensor.

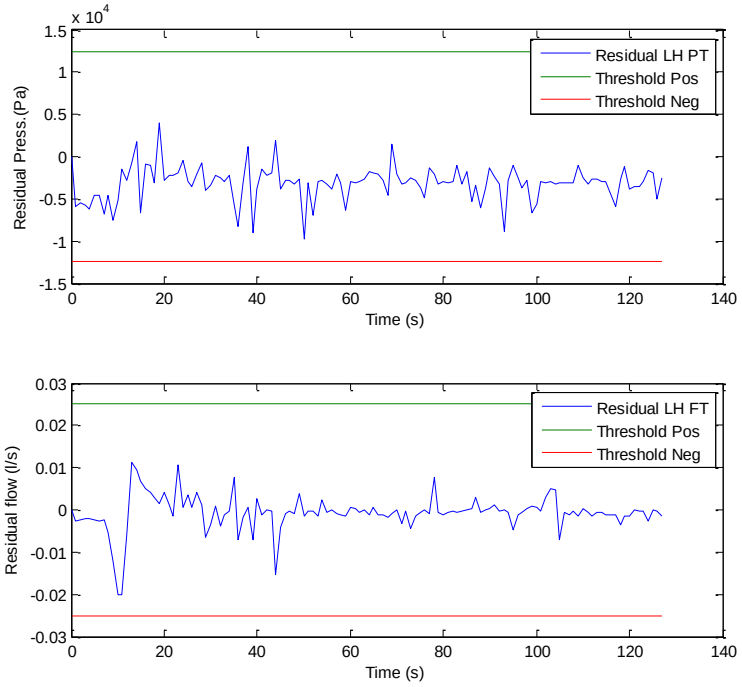

Figure 98: Residual signal and threshold for flow and pressure sensor.

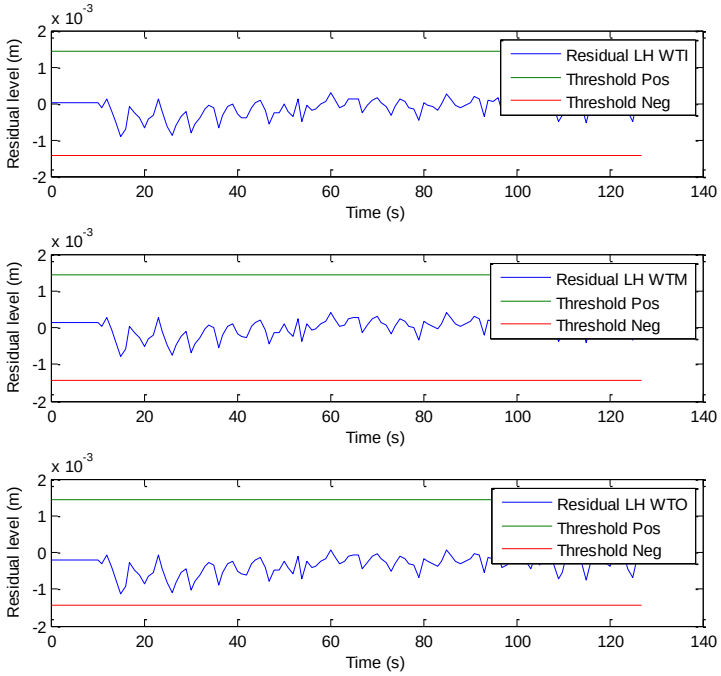

Figure 99: Residual signal and threshold for tank level sensor.

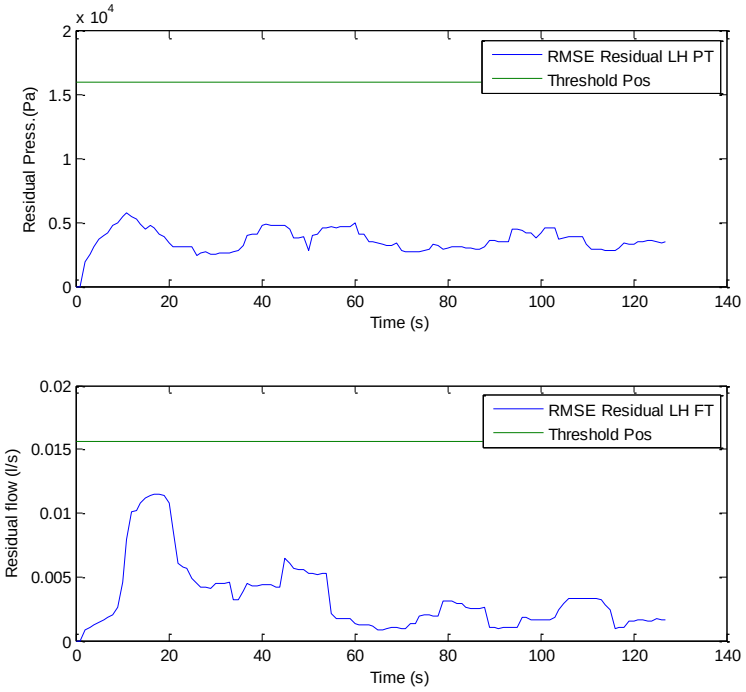

Figure 100: RMSE residual signal and threshold for flow and pressure sensor.

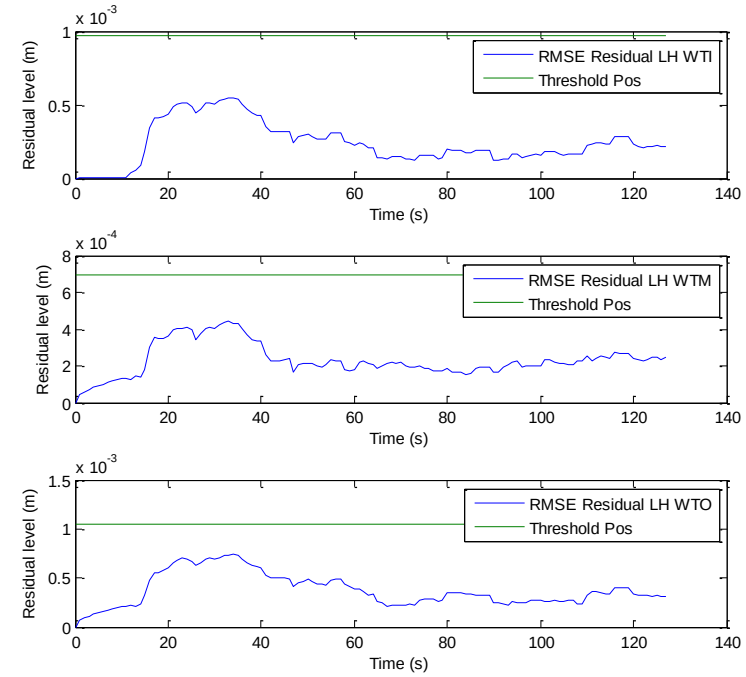

Figure 101: RMSE residual signal and threshold for tank level sensor.

7.3.2 Test 2

For this test case a leak in a tank is injected on the fuel rig in the left hand wing tank. The flow rate of the leak is unknown since it is injected by means of opening a manual valve at the bottom of the tank. The fault is injected at approximately 39 seconds. The simulation done in Chapter 6 with the Kalman filter being implemented on the simulink system model had the same fault injected at a similar time and this was done to allow for direction comparison to be achieved.

Figure 102 shows the left hand wing tank levels for inner, middle and outer tanks for the fuel rig and its corresponding Kalman filter estimation. Figure 103 shows the associated residuals for these tank levels and Figure 104 shows the root mean square error (RMSE) for these residuals.

The residual signals seen in Figure 103 shows a negative divergence from its normally zero position crossing the negative threshold at approximately 43 seconds.

The RMSE residual, seen in Figure 104, also crosses the threshold at approximately 43 seconds also. This plot also highlights the smoothing effect of the RMSE statistical implementation. It also shows that with the statistical measure the separation between the fault and threshold is greater for the same fault compared to the residual alone, showing the amplification of the error condition with the application of the statistical measure.

Referring back to the tabulation of fault conditions in Chapter 6 provides the information that a negative residual in the left hand wing tank leads the fault case being F18 which is a fault of a leak in the left hand wing tank.

A similar scenario would be if a fault was seen that showed a negative residual in the wing tank, as was the case in this example, but also a negative fault in flow and pressure sensors which indicates a leak fault in the pipe work between the wing tank and the engine. Alternatively if a left hand wing tank sensor failure has occurred then

it would also produce a negative residual as in this test scenario. However, the behaviour of the sensor signal itself would equal zero for a short to ground failure or constantly high for a high/ floating failure.

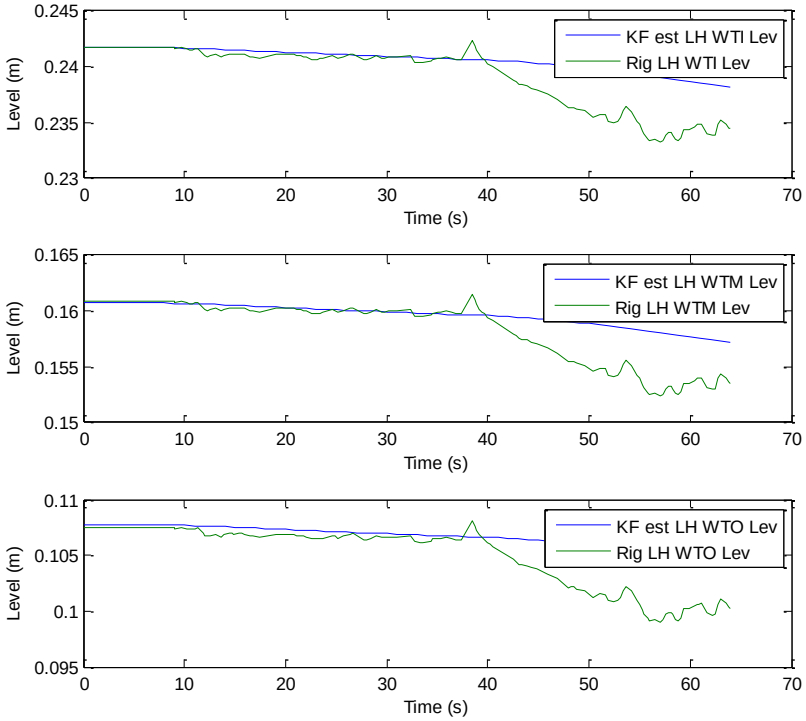

Figure 102: Left hand wing tank fuel rig sensor and Kalman filter estimate.

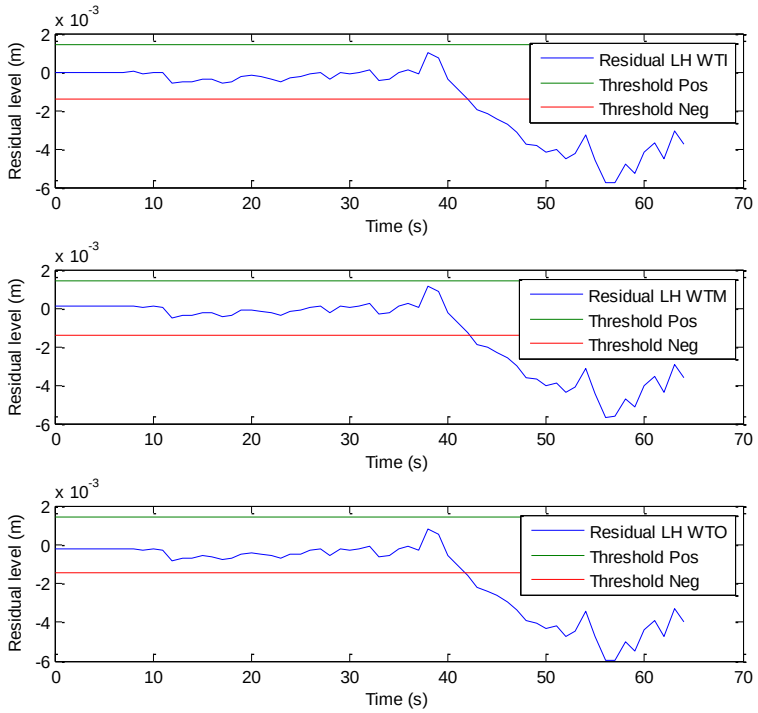

Figure 103: Left hand wing tank residual.

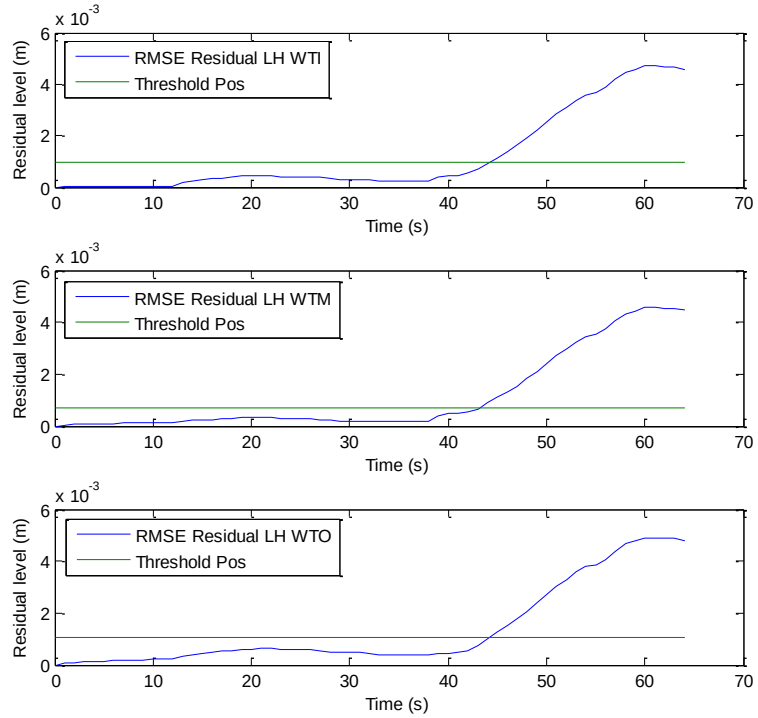

Figure 104: Left hand wing tank RMSE residual.

7.3.3 Test 3

This test scenario applies the fault condition of pump degradation to the fuel rig which in practice could be indicative of incipient mechanical failure limiting the action of the pump motor. To simulate this, a bias of -1V is applied to the left hand main pump, (i.e. intended voltage 2.5V but only 1.5V is applied), therefore limiting the fuel rig pump motor performance. This change occurs at 15 seconds.

The fuel rig sensor signal along with the Kalman filter estimate for the flow transducer and pressure transducer is shown in Figure 105. At the point of fault injection, divergence of both the pressure and flow signals is seen. Figure 106 shows the left hand wing tank levels and the corresponding Kalman filter estimation which also show divergence of the signals after the fault is injected.

The residuals for flow and pressure, seen in Figure 107, show the flow sensor residual exceeding the negative threshold, however although the pressure sensor showed considerable divergence, in Figure 105, the residual, in Figure 107, does not exceed the predetermined threshold level. This is due to the inaccuracy of the sensor at low pressure. As was explained in the previous chapter the noise seen on the sensor is so great at low system pressure, i.e. normal operational pressure, that the size of the threshold required eliminates the possibility of picking up negative Kalman filter fault conditions. The pressure sensor is still useful in the positive residual direction however which occurs in the presence of a blockage condition.

Figure 108 shows the left hand wing tank level residuals. Although this approaches and exceeds the thresholds periodically it bounces in and out of reliably determining a fault condition. It is therefore considered not to have triggered the fault condition as it did not remain in this state for long enough.

The root mean squared error (RMSE) for the residuals of flow and pressure are shown in Figure 109. The RMSE pressure transducer signal does not exceed the threshold, however it remains much further from the threshold bounds of the residual than when

no statistical processing was applied as seen in Figure 107 indicating the increased robustness due to the implementation of this method.

The RMSE flow transducer signal exceeds the threshold greatly and much more, proportionately, than with no statistical measure applied.

Figure 110 shows the tank levels which exceed the threshold indicating the presence of a fault condition. However, previously with no statistical processing applied, as seen in Figure 108, a fault condition was not reliably determined.

Therefore by assuming the presence of a fault condition is determined using the RMSE signal and the Kalman filter residual only determines the direction of the fault. Then in this case the flow transducer signal produces a negative fault and the left hand wing tank produces a positive fault. Mapping this back to the fault tables seen in Chapter 6 refers to F5, which is a pump under-run bias which would be correct.

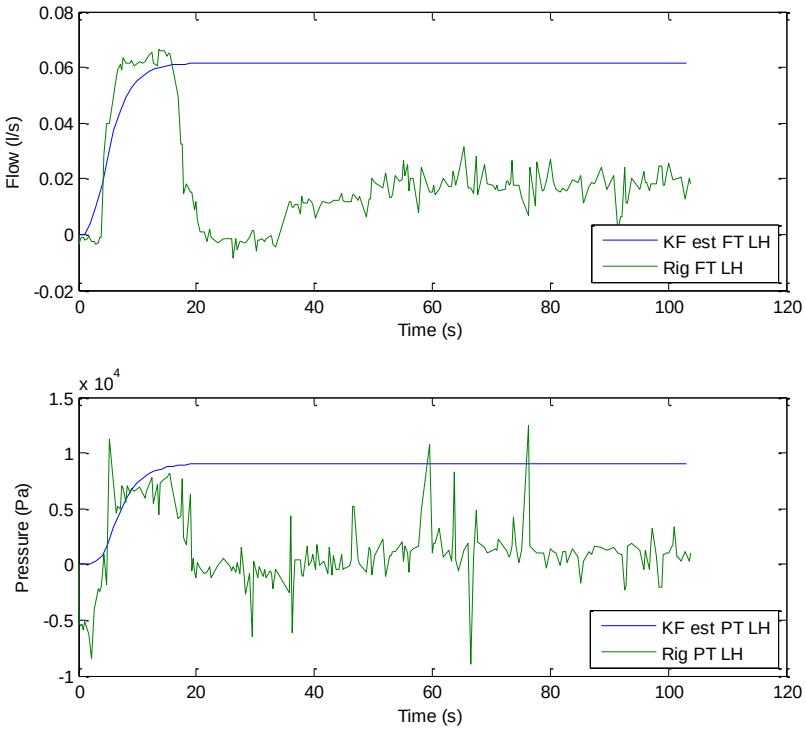

Figure 105: Left hand main pump flow and pressure rig sensor and Kalman filter estimate.

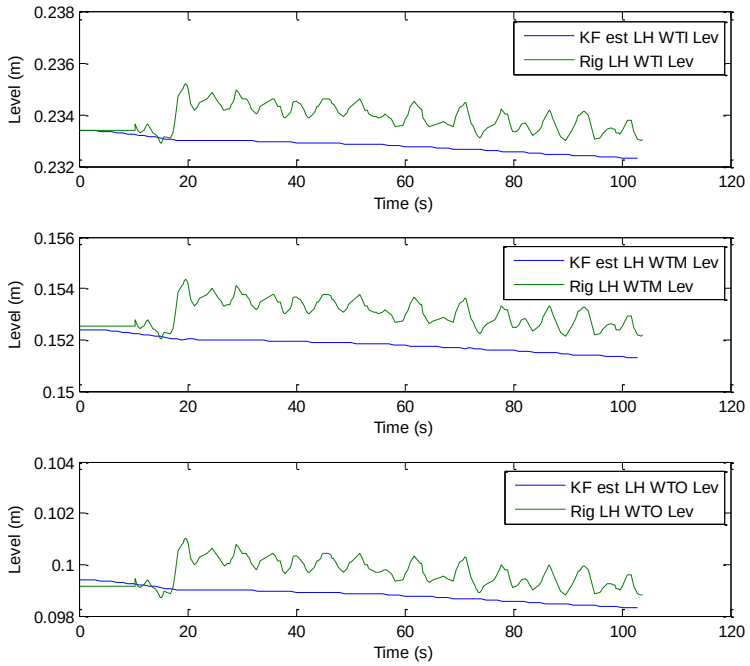

Figure 106: Left hand wing tank rig sensor and Kalman filter estimate.

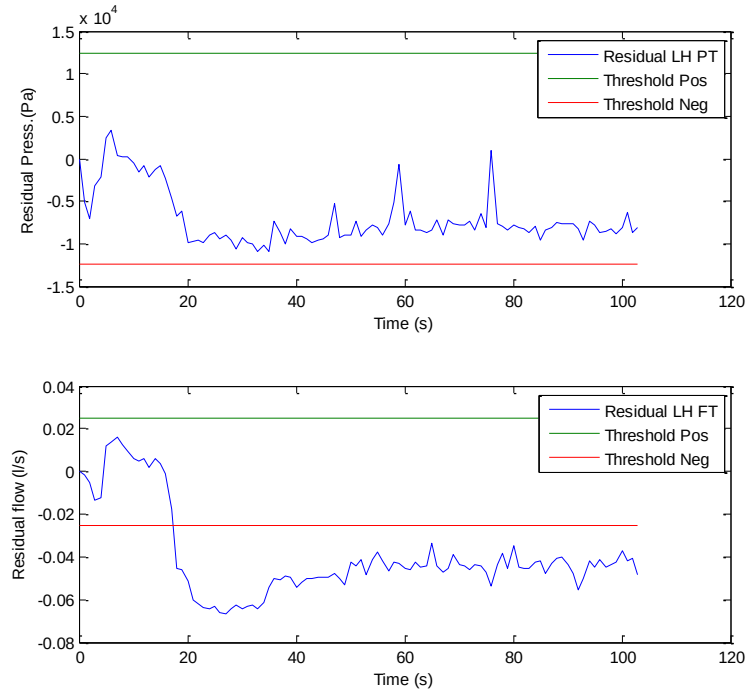

Figure 107: Left hand main pump flow and pressure residual.

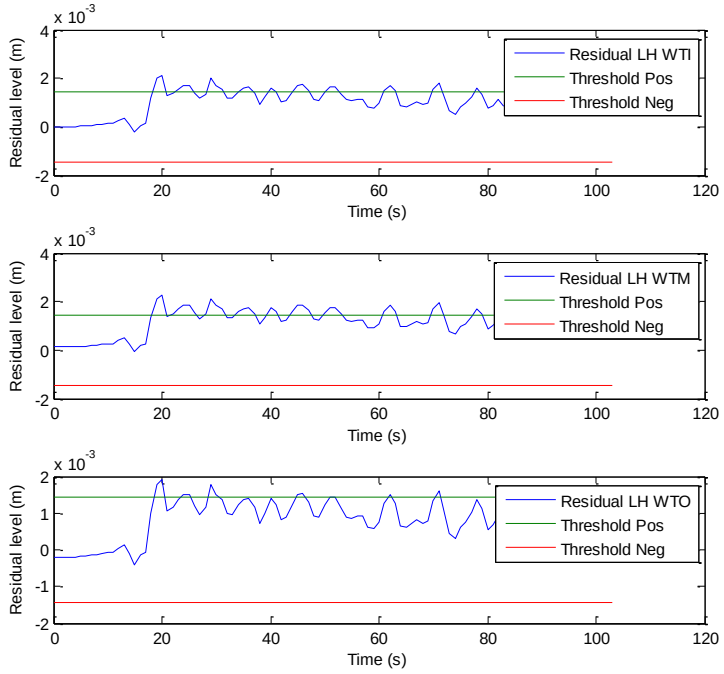

Figure 108: Left hand wing tank residual.

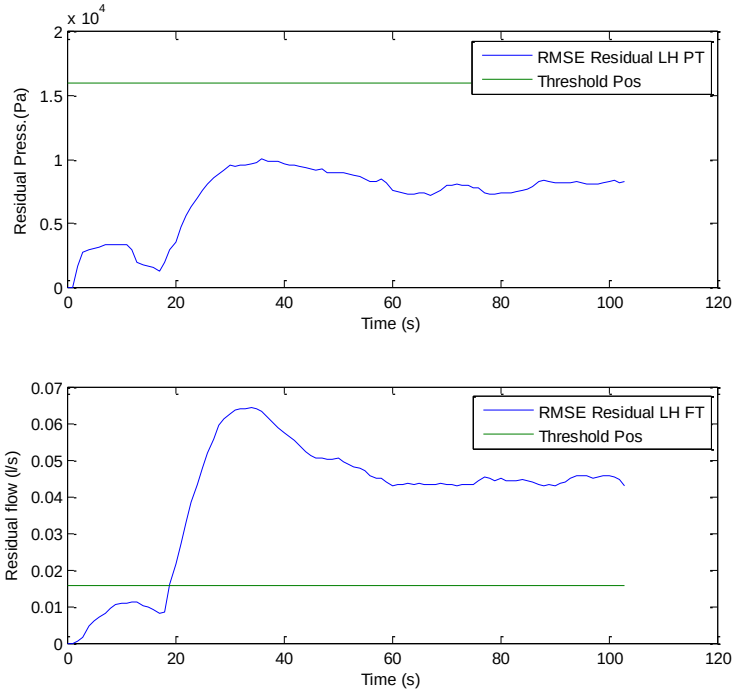

Figure 109: Left hand main pump flow and pressure RMSE residual.

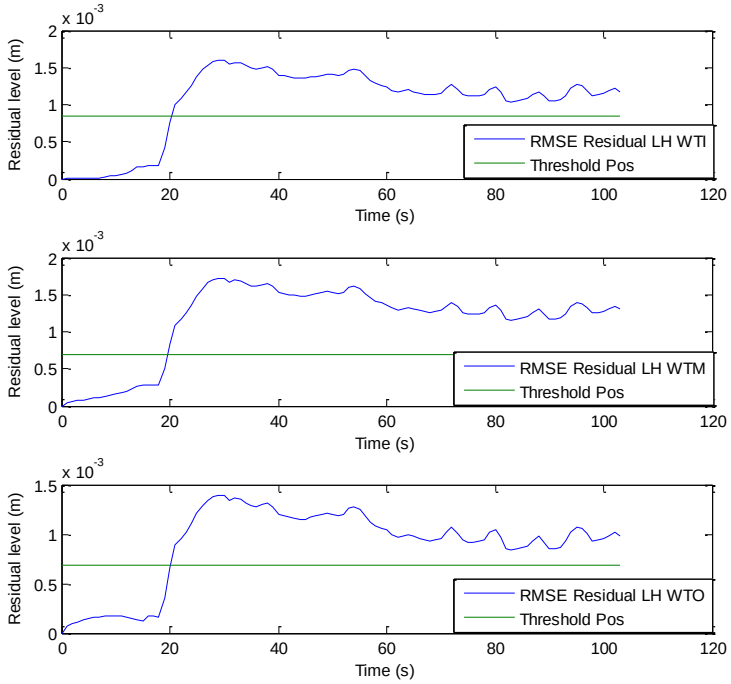

Figure 110: Left hand wing tank RMSE residual.

7.3.4 Test 4

In this fault case scenario an isolation valve is closed proportionately to represent a part blockage in the pipe work between the left hand pump and the engine. The first blockage is injected at approximately 30 seconds when the isolation valve position is changed to approximately 50% closed, then at 70 seconds approximately 80% closed and finally at 110 seconds the valve is fully closed.

The fuel rig flow transducer and pressure transducer along with the Kalman filter estimates for each signal are shown in Figure 111. The plot showing the pressure transducer signal highlights the divergence clearly by the increase in pressure each time the valve position is changed. As for the flow, when the valve position is moved to 50% closed position this does not affect the flow apart from a short transient at the time of the fault injection. When the valve position is changed to 85% closed the flow does diverge from its Kalman filter estimate, however, the flow does partially remain. When the valve is fully closed the flow sensor signal is seen to approach zero, however, the Kalman filter estimation remains and thus the divergence increases.

The residuals for the sensor signals seen in Figure 111 are shown in Figure 112. Again the pressure residual clearly increases at each stage of closure of the valve and for all position from 50% is beyond the bounds of the positive threshold.

The flow residual for 50% valve closure remains within the threshold. For 85% valve closure the flow residual bounces around the threshold although remaining mostly on the side of a fault condition, although this is very indeterminate. When the valve is fully closed the flow residual exceeds the negative threshold.

Figure 113 shows the root mean squared error (RMSE) for the flow and pressure transducer residuals. The pressure RMSE residual remains similar in performance to the residual alone, seen in Figure 112, both highlighting the increase in divergence for each valve position increment.

The flow transducer RMSE plot does not exceed the threshold for the valve position of 50% closed. However, for 85% valve closure it clearly exceeds the threshold identifying the presence of a fault whereby the residual signal alone, seen in Figure 112, did not identify this same fault.

Therefore the fault of part blockage simulated by closing the valve 50% caused a positive residual of pressure only which when referenced back to the tabulation of faults in Chapter 6 this identifies F27 which represents a blockage of 0% to 85% closed, i.e. a part blockage. However further investigation would be required as this fault signature is also representative of fault F52. This would need to be reported to the maintenance personnel dealing with the issue.

The faults injected of 85% closed and fully closed produce a positive residual for pressure and a negative residual for flow. Referencing this back to the fault permutations tables in Chapter 6 identifies F28, which is a blockage of 85% to 100%. This corresponds to the faults which were injected.

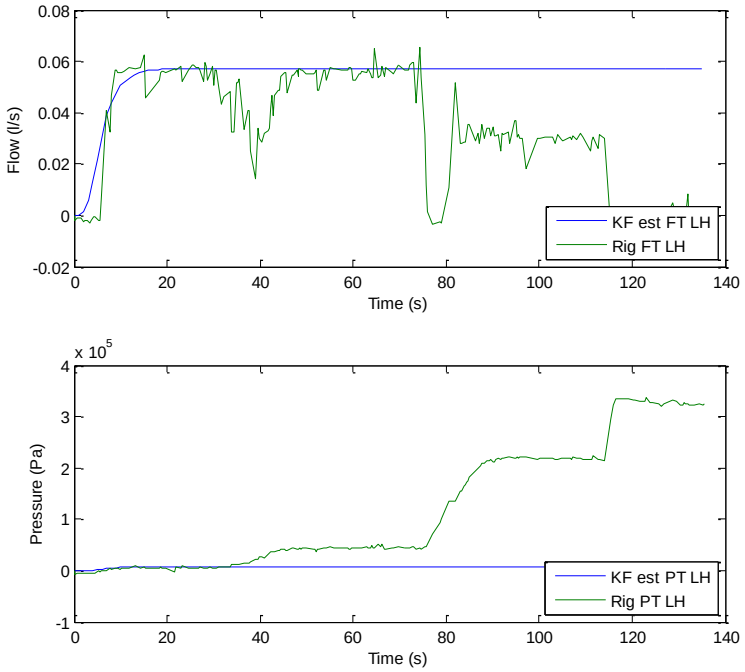

Figure 111: Left hand main pump flow and pressure rig sensor and Kalman filter estimate.

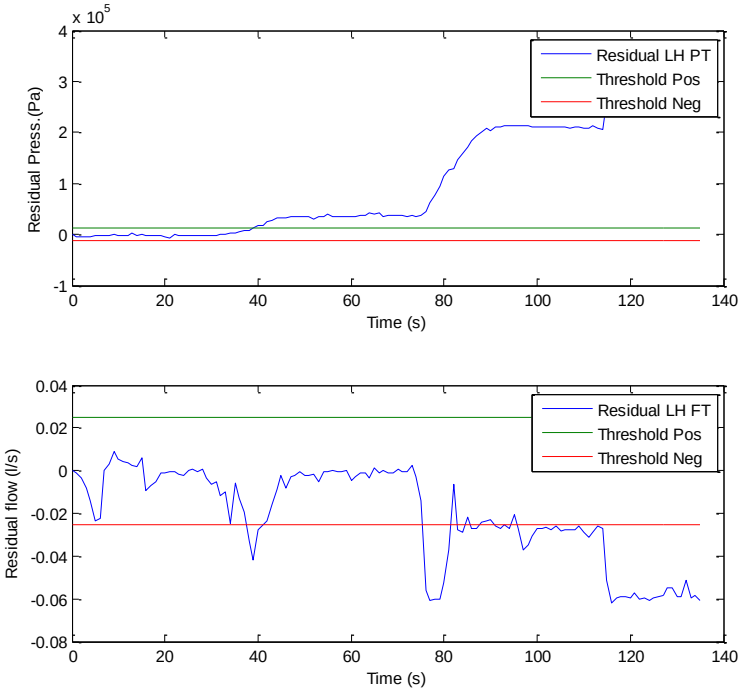

Figure 112: Left hand main pump flow and pressure residual.

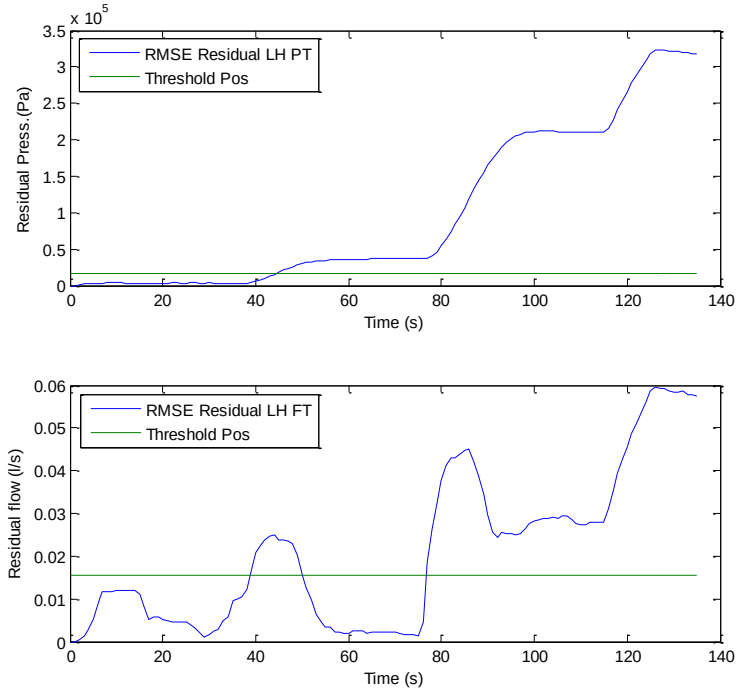

Figure 113: Left hand main pump flow and pressure RMSE residual.

7.3.5 Test 5

In this fault case scenario the left hand flow sensor is grounded at 40 seconds to simulate a short to ground failure mode of this sensor. Figure 114 shows the fuel rig sensor signals for flow and pressure and the relevant Kalman filter estimate for each. When the flow sensor fails at 40 seconds it clearly shows on the plot. The pressure sensor result is unaffected.

The residuals derived from the flow sensor is shown in Figure 115, whereby when the fault is injected a clear negative divergence of its normally zero position is observed. Again the result for the pressure residual is unaffected.

The root mean square error (RMSE) is shown in Figure 116 and this also shows large divergence greatly exceeding the threshold.

Therefore, a negative residual fault on the left hand main flow sensor when referenced back to the fault tabulation in Chapter 6 produces F59, which is an abrupt failure in the left hand flow transducer. In this case the activity of the flow sensor signal itself also aids in the discrimination of the fault identity being constant and equal to zero at the time at which the fault is present.

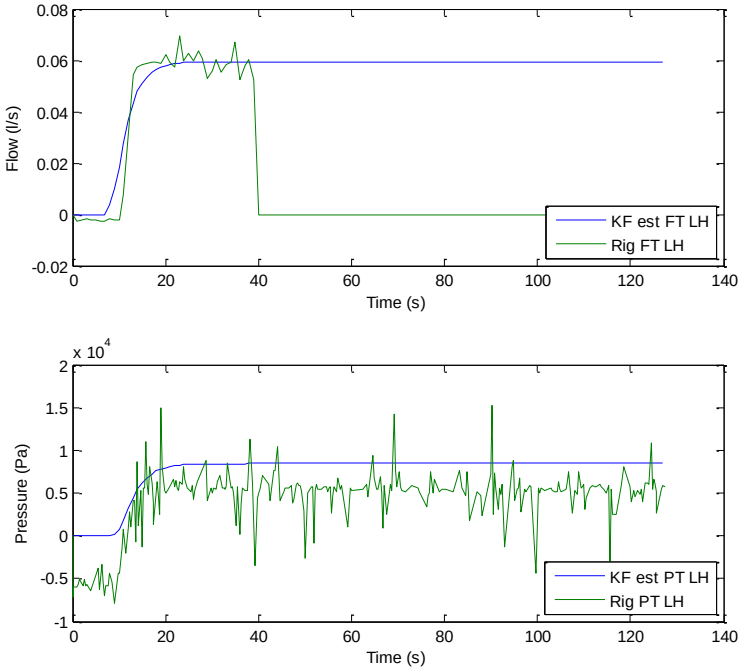

Figure 114: Left hand main pump flow and pressure rig sensor and Kalman filter estimate.

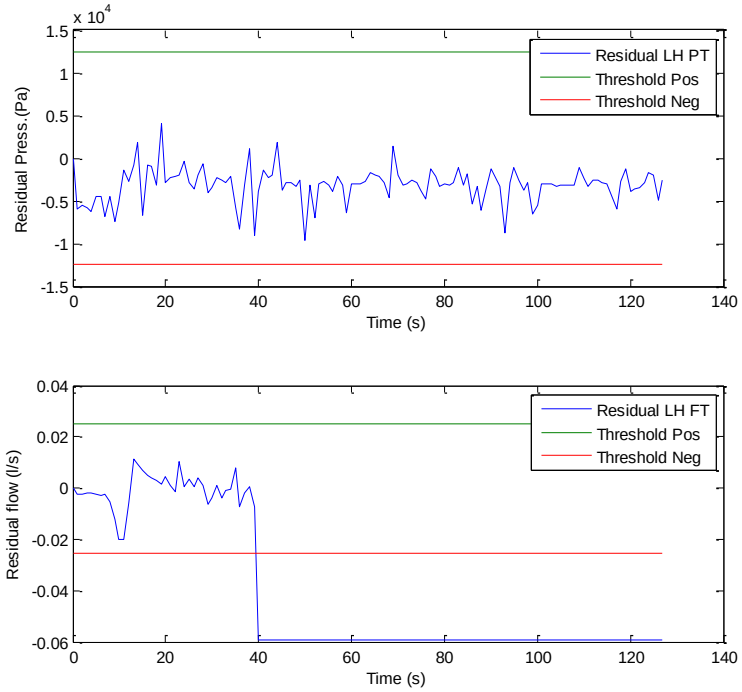

Figure 115: Left hand main pump flow and pressure residual.

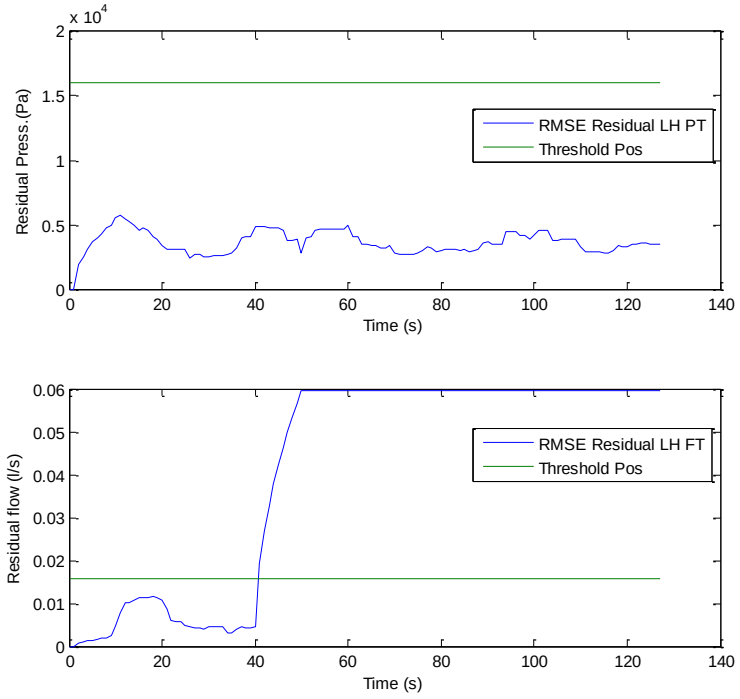

Figure 116: Left hand main pump flow and pressure RMSE residual.

7.4 Conclusion

A Kalman filter based Fault Detection and Identification (FDI) scheme has been applied to the fuel rig in order to detect and identify faults. The Kalman filter FDI developed upon the Simulink system model representing the fuel rig has been used for the detection and identification of faults injected on the fuel rig. In addition to the Kalman filter based FDI, statistical processing is applied to further improve the sensitivity to fault conditions and its robustness in order to eliminate false detection of fault conditions. The statistical evaluation of the residual used the root mean squared error (RMSE) for the residual with a window of 10 samples. This provides a smoothing of or filtering action on the residual signal which in theory will slow down the speed of fault detection. However, the smoothing of the comparatively noisy residual also then allows tighter thresholds to be applied reducing the delay in detection. In practice it was found that a number of faults which were not detectable with certainty using the raw residual alone are detected by the use of the RMSE of the residual. This was seen in test 3 and test 4 in this Chapter.

Another significant development to the FDI scheme in this Chapter is the automatic threshold level determination. In the previous chapter all threshold were determined heuristically which is a painstakingly time consuming process. This Chapter has introduced the automatic determination of threshold levels which utilises a function of the distribution of a known good data set and applies bounds at which a fault condition is judged to be present. It was found to be very effective.

Several test runs were performed, these are summarised below:

1. the first of which being of non-fault condition as a benchmark to show that no fault condition is detected in the presence of no fault condition being injected into the fuel rig. The test performed successfully.

2. The second test scenario was the injection of a tank leak fault in the left hand wing tank. The FDI scheme responded well to the detection of this fault

condition. The identification process led to correctly identifying the fault from the tabulation of possible fault permutations presented in the previous chapter.

3. The third test case applied a fault of pump performance degradation to the left hand main pump motor. This represents impaired performance of the pump and in practice could be due to mechanical failure within the pump or motor limiting its performance. The Kalman filter FDI scheme without the application of statistical evaluation of the residual did not reliably detect the fault. However when using the statistical evaluation of the residual it correctly detects and identifies the fault condition. This highlights the increased robustness and sensitivity obtained via the use of the RMSE statistic.

4. The fourth test scenario was the injection of a blockage into the pipe work between the left hand wing tank and left hand engine. A valve was closed to various positions to represent the blockage over the test case. The valve positions were 50% closed, 85% closed and fully closed. When utilising the RMSE measure all fault conditions were correctly detected and identified as per the fault matrix.

5. The fifth and last test case was a sensor failure of the left hand flow sensor. The fault was detected and identified reliably. However the identification process of the fault using the fault tables highlights the ability to further discriminate between fault conditions by using both the behaviour of the residual and the behaviour of the sensor at the time of the fault detection. In this case it is possible to determine exactly the cause of the fault as the behaviour of the sensor is to remain at zero or constant during the fault condition.

In summary, the FDI scheme with a Kalman filter bank and residual evaluation using raw data and RMSE combined with automatic threshold setting has been tested under various realistic fault scenarios. The result is that the scheme was found capable of reliably detecting a range of faults and was not triggering undesired false alarms.

Chapter 8

Conclusion

The subject of this thesis has been the development and application of a Fault Detection and Identification tool applied to an avionic fuel system simulator rig. This section contains the conclusions to the development.

8.1 Introduction

A Fault Diagnosis and Identification (FDI) tool has been successfully developed for the intended purpose of detection of faults on the fuel rig. The method utilized, as identified as the intended method early on, the use of a Kalman filter.

The Kalman filter is an observer which uses a linear model of the plant simulating the dominant dynamics with feedback correction to the model to correct any divergence between plant and model. It is, however, the feedback gain value, i.e. the Kalman filter gain, that is critical and determines this as an optimal observer. If the gain is too large then the model will track the output of the plant, including any faults present. Now if the Kalman filter gain is too small then the Kalman filter and plant outputs will diverge over time as no system is without disturbance. In fault detection the purpose of the Kalman filter gain is to overcome any disturbances due to modeling errors, etc, and not to track to such an extent that when a fault is present it masks this action. The Kalman filter gain is calculated using the Ricatti equation which uses the covariance of sensor noise, which is available by analysis of sensor data, and process noise which is estimated and this process used to tune the Kalman filter. Alternative adaptations of Kalman filter are available but it was thought unnecessary to add to the complexity as it would not achieve significantly improved result than the steady state Kalman filter used. One limitation of the approach adopted is it can only be applied to linear models, if a nonlinear model is required then use of an extended Kalman filter may be adopted. Another limitation is the ability to fully discriminate the identification of faults, although this system has exhibited almost full discrimination between faults providing an accurate fault position for the effect of the fault it had one fault with the same fault signature to another. The addition of further sensors can help with the fault identification process since the number of and position of the sensors influences the ability to discriminate between faults.

8.2 Chapter by Chapter Review

8.2.1 Chapter 2

Other, similar areas of diagnostic methodology were examined in the early stages of the project and some of the research presented in the literature survey in Chapter 2. Several other methods examined showed promising performance in several areas including neural networks, neuro-fuzzy methods and statistical classification methods. These alternative methods could be applied to the test rig in order to perform comparisons between methods.

A brief examination of literature concerning prognostics was explored identifying this as a possible path for extension of the project.

8.2.2 Chapter 3

Chapter 3 introduced the plant subject to the FDI scheme as an aircraft fuel system simulator rig. This fuel rig simulates, by hardware similarity, the function of an aircraft fuel system. It consists of an array of pipe work, pumps, valves and tanks similar in function to that found on a modern aircraft fuel system.

The initial stages of the project consisted of the assistance in the commissioning of the fuel rig for which the authors contribution included redesign of the power and motor control cabinet. The cabinet includes interface to all power supplies, motor control via inverters, the function of injection of physical faults and the ability to reconfigure the power supply in order to overcome a fault in the power system.

Additional to this project, the fuel rig has also been used in order to implement experimentation on other projects.

8.2.3 Chapter 4

The design process required a simulink nonlinear system model of the fuel rig to be created as was seen in Chapter 4. This simulink model is a nonlinear mechanistic/ physical model based upon the electromechanical interfaces and the fluid dynamics. As many parts of the fuel rig are repeated a library of component models are created which when interconnected create the overall system model. The library consists of generic model for tanks, pumps, pipes and valve, the parameters of which provide the capacity to model different physical attributes of the various parts of the fuel rig.

The modular design of the library of subsystem models necessitates a specific order of interconnection. The library models are considered capacitive or resistive elements. Capacitive elements are storage devices such as tanks and pipes, whereas resistive elements offer resistance to the fluid flow such as valves. The storage devices, i.e. capacitive, offer inputs of flow and output of pressure. Whereas resistive elements, such as a valve, require input of pressure and provide output of flow. Therefore the system simulink model can be built using interconnecting alternate type of model subsystem, i.e. capacitive, resistive, capacitive, etc. The overall simulink system model was created and validated successfully against the fuel rig. The least accurate part of the simulink system model is the pressure sensor, i.e. the pressure output from the pipe model. This is not due to the model as an average between sensors was taken to provide the model parameter due to differences between individual sensors. At low pressure, which covers most normal operating conditions, the pressure sensor seems to indicate some variability in its measurement, at higher pressures the accuracy of the pressure sensor functions more accurately. Due to this the pressure sensor fault condition thresholds have to be wider than if the sensor was more accurate, however, under testing in blockage conditions the pressure increases significantly for relatively small blockages and is therefore considered fine for the intended purpose.

8.2.4 Chapter 5

Chapter 5 presented an initial investigation into the performance of the Kalman filter, a simple Kalman filter was designed to detect a leak fault in a tank. A state space model was created using the already linear plant differential equations and a steady state Kalman filter applied to this. The tuning of the gain of the Kalman filter was achieved using the covariance of the sensor noise and an estimation of the covariance of process noise. The testing was performed using real fuel rig data. Four separate test cases were carried out. The first being a benchmark test of good data, i.e. no leak fault injected. The following three tests being variable degrees of leak flow rate from the fuel rig tank. The leak flow rates were 1.03l/s, 0.44l/s, and 0.22l/s. For the three fault cases the time taken for the Kalman filter to detect the fault was 8 seconds, 25.5 seconds and 26.8 seconds respectively.

For the fault condition test cases the residual signal was further processed with the intention on finding possible methods of improving the function of fault detection. Several statistical methods were applied to the Kalman filter residual to attempt to further optimize its performance, including mean deviation, mean absolute deviation, sum square of error, weighted sum square of error, root mean square of error, paired t-test, chi-squared mean and r-square methods. The residual evaluation tested each of the mentioned methods using varying sample window size to further improve the analysis. Sample window sizes of N=5, N=10, N=20, N=40, N=80 and N=160 were tested. In order to achieve fairness in comparison each test was performed offline using data collated previously from the test rig and the same as was used with the Kalman filter alone. In order to further achieve equality between tests a standardization of the threshold level was also required as heuristic determination could lead to an unfair comparative. A threshold setting was determined by taking a multiple of the standard deviation of the normally distributed residual signal and as each method is subjected to testing of the same residual this produced a fair comparative.

The results of evaluation of the statistical residual processing determined root mean square error produced the fastest fault detection response, sum square error and mean square error being a close second. As the sample window size, N, is increased the amount of noise seen on the resultant signal is attenuated. The downside of this though is the slower response to a fault, however, greater attenuation of the noise seen on the signal a "tighter" set of thresholds can be achieved overcoming the delayed reaction. It was found that between N=5 and N=20 samples produced the best result, ample sizes of greater than N=20 reduced the reaction time too much and sample sizes of less than N=5 proved to be too noisy in comparison.

Overall the addition of statistical residual evaluation produced positive results in providing an improved performance over the Kalman filter residual alone. The benefit of this was seen later on the complete system in Chapter 7.

8.2.5 Chapter 6

The next stage of the design flow, provided by Chapter 6, was to develop the Kalman filter bank and validate it on the simulink system model. For this it was required that linear state space models were to be developed for the subsystem models of pump, tank, pipe and valve which were created previously. The flow through the valve on the rig where the flow sensor is positioned considered the same as the flow through the pump when the rig is in a steady state. Therefore, for the purpose of the Kalman filter design, the flow of the pump model shall be compared to that of the measured flow through the pipe. Some nonlinearity is present on the pump control input which is caused by the action of the inverter control on the motors. Each of the tanks within the system has varying inputs and outputs dependant on what flows into and out of it. Therefore each of the tank models is slightly different. Two separate methods of applying the Kalman filter to the tank were tested. The first being the use of the flow sensor as an input to the Kalman filter in order to determine height in the tank. Although this would seem the most suitable it was deemed too noisy to give a stable tank height estimate. Much better performance was achieved by calculating the flow from the input voltage and using this input to determine tank height levels and

therefore the latter method was used. The flow to and from tanks is also subject to the position of the three way valves on the rig and logic is implemented to determine switching of the inputs to accommodate this.

The Kalman filter gains were tuned using calculated sensor noise covariance and estimated process noise covariance to provide good results, where small errors, such as model inaccuracies, would be tracked but system faults would not. A fault condition leading to divergence between sensor signal and estimate and thus a deviation from near zero of the residual signal.

It was also necessary to identify the location of the fault. Once a fault condition was determined this was achieved by manually injecting faults into the simulink system model and recording the resulting action of the residual and the sensor behavior in the presence of a fault condition. The permutation of possible fault condition was tabulated and the action of resultant behavior recorded. The faults injected are categorized into three fault types. The first being a process fault, whereby the cause of the fault is physical, such as a leak in a tank or a pipe blockage. The second is an actuator fault, whereby an actuation failure has occurred such as a valve position error or pump performance or inoperability issue. The last category being a sensor failure.

The behavior of both Kalman filter and sensor behavior recorded in these tables identified that discrimination between all faults is possible. It is not possible, however, by monitoring the action of the Kalman filter residual alone. An example of this is the discrimination between a tank level transducer failure and a leak in a tank. Both produce a negative residual for the flow measurement; however the action of the sensor subject to the failure will be discriminately different.

Testing of the Kalman filter applied to the simulink system model achieved positive results. The four failure scenarios tested include tank leak, pump performance degradation, pipe blockage and sensor failure. The four test cases with fault injected each capture the intended scenario.

8.2.6 Chapter 7

In Chapter 7, the bank of Kalman filters applied to the simulink system model were then applied to the fuel rig itself and the same set of fault types applied. The setup of the bank of Kalman filter first required some configuration in order to be adapted for this task. The first adaptation was to facilitate external input to the model from the fuel rig. This was achieved using a communication link between the NI labview control and data logging system and the bank of Kalman filter on an external PC running Matlab. This utilized UDP network protocol and some regularisation in the transmission timing at the Matlab end was required.

Statistical residual evaluation was also applied to the KF bank utilizing root-mean-square-error (RMSE) over a sample window size of 10 samples. This was chosen as it proved to have good overall performance in the evaluation of statistical methods carried out previously in Chapter 5.

Another further addition to the system was the ability to automatically determine threshold levels. This was achieved by analysis of a good set of data and calculating thresholds based upon a multiple of the standard deviation of the normally distributed residual data for a known good data set.

Faults injected into the fuel rig were a leak in a tank, pump performance degradation, part and full blockage of a pipe and failure of a sensor. The test case of a leak fault was performed on both the FDI tool applied to the simulink system model and to the FDI tool applied to the fuel rig. Similar fault rates were estimated and both injected at around the same time. Performance of the FDI tool was similar in both instances showing positive results and correct fault identification.

The pump performance degradation test case highlighted that the inaccuracy of the pressure transducer a low pressure due to the required threshold exceeding the normal operating range caused it not to be possible to accurately determine the presence of a negative residual fault condition to be determined except in the extreme circumstance

of abrupt sensor failure or abrupt pump failure. Faults identified by the pressure residual in the positive direction, such as blockages, still perform reliably, a blockage of 50% producing a residual pressure of five times greater than the threshold. The remainder of this test case of pump performance degradation performed suitably, identifying the fault condition correctly.

The third fault condition examined was a blockage of a pipe. Blockages of 50% closed, 80% closed and 100% closed were injected although this required estimation on the fuel rig as it was controlled by a manual valve. Two possible fault conditions are identifiable in this instance. The first is a blockage of 0% to 85% and is determined by the presence of a positive pressure transducer residual. The second is a blockage of 85% to 100% being determined by a positive pressure transducer residual and a positive flow transducer residual also, as the flow in the system becomes restricted. The simulink system model blockages behaved as expected. However, the 80% blockage on the fuel rig was identified as an 85% to 100% blockage highlighting a small discrepancy. It may be required to adjust this estimation of ranges of blockage after further testing to identify the point at which a blockage will cause the flow residual to also exceed its threshold.

The last test case was the grounding of a sensor input signal. For the case of the simulink system model FDI a pressure sensor is grounded. The fault as captured successfully, however identified that a fault of this nature is only able to be captured at a point when the pumps are running near to or at full output. This is due to the inaccuracy at low pressure identified earlier. For the fuel rig FDI test case the sensor failure was the grounding of a flow sensor and this was detected and identified without issue.

The addition of statistical residual evaluation caused faults to be detected that were not detected without its use in two of the test cases. However, this measure removes the possibility of identifying the direction of the residual which is used in discrimination between faults. Therefore the direction of the Kalman filter needs also

to be monitored although it is not as sensitive in reporting the presence of a fault condition.

The automatic threshold has proven a useful tool as it removes the requirement of manually determining threshold levels, a painstakingly time consuming task. It also increases the portability of these methods to another plant by removing this part of the design process. However, portability to another plant will still require development of a system model and tuning of the Kalman filter.

8.3 Considerations for Application to an Aircraft

A real life consideration extended from the development of the FDI tool is the action that could be taken by the aircraft in consideration of a fault condition.

The action taken by an aircraft in the case of a fuel leak, for example, can be overcome by redirection of the fuel to a fault free tank and to alert the pilot of the fault condition as it may affect aircraft performance. It is unlikely in modern aircraft in this case that the failure results in catastrophic failure as the use of multiple tanks and transfer pumps between them is usually present. Indeed with the aid of FDI it may be possible to detect such faults quick enough that preventative action be taken as to not disturb the planned flight at all, maintenance being carried out at a later time. Similarly, pipe leak faults can be accommodated by rerouting the fuel path to accommodate the situation as can pump failures and full bore pipe blockages.

Partial blockages of pipes and pump performance degradation issues can be accommodated via altering the control parameters to achieve the required performance as long as it remains within safe operating limits. The loss of sensor data can be accommodated utilizing the proposed Kalman filter scheme to provide estimates for missing sensor data based upon known other system states as discussed in previously mentioned publications (Dixon, 2004).

8.4 Design Methodology

The sequence of tasks leading to the development of the FDI scheme is shown in the numbered list below.

1) Create nonlinear simulink system model representing the fuel rig and validate against the fuel rig or in the case of a generic system to create the nonlinear model and validate against the system.

2) Develop a linear state space models representing the main dynamics of key components of the simulink system model.

3) Use the linear state space model to create a Kalman filter based FDI to apply to the simulink system model.

4) Apply tuning to the Kalman filter gains to attain sufficient tracking of the real life system without masking of faults.

5) Apply the Kalman filter based FDI to the fuel rig to correctly detect and identify fault conditions. Faults can be mapped to Kalman filter residual behavior. This is discrimination between faults is limited by the number of physical sensors on the system being diagnosed.

6) Develop improvements to the FDI scheme by using statistical residual evaluation and automatic threshold determination.

8.5 Summary of Contributions

The thesis contributions cover a number of areas and are as shown in the list below.

i) The contribution of Chapter 2, *literature survey*, is the identification of publications presenting current methodology concerned with the development of diagnostic systems or similar related material to aid the development of the fault detection and identification scheme.

ii) The contribution claimed in Chapter 3, *Fuel Rig Plant Description*, is to provide a full functioning fuel rig that can be used for the validation and evaluation of methods and algorithms for fault detection and health monitoring.

iii) The contribution of Chapter 4, *Fuel Rig Modelling and Validation*, is to create and document the development and validation of a simulink model based upon the fuel rig to be used in the production of a Kalman filter based Fault Diagnostic and Identification (FDI) development.

iv) The contribution claimed in Chapter 5, *Application of Fault Diagnosis to a Single Tank*, are application of fault detection to a real tank successfully detecting a leak and the evaluation of different methods utilised in detection of a fault to determine which offers greatest sensitivity whilst remaining robust to false alarms.

v) The contribution of Chapter 6, *Design and Evaluation of Fault Diagnosis and Identification for the System Simulation Model*, is the development of the fault detection and identification system and its correct operation in identifying faults correctly when applied to the simulink system model representing the fuel rig. This validates the design prior to applying it to the real system.

vi) The contribution claimed in Chapter 7, *Application of Fault Diagnosis and Identification to the UAV Fuel Rig*, is the application and successful demonstration of the Fault Detection and Identification scheme to the real life system in order to detect and identify faults reliably.

8.6 Future Work

Further possible research paths extending from this work could be the implementation of other diagnostic methodologies with a view to comparative measure against this work.

Another possible extension of this work is the exploration of prognostics with regard to identifying failure in the rig before it happens. A relatively easy start to developing prognostics could be upon detecting a leak fault in a tank to then estimate the rate of the leak from this data and to extrapolate to estimate the time at which the tank has no fuel left. With regard to prognostics of other areas of the rig, pumps for example tend to be subject to areas such as vibration analysis or current signatures to determine condition based on known life cycle performance data.

Another extension would be to combine the fault flags generated into a Bayesian reasoning approach to enable probabilities of fault conditions to contribute to the decision process.

An important extension, if this approach is to be used by engineers in general, is to embody the general approach in a generic design framework for FDI on MIMO systems.

A further extension is the application of the FDI scheme to a real in-service aircraft fuel system; however qualification issues arise, although it may not cause relevant re-qualification at system level since no positive interaction is made. The FDI scheme only observes system variables, which would hopefully be available as sensor data, and provides a system condition user output, useful to maintenance operatives in the monitoring of the fuel system condition. For piloted aircraft as opposed to UAV, diagnosed faults could be relayed to the pilot in flight, leading to ‘human in the loop’ reconfiguration.

Chapter 9

Bibliography and References

[1] Satnam Alag, Alice M. Agogino and Mahesh Morjaria, A Methodology for Intelligent Sensor Measurement, Validation, Fusion, and Fault Detection for Equipment Monitoring and Diagnostics, Artificial Intelligence for Engineering Practice, Analysis and Manufacturing 15, pp 307-320, (2001).

[2] N. Aretakis, K. Mathioudakis and A. Stamatis, Identification of Sensor Faults on Turbofan Engines using Pattern Recognition Techniques, Control Engineering Practice 12, pp827-836, (2004).

[3] Irtaza Barlas, Guangfan Zhang, Nicholas Propes, George Vachtsevenos, Thomas Galie, Ash Thakkar, Confidence Metrics and Uncertainty Management in Prognosis, AAAI Symposium, Stanford, California, (March 25-27 2002).

[4] Bartlett L. M., Hurdle E. E., Kelly E. M., Integrated system fault diagnostics utilising digraph and fault tree-based approaches, Reliability Engineering & System Safety Vol. 94, Issue 6, pp 1107-1115, (2008).

[5] Bennett P., Dixon R., Pearson J.; "Comparing residual evaluation methods for leak detection on an aircraft fuel system test-rig"; Systems Science Journal, Vol. 34, pp 63-74, (2008).

[6] Bennett P., Dixon R., Pearson J.; "Comparing residual evaluation methods for leak detection on an aircraft fuel system test-rig"; Proceedings of the 16th International Conference on Systems Science, Wroclaw, Poland, (4-6 September 2007).

[7] Bennett, P.J; Pearson, J. T.; Martin, A; Dixon, R., Application of diagnostic techniques to an experimental aircraft fuel rig, proc. of the 6th IFAC Symposium on Fault Detection, Supervision and Safety of Technical Processes (SAFEPROCESS), Beijing, China, (Sept 2006).

[8] Bennett P., Dixon R., Pearson J.; "Dynamic model development and validation for an aircraft fuel test-rig"; Proc of 6th UKACC International Control Conference, Glasgow, UK, (Aug 2006).

[9] Giovanni Betta and Antonio Pietrosanto, Instrument Fault Detection and Isolation: State of the Art and New Research Trends, IEEE Transactions on Instrumentation and Measurement, Vol. 49, No. 1, pp 100-107, (2000).

[10] Blanke, M., Kinnaert, M., Lunze, J., Starswiecki, M., Diagnosis and fault tolerant control, Springer, (2006).

[11] M. Blanke, R. Izadi-Zamanbadi, S. A. Begh and C. P. Lunau, Fault-Tolerant Control Systems – A Holistic View, Control Engineering Practice, Vol. 5, No. 5, pp 693-702, (1997).

[12] Piero Bonnisonne and Kai Goebel, Soft Computing for Diagnostics in Equipment Service, Artificial Intelligence for Engineering Practice, Analysis and Manufacturing 15, pp 267-279, (2001).

[13] Byington, C. S., Roemeer, M. J., Galie, T., Prognostic Enhancements to Diagnostic Systems for Improved Condition Based Maintenance, Aerospace Conference Proceedings, Vol. 6, pp 2815-2824, (2002).

[14] Candy, J. V.; Mcclay, W.; Awwal, A.; Ferguson, W., Optimal Centroid Position Estimation, SPIE 49th Annual Meeting 2004, Denver, CO, United States, (2004).

[15] Calisto, H., Martins, N., Afgan, N., Diagnostic System for Boiler and Furnacesusing CFD and Nueral Networks, Expert Systems with Applications Vol. 35, pp 1780-1787, (2008).

[16] Chen, J.; Patton, R., Robust Model-Based Fault Diagnosis for Dynamic Systems, Kluwer Acedemic Publishers, Massachusetts, United States, (1999).

[17] Luca Chitaro, Roberto Ranon and Alfredo Soldati, Introducing Deviations and Multiple Abstraction Levels in the Functional Diagnosis of Fluid Transfer Systems, Artificial Intelligence in Engineering 12, pp 355-373, (1998).

[18] Davies, J., Steffen, T. Dixon, R., Goodall, R. M., Zolatas, A. C. Pearson, J. T., Modelling of High Redundancy Actuation utilising Multiple Moving Coil Actuators, 17th IFAC World Congress, (July 2008).

[19] Paulo Sergio Ramirez Diniz, Eduardo A. B. Da Silva, Sergio L. Netto, Digital Signal Processing: System Analysis and Design. Cambridge University Press, (2002).

[20] R. Dixon, Observer-Based FDIA: Application to an Electromechanical Positioning System, Control Engineering Practice 12, pp 113-125, (2004).

[21] E. L. Ding, H. Fennel, S. X. Ding, Model-based Diagnosis of Sensor Faults for ESP Systems, Control Engineering Practice 12, pp 847-856, (2004).

[22] Dorf, R. C., Bishop, R. H., Modern control systems, 9th edition, Prentice Hall, (2001).

[23] Dragan Djurdjanovic, Jay Lee and Jun Ni, Watchdog Agent – An infotronics based prognostics approach for product performance degradation assessment and prediction, Advanced Engineering Informatics 17, pp109-125, (2003).

[24] Du, X., Dixon, R. Goodall, R, Zolatas, A. C., LQG Control for a Highly Redundant Actuator, 2007 IEEE/ASME International Conference on Advanced Intelligent Mechatronics, pp 1-6, (Sept 2007).

[25] R. Du and K. Yeung, Fuzzy Transition Probability: Anew Method for Monitoring Progressive Faults. Part 1: The Theory, Engineering Applications of Artificial Intelligence 17, pp 457-467, (2004).

[26] Levent Eren and Michael J. Devaney, Bearing Damage Detection via Wavelet Packet Decomposition of the Stator Current, IEEE transactions on instrumentation and measurement, vol. 53, No. 2, pp 431-436, (2004).

[27] P. M. Frank, S. X. Ding and T. Marcu, Model-based Fault Diagnosis in Technical Processes, Transactions of the Institute of Measurement and Control 22, No. 1, pp 57-101, (2000).

[28] Frank, P. M.; Ding, X., Survey of robust residual generation and evaluation methods in observer-based fault detection systems, Journal of Process Control, Vol. 7, No. 6, pp 403-424, (1997).

[29] Franklin, G. F., Powell, J. D., Workman, M. L., Digital control of dynamic systems, 2nd edition, Addison Wesley, (1990).

[30] Franklin, G. F., Powell, J. D., Emami-Naeini, A., Feedback control of dynamic systems, 3rd edition, Addison Wesley, (1994).

[31] Friedland, B., Control Systems Design, McGraw-Hill, Singapore, (1987).

[32] F. Javier Garcia, Virginia Izquierdo, Luis J. de Miguel and Jose R. Peran, Fault-Diagnostic System using Analytical Fuzzy Redundancy, Engineering Applications of Artificial Intelligence 13, pp 441-450, (2000).

[33] Kai Goebel, Architecture and Design of a Diagnostic Information Fusion System, Artificial Intelligence for Engineering Design, Analysis and Manufacturing 15, pp 335-348, (2001).

[34] Grainger, R. W.; Holst, J.; Isaksson, A. J.; Ninness, B. M., A parametric statistical approach to FDI for the industrial actuator benchmark, Control Engineering Practice, Vol. 3, No. 12, pp 1757-1762, (1995).

[35] George D. Hadden, , Peter Bergstrom, Tariq Samad, Bonnie Holte Bennett, George J. Vachtsevanos, Joe Van Dyke, Application Challenges: Systems Health Management for Complex Systems, proceedings from IPDPS workshop, Cancun, Mexico, (May 2000).

[36] Chingiz Hajiyev and Fikret Caliskan, Sensor/ Actuator Fault Diagnosis based on Statistical Analysis of Innovation Sequence and Robust Kalman Filtering, Aerospace Science Technology 4, pp 415-422, (2000).

[37] D. Henry, A. Zolghadri, M. Monsion, S. Ygorra, Off-line Robust Fault Diagnosis using the Generalized Structured Singular Value, Automatica 38, pp 1347-1358, (2002).

[38] E. H. Higham and S. Perovic, Predictive Maintenance of Pumps based on Signal Analysis of Pressure and Differential Pressure (Flow) Measurements, Transactions of the Institute of Measurement and Control, 23, No. 4, pp 226-248, (2001).

[39] Isermann, R. Model based fault detection and diagnosis – Status and Application, 16th IFAC symposium on Automatic Control – ACA2004, Petersburg, Russia, (2004).

[40] R. Isermann, "Supervision, fault-detection and fault diagnosis methods - an introduction". Control Engineering Practice, Vol. 5, No. 5, pp. 639-652, (1997).

[41] R. B. Joly, S. O. T. Ogaji, R. Singh, S. D. Probert, Gas-turbine Diagnostics using Artificial Neural Networks for a High Bypass Ratio Military Turbofan Engine, Applied Energy 78, pp 397-418, (2004).

[42] Kelly, E. M. and Bartlett, L. M., Aircraft fuel rig system fault diagnostics based on the application of digraphs, Proc. of the institution of mechanical engineers, Part O: Journal of Risk and Reliability Vol. 221, No. 4, pp 275-284, (2007).

[43] Kobayashi, Takahisa; Simon, Donald L., Application of a bank of Kalman filters for aircraft engine fault diagnostics, Turbo Expo 2003, Atlanta, Georgia, (June 2003).

[44] Chang-duk Kong, Fa-young Ki, Myoung-cheol Kang and Seong-hee Kho, Intelligent Performance Diagnostics of a Gas Turbine Engine using User-friendly Interface Neural Networks, Aircraft Engineering and Aerospace Technology, Vol. 76, No. 4, pp 391-397, (2004).

[45] R. J. Kuo, Intelligent Diagnosis for Turbine Blade Faults using Artificial Neural Networks and Fuzzy Logic, Engineering Applications of Artificial Intelligence, Vol. 8, No. 1, pp 25-34, (1995).

[46] Landau, I. D., Zito, G., Digital control systems, Springer, (2005).

[47] Jianhui Leo, Madhavi Namburu, Krishna Pattipati, Liu Quao, Masyuki Kawamoto, Shunsuke Chigusa, Model-based Prognostic Techniques, Autotestcon., pp 330-340, (2003).

[48] S. Leonhardt and M. Ayoubi, Methods of Fault Diagnosis, Control Engineering Practice 5, pp 683-692, (1997).

[49] Daming Lin, Murray Wiseman, Dragan Banjevic, Andrew K. S. Jardine, An Approach to Signal Processing and Condition Based Maintenance for Gearboxes subject to Tooth Failure, Mechnical Systems and Signal Processing 18, pp 993-1007, (2004).

[50] Jian, F., Huaguang, Oil Pipeline Leak Detection and Location Using Double Sensor Pressure Gradient Method, Proceedings of the 5th World Congress on Intelligent Control and Automation, pp 3134-3137, (June 2004).

[51] Jianhui Luo, Madhavi Namburu, Liu Qiao, Masayuki Kawamoto, Shunsuke Chigusa, Model Based Prognostic Techniques, SPIE Conference Proceedings, Orlando, (2003).

[52] Jianhui Luo, Krishna Pattipati, Liu Qiao, Shunsuke Chigusa, Model Based Prognostic Techniques Applied to a Suspension System, IEEE Transactions on Systems, Man and Cybernetics – Part A: Systems and Humans, Vol. 38, No. 5, (2008).

[53] Ajay Mahajan, Kaihong Wang and Probir Kumar Ray, Multisensor Integration and Fusion Model that Uses a Fuzzy Inference System, IEEE ASME Transactions on Mechatronics, Vol. 6, No. 2, pp 188-196, (2001).

[54] Eric J. Manders, Lee A. Barford and Gautam Biswas, An Approach for Fault Detection and Isolation in Dynamic Systems From Distributed Measurements, IEEE Transactions on Instrumentation and Control, Vol. 51, No. 2, pp 235-240, (2002).

[55] Luca Marinai, Douglas Probert and Riti Singh, Prospects for Aero Gas Turbine Diagnostics: A Review, Applied Energy 79, pp 109-126, (2004).

[56] Donald McLean, Measurement and Control in Aviation, Aircraft Engineering and Aerospace Technology, Vol. 76, No. 5, pp 458-460, (2004).

[57] Stan Ofsthun, Integrated Vehicle Health Management for Aerospace Platforms, IEEE Instrumentation and Measurement Magazine, pp 21-24, (September 2002).

[58] Maciej Petko and Tadeusz Uhl, Smart Sensor for Operational Load Measurement, Transactions of the Institute of Measurement and Control 26, No. 2, pp 99-117, (2004).

[59] Yiannis Popadopoulos, Model-based System Monitoring and Diagnosis of Failures Using Statecharts and Fault Trees, Reliability Engineering and System Safety 81, pp 325-341, (2003).

[60] Piatyszek, E.; Voignier, P.; Graillot, D., Fault detection on a sewer network by combination of a Kalman filter and a binary sequaential probability ration test, Journal of Hydrology, No. 230, pp 258-268, (2000).

[61] Presatiawan, E. A., Modelling, Simulation and Control of an Earthmoving Vehicle Powertrain Simulator, MSc. Thesis, University of Illinios, (2001).

[62] R. Rengaswamy, Dinkar Mylaraswamy, MN, K. E. Arzen , V. Venkatasubramanian, A Comparison of Model-Based and Neural Network-Based Diagnostic Methods,; Engineering Applications of Artificial Intelligence 14, pp 805-818, (2001).

[63] Michael J. Roemer and Gregory J. Kaeprzynski, Advanced Diagnostics and Prognostics for Gas Turbine Engine Risk Assessment, Impact Technologies, IGTI/ASME Turbo Expo, Munich, Germany, (May 2000).

[64] Sandborn, P. A., Wilkinson, C., A Maintenance Planning and Business Case Development Model for the Application of Prognostics and Health Management (PHM) to Electronic Systems, Microelectronics Reliability 47, pp 1889-1901, (2007).

[65] Schroer, R., Reolutionary Ideas in Test, IEEE AESS Systems Magazine, pp36-41, (June 2002).

[66] Simani, S., Identification and Fault Diagnosis of a Simulated Model of an Industrial Gas Turbine, IEEE Transactions on Industrial Informatics, Vol. 1, No. 3, pp 202-216, (August 2005).

[67] V. A. Skormin, V. I. Gorodetski, L. J. Popyack, Data Mining Technology for Failure Prognostic of Avionics, IEEE Transactions on Aerospace and Electronic Systems, Vol. 38, No. 2, pp 388-403, (2002).

[68] Sohlberg, B., Monitoring and failure diagnosis of a steel strip process, IEEE Transactions on Control Systems Technology, Vol. 6, No. 2, pp 294-303, (March 1998).

[69] Soong, T. T., Fundamentals of probability and statistics for engineers, Wiley-Interscience, (2004).

[70] Thomas, P., Simulation of industrial processes for control engineers, Butterworth Heinemann, (1999).

[71] Dejan Tinta, Janko Petrovcic, Uros Benko, Dani Juricic, Andrej Rakar, Mina Zele, Joze Tavcar, Jozica Rejec and Aneta Stefanovska, Fault Diagnosis of Vacuum Cleaner Motors, Control Engineering Practice 13, pp 177-187, (2005).

[72] Venkat Venkatasubramanian, Raghunathan Rengaswamy, Keyen Yin, Surya N. Kavuri, A review of Process Fault Detection and Diagnostics, Part I: Quantitative Model-based Methods, Computers and Chemical Engineering 27, pp 293-311, (2003).

[73] Venkat Venkatasubramanian, Raghunathan Rengaswamy, Keyen Yin, Surya N. Kavuri, A review of Process Fault Detection and Diagnostics, Part II: Qualitative Models and Search Strategies, Computers and Chemical Engineering 27, pp 313-326, (2003).

[74] Venkat Venkatasubramanian, Raghunathan Rengaswamy, Keyen Yin, Surya N. Kavuri, A review of Process Fault Detection and Diagnostics, Part III: Process History Based Methods, Computers and Chemical Engineering 27, pp 327-346, (2003).

[75] Shengwei Wang and Jin-Bo Wang, Robust Sensor Fault Diagnosis and Validation in HVAC Systems, Transactions of the Institute of Measurement and Control 24,3, pp 231-262, (2002).

[76] Peng Wang and George Vachtsevanos, Fault Prognostics Using Dynamic Wavelet Neural Networks, Georgia Institute of Technology, Atlanta, Artificial Intelligence for Engineering Design, Analysis and Manufacturing 15, pp349-365, (2001).

[77] Wilson Q. Wang, M. Farid Golnaraghi and Fathy Ismail, Prognosis of Machine Health Condition Using Neuro-Fuzzy Systems, Mechanical Systems and Processing 18, pp 813-831, (2004).

[78] Xiaochun George Wang and Wei Liu, A Singular Pencil Model and Neural Network Cascade Fault Diagnosis Strategy for the Lumber Drying Process, Transactions of the Institute of Measurement and Control 25, No. 4, pp 335-351, (2003).

[79] Wesley G. Zanardelli, Elias G. Strangas, Hassan K. Khalil and John M. Miller., Wavelet based methods for the prognosis of mechanical and electrical failures in electric motors, Mechanical Systems and Signal Processing 19, pp 411-426, (2005).

[80] G Zhang, S Lee, N Propes, Y Zhao, G Vachtsevanos, A Novel Architecture for an integrated fault diagnostic/ prognostic system, AAAI Symposium, Stanford, California, (March 25-27 2002).

[81] Z. Zoouaoui and H. Rami, Flight Control System Reconfiguration for "Locked and Centred" and "Non-Neutral Position" Control Surface Failures, Aircraft Engineering and Aerospace Technology, Vol. 76, No. 5, pp 461-466, (2004).

Appendix A

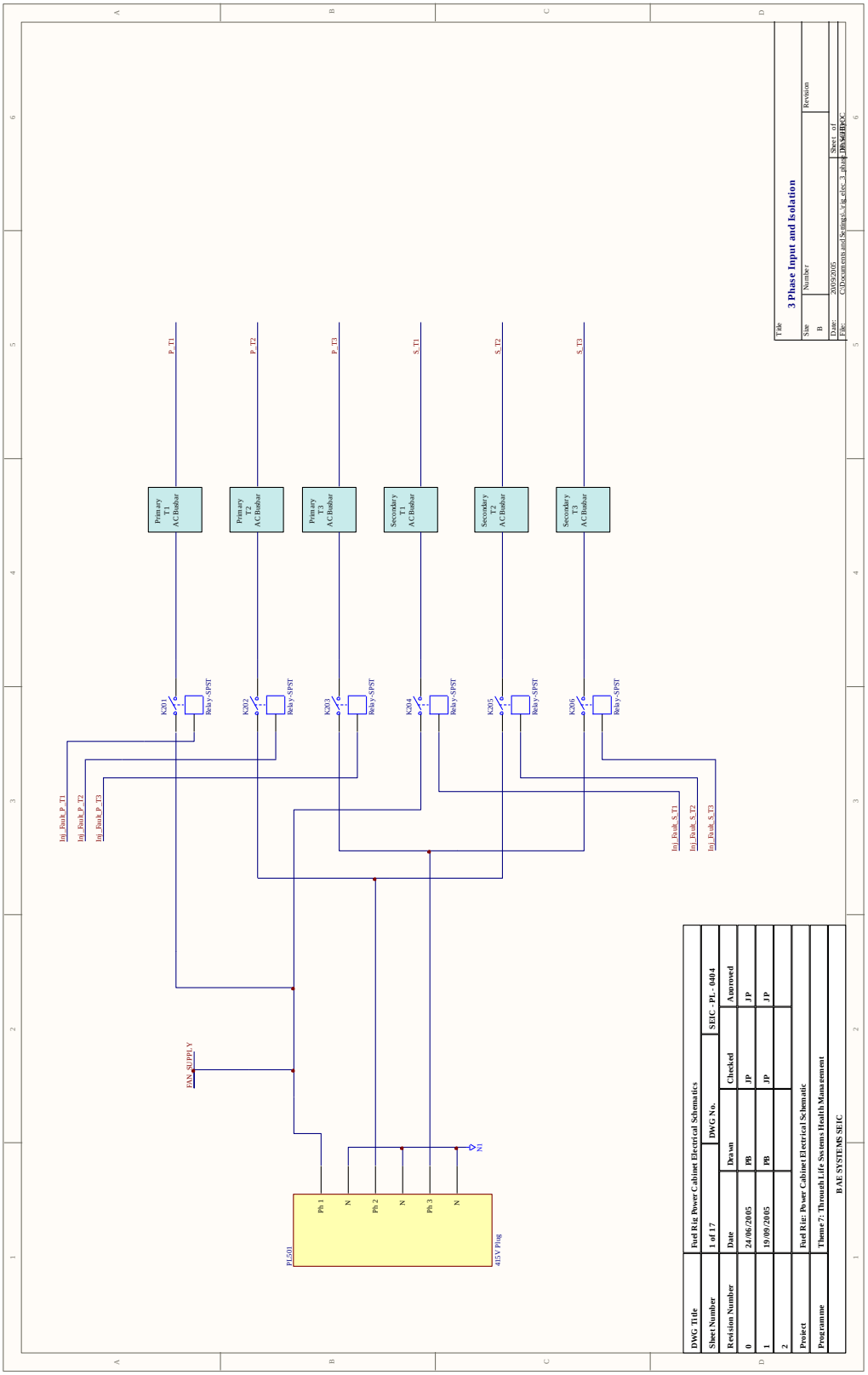
3 Phase Input and Isolation
P_T1
P_T2
P_T3
S_T1
S_T2
S_T3
Primary T1 AC Busbar
Primary T2 AC Busbar
Primary T3 AC Busbar
Secondary T1 AC Busbar
Secondary T2 AC Busbar
Secondary T3 AC Busbar
K201
K202
K203
K204
K205
K206
Relay-SPST
Inj_Fault_P_T1
Inj_Fault_P_T2
Inj_Fault_P_T3
Inj_Fault_S_T1
Inj_Fault_S_T2
Inj_Fault_S_T3
FAN_SUPPLY
N1
Ph 1
Ph 2
Ph 3
N
P1501
415V Plug
DWG Title
Fuel Rig: Power Cabinet Electrical Schematics
Sheet Number
1 of 17
DWG No.
SEIC - PL - 0404
Revision Number
Date
Drawn
Checked
Approved
0
24/06/2005
PB
JP
JP
1
19/09/2005
PB
JP
JP
2
Project
Fuel Rig: Power Cabinet Electrical Schematic
Programme
Theme 7: Through Life Systems Health Management
BAE SYSTEMS SEIC

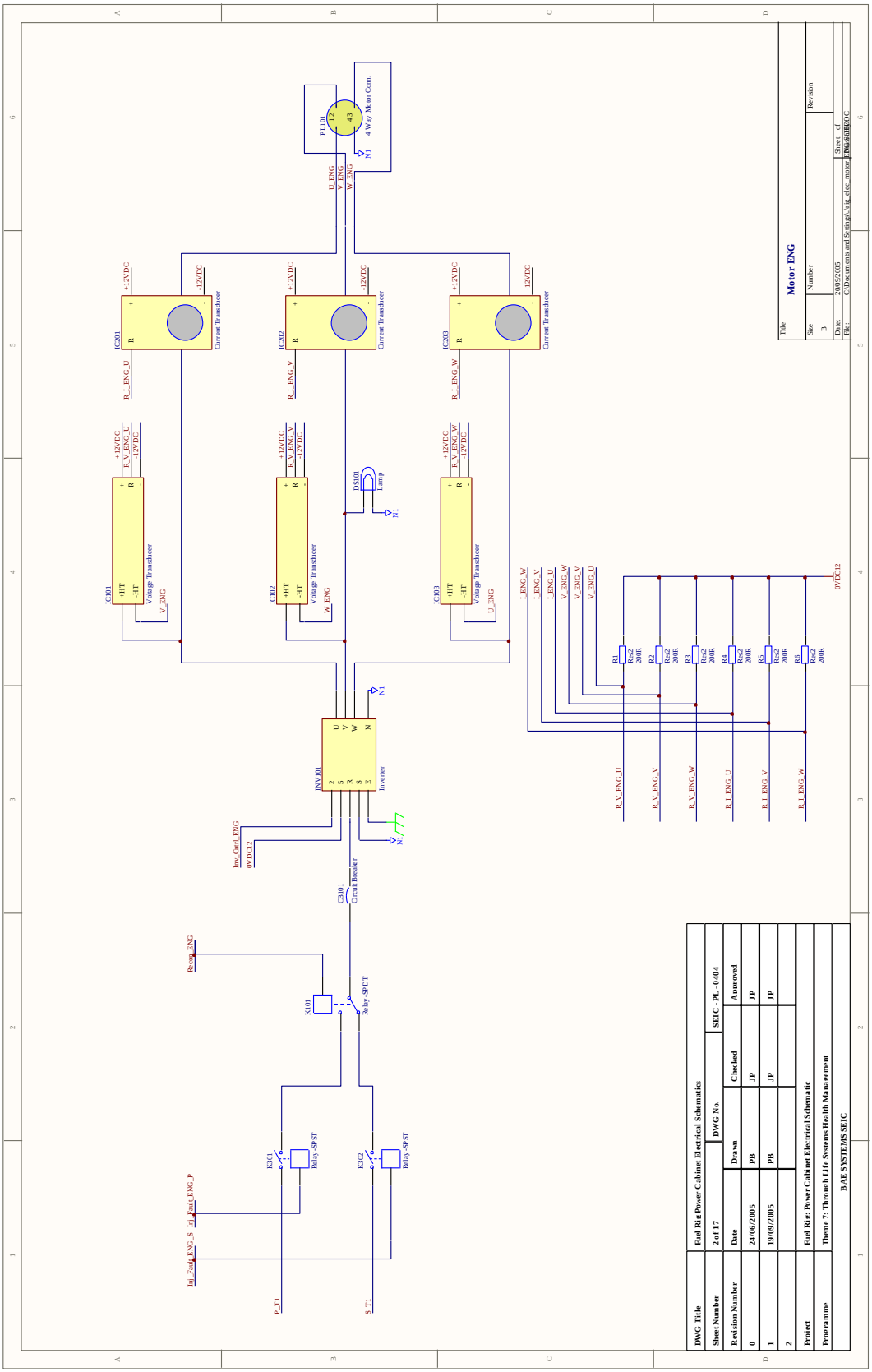
Motor ENG
Fuel Rig Power Cabinet Electrical Schematic
SEIC - PL - 0404
BAE SYSTEMS SEIC
Theme 7: Through Life Systems Health Management
Current Transducer
Voltage Transducer
Inverter
Circuit Breaker
Relay -SPDT
Relay -SPST
Lamp
4 Way Motor Conn.
Resistor 200R

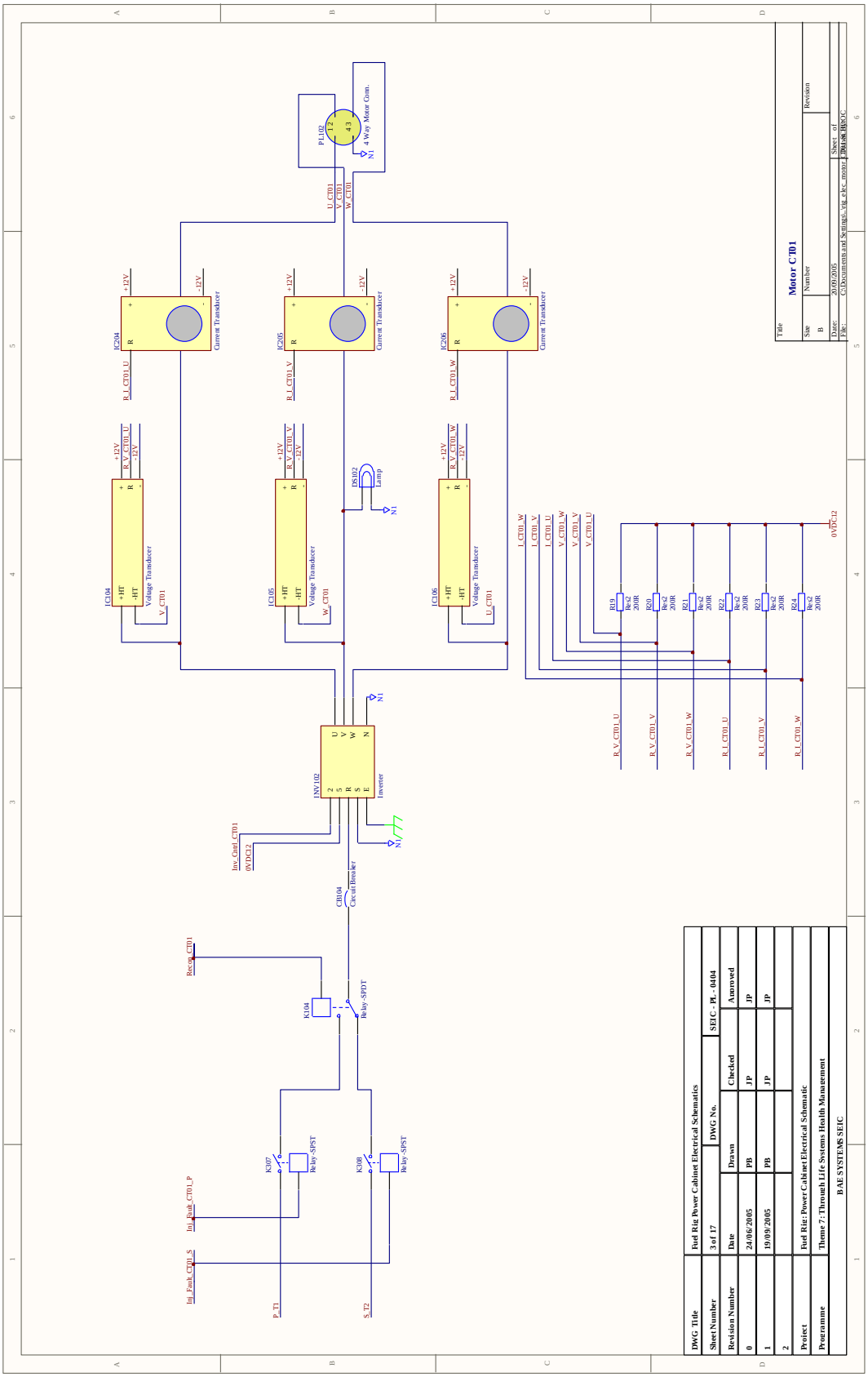
Motor C701
Current Transducer
Voltage Transducer
Inverter
Circuit Breaker
Relay-SPDT
Relay-SPST
Lamp
4 Way Motor Conn.
Fuel Rig Power Cabinet Electrical Schematics
Fuel Rig: Power Cabinet Electrical Schematic
Theme 7: Through Life Systems Health Management
BAE SYSTEMS SEIC

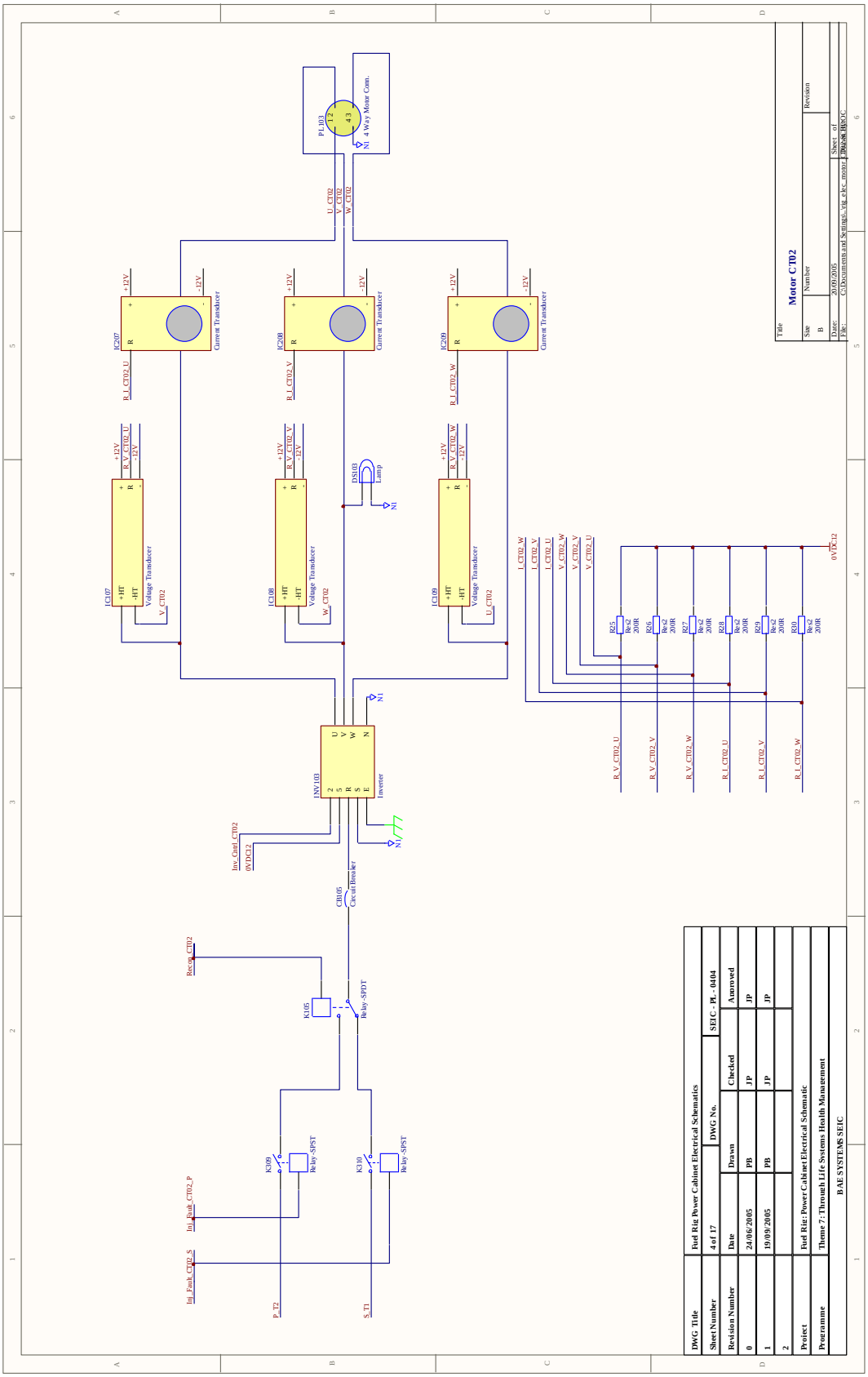
Motor CT02
DWG Title
Fuel Rig Power Cabinet Electrical Schematics
Sheet Number
4 of 17
Revision Number
Date
Drawn
Checked
Approved
Project
Fuel Rig: Power Cabinet Electrical Schematic
Programme
Theme 7: Through Life Systems Health Management
BAE SYSTEMS SEIC
SEIC - PL - 0404
4 Way Motor Conn.
Current Transducer
Voltage Transducer
Lamp
Inverter
Circuit Breaker
Relay-SPDT
Relay-SPST

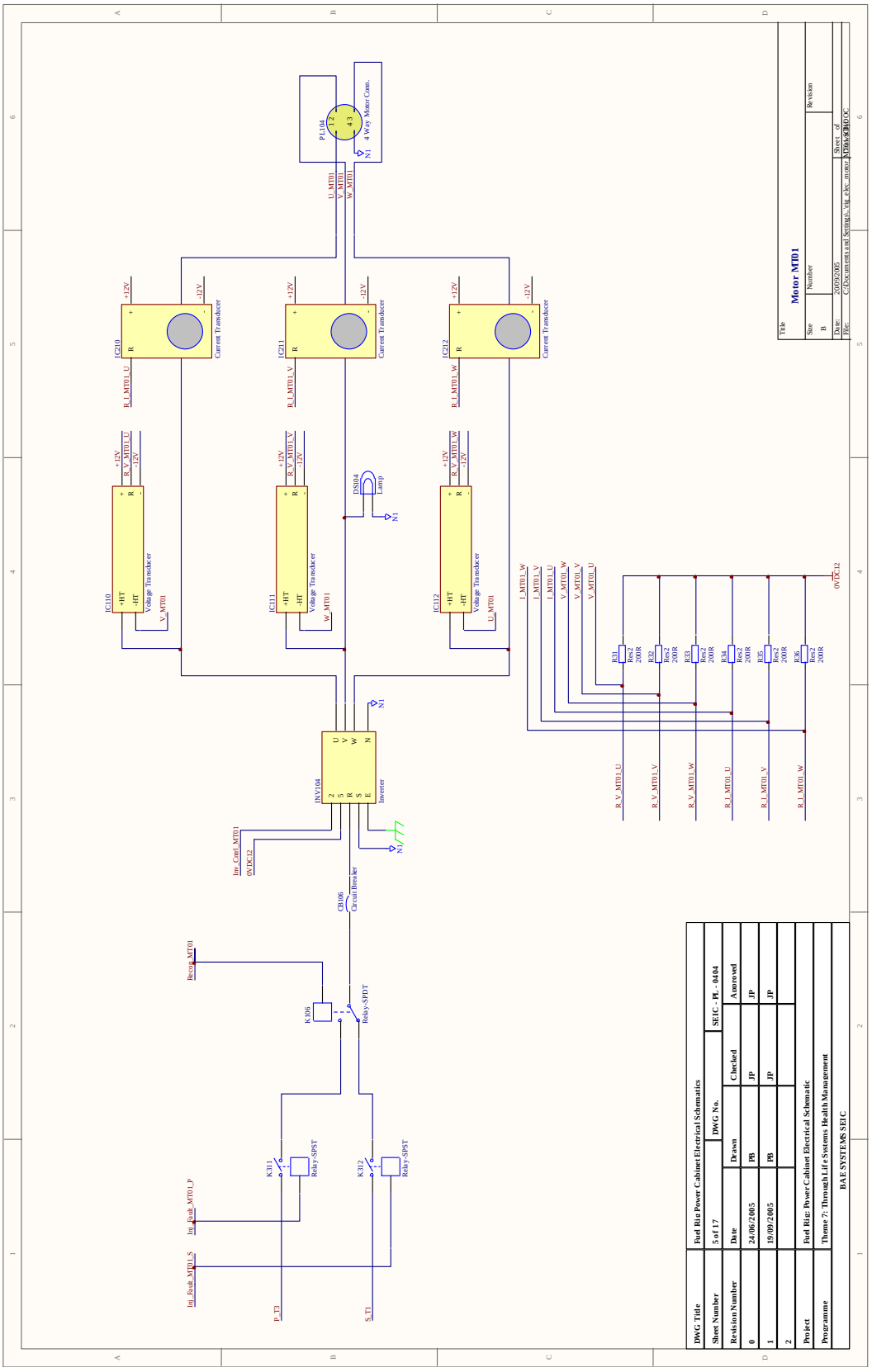
Motor MT01
Fuel Rig: Power Cabinet Electrical Schematic
Theme 7: Through Life Systems Health Management
BAE SYSTEMS SELC
Current Transducer
Voltage Transducer
Inverter
Relay-SPDT
Relay-SPST
Lamp
Res2
4 Way Motor Conn.
CircuitBreaker

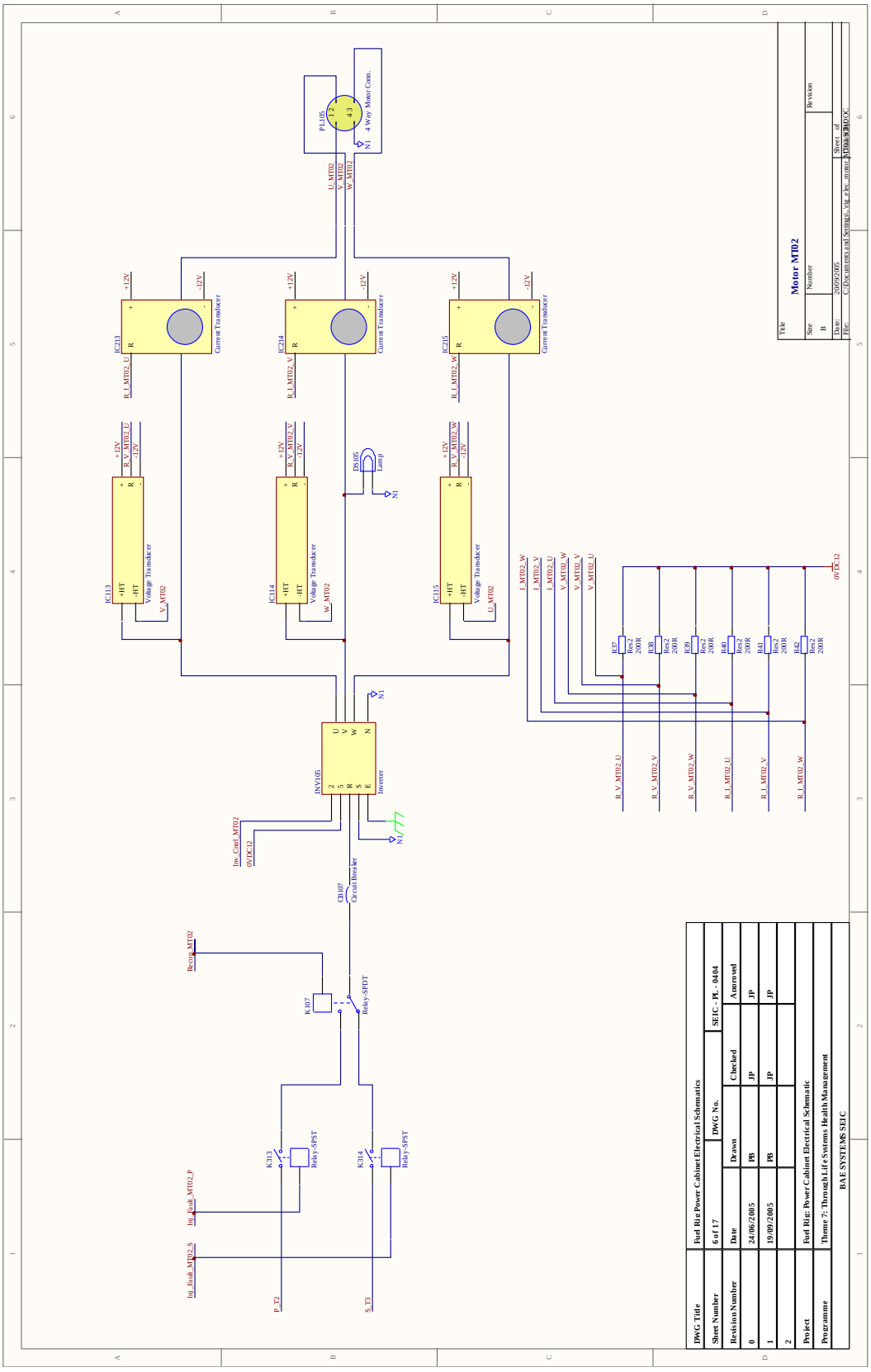
Motor MT02
DWG Title
Fuel Rig Power Cabinet Electrical Schematics
Sheet Number
6 of 17
DWG No.
SEIC - PL - 0404
Revision Number
Date
Drawn
Checked
Approved
0
24/06/2005
PB
JP
JP
1
19/09/2005
PB
JP
JP
2
Project
Fuel Rig: Power Cabinet Electrical Schematic
Programme
Theme 7: Through Life Systems Health Management
BAE SYSTEMS SEIC
4 Way Motor Conn.
Current Transducer
Voltage Transducer
Lamp
Inverter
Circuit Breaker
Relay-SPDT
Relay-SPST
Res2 200R

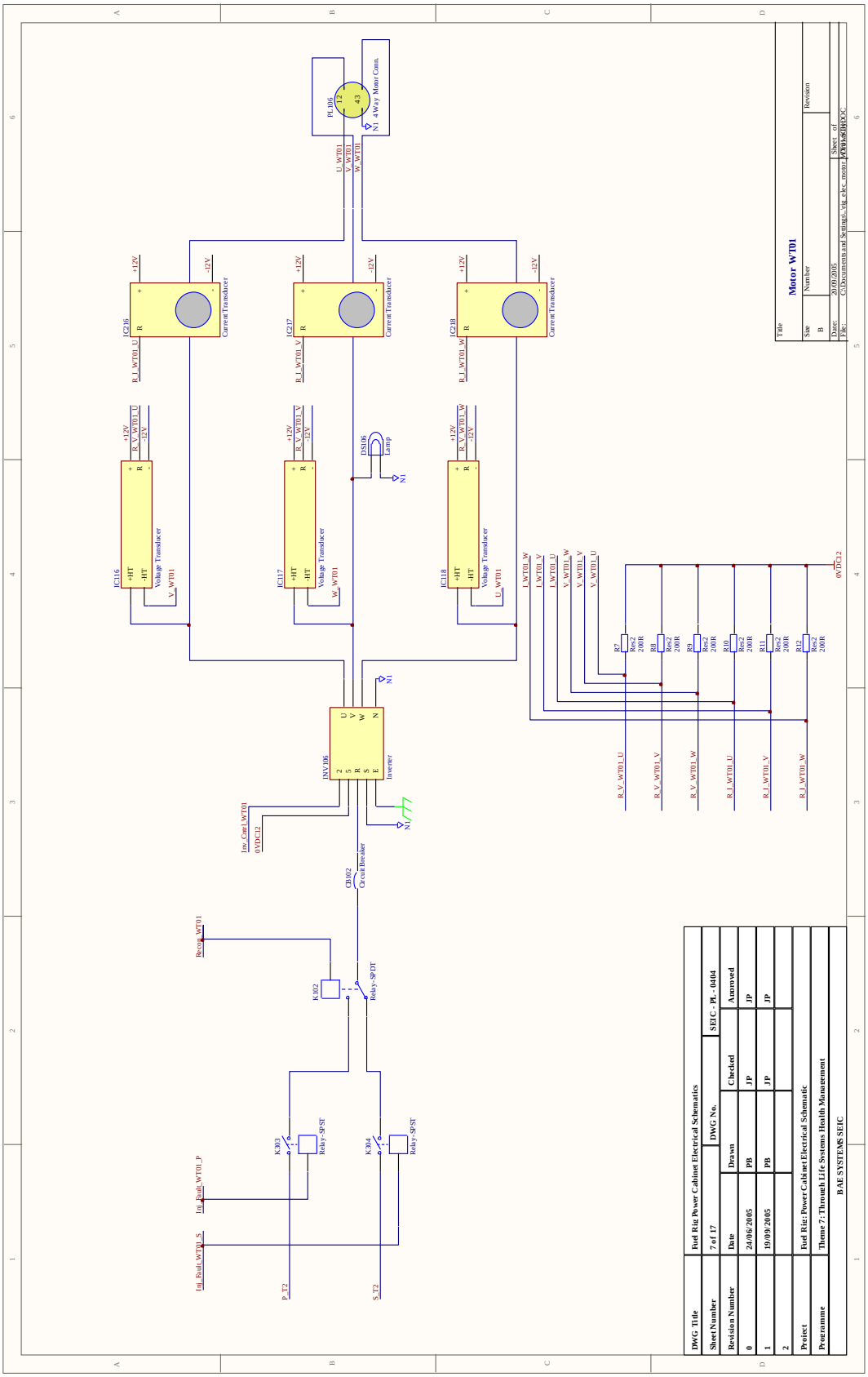
Motor WT01
DWG Title
Fuel Rig Power Cabinet Electrical Schematics
Sheet Number
7 of 17
Revision Number
Date
24/06/2005
19/09/2005
Project
Fuel Rig: Power Cabinet Electrical Schematic
Programme
Theme 7: Through Life Systems Health Management
BAE SYSTEMS SEIC
SEIC - PL - 0404
Drawn
Checked
Approved
PB
JP
Inverter
Circuit Breaker
Relay-SPDT
Relay-SPST
Voltage Transducer
Current Transducer
Lamp
4 Way Motor Conn.

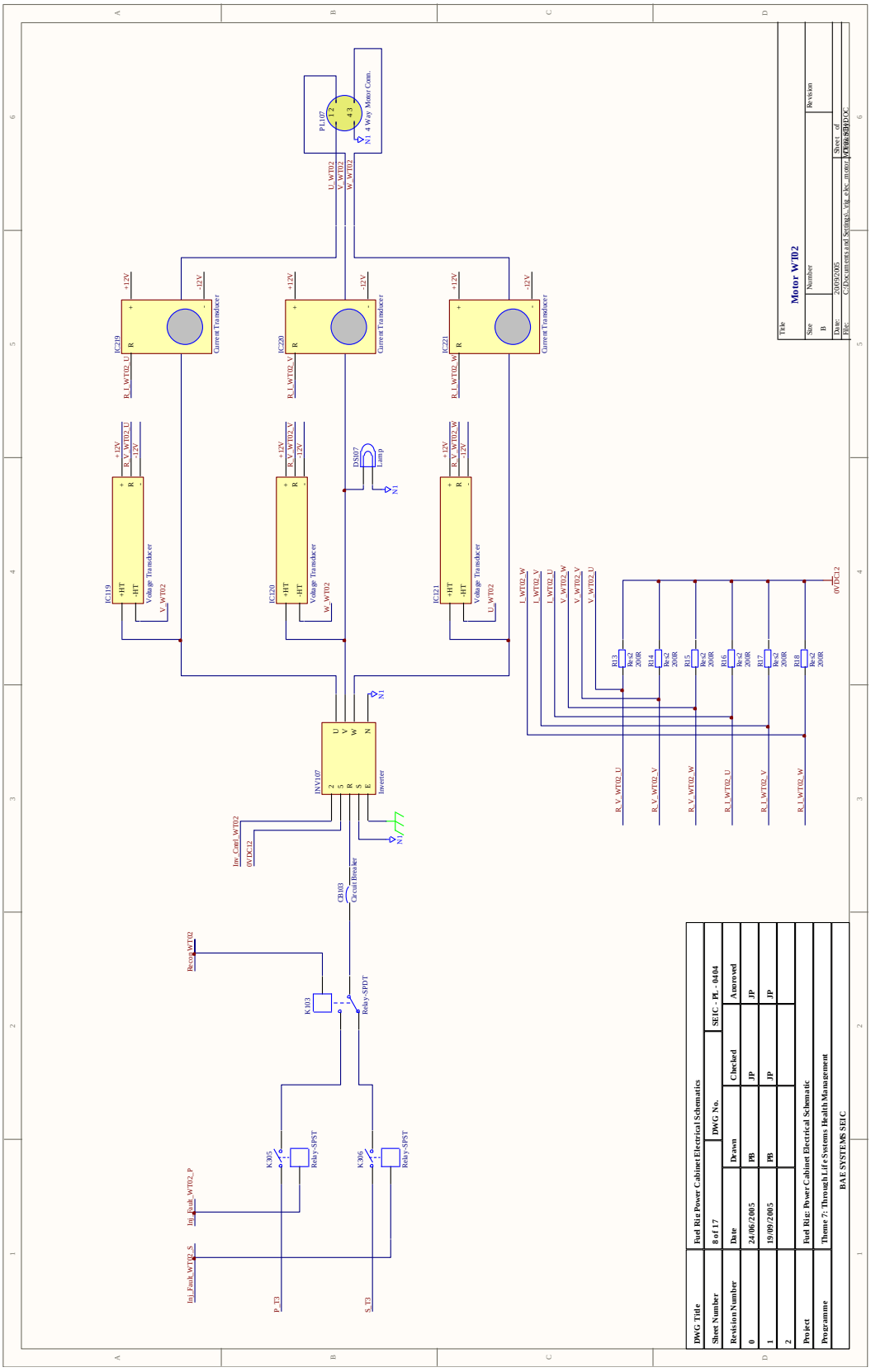
Motor WT02
Fuel Rig: Power Cabinet Electrical Schematic
Theme 7: Through Life Systems Health Management
BAE SYSTEMS SEIC
Current Transducer
Voltage Transducer
Inverter
Circuit Breaker
Relay-SPDT
Relay-SPST
4 Way Motor Conn.
Lamp

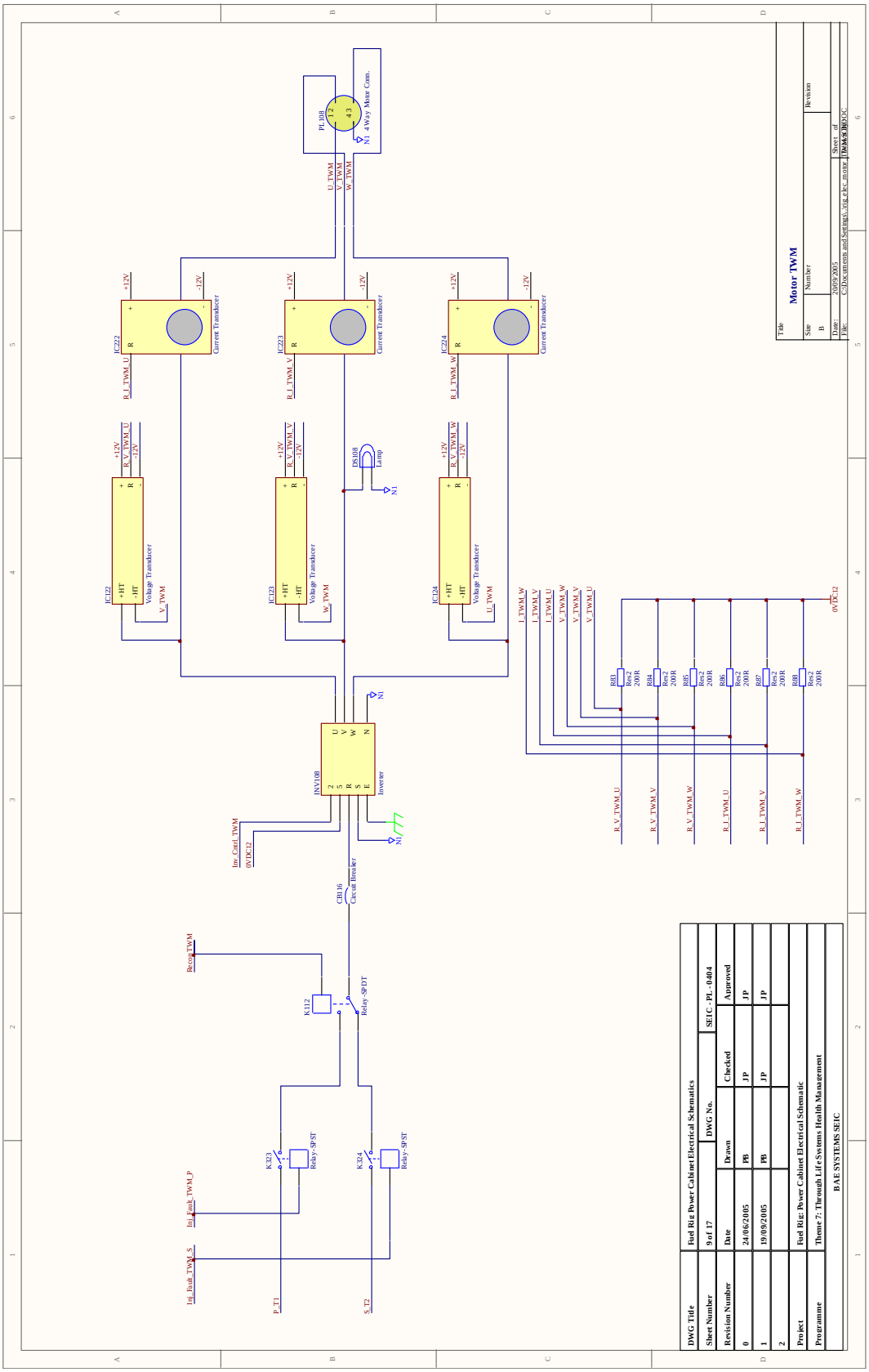
Motor TWM
Current Transducer
Voltage Transducer
Inverter
Relay-SPDT
Relay-SPST
Circuit Breaker
Lamp
4-Way Motor Conn.
Fuel Rig Power Cabinet Electrical Schematics
Fuel Rig: Power Cabinet Electrical Schematic
Theme 7: Through Life Systems Health Management
BAE SYSTEMS SEIC

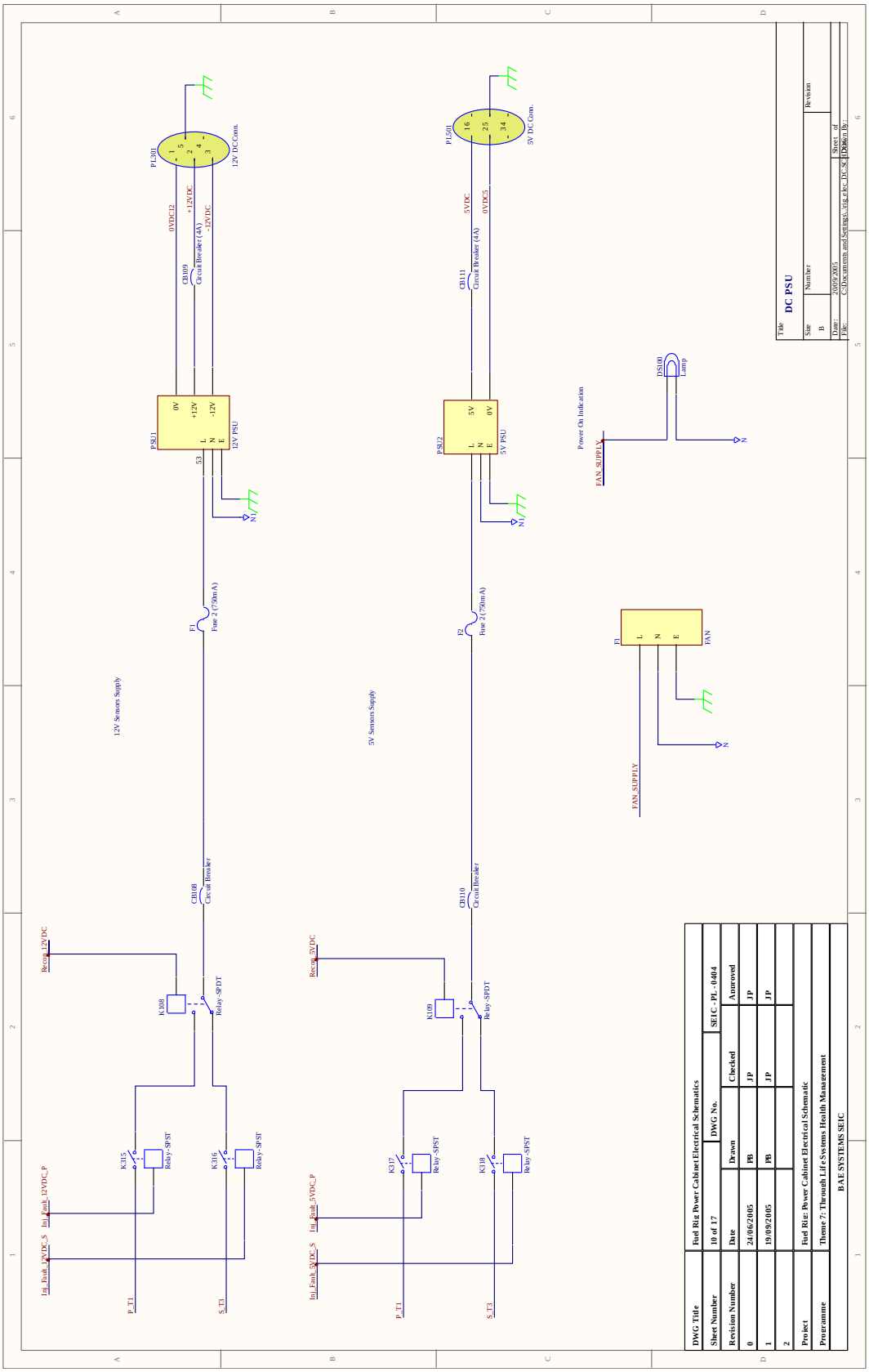
DC PSU
Fuel Rig Power Cabinet Electrical Schematics
BAE SYSTEMS SEIC
Theme 7: Through Life Systems Health Management
Fuel Rig: Power Cabinet Electrical Schematic
SEIC - PL - 0404
12V Sensors Supply
5V Sensors Supply
Power On Indication
12V PSU
5V PSU
Fuse 2 (750mA)
Circuit Breaker
Relay -SPDT
Relay -SPST
Lamp
FAN

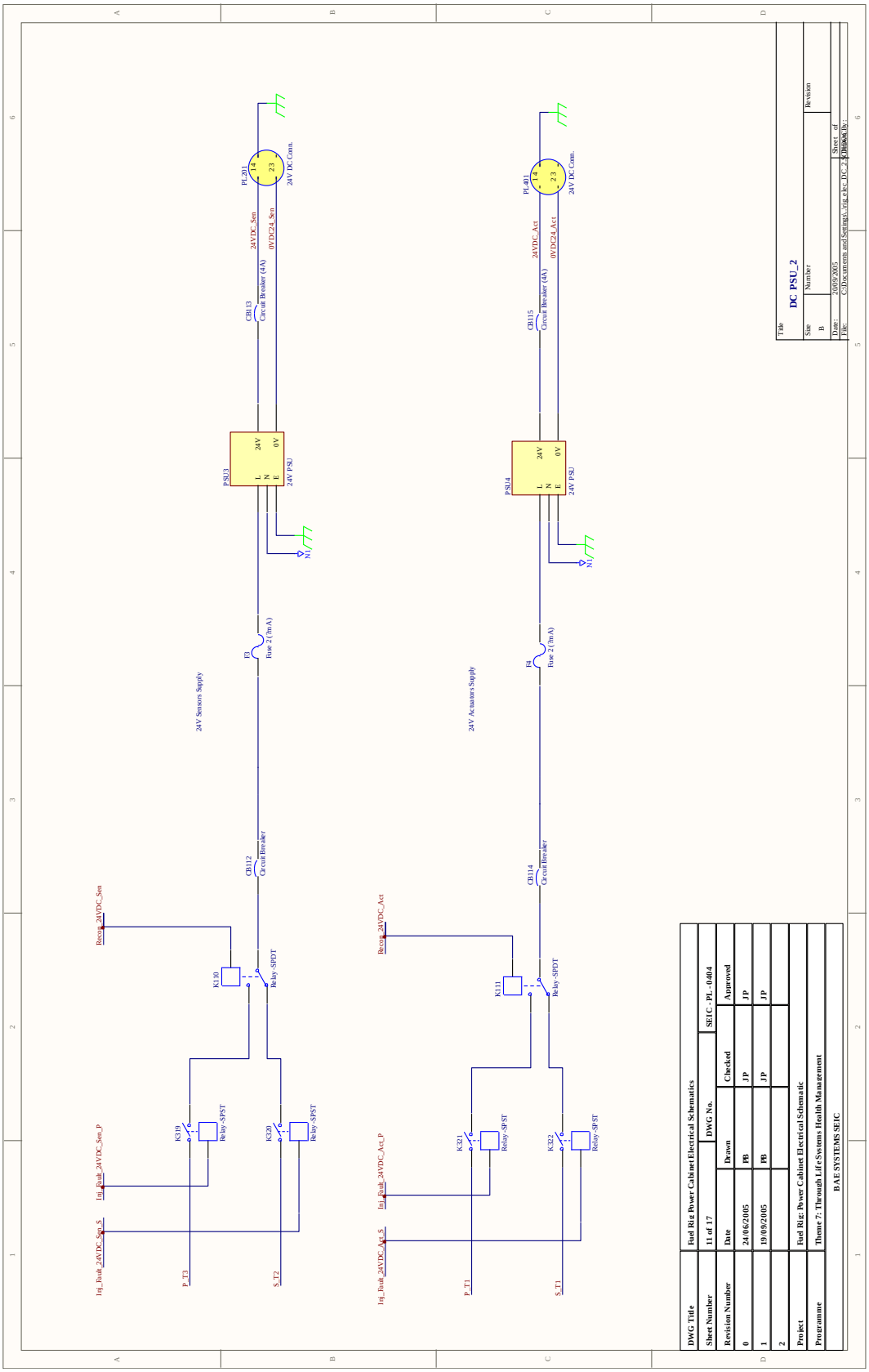
DC_PSU_2
DWG Title
Fuel Rig Power Cabinet Electrical Schematics
Sheet Number
11 of 17
DWG No.
SEIC - PL - 0404
Revision Number
Date
Drawn
Checked
Approved
0
24/06/2005
PB
JP
JP
1
19/09/2005
PB
JP
JP
2
Project
Fuel Rig: Power Cabinet Electrical Schematic
Programme
Theme 7: Through Life Systems Health Management
BAE SYSTEMS SEIC
24V Sensors Supply
24V Actuators Supply
PSU3
PSU4
24V PSU
CB112
CB114
CB113
CB115
Circuit Breaker
Circuit Breaker (4A)
F3
F4
Fuse 2 (3mA)
PL201
PL401
24V DC Conn.
24VDC_Sen
0VDC24_Sen
24VDC_Act
0VDC24_Act
K110
K111
K319
K320
K321
K322
Relay -SPDT
Relay -SPST
Recog_24VDC_Sen
Recog_24VDC_Act
Inj_Fault_24VDC_Sen_P
Inj_Fault_24VDC_Sen_S
Inj_Fault_24VDC_Act_P
Inj_Fault_24VDC_Act_S
P_T3
S_T2
P_T1
S_T1

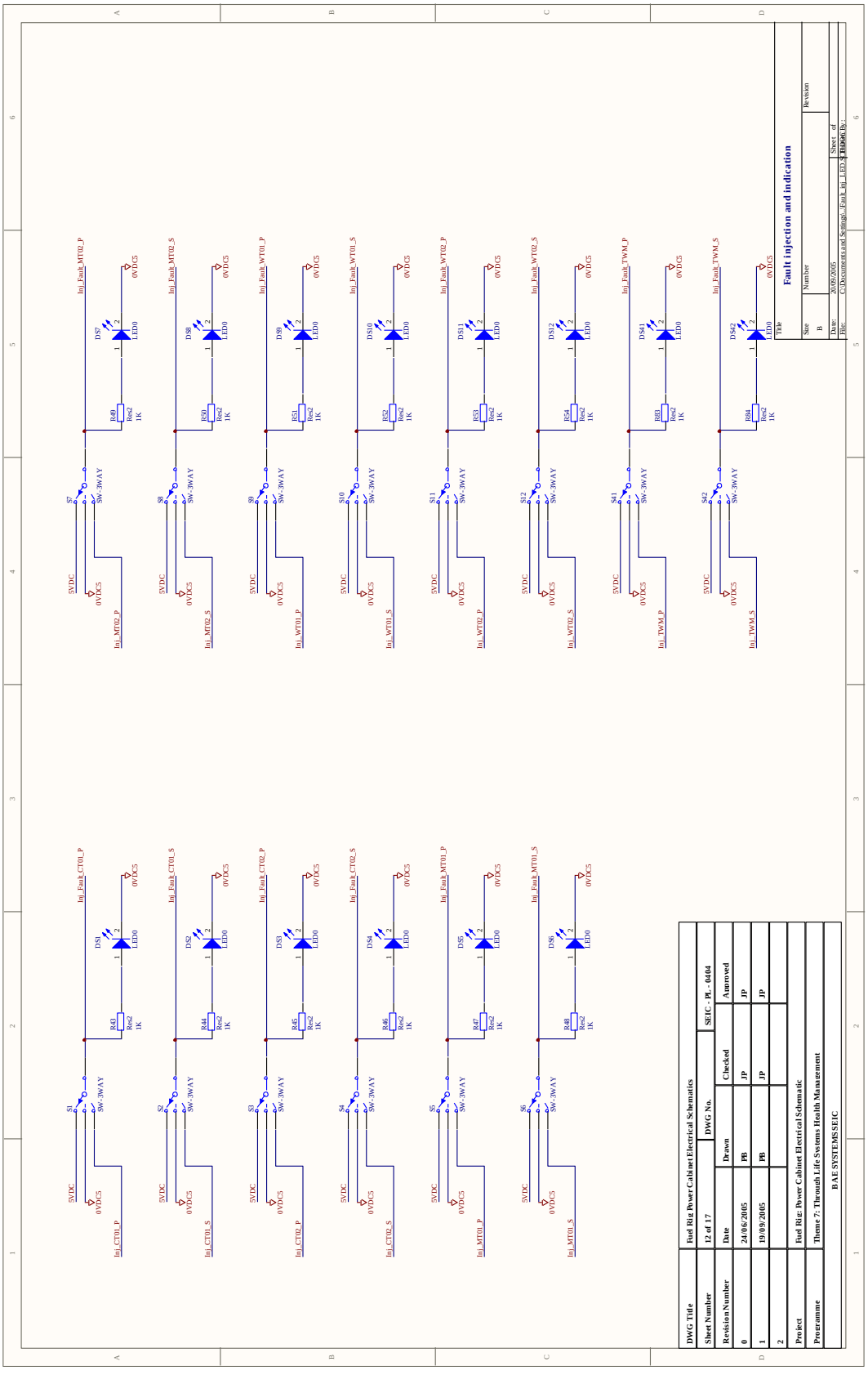
Fault injection and indication
DWG Title
Fuel Rig Power Cabinet Electrical Schematics
Sheet Number
12 of 17
DWG No.
SEIC - PL - 0404
Revision Number
Date
Drawn
Checked
Approved
0
24/06/2005
PB
JP
JP
1
19/09/2005
PB
JP
JP
2
Project
Fuel Rig: Power Cabinet Electrical Schematic
Programme
Theme 7: Through Life Systems Health Management
BAE SYSTEMS SEIC
Inj_Fault_CT01_P
Inj_Fault_CT01_S
Inj_Fault_CT02_P
Inj_Fault_CT02_S
Inj_Fault_MT01_P
Inj_Fault_MT01_S
Inj_Fault_MT02_P
Inj_Fault_MT02_S
Inj_Fault_WT01_P
Inj_Fault_WT01_S
Inj_Fault_WT02_P
Inj_Fault_WT02_S
Inj_Fault_TWM_P
Inj_Fault_TWM_S
5VDC
0VDC5
LED0
SW-3WAY
Res2
1K

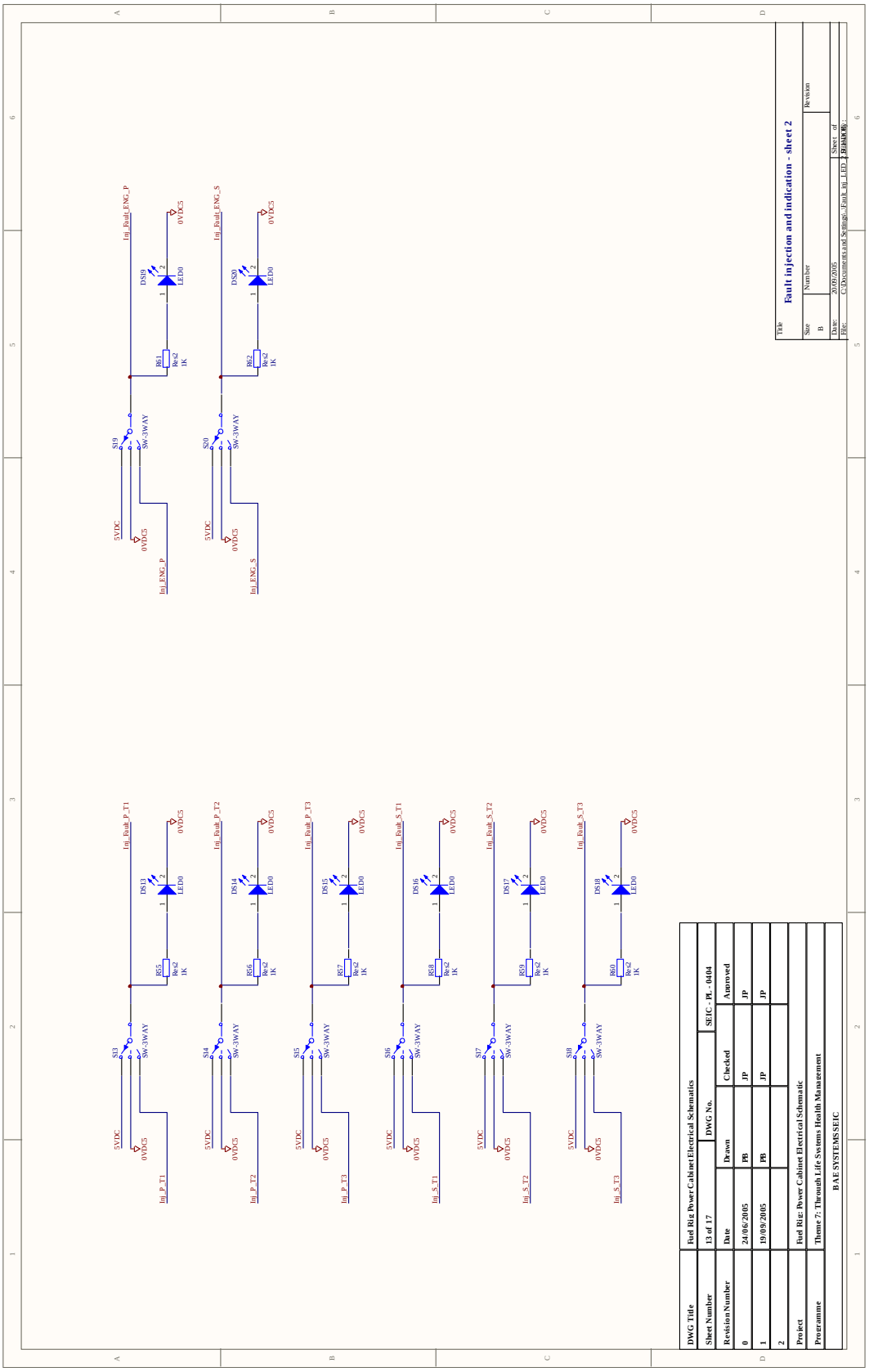
Inj_Fault_ENG_P
Inj_Fault_ENG_S
Inj_Fault_P_T1
Inj_Fault_P_T2
Inj_Fault_P_T3
Inj_Fault_S_T1
Inj_Fault_S_T2
Inj_Fault_S_T3
5VDC
0VDC5
Inj_ENG_P
Inj_ENG_S
Inj_P_T1
Inj_P_T2
Inj_P_T3
Inj_S_T1
Inj_S_T2
Inj_S_T3
Fault injection and indication - sheet 2
Fuel Rig Power Cabinet Electrical Schematics
13 of 17
SEIC - PL - 0404
Fuel Rig: Power Cabinet Electrical Schematic
Theme 7: Through Life Systems Health Management
BAE SYSTEMS SEIC

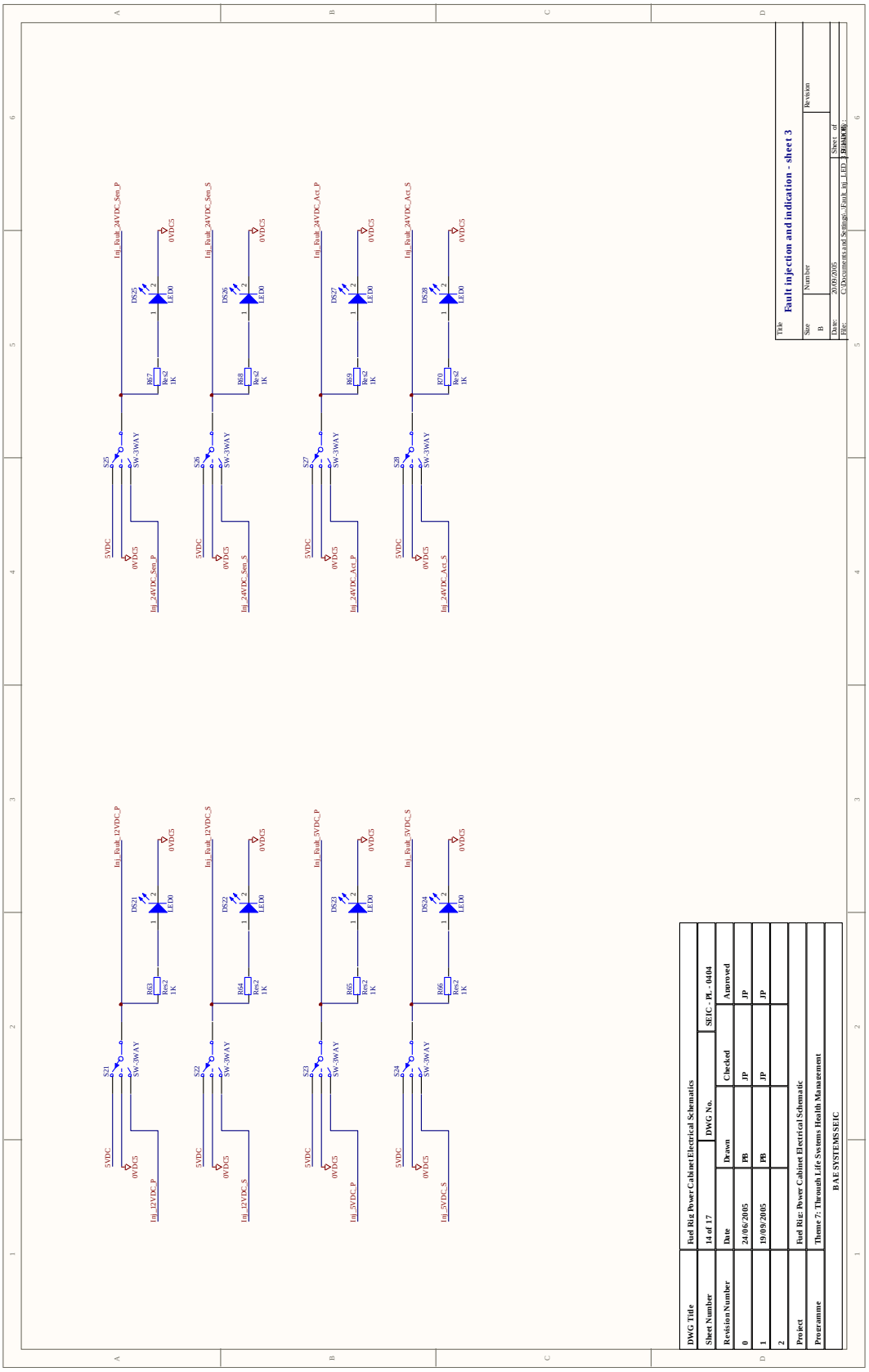
Inj_Fault_24VDC_Sen_P
Inj_Fault_24VDC_Sen_S
Inj_Fault_24VDC_Act_P
Inj_Fault_24VDC_Act_S
Inj_Fault_12VDC_P
Inj_Fault_12VDC_S
Inj_Fault_5VDC_P
Inj_Fault_5VDC_S
DS25
DS26
DS27
DS28
DS21
DS22
DS23
DS24
LED0
R67
R68
R69
R70
R63
R64
R65
R66
Res2
1K
S25
S26
S27
S28
S21
S22
S23
S24
SW-3WAY
5VDC
0VDC
Inj_24VDC_Sen_P
Inj_24VDC_Sen_S
Inj_24VDC_Act_P
Inj_24VDC_Act_S
Inj_12VDC_P
Inj_12VDC_S
Inj_5VDC_P
Inj_5VDC_S
Title
Fault injection and indication - sheet 3
Size
B
Number
Revision
Date:
20/09/2005
File:
C:\Documents and Settings\...\Fault_inj_LED_1.ddb
Sheet of
Drawn:
DWG Title
Fuel Rig Power Cabinet Electrical Schematics
Sheet Number
14 of 17
DWG No.
SEIC - PL - 0404
Revision Number
Date
Drawn
Checked
Approved
0
24/06/2005
PB
JP
JP
1
19/09/2005
PB
JP
JP
2
Project
Fuel Rig: Power Cabinet Electrical Schematic
Programme
Theme 7: Through Life Systems Health Management
BAE SYSTEMS SEIC

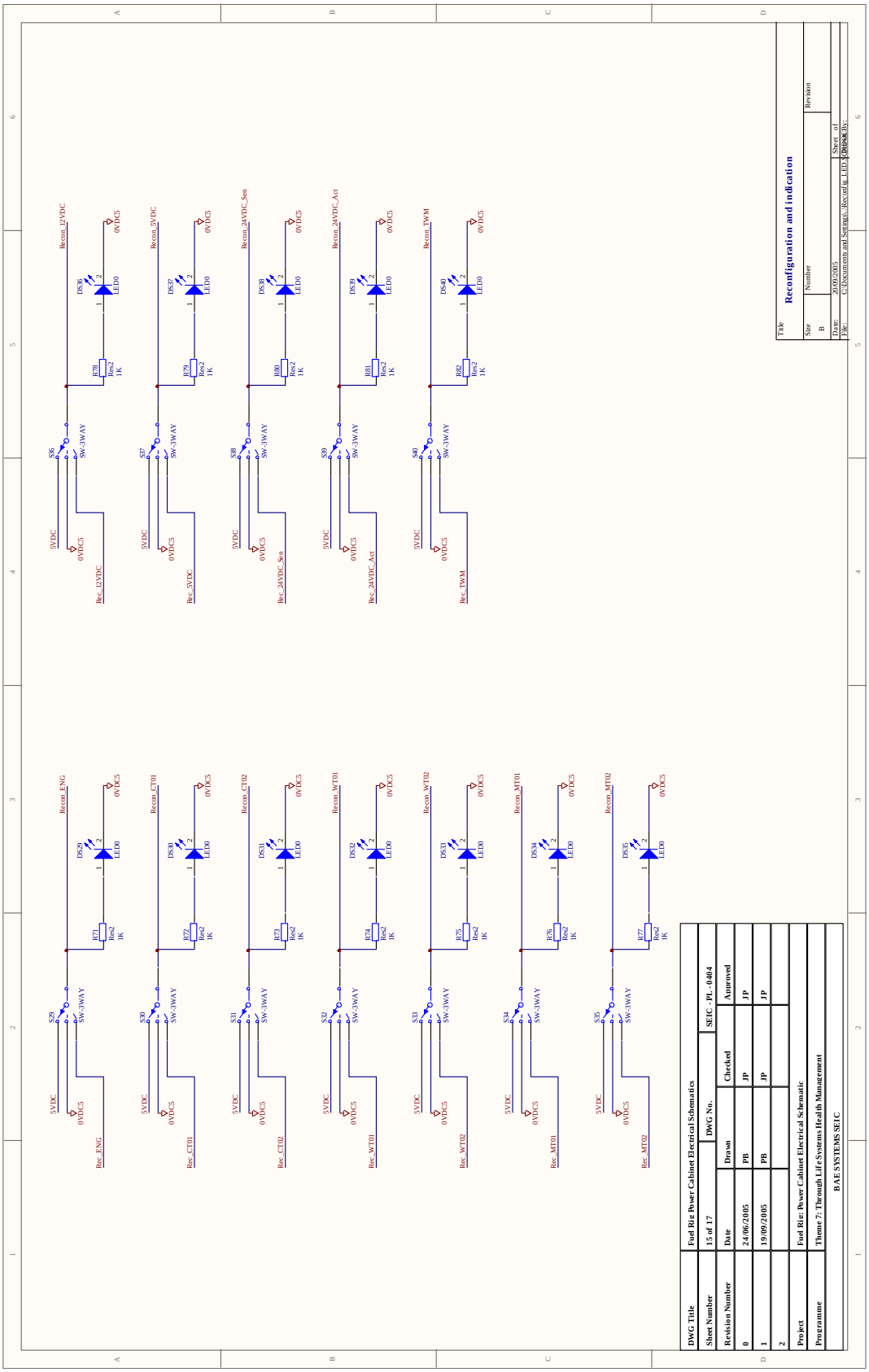
Recon_12VDC
Recon_5VDC
Recon_24VDC_Sen
Recon_24VDC_Act
Recon_TWM
Recon_ENG
Recon_CT01
Recon_CT02
Recon_WT01
Recon_WT02
Recon_MT01
Recon_MT02
Rec_12VDC
Rec_5VDC
Rec_24VDC_Sen
Rec_24VDC_Act
Rec_TWM
Rec_ENG
Rec_CT01
Rec_CT02
Rec_WT01
Rec_WT02
Rec_MT01
Rec_MT02
5VDC
0VDCS
SW-3WAY
LED0
Res2
1K
Reconfiguration and indication
Fuel Rig Power Cabinet Electrical Schematics
Fuel Rig Power Cabinet Electrical Schematic
Theme 7: Through Life Systems Health Management
BAE SYSTEMS SEIC

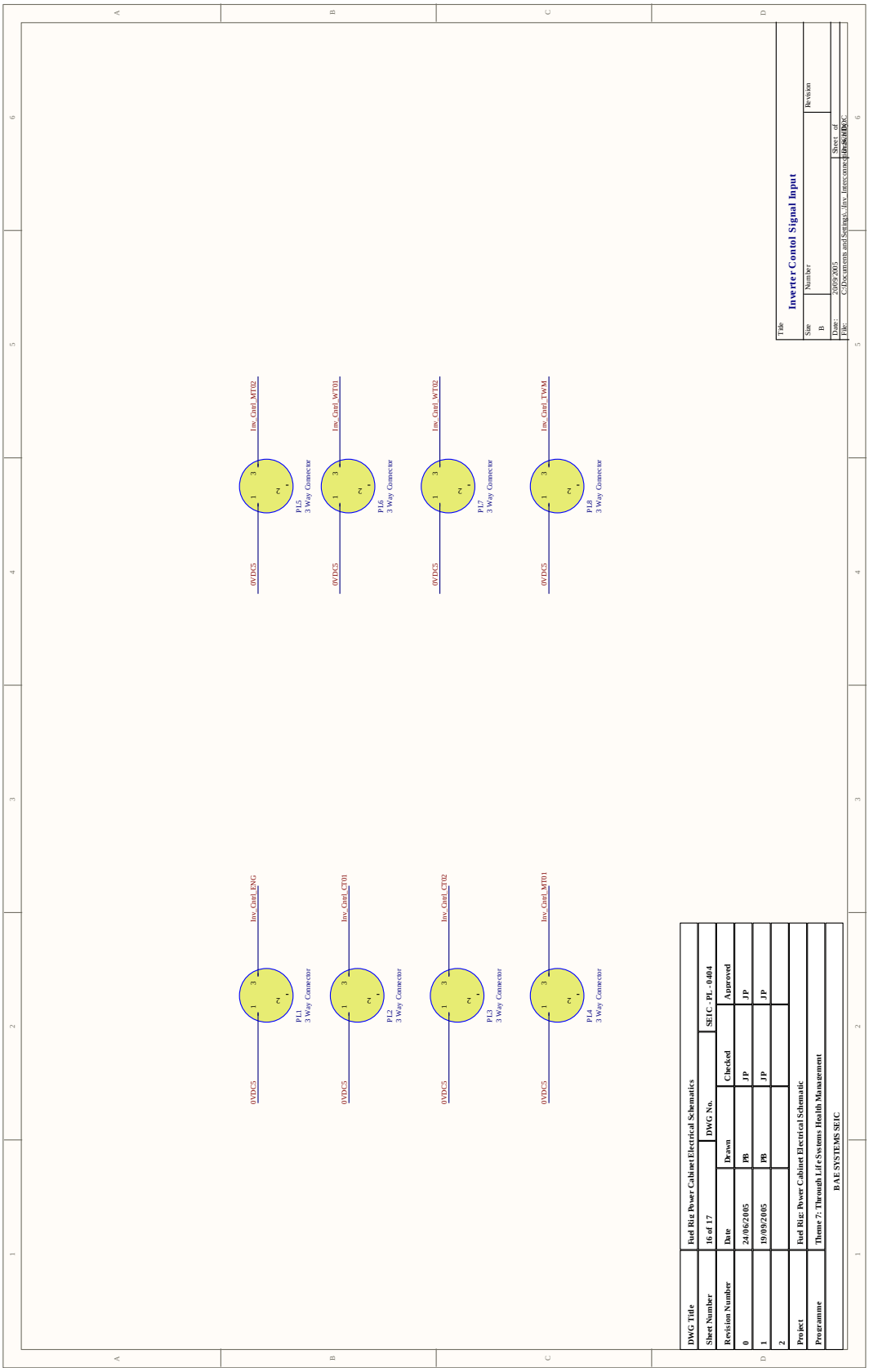
Inv_Cntrl_ENG
Inv_Cntrl_CT01
Inv_Cntrl_CT02
Inv_Cntrl_MT01
Inv_Cntrl_MT02
Inv_Cntrl_WT01
Inv_Cntrl_WT02
Inv_Cntrl_TWM
0VDC5
P1.1 3 Way Connector
P1.2 3 Way Connector
P1.3 3 Way Connector
P1.4 3 Way Connector
P1.5 3 Way Connector
P1.6 3 Way Connector
P1.7 3 Way Connector
P1.8 3 Way Connector
Inverter Contol Signal Input
Size B
Number
Revision
Date: 20/09/2005
File: C:\Documents and Settings\..\Inv_Interconnect.SchDoc
Sheet of
DWG Title Fuel Rig Power Cabinet Electrical Schematics
Sheet Number 16 of 17
DWG No. SEIC - PL - 0404
Revision Number Date Drawn Checked Approved
0 24/06/2005 PB JP JP
1 19/09/2005 PB JP JP
2
Project Fuel Rig: Power Cabinet Electrical Schematic
Programme Theme 7: Through Life Systems Health Management
BAE SYSTEMS SEIC

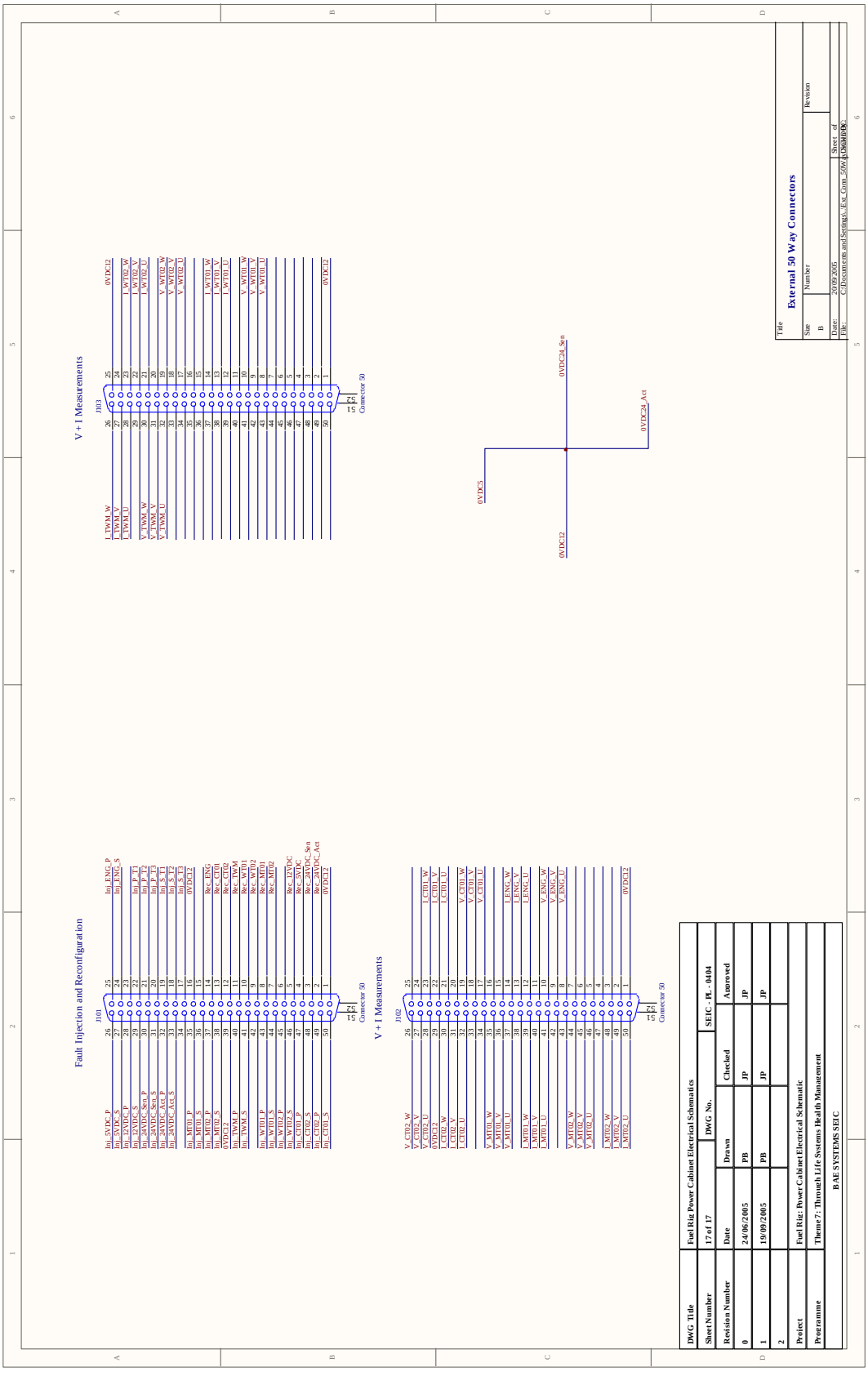
Fault Injection and Reconfiguration
V + I Measurements
V + I Measurements
External 50 Way Connectors
Connector 50
Connector 50
Connector 50
0VDC12
0VDC5
0VDC24_Sen
0VDC24_Act
DWG Title
Fuel Rig Power Cabinet Electrical Schematics
Sheet Number
17 of 17
DWG No.
SEIC - PL - 0404
Revision Number
Date
Drawn
Checked
Approved
0
24/06/2005
PB
JP
JP
1
19/09/2005
PB
JP
JP
2
Project
Fuel Rig: Power Cabinet Electrical Schematic
Programme
Theme 7: Through Life Systems Health Management
BAE SYSTEMS SEIC